# STRESS CONCENTRATION FACTOR AND HOT SPOT STRESS STUDIES OF PARTIALLY OVERLAPPED CIRCULAR HOLLOW SECTION K-JOINTS

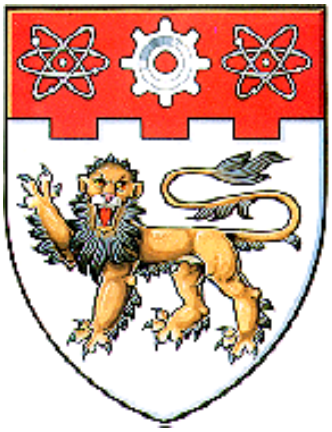

**SOPHA THONG**

**School of Civil & Environmental Engineering**

**Nanyang Technological University**

2010

# STRESS CONCENTRATION FACTOR AND HOT SPOT STRESS STUDIES OF PARTIALLY OVERLAPPED CIRCULAR HOLLOW SECTION K-JOINTS

**SOPHA THONG**

**School of Civil & Environmental Engineering**

A Thesis submitted to the Nanyang Technological University

in fulfillment for the degree of

Doctor of Philosophy

2010

# *ACKNOWLEDGEMENTS*

The author wishes to acknowledge the Nanyang Technological University for providing a scholarship to undertake the research study. The author would like to express sincere gratitude and appreciation to A/P. Lee Chi King for his supervision. Throughout this research, the author has received much invaluable advice and encouragement from his supervisor. His constructive instructions and comments gave the author a very deep impression.

Special thanks are given to A/P Chiew Sing Ping, A/P. Lie Seng Tjhen and for their valuable advice and support in connection with relevant aspects of this work.

The author wishes to thank his friends, especially Dr Nguyen Thi Bich Ngoc, Dr Yang Zhengmao, Dr Ji Hongli, and all the technical staff at Construction Technology Laboratory, namely Mr Goh C. K., Ms Ong S. H., Mrs Peck-Leong Y. L., Mrs Yuen-Ng S. J. for their assistances in the testing of the specimens.

Finally, the author wishes to express his appreciation to his wife, daughter and son for their love, concern, selfless and diligent support to effect the completion of this work.

# *ABSTRACT*

Circular hollow sections (CHS) are widely adopted in fixed jacket and topside structures due to their excellent structural and mechanical properties. Virtually in almost all off-shore structures, one of the main design considerations when using CHS is to optimize the structural joints which are susceptible to fatigue failure due the dynamic and cyclic loading natural of the structures. Recently, partially overlapped CHS tubular K-joints become more and more popular due to their optimum strengths when compared to other alternative joint configurations such as non-overlapped (gapped) or completely overlapped K-joints. However, in the past, few research works were carried out to study the fatigue behaviour of partially overlapped CHS K-joints. In fact, currently, only a very limited information regarding the fatigue life of CHS overlapped K-joints are available. Hence, there is a need to investigate the *stress concentration factors* (SCF) and *the hot spot stress* (HSS) distributions of this kind of joints in the current research.

In the current research, carefully planned experimental studies were firstly carried out to investigate the SCF and the HSS distributions along the joint intersection of three full-scale partially overlapped CHS K-joints. The experimental results show that depending on the geometrical parameters of the partially overlapped K-joints, the maximum SCF could locate on either the brace side or the chord side of the joint. The experimental results show that Efthymiou formulae are conservative only when the partially overlapped K-joints are subjected to in-plane bending (IPB) loading, but not for the case of axial (AX) loading. In addition, it is observed that the S-N curves are found to be on the conservative side of the test results.

After the experimental study, finite element (FE) models were created to simulate the test specimens. The FE models were based on mesh generator developed by Nguyen at NTU in 2008. These FE models were conducted by using the FE program ABAQUS. A comparison between tests results with FE analyses showed that reliable SCF and HSS values could be obtained. However, using such method in a normal day-to-day design

office operation is not unfeasible. Thus, a large scale parametric study is carried out to study the general fatigue performance of this type of joint. A total of 3500 FE models with wide range of geometrical parameters of partially overlapped K-joints were created. From the parametric study, it is seen that the SCF values increase generally as $\gamma$, $\tau$ and $\theta$ increase, but as Ov and $\beta$ increases the SCF values decrease. In general, all these parameters have a large impact on SCFs for the partially overlapped CHS K-joint. A set of parametric equations was subsequently proposed for predicting the SCF of partially overlapped CHS K-joints under axial and in-plane bending load cases. The equations were verified against the acceptance criteria of the Fatigue Guidance Review Panel. Further analysis on the accuracy and reliability of these regression equations shows that they are reasonable accuracy, but improvement is needed in order to come up better SCF/HSS estimations. As part of an attempt to gain a more accurate prediction, a new interpolation method is used for estimating the SCF and HSS values of partially overlapped CHS K-joint. The assessment confirms the efficiency and reliability of the new method for predicting the SCF and HSS of partially overlapped CHS K-joints under basic AX, IPB and combined loadings.

Finally, a comparison study between the gapped and the partially overlapped CHS K-joints has been made. It is observed from the comparison results that the partially overlapped CHS K-joints are mainly in favour when they are working under the AX load case, especially where the joints of having braces with low and medium $\gamma$ values. It is also observed that under the combined AX and IPB loading, the partially overlapped CHS K-joints gain more benefits than the gapped. The gapped CHS K-joints are in favour on working under the IPB loading. However, it should be noted that some researchers suggested that in design of trusses or frames it is usually to assume that the members are pin-ended, meaning bending moment can be neglected as far as the joint design is concerned provided the eccentricity associated with them falls within the certain limits stipulated in CIDECT Design guide No. 8. In this case, it could be concluded that the partially overlapped K-joints could be regarded as a favourite joint type when compared to gapped CHS K-joints in terms of fatigue performance.

# *CONTENTS*

# *LIST OF TABLES*

# *LIST OF FIGURES*

# *LIST OF SYMBOLS*

| | |
|---|---|
| D, $d_1$, | Outside chord diameter |
| d, $d_2$ | Outside brace diameter |
| $D_{Ov-Gap}(HSS)$ | Relative difference between the HSS values obtained from the proposed LIM for the partially overlap CHS K-joints and from the DEn parametric SCF equations for the gapped CHS K-joints |
| $D_{Gap-Ov}(FL)$ | Relative difference between the numbers of cycles based on S-N curve [5] obtained from the partially overlapped CHS K-joints and the gapped CHS K-joints |
| e | eccentricity |
| E | Young's modulus |
| $E_{PRM-FEM}(SCF)$ | Relative error between the estimated SCF values from the PRM and the FE analyses |
| $E_{PIM-FEM}(SCF)$ | Relative error between the estimated SCF values from the PIM and the FE analyses |
| $E_{LIM-FEM}(SCF)$ | Relative error between the estimated SCF values from the LIM and the FE analyses |
| F, $F_{ax}$ | Axial load |
| $F_{IBP}$ | In-plane bending load |
| $F_{OPB}$ | Out-of-plane bending load |
| $f_{ax}$ | Nominal stresses due to axial load |
| $f_{ipb}$ | Nominal stresses due to in-plane bending load |
| $f_{opb}$ | Nominal stresses due to out-of-plane bending load |
| g | Gap between two braces |
| I | Moment of inertia of cross section |
| $K_A(\varphi)$ | Stress concentration factors (SCFs) around the intersection of joint subjected to axial load |
| $K_{Bi}(\varphi)$ | Stress concentration factors (SCFs) around the intersection of joint subjected to in-plane bending load |

| | |
|---|---|
| $K_{Bo}(\varphi)$ | Stress concentration factors (SCFs) around the intersection of joint subjected to out-of-plane bending load |
| L | Chord length |
| l | Brace length |
| $l_{r,\ min}$ | Minimum distance measured from weld toe |
| $l_{r,\ max}$ | Maximum distance measured from weld toe |
| $M_{IPB}$, $M_1$, $M_2$, $M_3$, $M_4$ | in-plane bending moment |
| $M_o$, $M_{OPB}$ | Out-of-plane bending moment |
| N, $N_f$ | Number of cycles |
| Ov | Percentage of overlap |
| q | Length of overlap between two braces |
| R, $r_o$ | Radius of chord |
| r, $r_1$ | Radius of brace |
| $S$, $S_{rhs}$ | Hot spot stress (HSS) range |
| $SCF_{PRM}$ | SCF value estimated from the PRM |
| $SCF_{PIM}$ | SCF value estimated from the PIM |
| $SCF_{LIM}$ | SCF value estimated from the LIM |
| $SCF_{FEM}$ | SCF value obtained from the FE analyses. |
| T | Chord thickness |
| t, $t_1$ | Brace thickness |
| $T_{AWS}$ | Minimum specification of American Welding Society [9] for weld thickness |
| $T_W$ | Weld thickness |
| $t_B$ | Reference thickness (16mm for tubular joints) |
| $\alpha$ | Chord length parameter (2L/D) |
| $\beta$ | Brace-to-chord diameter ratio (d/D) |
| $\gamma$ | Chord radius-to-wall thickness ratio (D/2T) |
| $\theta$ | Angle between chord and brace |
| $\theta_1$ | Angle between chord and through brace |
| $\theta_2$ | Angle between chord and overlapping brace |
| $\sigma_b$ | Nominal stress due to bending load |

| | |
|---|---|
| $\sigma_{HSS}$ | Hot spot stress |
| $\sigma_{max}$ | Maximum stress |
| $\sigma_{min}$ | Minimum stress |
| $\sigma_x$ | Nominal stress component in x-direction in global coordinate system |
| $\sigma_y$ | Nominal stress component in y-direction in global coordinate system |
| $\sigma_{nom}$, $\sigma_n$ | Nominal stress |
| $\tau$ | t/T, wall thickness ratio |
| $\upsilon$ | Poisson's ratio |
| $\xi_n$ | Nominal strain |
| $\xi_{\perp}$ | Hot spot strain (HSSN) |
| $\xi_{//}$ | The strain at weld toe position perpendicular to $\xi_{\perp}$ |

***Abbreviation***

| | |
|---|---|
| AX | Axial load |
| AX11 | Axial load at the end of the through brace |
| AX21 | Axial load at the end of the overlapping brace |
| AX11tA | under AX11 load case on the weld toe of through brace along Curve A |
| AX11oA | under AX11 load case on the weld toe of overlapping brace along Curve A |
| AX11tC | under AX11 load case on the weld toe of through brace along Curve C |
| AX11cC | under AX11 load case on the weld toe of chord along Curve C |
| AX21oA | under AX21 load case on the weld toe of overlapping brace along Curve A |
| AX21tA | under AX21 load case on the weld toe of through brace along Curve A |
| AX21oB | under AX21 load case on the weld toe of overlapping brace along Curve B |
| AX21cB | under AX21 load case on the weld toe of chord along Curve A |
| CHS | Circular hollow section |
| 3D | Three-dimensional |

| | |
|---|---|
| 1D | One-dimensional |
| 2D | Two-dimensional |
| FE | Finite element |
| FL | Fatigue life |
| $F_{Gap}$ | Number of cycles based on S-N curve [5] estimated from the HSS value based on DEn parametric equations results, |
| $F_{Ov}$ | Number of cycles based on S-N curve [5] estimated from HSS value obtained from the proposed LIM. |
| IPB | In-plane bending |
| IPB11 | + ve in-plane bending load at the end of the through brace |
| IPB12 | - ve in-plane bending load at the end of the through brace |
| IPB21 | + ve in-plane bending load at the end of the overlapping brace |
| IPB22 | - ve in-plane bending load at the end of the overlapping brace |
| IPB11tC | under IPB11 load case on the weld toe of through brace along Curve C |
| IPB11cC | under IPB11 load case on the weld toe of chord along Curve C |
| IPB12tA | under IPB12 load case on the weld toe of through brace along Curve A |
| IPB12oA | under IPB12 load case on the weld toe of overlapping brace along Curve A |
| IPB21oB | under IPB21 load case on the weld toe of overlapping brace along Curve B |
| IPB21cB | under IPB21 load case on the weld toe of chord along Curve B |
| IPB22oA | under AX11 load case on the weld toe of overlapping brace along Curve C |
| IPB22tA | under IPB22 load case on the weld toe of through brace along Curve A |
| LIM | Line interpolation method |
| *HSS* | Hot spot stress |
| $HSS_{Ov}$ | HSS values estimated from the proposed LIM |
| $HSS_{Gap}$ | HSS values estimated from the DEn parametric equations. |
| *HSSN* | Hot spot strain (s) |
| OPB | Out-of-plane bending |
| PIM | Point interpolation method |

| | |
|---|---|
| PRM | Parametric regression method |
| RHS | Rectangular hollow section |
| SCF | Stress concentration factor |
| $SCF_{av}$ | Average stress around the intersection of the joint |
| $SCF_{ax}$ | Stress concentration factor for axial load |
| $SCF_{ipb}$ | Stress concentration factor for in-plane bending load |
| $SCF_{opb}$ | Stress concentration factor for out-of-plane bending load |
| $SCF_{OV}$ | SCF values estimated from program PIM |
| $SCF_{Gap}$ | SCF values estimated from program DEnPRM |
| $SCF_{CS}$ | SCF at the chord saddle |
| $SCF_{CC}$ | SCF at the chord crown heel |
| $SCF_{C}$ | Maximum SCF on the chord side |
| $SCF_{BS}$ | SCF at brace saddle |
| $SCF_{BC}$ | SCF at the brace crown heel |
| $SCF_{B}$ | Maximum SCF on the brace side |
| $HSS_{OV}$ | HSS values estimated from program LIM |
| $HSS_{Gap}$ | HSS values estimated from program DEnPRM |
| SHS | Structural hollow section |
| SNCF | Strain concentration factor |

# *CHAPTER 1*
# *INTRODUCTION*

## 1.1 RESEARCH BACKGROUND

Steel hollow sections are commonly used as supporting structures in onshore and offshore engineering. In these structures, the members are jointed together by welding the profiled ends of the brace into the circumference of the chord. The connections between the brace and the chord are defined as structural joints. According to different sectional shapes, the types of structural joints can be classified either as circular or rectangular joints. *Circular hollow sections* (CHS) are more widely adopted in practice due to their excellent structural and mechanical properties such as having high strength and low weight ratio. The continuous smooth curved surfaces also decrease the frictional forces caused by wind/wave, and thus increase the capacity of resistance against the environmental loads. In addition, the stress concentration, which will reduce the life of the structures subjected to cyclic loads, is smaller than that of *rectangular hollow section* (RHS) joints.

Fatigue is regarded as one of the major problems that cause the degradation of offshore steel structures in the long-term integrity. A significant feature of fatigue is that the applied load is not necessarily large to cause immediate failure at members and joints of the structures. Instead, the failure of structural components occurs after a certain number of load fluctuations have been experienced. The Health & Safety Executive statistic data of the North Sea steel structures revealed that the fatigue damage of offshore steel jackets was the most frequent single cause of repairs which represented about 25% of all repair works [1]. Thus, the fatigue failure is one of the most important failure modes to be considered in the design for offshore steel jacket. The offshore steel jacket is a truss-work structure consisting of tubular members resting on the seabed. It supports several modules on topside with piles running inside the main legs of structure

and penetrating beneath the seabed as shown in Figure 1.1.

The *structural hollow section* (SHS) joints may be classified according to the geometric configurations, transfer action of loads among braces, and types of design. For the purpose of design, Underwater Engineering Group [2] classified the tubular joints into four (4) categories as follow.

- Simple welded joint
- Complex welded joint
- Cast steel joint
- Composite joint

Some of the different types of tubular joints are illustrated in Figure 1.2. Cyclic loadings would be occurred to tubular joints by three basic load cases namely *axial load* (AX), *in-plane bending* (IPB) and *out-of-plane bending* (OPB) as shown in Figure 1.3. Each load case has its particular distribution of stresses along the joint intersection of members. The geometrical parameters of typical welded joints are shown in Figure 1.4.

Simple tubular joints are the most widely used connection details for the construction of offshore steel jackets in the industry. The popularity is attributed to the available parametric equations and direct calculation methods to assess the joint capacity. It is also because of ease of fabrication, non-destructive testing and inspection that can apply to them. However, due to the gap between braces and eccentricity, additional moments on the chord member should be carefully considered. BOMEL [3], in an industry project investigating the strengths of tubular frames, found that gapped K-joints exhibited a typical brittle response and shed a large proportion of the load. It is also important to note that with the progressive development of offshore exploration in deeper waters and arctic conditions, the offshore platforms are now becoming larger and more demanding. As a result, the use of simple tubular joints for larger offshore steel jackets may not be appropriate and becomes uneconomical as long thick wall cans

are required to be used at every connection in order to avoid the overlapping of structural members.

In contrast, partially overlapped K-joint has a high residual capacity as a result of their optimized load transfer pattern. This advantage, however, is offset by higher fabrication costs due to the complex end profile of the overlapping brace and difficulty of the inspection of the hidden weld. However, Tizani et al. [4] reported a case study comparing the costs of three K-joints design options. Having considered a material based on, however, only ultimate strength of the joints and fabrication costs, it was concluded that the specification of tubular overlapped joints was the cheapest solution, with the fabrication cost actually being significantly cheaper than that of the alternative canned gapped joints. However, up to now, only a few research works were carried out to study the fatigue behaviour of partially overlapped CHS K-joints. In fact, currently, very few information regarding the fatigue life of partially overlapped CHS K-joints are available. Hence, there is a need to investigate the *stress concentration factors* (SCF) and the *hot spot stress* (HSS) of this kind of joints in the current research.

## 1.2 OBJECTIVES OF CURRENT RESEARCH

The main objectives of the current research are focused on the SCF and HSS of partially overlapped CHS K-joints and are listed below.

1. To experimentally and numerically investigate the HSS and SCF distributions at the joint intersections under different load cases.
2. To evaluate the applicability of present S-N curve [5] in design of partially overlapped CHS K-joints.
3. To study numerically the influence of geometrical parameters on the SCF distributions of the joint under AX and IPB load cases.
4. To propose parametric equations to predict the SCF of the joint under AX and IPB load cases.

5. To propose a new method that based on interpolation method for the more accurate estimation of SCFs and HSSs of partially overlapped CHS K-joints.
6. To compare, in general, the fatigue performance of partially overlapped CHS K-joints with their counterparts, gapped CHS K-joints.

## 1.3 SCOPE OF CURRENT RESEARCH

The current research involves experimental and numerical investigations of SCF and HSS of partially overlapped CHS K-joints under both basic and combined load cases. In Chapter 1, an introduction of the use of tubular joints in the offshore construction industry is presented. The objectives of the current research are also given. In Chapter 2, a literature review on the past research findings related to the partially overlapped K-joints is reviewed in detail. Some basic understandings on the stress and concentration distributions of various tubular joints are also included.

Chapter 3 describes the experimental set up for three full-scale partially overlapped CHS K-joints. The stress distributions and stress concentration along these joints intersections are studied. The test data are also used for the verification and calibration of the *finite element* (FE) model. The applicability of the present S-N curve [5] in design of partially overlapped CHS K-joints is evaluated. Then, the influence of various geometrical parameters on the SCF of partially overlapped CHS K-joints is presented in Chapter 4. In this chapter, based on the data obtained from the FE analysis, a set of regression equations is proposed to predict the SCFs of partially overlapped CHS joints under AX and IPB loading. In order to further improve the accuracy of the SCF/HSS predictions, an interpolation method to calculate HSS and SCF values of partially overlapped CHS K-joints is presented in Chapter 5. A comparison fatigue performance, in general, between the partially overlapped CHS K-joints and the gapped counterparts is presented in Chapter 6. Finally, in Chapter 7, conclusions of the present research project are given. The recommends concerning future research programmes on the behaviour of the partially overlapped CHS K-joints are also highlighted.

To date, equations for the fatigue design of partially overlapped CHS K-joints are not commonly available in any design code. The originality of this study is to propose new method, which is based on interpolation method, to predict the SCF and HSS of partially overlapped CHS K-joints. It is believed that this new method would help engineers to successfully and effectively carry out the SCF/HSS analysis of any partially overlapped CHS K-joint.

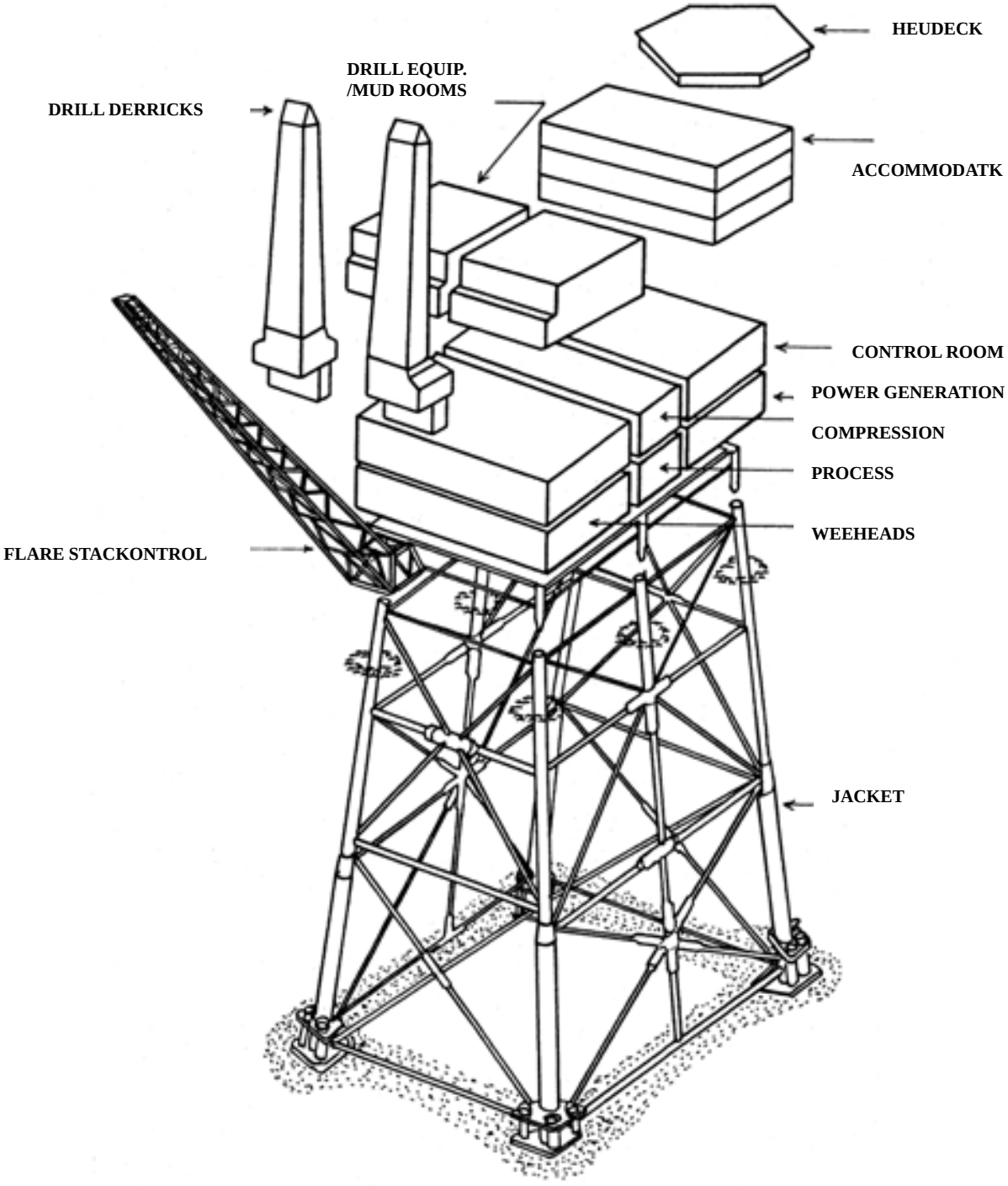


Figure 1.1 A typical offshore steel jacket structure [2]

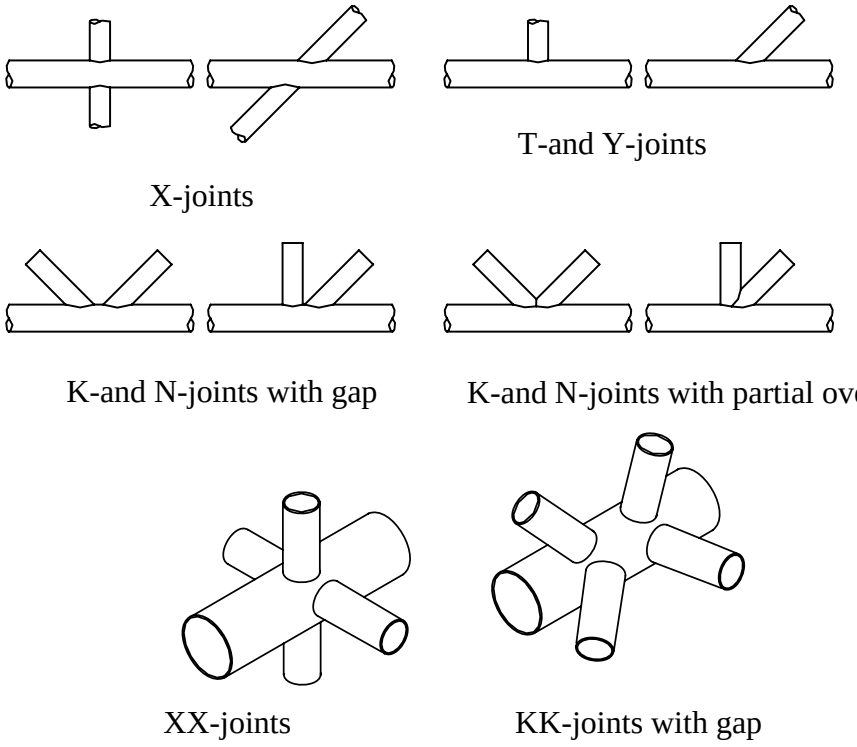


Figure 1.2 Different types of tubular joints

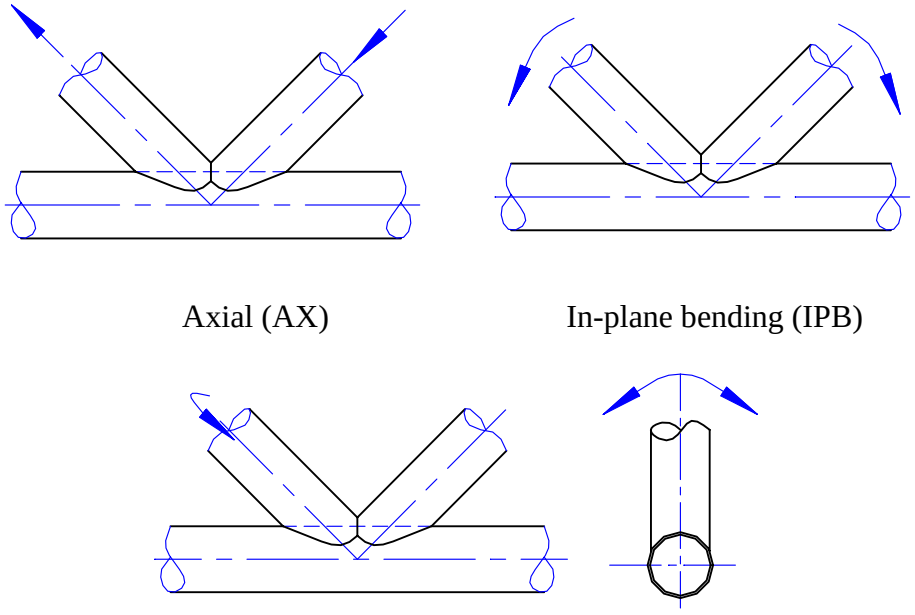


Figure 1.3 Basic load cases for tubular joints

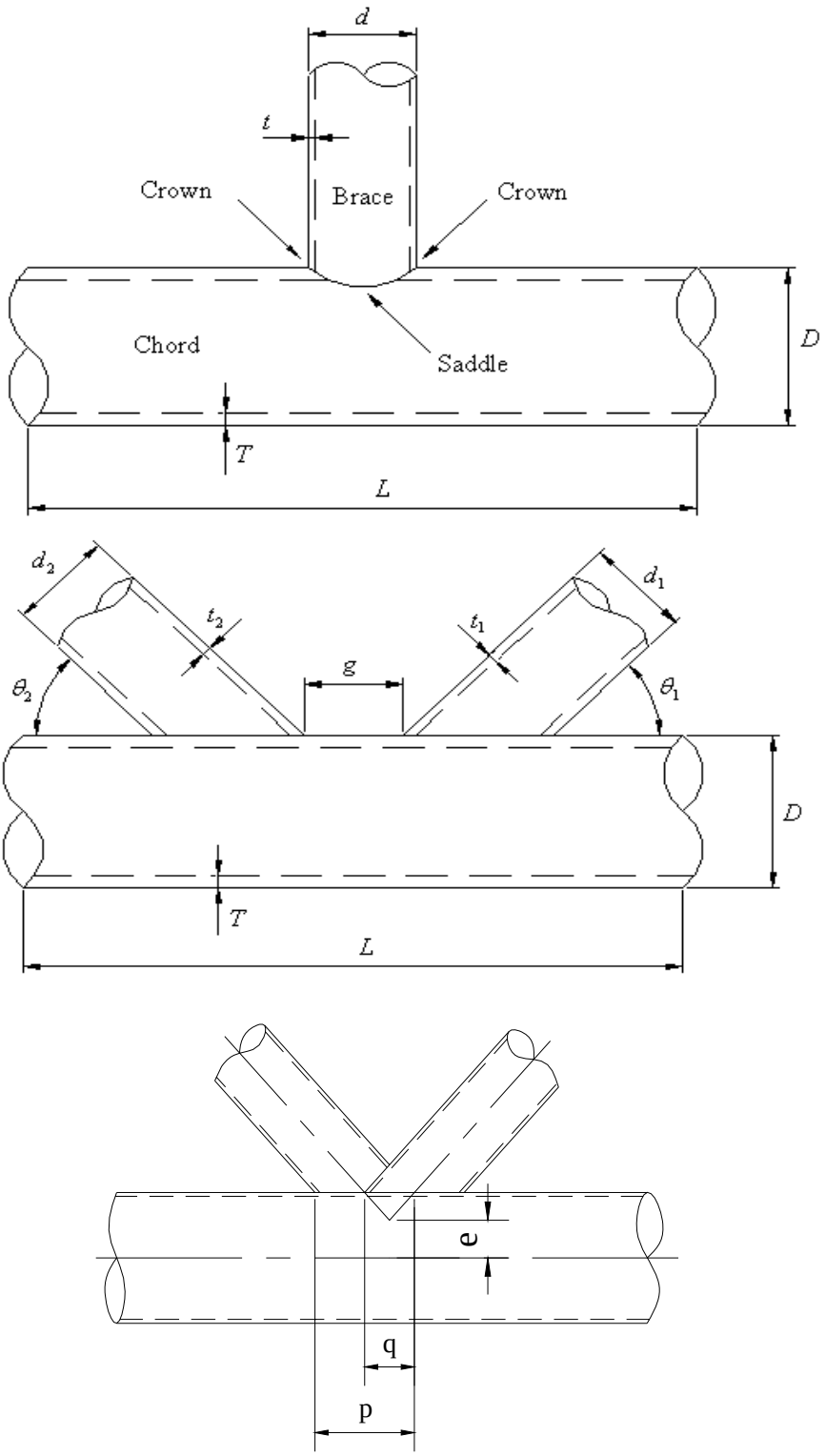


Ov = q / p x 100%

Figure 1.4 Definition of geometrical parameters

# *CHAPTER 2*

# *LITERATURE REVIEW*

## 2.1 STRESS ANALYSIS OF TUBULAR JOINTS

Tubular joints have been used extensively as supporting structures in offshore engineering. The joints are formed by welding the brace and the chord together. In these welded tubular joints, the stiffness around the intersection is not uniform. This will result in a non-uniform geometrical stress distribution. A typical stress distribution along the weld toe is shown in the Figure 2.1. This non-uniform stress is usually caused by curvature discontinuity at the intersecting curve, which will then cause stress concentration at this region. The peak stress around the intersection is known as the *hot spot stress* (HSS) which is the place of the crack initiation site and relates to fatigue life of tubular joints, and thus it is an important parameter used in design and analysis. The HSS is normally dependent on the geometry of the joints as well as on the external loadings. In addition, the HSS is also affected by fabrication factors such as the configuration of the weld (flat, convex, concave), and the local condition of the weld toe (radius of weld toe, undercut).

### 2.1.1 Nominal Stress

The nominal stress ($\sigma_n$) is calculated using the simple beam theory and the superposition method without taking accounts the geometric discontinuity and other localizing effects. The nominal stress of a tubular K-joint subjected under basic load can be expressed as follows:

For balanced axial load (Figure 1.3a),

$$\sigma_n = \frac{4F}{\pi(d^2 - (d-2t)^2)} \tag{2.1}$$

For in-plane bending (Figure 1.3b),

$$\sigma_n = \frac{32\, d\, M_{IPB}}{\pi(d^4 - (d-2t)^4)} \tag{2.2}$$

For out-of-plane bending (Figure 1.3c),

$$\sigma_n = \frac{32\, d\, M_{OPB}}{\pi(d^4 - (d-2t)^4)} \tag{2.3}$$

where $F$ is the axial load, $d$ is diameter of the brace, $t$ is thickness of the brace, $M_{IPB}$ and $M_{OPB}$ are in-plane bending and out-of-plane bending moments respectively.

In the case of a CHS overlapped K-joint under combined axial load and in-plane bending, the nominal stress can be superimposed by the two nominal stresses. That means the nominal stress can be expressed as

$$\sigma_n = \frac{4F}{\pi(d^2 - (d-2t)^2)} + \frac{32\, d\, M_{IPB}}{\pi(d^4 - (d-2t)^4)} \tag{2.4}$$

Accordingly, the nominal stress of a tubular K-joint under combined axial load and out-of-plane bending can also be expressed as

$$\sigma_n = \frac{4F}{\pi(d^2 - (d-2t)^2)} + \frac{32\, d\, M_{OPB}}{\pi(d^4 - (d-2t)^4)} \tag{2.5}$$

### 2.1.2 *Hot Spot Stress* (HSS) Classification

There are several methods available to determine the fatigue resistance of welded connections [5]. The commonly used methods are the classification method, the HSS method, the local notch stress method and the fracture mechanics approach. The

classification method is based purely on the nominal stresses. The HSS and the local notch stress methods are based on the HSS at weld toe and the local peak notch stresses at weld root respectively. However, the HSS method is regarded to be the most practical approach as it relates different structural geometry of the joints to the same S-N curve by introducing SCF for fatigue calculation [6]. Hence, the HSS method is adopted in the current study to determine the stress concentrations of partially overlapped CHS K-joints.

It should be noted that the points of higher localized stresses at the joint intersection of members are called as "hot-spots" and the associated stresses are known as HSS. Based on a large amount of data on stress analysis of tubular joints obtained by UKOSRP programme, Irvine [7] suggested that the HSS should be defined as "the linear stress distribution outside the notch region on a tubular joint extrapolated to the weld toe to obtain experimental values of tubular joint hot spot stress". Additionally, rosette gauges were recommended to be used to obtain the maximum principal stresses so that the stresses could be conservatively extrapolated to obtain the HSS.

On the other hand, DEn [6] recommended that "the stress, which is used to describe the fatigue performance of a tubular joint, should incorporate the effects of overall tube geometry (i.e. the relative sizes of the brace and chord) but omit the concentrating influence of the weld geometry which changes around the periphery of any brace/chord intersection and, although weld profiling is specified by codes of practice such as AWS D1.1 [8], will in practice vary from joint to joint". The greatest value of the maximum principle stress extrapolated to the weld toe through the local stress region around the brace and the chord periphery conservatively determines the HSS.

It should be stated that not all tubular joints will exhibit a region of stress linearity near the weld toe. K and Y joints in particular can, in certain locations, exhibit geometric stress distributions which are non-linear, and to maintain the general definition of HSS as given above, i.e. that found at the weld toe but omitting the concentration caused by

weld geometry, non-linear extrapolation through the region of local stress is necessary. Thus, a more general definition of HSS can be defined as the peak value of geometric stress at the weld toe. Furthermore, van Wingerde et al. [9] proposed a more precise approach based on the HSS method to replace the previous nominal stress and HSS approaches for the fatigue analysis of steel connections. The following guideline was proposed for the fatigue design of hollow section connections.

*(a) Type of stress*

Only stresses perpendicular to the weld toe were considered.

*(b) Extrapolation approach*

A quadratic extrapolation was recommended to exclude local stress concentrations. This extrapolation approach accurately described a nonlinear stress increase near the weld toe as more data was obtained. It is certain that for most simple tubular joints, the stress increase within the extrapolation region was linear. However, a quadratic extrapolation would be needed to determine the HSS at the weld toe in certain location of the overlapped CHS K-joints.

*(c) Position of HSS at weld toe*

The exact position of SCF at weld toe had to be established to determine the HSS caused by axial forces, in-plane and out-of-plane bending moments. For tubular joints, these positions were located at the heel crown and saddle of the chord and the braces.

It should be noted that the HSS is the extrapolated stress at the weld toe. For simple welded joints, the SCF is defined as the HSS divided by the nominal stress of the loaded brace that causes the HSS. Therefore, the HSS at the weld toe is a function of all the nominal stresses in the members of the connection multiplied by their corresponding SCF.

In the latest International Institute of Welding fatigue design guide [10], the use of the HSS range had similar concept as the HSS method proposed by van Wingerde et al. [9] with procedure described below. The HSS range at a specific location of a joint under a load case was the product of the nominal stress range and the corresponding SCF. The HSS ranges at the same location of a joint under combined load cases could be superimposed. If the position of the maximum HSS in a member under a relevant loading could not be determined, the maximum SCF must be applied for all the points around the periphery of the member at a joint. The HSS ranges must be calculated for both the chord and the brace.

From the above, it could be seen that the principal stress and the stress perpendicular to the weld toe were the two commonly used stresses to determine the HSS at the weld toe. For simple welded joints, owing to the stiffening effect of the weld and the member wall thickness, the principal stress tended to divert to a perpendicular direction as it moved toward the weld toe. That is the ratio of the principal stress to the stress perpendicular to the weld toe decreased with the distance to the weld [11, 12]. It was important to note that the direction of the maximum principal stress at the crown toe and heel positions was perpendicular to the weld toe. However, in certain location of tubular joints, the geometric stress perpendicular to the weld toe may not be the maximum principal stress [6]. In this case, one of the above methods should be chosen to calculate the HSS.

Van Wingerde et al. [9] also summarized the advantages of using the stress perpendicular to the weld toe to determine the HSS. The stresses perpendicular to the weld toe could easily be measured using simple strain gauges. All the stress components were still required to be separately considered even when the principal stresses were determined. The hot spot principal stresses caused by various load cases could not be superimposed. The stress component perpendicular to the weld toe was enlarged by the presence of global weld shape and notch. This view was supported by the direction of crack growth.

### 2.1.3 Extrapolation Methods

Owing to the effect of localized weld shape and notch stresses, HSS cannot be directly obtained by using strain gauges installed at the vicinity of the weld toe. Thus, the extrapolation of stresses within the specific region is adopted to determine the HSS. Generally, the extrapolation region is defined by specified minimum and maximum distance measured from the weld toe of the joint. The region is defined in such a way that the effect of the geometry of the weld and the condition at the weld toe are not included in the HSS [13].

Two extrapolation methods were employed in the ECSC and CIDECT research programmes [14, 15, 16, 17, 18, 19, 20 and 21] simultaneously, to enable a comparison between the two methods to be made. Both methods start by fitting a curve through all available data points (by hand or numerically), shown as a heavy line in Figure 2.2.

1. Linear extrapolation. Two points on the curve determined from all data points are used for the extrapolation: the first is 0.4$t$ from the weld toe, with a minimum of 4 mm. The second point is taken to be 0.6$t$ further from the weld toe.

2. Quadratic extrapolation. The first point is 0.4$t$ from the weld toe, with a minimum of 4 mm. The second point on the curve used for the quadratic extrapolation is taken 1.0$t$ further from the weld toe. The quadratic extrapolation is carried out through the first and second points on the curve based on all data points, shown as squares in Figure 2.2.

It was also recommended by DEn [6] that "the maximum extent of local notch region is defined as $0.2(rt)^{1/2}$ (and not less than 4 mm), where $r$ and $t$ are the brace outside radius and thickness respectively". The dependence of $(rt)^{1/2}$ was derived from the study of bending stresses in tubes [23]. This parameter was modified according to the analysis of large-scale tests on tubular joints in ECSC and UKOSRP projects. Based on DEn

guidance [6], the requirements for the extrapolation region of the chord and the brace can be seen in Figure 2.3.

An alternative approach to determine the HSS was to specify a minimum strain gauge distance of 0.4$t$ from the weld toe as highlighted by Gurney [22]. Gurney's recommended distance was actually derived from the finite element analysis of simple fillet weld joints in plates. The region of the notch stress was a function of plate thickness. Swensson et al. [23] and Wardenier [24] commented that for joints with pronounced 3-dimensional effects, Gurney's recommendation described the notch region better than DEn [6]. ECSC Working Group III eventually adopts the requirement of 0.4$t$ minimum distance as the extrapolation region with details summarized in Table 2.1 [13]. These requirements for the extrapolation region to determine the HSS near the weld toe of the joint are also included in IIW [10] and Zhao et al. [5].

van Wingerde et al [25] recommended that linear extrapolation is suitable only for non-overlapped CHS connections, where the stresses near the weld toe would increase almost linearly noted by the DEn design recommendations [26], since in this case the difference between linear and quadratic extrapolation would be negligible. As for RHS connections, the geometric strain can be strongly non-linear, and the quadratic extrapolation method should therefore give more realistic values for the SNCF at the weld toe. It is also noted that another advantage of the quadratic extrapolation is a better agreement between characteristic S-N lines based on experiments and those based on parametric formulae. This allows the same classification according to EC3 [27], without any correction factors on the parametric formulae being necessary. Having learned from all above researchers, although the quadratic extrapolation is slightly more difficult to carry out, this extrapolation method has been used in the current study.

### 2.1.4 *Stress Concentration Factor* (SCF)

In the design guides the HSS is usually defined and obtained by a parameter called *Stress Concentration Factor* (SCF). The relationship between the HSS and the SCF can be illustrated in Figure 2.1. The HSS is the peak stress, and it can be expressed as follow:

$$\sigma_{HSS} = \sigma_{nominal} \times SCF \tag{2.6}$$

From Equation (2.6), the *HSS* is obtained if the *SCF* and nominal stress are determined. The nominal stress can be obtained from Equations (2.1) to (2.3) for basic loads.

Research into fatigue behaviour of overlapped K-joints can be found in Almar [28], Efthymiou & Durkin [29], Gibstein [30], Lalani and Forsyth [31] and Moe [32]. Systematic research into the fatigue behaviour of overlapped K-joints was carried out at VERITAS in years 1982 -1984. Stress analysis was carried out with objective of deriving parametric formulas for SCF. Fatigue tests were conducted in order to verify the validity of hot spot definitions and the applicability of S-N curves for overlapping joints. It is noted that overlapped K-joints can be designed to provide some improvement of fatigue strength properties comparing to K-joints with gap, provided that d/D should be less than 0.85. However, the parametric SCF formulas for overlapped CHS K-joints are presently not available in literature [28].

Efthymiou and Durkin [29] carried out the stress analysis of 100 FE models of K-joints using PMBSHELL FE program. The emphasis was on overlapped joints but a large number of gapped joints were also examined. The SCF parametric equations of the partially overlapped K-joints were developed under both balanced and unbalanced basic load cases. It is noted that the unbalanced axial load overlapping always reduces chord SCFs significantly, whereas braces SCFs are also reduces when $\gamma_{brace} \leq \gamma_{chord}$. The benefit of overlapping is more pronounced in joints with brace inclinations 90°/45°

than for inclinations 45°/45°. It is also noted that overlapped K-joints is, however, not beneficial while subjecting to in-plane bending load case. Furthermore, it is noted that SCFs are low in balanced out-of-plane bending load case, while in unbalanced are high. These equations for overlapped K-joints are shown in Table 2.3 in the present study. However, they were not adopted in the EC3 [27].

Gibstein [30] studied the stress concentrations of 19 FE models of K-joints with $\beta$ =1 under five different load cases. A set of parametric equations was derived to estimate the SCF of gapped K-joints as well as overlapping K-joints with and without stiffeners. The SCF formulas for $\beta$ =1 of the overlapped K-joints are shown in Table 2.4. However, the investigation did not cover fully the range of geometric parameters of the joints. According to that study, the locations of maximum SCF were depended on the brace-chord thickness ratio *(t/T)* and load type: for the $t/T$ =1 the maximum SCF is usually located in the chord, whereas $t/T < 1$ the maximum SCF can be found in chord or brace, depending on the load type and design considered.

Lalani and Forsyth [31] also investigated a series of elastic and fatigue tests on overlapping K(N)-joints. A total of ten elastic and fatigue tests were undertaken, including four axial load tests, three in-plane moment load tests and three out- of- plane bending tests. The HSS approach was used to determine the SCF of the joints. According to this study, for the joints under balanced axial load case, the maximum SCF occurred at the crown heel of the 45° diagonal brace. Similarly, for the brace perpendicular to the chord, the maximum SCF occurred at the crown position. However, the peak stress of the joint did not always occur at the crown or the saddle position of members. It is also noted that all cracks occurred on the brace side of the weld, in line with maximum stress locations. It is further noted that the use of the HSS range concept is valid for overlapped CHS K-joints studied.

Moe [32] performed the stress analysis based on the fatigue tests of overlapped CHS K-joints and overlapped CHS K(N)-joint subjected to balanced axial loads. It is observed

that brace failure mode in overlapped joints is more critical than previously observed chord failure due to the acceleration of the crack development from relatively short surface crack, which to some extent reduces the time in-service for possible crack detection, meaning that this mode of failure may lead to somewhat shorter fatigue lives compared with previous results.

### 2.1.5 *Hot Spot Stress* (HSS) determination

Although the HSS can be determined by nominal stress and SCF together, it is still not easy to estimate its value and the location of peak stress when overlapped K-joint is subjected to complicated loads. This is because all SCF equations proposed by the researchers have considered only the basic loads and disregard where the maximum SCF point located. For combined loading cases, it is uncertain because there is no general definition on nominal stress and also the position of the HSS could shift from one location to another depends on different proportions of the basic loads in the combined loading cases. Actually, the HSS can be located at any point along the intersection under combined loads. API RP-2A [33] proposed a method to determine the peak hot spot stress as follow:

$$Peak\ HSS = \left|SCF_{AX} f_{AX}\right| + \left[(SCF_{IPB} f_{IPB})^2 + (SCF_{OPB} f_{OPB})^2\right]^{\frac{1}{2}} \tag{2.7}$$

where *peak HSS* is the peak HSS, $SCF_{AX}$, $SCF_{IPB}$, $SCF_{OPB}$ are concentration factors (SCFs) for AX, IPB and OPB respectively. $f_{AX}$, $f_{IPB}$ and $f_{OPB}$ are the corresponding nominal stresses.

Obviously, Equation (2.7) is simply summing up the products of the nominal stress due to each load type and the corresponding maximum SCFs. This will make the results conservative because in general the HSS caused by each basic load could be located at different positions. Therefore, the sum of the HSS from Equation (2.7) will

overestimate the peak stress value. This had been proven by Pang and Lee [34] in their study on tubular T-joints. To avoid this disadvantage, Gulati et al. [35] had suggested superimposing the stress distributions from each of basic load modes to obtain the HSS. Subsequently, a new equation was proposed as follow:

$$\sigma(\varphi) = K_A(\varphi) f_{AX} + K_{Bi}(\varphi) f_{IPB} + K_{Bo}(\varphi) f_{OPB} \tag{2.8}$$

where $K_A(\varphi)$, $K_{Bi}(\varphi)$, $K_{Bo}(\varphi)$ specify the stress concentration factors (SCFs) around the intersection of joint subjected to AX, IPB and OPB respectively. $f_{AX}$, $f_{IPB}$ and $f_{OPB}$ are the corresponding nominal stresses.

The position and value of the HSS can be determined from Equation (2.8) if $K_A(\varphi)$, $K_{Bi}(\varphi)$, $K_{Bo}(\varphi)$ can be explicitly provided. However, the explicit expressions were not provided in the literature. Chang and Dover [1] suggested that $K_A(\varphi)$, $K_{Bi}(\varphi)$, $K_{Bo}(\varphi)$ can be obtained using equations of Hellier et al. [36] for tubular T and Y-joints. Yeoh et al. [37] verified this method by conducting a test on a tubular T-joint and found that stress distributions obtained by superposition method of Equation (2.8) compared well with the results obtained directly from the full-scale test. Soh and Soh [38] also studied the superposition method by conducting a test on tubular K-joint and found the results from this method agreed well with experimental results. Although this method can provide more accurate information of hot spot stress, it is still not easy to be applied in practice because the accuracy of the HSS from Equation (2.8) depends on the accurate expressions of $K_A(\varphi)$, $K_{Bi}(\varphi)$, $K_{Bo}(\varphi)$.

Therefore, in the present study a new tool is suggested to predict the HSS values which base on Equation (2.8). The created database is able to provide all positions and $K_A(\varphi)$, $K_{Bi}(\varphi)$, $K_{Bo}(\varphi)$ along the intersection of partially overlapped K-joints.

## 2.2 S-N Curves for Fatigue Design

The fatigue life prediction of welded components requires appropriate stress analyses. The dominant parameter in the fatigue analysis is the stress range which can be defined as the stress difference between the maximum stress ($\sigma_{max}$) and the minimum stress ($\sigma_{min}$). The mean or the peak levels of loading are found to be less significant as compared to the range of stresses. In the case of constant amplitude loading, the stress range is defined as follow.

$$\Delta\sigma = \sigma_{max} - \sigma_{min} \tag{2.9}$$

The constant amplitude of stress histories is illustrated in Figure 2.4a. For welded structures, the variable amplitude loading (Fig. 2.4b) is more common than the constant amplitude loading.

The S-N curves for assessing the fatigue performance of tubular joints are commonly used in offshore structures [5 and 10]. The S-N curves are a plot of the stress range versus the number of load cycles to failure. The typical S-N curves for structural hollow section connections are shown in Figure 2.5. These S-N curves are obtained from series of the experimental tests on representative geometries and materials. The primary advantage of using these curves is that it allows the use of a single S-N curve and thickness correction for all hollow section connections. The validity of wall thickness for circular hollow section connections is limited to 50 mm. The effect of wall thickness of hollow sections can partly be explained by fracture mechanics and partly by technological and statistical factors. It can be seen from Figure 2.5 that thicker walled elements have shorter fatigue life than thinner walled elements. As a result, thicker walled elements would fail at lower number of load cycles than the thinner walled elements in the same hot spot stress range. Therefore, a proper design of welded tubular joints against fatigue failures must be based on the magnitude of SCF,

which is defined as the ratio of the highest stress to the member nominal stress obtained from the global stress analysis.

Actually, a basic S-N curve is used for hollow section joints with a wall thickness of 16 mm [9, 39-43]. For joints with wall thickness other than 16 mm, the thickness correction factors are introduced. The influence of the thickness effect on fatigue behaviour of hollow section joints has been widely investigated by Gurney [23], van Delft [44], Marshall [45, 46], van Delft et al. [47], Berge and Webster [48], Haagensen [49], Thorpe and Sharp [40] and van Wingerde [11]. The thickness effect is also recognized in the design recommendations [50], [26, 27] and [10]. A common set of S-N curves and thickness correction formulae have been established by van Wingerde et al. [51, 52]. The equations for S-N curves are presented in Table 2.2. However, an attention should be paid as Figure 2.5 and Table 2.2 only apply to CHS joints with thickness between 4 mm and 50 mm and RHS joints with thickness between 4 mm and 16 mm.

Some research works concerning overlapped K-joints have been done by Lalani and Forsyth [31], and Moe [32]. Lalani and Forsyth [31] investigated a series of elastic and fatigue tests on overlapping K(N)-joints. According to them, test results indicated that S-N curves approaches would yield a conservative estimate of fatigue life. Another researcher Moe [32] performed the stress analysis based on the fatigue tests of two overlapped K-joints subjected to balanced axial loads. It is also noted that the S-N curves were found to be on the conservative side of the test results.

## 2.3 Interpolation Method for SCF and HSS Estimation

In the mathematical subfield of numerical analysis, interpolation is a method of constructing new data points within the range of a discrete set of known data points.

In engineering and science one often has a number of data points, as obtained by sampling or experimentation, and tries to construct a function which fits those data points. This is called curve fitting or regression analysis. Interpolation is a specific case of curve fitting, in which the function must go exactly through the data points.

An interpolation method was firstly applied to analyze *stress intensity factors* (SIFs) of gapped CHS K-joints by Shao [53]. According to the results of the study, the accuracy of the SIFs obtained from interpolation method is higher than that of SIFs obtained from the proposed parametric equations. Having compared the interpolation method with the proposed equations for tubular T and Y-joints [54 and 55], the interpolation method appears to be more accurate, feasible and practical.

Presently, there is almost no parametric equation available for fatigue design of partially overlapped CHS K-joints. An extensive research is therefore needed in this area before the joint configuration could be considered to be used in practice. In this current research, the determination of the SCF and HSS of the partially overlapped CHS K-joint is the primary focused. As far as the new method is concerned, both experimental and numerical investigations are needed to be carried out as they would have been performed in next chapters.

Table 2.1 Extrapolation region recommended by IIW [10] and Zhao et al. [5]

| Chord member | | Brace member |
|---|---|---|
| Crown | Saddle | Crown and saddle |
| $3l_{r,min} = 0.4T \quad l_{r,min} \geq 0.4\ mm$ | | $l_{r,min} = 0.4t \quad l_{r,min} \geq 0.4\ mm$ |
| $l_{r,max} = 0.4(rtRT)^{1/4}$ | $l_{r,max} = 0.09R$ | $l_{r,max} = 0.65(rt)^{1/2}$ |
| $l_{r,min}$ $(l_{r,max})$: minimum (maximum) distance measured from the weld toe location in a direction perpendicular to the weld toe (for chord member location) or/and a direction parallel to axis of the brace member (for brace member location) | | |

Table 2.2 Equations for the $S_{rhs}$-$N_f$ curves for CHS joints (4 mm ≤ t ≤ 50 mm ) and RHS joints (4 mm ≤ t ≤ 50 mm ) [5, 10]

| | |
|---|---|
| for $10^3 < N_f < 5x10^6$ | $\log(S_{rhs}) = \frac{1}{3}(12.476 - \log(N_f) + 0.06\log(N_f)\log(\frac{16}{t})$<br>or<br>$\log(N_f) = \frac{12.476\text{-}3\log(S_{rhs})}{1\text{-}0.18\log(\frac{16}{t})}$ |
| for $5.10^6 < N_f < 10^8$<br>(variable amplitude) | $\log(S_{rhs}) = \frac{1}{5}(16.327 - \log(N_f) + 0.402\log(\frac{16}{t})$<br>or<br>$\log(N_f) = 16.327 - 5\log(S_{rhs}) + 2.01\log(\frac{16}{t})$ |

Table 2.3 Parametric equations for overlapped K-joints [29]

| Load type | SCF equation |
|---|---|
| Load on one brace only 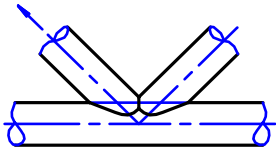 | Chord SCF: $\gamma\tau^{1.1}\left[1.11-3(\beta-0.52)^2\right]\sin^{1.6}\theta$ Brace SCF: $1.3+\gamma\tau^{0.52}\alpha^{0.1}\left[0.187-1.25\beta^{1.1}(\beta-0.96)\right]\sin^{(2.7-0.01\alpha)}\theta$ |
| Balanced IPB 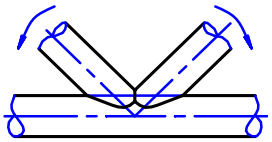 | Chord SCF: $1.45\beta\tau^{0.85}\gamma^{(1-0.68\beta)}\sin^{0.7}\theta\left[0.87\tau^{-0.3}\right]$ Brace SCF: $1+0.48\beta^{0.24}\tau^{-0.2}\gamma^{0.7}\sin^{0.55}\theta_{\max}\left(\frac{\sin\theta_{\min}}{\sin\theta_{\max}}\right)^{1.8}$ |
| IPB on one brace only 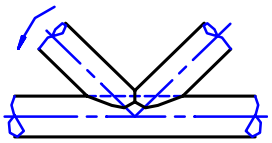 | Chord SCF: $1.45\beta\tau^{0.85}\gamma^{(1-0.68\beta)}\sin^{0.7}\theta$ Brace SCF: $1+0.65\beta\tau^{0.4}\gamma^{(1.09-0.77\beta)}\sin^{(0.06\gamma-1.16)}\theta$ |
| Unbalanced IPB 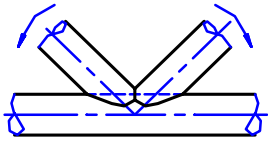 | Chord SCF: $1.45\beta\tau^{0.85}\gamma^{(1-0.68\beta)}\sin^{0.7}\theta$ $(O_V \le 30\%)$ $1.776\beta\tau^{0.85}\gamma^{(1-0.68\beta)}\sin^{0.7}\theta$ $(O_V > 30\%)$ Brace SCF: $1+0.65\beta\tau^{0.4}\gamma^{(1.09-0.77\beta)}\sin^{(0.06\gamma-1.16)}\theta\ *(0.9+0.4\beta)$ |

VALIDITY RANGE

The above equations are generally valid for geometrical parameters within the following limits:

$0.2 \le \beta \le 1.00$

$8.0 \le \gamma \le 32$

$0.2 \le \tau \le 1.00$

$20^\circ \le \theta \le 90^\circ$

$4 \le \alpha$

$60\% \le Ov \le 100\%$

Table 2.4 SCF Formulas for $\beta$=1 of overlapped K-joints [30]

| Load type | SCF equation |
|---|---|
| Axial Load 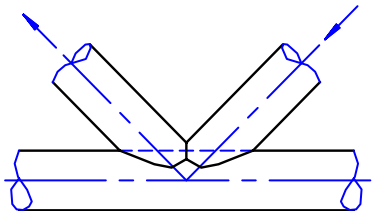 | Chord SCF: $1.49(t/T)^{0.73}\,\gamma^{0.37}$ Brace SCF: $1.61(t/T)^{-0.23}\,\gamma^{0.32}$ |
| In Plane Bending 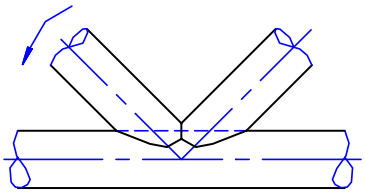 | Continuous brace Chord SCF: $1.76(t/T)^{0.89}\,\gamma^{0.22}$ Brace SCF: $0.78(t/T)^{0.41}\,\gamma^{0.37}$ Non continuous brace Chord SCF: $1.93(t/T)^{0.89}\,\gamma^{0.21}$ Brace SCF: $1.24(t/T)^{-0.17}\,\gamma^{0.28}$ |
| Out of Plane Bending 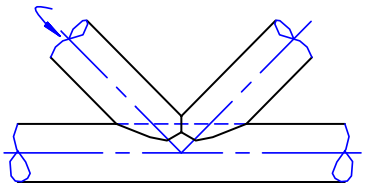 | Continuous brace Chord SCF: $1.54(t/T)^{1.31}\,\gamma^{0.37}$ Brace SCF: $1.11(t/T)^{0.22}\,\gamma^{0.53}$ Non continuous brace Chord SCF: $0.90(t/T)^{1.21}\,\gamma^{0.58}$ Brace SCF: $1.16(t/T)^{0.29}\,\gamma^{0.51}$ |

VALIDITY RANGE

The above equations are generally valid for geometrical parameters within the following limits:

$\beta = 1.00$

$\gamma = 15 - 35$

$\tau \geq 0.5$

$\theta_1 = \theta_2 = 55^\circ$

Ov = $q / p \times 100 = 21\%$

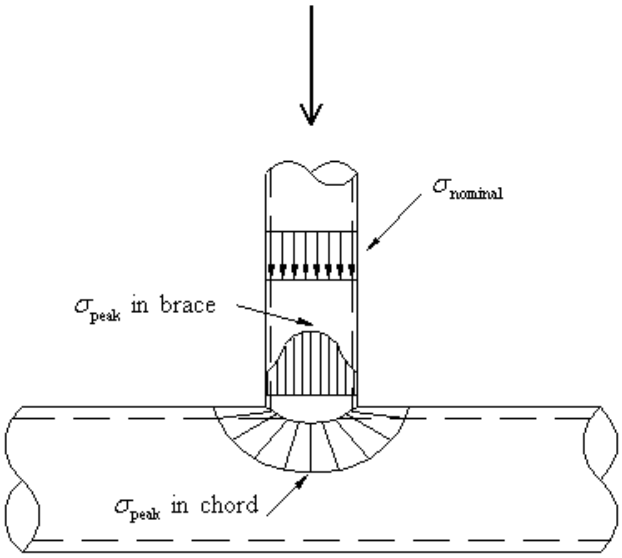


Figure 2.1 Stress distributions at joint intersection of chord and brace [6]

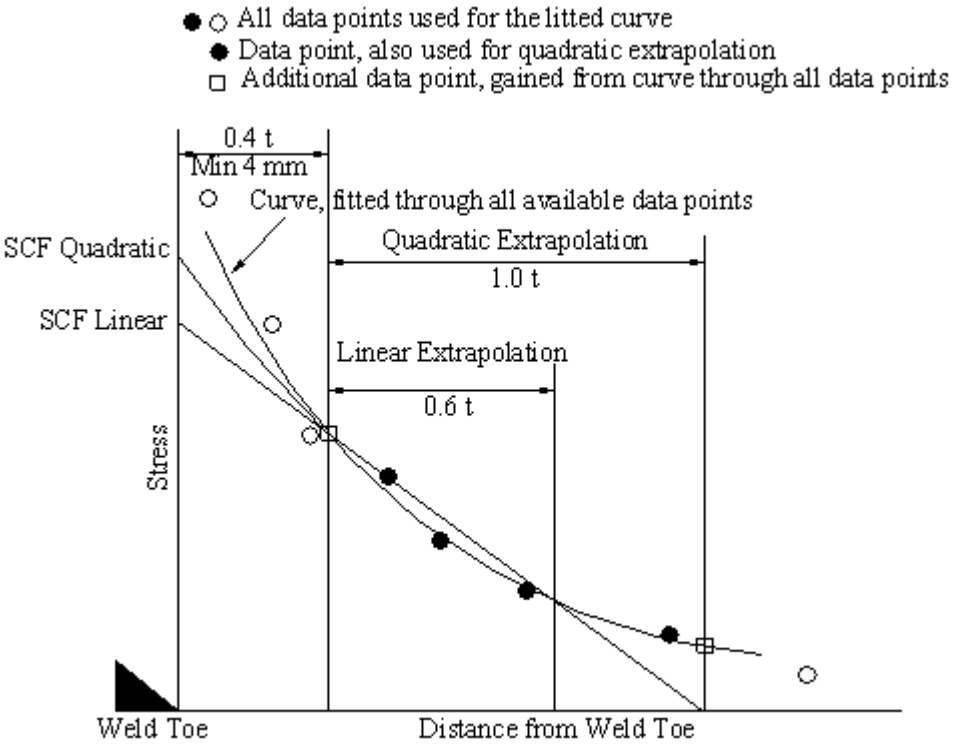


Figure 2.2 Linear and quadratic extrapolation procedure [6]

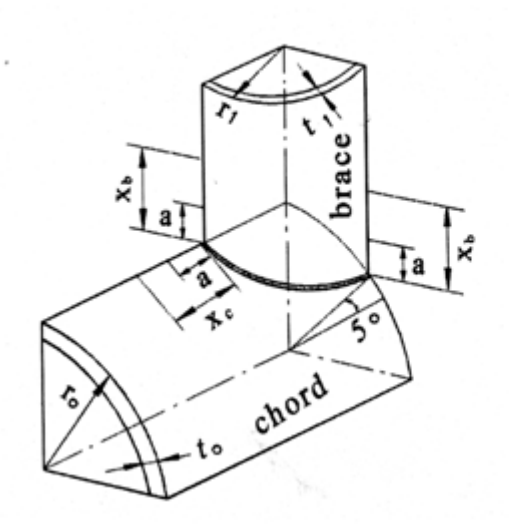


Minimum distance

$a=0.2(r_1t_1)^{1/2}$, $a \geqslant 4$ mm

Maximum distance

Chord member

Saddle 5°

Crown $x_c=0.4(r_1t_1r_0t_0)^{1/4}$

Brace member

Saddle and crown $x_b=0.65(r_1t_1)^{1/2}$

Figure 2.3 Extrapolation region defined by DEn [6]

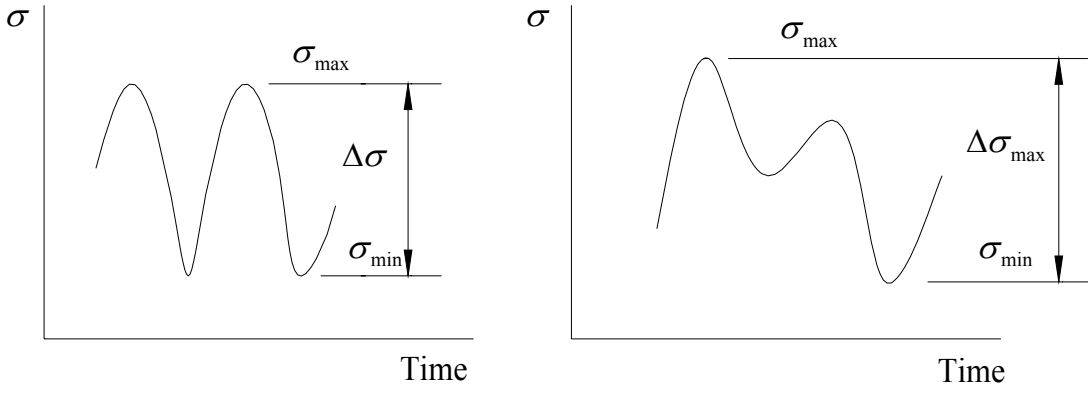


(a) Constant amplitude (b) Variable amplitude

Figure 2.4 Stress (σ) –Time history [5, 10]

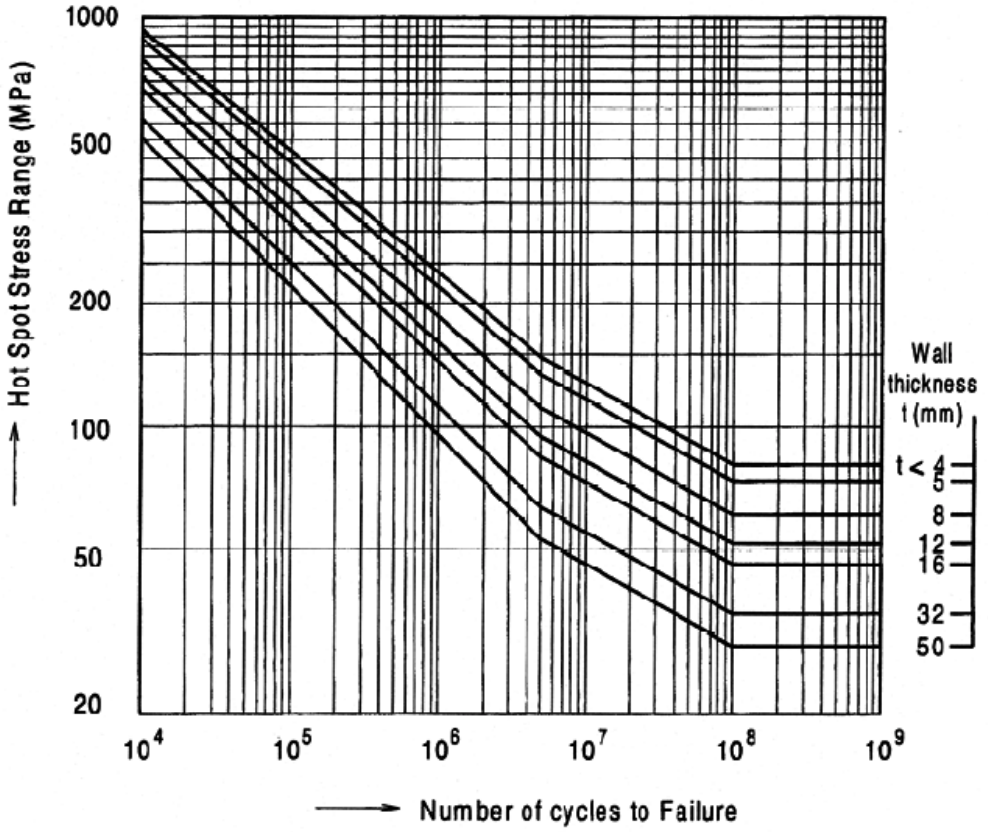


Figure 2.5 Typical S-N curves for fatigue design of structural hollow section connections [5, 10]

# *CHAPTER 3*
# *EXPERIMENTAL INVESTIGATION*

## 3.1 INTRODUCTION

Simple non-overlapped CHS K-joint is one of the most widely used connection types in offshore structures. However, due to the existence of a gap between the braces, under some geometrical configurations, eccentricity and unbalanced moment could be generated on the chord and this may lead to undesirable brittle responses of the joints [3]. Hence, in many design codes [5, 27] an upper limited is imposed on the eccentricity for non-overlapped CHS K-joints. In practice, any eccentricity for a non-overlapped CHS K-joint could be eliminated by partially overlapping the braces. When compared with a non-overlapped K-joint, the partially overlapped CHS K-joint normally has a higher fabrication cost due to the more complex intersection profile. However, due to their optimized load transfer pattern and zero eccentricity property, partially overlapped CHS K-joints often offer a higher residual capacity and ultimate strength [56, 57]. In a study carried out by Healy [58], it was found that in case the through brace was in tension, the capacity of partially overlapped joint was much better than when it was otherwise loaded. Dexter and Lee [59, 60] examined numerically the effects of several geometrical parameters and the overlapping percentage on the behaviour of overlapped joints. It was found that, in general, overlapping the braces has a beneficial effect on joint strength for the joints with relatively thick brace walls. Furthermore, it was also reported from Dexter et al. [61] that partially overlapped CHS K-joints are expected to have increased strength up to a certain amount of overlap and then decrease when the joint is completely overlapped. Besides strength enhancement, partially overlapped joint could also lead to more cost effective joint design. In a study carried out by Tizani et al. [4], it is found that after considering both material and fabrication costs, the use of a partially overlapped joint could lead to the cheapest solution with the addition fabrication cost actually offset by avoiding the use of canned gapped joint as an alternative.

In the study of fatigue performance of partially overlapped CHS K-joints, works done by Bouwkamp [56, 57] found that the SCF could be reduced by more than 30% when compared with the non-overlapped CHS K-joints having the same parameters and properties. Fessler et al. [62] also observed that the HSS of a partially overlapped CHS K-joint is 40%-45% less than that of the gapped joint. Furthermore, having compared the results of overlapped and gapped CHS K-joints, Gibstein [30], however, concluded that fatigue strength improvements could be obtained by using a partially overlapped joint with same chord and brace diameter. So far, the most detailed work related to the SCF and the HSS distributions of this joint type was published by Efthymiou and Durkin [29]. Over 100 partially overlapped CHS K-joints were analyzed using FE models for nine different load cases. Parametric equations were then developed for each load case and the results were experimentally verified by Dharmavasan and Seneviratne [63] using acrylic models. It was found that overlapping helps reduce the chord SCFs significantly.

Despite the above mentioned advantages of the partially overlapped K-joint, equations for the fatigue design of this type of joints are not commonly available in design code. Efthymiou and Durkin [29] had published some formulae but they were not adopted in the EC3 [27]. Furthermore, not many full scale testing results related to the SCF and the HSS values for partially overlapped CHS K-joints were reported [64-69].

In this study three specimens were designed for testing in such a way that partially overlapping is inevitable in order to eliminate the eccentricity of the resulted joints. Experimental studies were carried out by applying static loadings at the end of the through braces of the joints. The stress distributions of the partially overlapped CHS K-joints tested under the three basic loading cases AX, IPB and OPB and their combinations were carefully recorded during the test. For each specimen, experimental study was carried out to investigate SCF and the HSS distributions along the brace-chord intersections. In addition, fatigue test of all three specimens were also carried

out, and their fatigue life was also compared with S-N curves as to evaluate the applicability of present S-N curves [5] in design of partially overlapped CHS K-joints.

## 3.2 STATIC TESTS OF PARTIALLY OVERLAPPED CHS K-JOINTS

### 3.2.1 Set up of the Test Rig and the Loading System

The tests of the partially overlapped CHS K-joints were carried out using the "Orange" rig (Figure 3.1) located in the Construction Technology Laboratory, School of Civil and Environmental Engineering, Nanyang Technological University. This test rig is designed for static and fatigue tests of hollow section joints under AX, IPB and OPB loads or combinations of them. The test rig has three actuators namely, Actuators 1, 2 and 3 (Figure 3.2) installed at one end of the rig which are able to apply cyclic loadings with adjustable frequency to the specimen along three mutually perpendicular axes. In this study, Actuators 1 and 2 which have a maximum capacity of 250 kN were employed to apply AX and IPB loadings, respectively. Actuator 3 with a maximum capacity of 150 kN was employed for the generation OPB loading. All three actuators can apply both tension and compression loadings and they can be operated individually or concurrently to create combined loading conditions.

### 3.2.2 The Specimens Tested

In this study, three full-scale partially overlapped CHS K-joints (Specimen SI, Specimen SII and Specimen SIII) were tested. The typical test set up of the three specimens and their geometrical properties are shown in Figures 3.1 and 3.3. Each joint specimen comprises the chord, a through brace and an overlapping brace. The angles between the braces and the chord are equal to 45° for Specimen SI and Specimen SII, and 60° for Specimen SIII. These three joints were fabricated using structural steel

pipes complied with the BS EN10210-S355 J2H standard. The joints were welded according to the AWS specifications [8]. Ultrasonic checking was conducted along all the welding paths to ensure that the welding at the intersections of the chord and braces was complete penetration groove weld with standard flat profile. In the set up of each specimen, both ends of the chord and the overlapping brace were welded onto the flat plates and bolted directly onto strong reaction panels of the rig. The end of the through brace was welded onto a flat plate and bolted directly onto the actuators (Figure 3.2). The physical dimensions and other important non-dimensional parameters of the specimens are listed in Table 3.1. The material properties of the sections obtained from standard coupon tests are summarized in Table 3.2. Note that the section sizes and configurations of these three specimens were carefully selected in such a way that if they are fabricated as non-overlapped joints with minimum gap spacing, the eccentricity of the resulted joints shall exceed the maximum limit imposed by the EC3 [27].

### 3.2.3 Strain and Stress Measurements

Since the main objective of this study is to investigate the HSS and the SCF distributions along the intersections of the tubular sections, extensive strain measurements were conducted by installation of strain gauge arrays at the joint. At the joint intersections, three curves, namely, Curves A, B and C were identified (Figure 3.4). Curve A is the intersection between the through and the overlapping brace. Curves B and C are the intersections between the chord and the overlapping and the through braces, respectively. From Figure 3.4, it can be seen that for each side of the joint, these three curves meet at a junction point. Along these three curves, strain gauges were installed at locations near the weld toe of the chord and the braces to record the strain distributions. As from many past studies [65, 66], the quadratic extrapolation method [5] is needed to obtain accurate strain measurements, three rows of strain gauges were installed at each measurement location along the line perpendicular to the weld toe at distances equal to 0.4$t$, 1.0$t$ and 1.4$t$ ($t$ is the thickness

of member) from the weld toe (Figures 3.4 and 3.5). Three types of strain gauge arrangements were deployed in this study (Figure 3.5). At locations far way from the junction point and the saddle and crown toe of the intersections, a single perpendicular strain gauge arrangement is used. At the saddle and crown toe of the intersections, an arrangement of a pair of strain gauges arranged in the perpendicular and the parallel directions to the weld toe was adopted. Finally, in order to capture the complex strain pattern, rosettes were deployed at regions close to the junction point. Besides along the intersection curves, eight strain gauges were also installed at the two cross-sections along the through brace to detect any secondary bending moment caused by load eccentricity and joint flexibility (Figure 3.6). During the test, all strain gauges were connected to four TML ASW-50 switchboxes and a TML TDS-801 data logger. The data logger was then connected to a personal computer where special software for monitoring, collecting and processing of the testing data was installed.

### 3.2.4 Static Test Procedure

In the static test, a series of basic loading cases and combinations of them were applied. The basic load cases were employed to obtain the SCF and the HSS distributions from the specimens and to validate the results against the published equations [29]. Prior to the actual test, the specimen was subjected to at least six loading and unloading sequences. This precaution shall test for the satisfactory performance of strain gauges and eliminated any drift of strain measurements due to the fabrication of the joints. In the actual test, each specimen was first subjected to an incremental static load on one axis, and the strains were checked against linearity and zero drift to indicate shakedown of residual stress. The eight strain gauges installed at the cross sections of the through brace were monitored by data logger to manage the applied loads in such a way that secondary loads would not be involved. The actuators were then ramped to the predetermined loads. During the static test, in order to ensure that the joint remained fully elastic, the maximum static load applied was carefully computed so that the peak HSS generated in all loading cases shall not exceed 85% of the corresponding material

yield stress of the sections (Table 3.3). It should be mentioned that while only positive value of AX and OPB loadings were applied in the test, both positive and negative IPB loadings (Figure 3.3) were applied. During the tests, the actuators were ramped to the maximum load in at least six loading increments. At each step, the actuators were held in place and the strain readings were recorded. The loads were then increased to the next level and measurements were repeated. After having reached the maximum load, the above steps were repeated by releasing the applied load in several increments to zero.

### 3.2.5 Static Test Results

*SCF computations*

At locations where only the single strain gauge arrangement was used, the strain values measured were directly converted to the stress values by multiple them with the Young's modules and the stress-strain conversion factors [65 and 66]. Quadratic extrapolation was then applied to obtain the stress at the weld toe for SCF computation. At locations where the two strain gauges arrangement was used, the corresponding *strain concentration factor* (*SNCF*) is first computed as

$$SNCF = \frac{HSSN}{SN_{nominal}} \tag{3.1}$$

where $SN_{nominal}$ is the nominal strain computed from the eight strain gauges readings at the center of brace sides. The SCF value is then computed using the following equation:

$$SCF = SNCF \frac{(1 + \nu\xi_{||}/\xi_{\perp})}{(1 - \nu^2)} \tag{3.2}$$

In Eqn. (3.2) strains $\xi_{\perp}$ and $\xi_{//}$are, respectively the perpendicular and the parallel strain components recorded by the strain gauges and $\nu$ = 0.3 is the Poisson's ratio.

Eventually, quadratic extrapolation was again employed to compute the *SCF* at the weld toe. At location where rosettes were deployed, the principal strain and stress could be directly computed and the SCF values at weld toe were then obtained by extrapolations.

*SCF distributions*

For Specimens SI and SII, it is found that critical SCF values were induced along Curve A and Curve C. In particular, a positive and a negative IPB loading induced high values of SCF along Curve A and Curve C, respectively. The SCF distributions along Curves A and C for Specimens SI and SII under different basic loading cases are shown in Figure 3.7(a) and Figure 3.7(b), respectively. In Figure 3.7(a), the SCF distributions along both the through and the overlapping braces are plotted. From Figure 3.7(a), it can be seen that in general, the SCF distributions along the through brace are higher than that along the overlapping brace. For Curve C, as shown in Figure 3.7(b) for the SCF distributions along the chord and the through brace, the SCF distributions along the through brace are higher than that along the chord.

For Specimen SIII, similar plots for the SCF distributions are shown in Figure 3.8(a) and Figure 3.8(b) for Curve A and Curve C, respectively. From Figure 3.8(a), it is again observed that for Curve A under the same basic loadings, the SCF induced along the through brace are in general higher than that along the overlapping brace. However, for Curve C, it is found that the maximum SCF induced along the chord is higher than that along the through brace. Hence, it could be concluded that besides the magnitude, the location of maximum SCF could also be influenced by the geometrical parameters of the joint.

*HSS distributions*

In this study, two different approaches were employed to evaluate the HSS of the joints tested under combined loading conditions. Besides direct strain and stress measurements obtained during the experimental study, the standard superposition

method [5] was also employed to compute the HSS from the SCF values obtained from the basic load cases. When the superposition method is used, for the combined load cases, $\sigma(\boldsymbol{p})$, the stress at a given point $\boldsymbol{p}$ at the weld toe is calculated as

$$\sigma(\boldsymbol{p})=SCF_{AX}(\boldsymbol{p})\times\sigma_{n\text{-}AX} + SCF_{IPB}(\boldsymbol{p})\times\sigma_{n\text{-}IPB} + SCF_{OPB}(\boldsymbol{p})\times\sigma_{n\text{-}OPB} \quad (3.3)$$

where $SCF_{AX}(\boldsymbol{p})$, $SCF_{IPB}(\boldsymbol{p})$ and $SCF_{OPB}(\boldsymbol{p})$ are, respectively, the SCFs at point $\boldsymbol{p}$ for the AX, the IPB and the OPB loads. $\sigma_{n\text{-}AX}$, $\sigma_{n\text{-}IPB}$ and $\sigma_{n\text{-}OPB}$ are the corresponding nominal stresses. Hence, the HSS values obtained from the superposition method could be directly compared with the corresponding results obtained from the experiments measurements.

After some detail comparisons among all the results obtained, it is found that when the joints were subjected to combined AX and IPB loadings, peak HSS was induced along Curve C. Figure 3.9(a) and Figure 3.9(b) show the HSS distributions obtained by the two approaches along Curve C for Specimens SI, SII and SIII, respectively. For Specimens SI and SII, it can be seen from Figure 3.9(a) that for all the two approaches used, HSS distributions along the through brace are higher than the corresponding distribution along the chord. Note that this observation is different from most results obtained in other T/Y and gapped K-joints studies in which the peak HSS location was almost all reported to be located along the chord side of the joint. For Specimen SIII, from Figure 3.9(b), it can be concluded that under the AX and IPB loading combination, the peak HSS is located along the chord side of the joint. It is important to note that the results obtained from the experiments and superposition method show reasonable agreement. Hence, it can be concluded that when one would like to carry out fatigue assessment of an uncracked partially overlapped CHS K-joint, cares shall be paid on the locations of the peak HSS which could either be located along the chord side or the brace side of the joint.

It is important to emphasize on the peak HSS location. The peak HSS for Specimen SI and Specimen SII is located along the brace side, while for Specimen SIII – along the chord side. This could be contributed to the fact that these three specimens are different in generated parameters, such as $\beta$, $\tau$, $\gamma$, $\theta$ and Ov. The experimental results also confirm previous researchers' results. According to Gibstein [30], the locations of maximum SCF are depended on the brace-chord thickness ratio *(t/T)* and load type: for the *t/T* =1 the maximum SCF is usually located in the chord, whereas *t/T* < 1 the maximum SCF can be found in chord or brace, depending on the load type and design considered.

### 3.2.6 Comparison with Efthymiou's Formulae

It seems sensible to compare the experimental tests results with that of Efthymiou's formula as this formula only gives SCFs at either the saddle or crown location, and also this formula was derived using models based on shell elements. However, as mentioned in the amended thesis that up to now, equations for the fatigue design of partially overlapped CHS K-joints are not commonly available in any design code. The Efthymiou's formulae are the only found in literature.

Furthermore, it is important to note that several previous researchers who did researches in this field were satisfied with Efthymiou's formula. Moe [32] performed the stress analysis based on the fatigue tests of overlapped CHS K-joints and overlapped CHS K(N)-joint subjected to balanced axial loads. According to Moe [32], the Efthymiou's formulae gave a very satisfactory with the maximum values measured in his study. Lalani and Forsyth [31] also investigated a series of elastic and fatigue tests on overlapping K(N)-joints. It is noted that the SCF values obtained from using Efthymiou's formulae are reportedly conservative to their test results.

The maximum SCF values obtained from the tests under the AX and IPB load cases and the corresponding values obtained by using Efthymiou's formulae [29] along the

Curve C are plotted in Figure 3.10 and Figure 3.11 for Specimens SI, SII and SIII, respectively. In addition, the maximum SCF values for all loading cases obtained from the test, from the Efthymiou's formulae are summarized in Table 3.4. Note that in Figures 3.10 and 3.11, the SCF values from Efthymiou's formulae were plotted as horizontal lines since the these formulae only give a single SCF value but not the distribution along the weld toe. Furthermore, since Efthymiou's formulae do not give any value for the load case of OPB, no comparison was made between the formulae and the experimental results. From Figures 3.10 and 3.11 and Table 3.4, it can be concluded that the Efthymiou's formulae is conservative for all specimens for the IPB loading case.

However, they are not always conservative for the AX loading case (e.g. Specimens SI and SII, AX loading for both chord and brace side). Hence, the use of these formulae in practical applications may not be always able to yield conservative estimation of the fatigue life of a partially overlapped CHS K-joint. It could also be due to the fact that the range of validity of the current specimens' parameters is not within the range validity for the Efthymiou's formulae in terms of percentage of overlap.

### 3.2.7 Comparison with Finite Element Models

Based on the dimensions of the actual specimens, the finite element (FE) models were generated and analyzed by using a finite element mesh generator which had been developed previously [65]. Figure 3.12 shows the 3D solid finite element meshes adopted in the numerical modelings. The FE models have been created in such a manner that smallest elements are used in regions of high stress gradients, with gradually increasing element sizes further away from the high stress gradient regions. For all FE models tested, the boundaries, loading conditions and material properties are identical as the respectively tested specimens. The analysis has been conducted by using the FE program ABAQUS [70].

*Comparison of SCF under AX load case*

The SCF distributions obtained from the tests and the FE analyses under AX load cases for Specimens SI, SII and SIII are shown in Figures 3.13(a), 3.15(a) and 3.17(a), respectively and their maximum SCF values under AX load case are also presented in Table 3.4. From Figures 3.13(a), 3.15(a), 3.17(a) and Table 3.4, it can be concluded that the FE analyses results are conservative for all specimens. Note that the maximum and minimum differences of SCF values between FE analyses and tests results are 23.3% and 4.6%, respectively.

It is observed from Figures. 3.13(a) and 3.15(a) that the trends of the experimental and finite element SCF curves for the +ve AX loadings are not agree well. The trends of the SCFs curves obtained from experimental tests are located near the crown heel, but the finite elements SCFs curves have no clear cut about their positions. Nonetheless, the trends of SCFs curves from finite element are likely towards to the crown heel, where the SCFs curves are located.

*Comparison of SCF under +ve IPB load case*

Figures 3.13(b), 3.15(b) and 3.17(b) show the SCF distributions obtained from the tests and the FE analyses under +ve IPB load cases for Specimens SI, SII and SIII, respectively. The maximum SCF values of the tests and the FE analyses under +ve IPB load case for all specimens are also presented in Table 3.4. From Figures 3.13(b), 3.15(b), 3.17(b) and Table 3.4, it can be concluded that the FE analyses results are conservative for all specimens. Note that the maximum and minimum differences of SCF values between FE analyses and tests results are 16.3% and 2.05%, respectively.

*Comparison of SCF under –ve IPB load case*

Figures 3.14(a), 3.16(a) and 3.18(a) show the SCF distributions obtained from the tests and the FE analyses under –ve IPB load cases for Specimens SI, SII and SIII, respectively. The maximum SCF values of the tests and the FE analyses under –ve IPB load case for all specimens are also presented in Table 3.4. From Figures 3.14(a),

3.16(a), 3.18(a) and Table 3.4, it can be concluded that the trends of FE analyses SCF curves agree well with the SCF curves obtained for the tests for all specimens. Note that the differences of SCF values between FE analyses and tests results are 2.14%, -4.00% and -2.67% for Specimens SI, SII and SIII, respectively.

It is observed that the SCFs obtained from the experimental tests and the finite element results under the negative IPB load cases are much better compared to the AX load cases. This could be due to the fact the SCFs under the AX load case, the responses of the joint is much more sensitive to small misalignment and fabrication error while it is not so sensitive for the case of IPB and OPB.

*Comparison of SCF under OPB load case*

The SCF distributions obtained from the tests and the FE analyses under OPB load cases for Specimens SI, SII and SIII are shown in Figures 3.14(b), 3.16(b) and 3.18(b), respectively, and their maximum SCF values under OPB load case are also presented in Table 3.4. From Figures 3.14(b), 3.16(b), 3.18(b) and Table 3.4, it can be concluded that the trends of FE analyses SCF curves agree well with the SCF curves obtained for the tests for all specimens. Note that the differences of FE analyses SCF results to the tests SCF results of SCF values are 32.6%, -8.67.00% and 7.14% for Specimens SI, SII and SIII, respectively.

In conclusion, a comparison between tests results with FE analyses shows that reliable SCF and HSS values could be obtained. However, it appears that numerical and measured SCFs do not agreed well, particularly when the overlapped K-joints were subjected under axial (AX) and out-of plane bending (OPB) load cases. The maximum difference can be as high as 23.3 % for AX and 32.6% for OPB. It could, probably, be due to many factors. The test set up definitely could be not 100% identical with the numerical model. The test section specimen might not the same thickness throughout the length of specimen as in numerical model. Weld profile might not be exactly reproduced in the numerical model.

Nonetheless, the numerical results shown are always conservative when compared with the measured one. In addition, please do note that in the current research the axial (AX) and in plane bending (IPB) load cases have only been studied for new method suggested as these two load cases are most likely happened in practice. Due to time limitation, the OPB loading case has been recommended for future works.

*Comparison of HSS under Combined load case of AX+IPB*

The HSS distributions obtained from the tests and the FE analyses under combined AX and IPB load cases for Specimens SI and SIII are shown in Figures 3.19(a) and 3.19(b), respectively. From Figures 3.19(a) and 3.19(b), it can be concluded that the trends of FE analyses HSS distribution curves agree well with the HSS distribution curves obtained for the tests for all specimens. The differences of HSS values between FE analyses and tests results for Specimens SI and SIII are 3.2% and 5.1%, respectively, which are less than the limit of 10% recommended by Gibstein [30].

From Figures 3.13 to 3.19, it can be seen that the generated finite element models of the partially overlapped CHS K-joints are not only validated against the experimental tests data. While the FE results do not shown excellent agreement along all curves, the results shown that good and conservative estimation of HSS (see Figure 3.19) is possible. However, for the comparison of HSS under combined load case of AX+IPB, which the current research concentrate on, the differences of HSS values between FE analyses and tests results for Specimens SI and SIII are 3.2% and 5.1%, respectively. Hence, the model could certainly be used to develop the PIM and LIM as a new method to predict the SCF and HSS of partially overlapped CHS K-joints (see Chapter 5 for details).

## 3.3 FATIGUE TESTS OF PARTIALLY OVERLAPPED CHS K-JOINTS

In practice, to carry out full-scale fatigue test on any joint is expensive and time consuming. It is also difficult to actually monitor the crack initiation and propagation accurately, since the behaviour of the crack initiation and propagation is influenced by many factors such as loading cases, environmental effects, boundary conditions, geometrical parameters, weld size, etc. However, recently tests by using the alternating current potential drop (ACPD) technique on a series of tubular joints had been completed successfully by [71-75]. According to those studies, the results showed that the captured crack profile by the ACPD technique agreed well with the actual crack shape.

### 3.3.1 Fatigue Test Preparation and Procedure

The alternating current potential drop (ACPD) technique [71, 72, 73, 74 and 75] was used to monitor the growth of surface crack at expected crack growth location. 32 ACPD probes were placed at equal intervals of 10 mm along the weld toe accordingly to the peak HSS locations detected during the static test. The plans of probes locations and typical views of probes sitting are shown in Figures 3.20 and 3.21, respectively. After all probes were spot-welded securely, special twisted cables were used to connect the probes to the U10 Crack Microgauge [76] channels, which were then connected to a personal computer where special software for monitoring, collecting and processing of the testing data was installed. The special software Flair software [77] was able to provide automated instrument control, data storage facilities and dedicated graphical output under the WINDOWS environment. In addition, the Flair software was also capable to record the growing fatigue crack information such as process of the crack initiation and propagation.

In the fatigue test, the combined AX and IPB were applied at the end of through brace. All three specimens were tested in air under sinusoidal constant amplitude loading with load frequency of 0.2 Hz through out the test, as shown in Figure 3.22. The mean values of AX and IPB of the Specimen SI were 100 kN and 22.5 kN respectively, while for the Specimen SII, the mean values of AX and IPB were the same values but with the IPB in negative direction as a part of comparison. Note that Specimens SI and SII have almost the same dimensions and material properties. For the Specimen SIII the mean values of AX and IPB were 50 kN and 6 kN, respectively.

The peak HSS of 382.3 MPa was located at the crown heel of through brace of Specimen SI subjected to combined loading of (AX200+IPB45). For the Specimen SII subjected to combined loading of (AX200-IPB45), the peak HSS of 285.92 MPa was in the crown toe position of through brace. The peak HSS of 121.9 MPa was located at the crown heel of the chord of Specimen SIII subjected to combined loading of (AX100+IPB12). Those mentioned above peak HSSs were set for studying fatigue life of partially overlapped CHS K-joints.

During the fatigue test, crack profiles were recorded using a scan interval equivalent to 180 cycles of the cyclic loading applied. For both specimens, the cyclic loading was applied until the crack had well penetrated the through brace thickness.

### 3.3.2 Fatigue Test Results

Figures 3.23(a), 3.23(b) and 3.23(c) show the crack surfaces of Specimens SI, SII and SIII, respectively. In order to check the actual crack shapes, the tested joints were spilt into two parts along the crack surface. The typical ACPD crack development plots obtained from the results recorded by Flair Software [77] are shown in Figure 3.24. The surface crack of Specimen SI was initiated at the crown heel of the through brace near the ACPD probe P-SI-0 and propagated symmetrically towards to saddle in the

initiation stage. However, as the surface crack propagated, it no longer remained symmetric, but the second surface crack of Specimen SII was initiated at the crown toe of the through brace near the ACPD probe P-SII-0 and propagated towards to saddle symmetrically. It was observed that the peak HSS positions were corresponding to the deepest position of the crack. The surface crack of Specimen SIII was, however, at the crown heel of the chord, but the ACPD probes failed capture the surface crack. It was observed that the peak HSS positions were corresponding to the deepest position of the crack.

Fatigue life based on S-N curve for through braces of Specimen SI, Specimen SII and Specimen SIII is plotted in Figure 3.25a, while the fatigue life based on S-N curve for chords of Specimen SI, Specimen SII and Specimen SIII is plotted in Figure 3.25b. Based on criteria of failure, the test results obtained in terms of cycles to through thickness cracking are plotted together with the similar data from S-N curves [5, 10] in Figure 3.25c.The tested fatigue life for Specimen SI, Specimen SII and Specimen SIII was 57000, 90000 and 4499238 cycles, respectively. It is important to note that since the ACPD probes failed to capture the surface crack due to unforeseen difficulties, the number of cycles was only any estimation obtained from the loading control unit. It is observed from Figure 3.25c that the S-N curve is conservative when predicting the fatigue life of the joint Specimens SI and SIII, but for Specimen SII the S-N curve is marginally conservative, although the peak HSS in Specimen SII was much lower that in Specimen SI.

## 3.4 CONCLUDING REMARKS

In this experimental investigation, a carefully planned experimental study was carried out to investigate the SCF and the HSS distributions along the joint intersection of three full-scale partially overlapped CHS K-joints. The experimental results show that, depending on the geometrical parameters of the joint, the maximum SCF could locate on either the brace side or the chord side of the joint. This is different from the previous

research findings on T-, Y and gapped K-joints in which the maximum SCF normally locates on the chord side only.

In addition, the experimental results also show that Ethymiou's formulae [29] are conservative only when the joints were subjected to IPB loading, but not for the case of AX loading. Hence, it is probably fair enough to say that the Efthymiou's formulae, which are currently the only formulae available in literature, may not be completely suitable for the design of partially overlapped CHS K-joints. Therefore, there is a need to develop a new design recommendation. A comparison of FE and tests results has shown that reliable SCF values could be obtained from a carefully constructed FE model. Hence, further research works on parametric numerical studies could be conducted to obtain a more complete picture for the responses of this type of joints under different loading conditions.

Finally, Fatigue tests were carried out to examine the fatigue life of three partially overlapped CHS K-joints under combined AX and IPB loadings, the results of which have given some thoughts over fatigue life of a partially overlapped CHS K-joint. They are following:

1. The current S-N curve can be regarded as a save approach to predict the fatigue life of partially overlapped CHS K-joints (see Figure 3.25).
2. From Figure 3.25 again, it can also conclude that the highest peak HSS does not always be crucial, when it comes to the fatigue life of the partially overlapped CHS K-joint. All loading cases possible to be occurred with the partially overlapped K-joint. Therefore, both proposed parametric equations and the new method to predict SCF and HSS for the partially overlapped CHS K-joint would be done for all load cases possible to occur with this kind of joint.

Table 3.1 Dimension of specimens

(a) Physical dimensions

| Specimens | Chord diameter (mm), D | Chord thickness (mm), T | Brace diameter (mm), d | Brace thickness (mm), t | Eccentricity (mm), e |
|---|---|---|---|---|---|
| SI | 273 | 25 | 244.5 | 19.1 | 0 |
| SII | 273 | 26 | 244.5 | 20.0 | 0 |
| SIII | 355.6 | 16 | 323.9 | 16 | 0 |

(b) Non-dimension parameters

| Specimens | $\beta = \frac{d}{D}$ | $2\gamma = \frac{D}{T}$ | $\tau = \frac{t}{T}$ | $\alpha = \frac{2L}{D}$ | $\theta$ (°) | $O_v$ (%) |
|---|---|---|---|---|---|---|
| SI | 0.89 | 10.92 | 0.77 | 42.79 | 45 | 21 |
| SII | 0.89 | 10.50 | 0.77 | 42.79 | 45 | 21 |
| SIII | 0.91 | 22.22 | 1.00 | 27.15 | 60 | 45 |

Table 3.2 Material properties of the specimens

| Specimens | Member | Yield strength (MPa) | Modulus of Elasticity (GPa) |
|---|---|---|---|
| SI | Chord | 355 | 205 |
| | Brace | 404 | 204 |
| SII | Chord | 404 | 207 |
| | Brace | 427 | 201 |
| SIII | Chord | 428 | 204 |
| | Brace | 424 | 201 |

Table 3.3 Peak HSS for the maximum basic and combined cases applied in the tests

| Specimen | Load cases | HSS (MPa) | |
|---|---|---|---|
| | | Chord | Brace |
| SI | AX (200 kN) | 35.6 | 40.7 |
| | IPB (+40 kN) | 110.4 | 333.2 |
| | IPB (-40 kN) | 202.1 | 111.1 |
| | OPB (30 kN) | 89.9 | 125.7 |
| | AX (200 kN) + + IPB (+45 kN) | 144.9 | 382.3 |
| | AX (200 kN) + IPB (-45 kN) | 276.9 | 127.6 |
| SII | AX (200 kN) | 41.0 | 41.5 |
| | IPB (+45 kN) | 110.6 | 345.1 |
| | IPB (-45 kN) | 253.6 | 111.2 |
| | OPB (30 kN) | 89.9 | 127.0 |
| | AX (200 kN) + + IPB (+45kN) | 178.9 | 364.7 |
| | AX (200kN) + IPB (-45 kN) | 285.9 | 125.4 |
| SIII | AX (100 kN) | 14.8 | 7.9 |
| | IPB (+12 kN) | 113.5 | 71.5 |
| | IPB (-12kN) | 116.2 | 72.1 |
| | OPB (16 kN) | 109.6 | 80.1 |
| | AX (100 kN) + +IPB (+12 kN) | 121.9 | 95.4 |
| | AX (100 kN) + IPB (-12 kN) | 97.4 | 56.4 |

Table 3.4 Summary of SCF for basic loading cases obtained from tests, Efthymiou's Formulae and FE analyses

| Load cases | Methods | Specimens | | | | | |
|---|---|---|---|---|---|---|---|
| | | SI | | SII | | SIII | |
| | | Chord | Brace | Chord | Brace | Chord | Brace |
| AX | Test | 2.48 | 2.85 | 2.34 | 2.90 | 5.39 | 4.35 |
| | Efthymiou | 1.60 | 2.11 | 1.47 | 2.30 | 5.75 | 3.94 |
| | FE | 2.04 | 3.72 | 1.91 | 3.35 | 5.65 | 5.02 |
| +IPB | Test | 1.19 | 2.57 | 0.68 | 2.13 | 2.87 | 2.22 |
| | Efthymiou | 1.57 | 2.73 | 1.56 | 2.72 | 2.98 | 3.05 |
| | FE | 1.76 | 3.07 | 1.49 | 2.55 | 2.93 | 2.13 |
| -IPB | Test | 1.87 | 1.03 | 1.56 | 0.68 | 1.54 | 1.95 |
| | Efthymiou | - | - | - | - | - | - |
| | FE | 1.83 | 1.29 | 1.50 | 1.09 | 1.50 | 1.47 |
| OPB | Test | 1.28 | 1.81 | 1.15 | 1.63 | 1.82 | 1.53 |
| | Efthymiou | - | - | - | - | - | - |
| | FE | 1.90 | 1.60 | 1.54 | 1.50 | 1.96 | 1.16 |

Table 3.5 Key data from the fatigue tests of Specimens SI, SII and SIII.

| Parameter | | Specimen SI | Specimen SII | Specimen SIII |
|---|---|---|---|---|
| HSS (MPa) | Brace | 382 | 285 | 122 |
| | Chord | 146 | 125 | 95 |
| Predicted fatigue life [5] (Cycles) | Brace | 44467 | 108990 | 2485734 |
| | Chord | 773217 | 126250 | 1938820 |
| Tested fatigue results (Cycles) | | 57000 | 90000 | 4499238 |
| Failed members | | Through brace | Through brace | Chord |

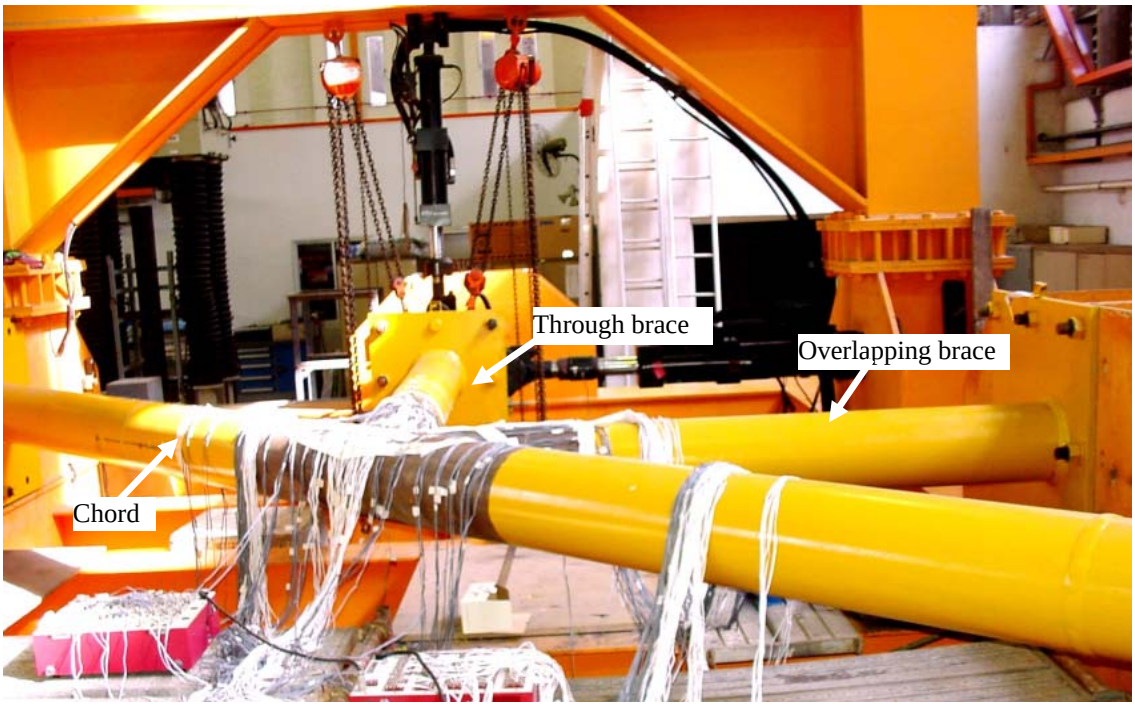


Figure 3.1 The "Orange" rig and the partially overlapped CHS K-joint specimen

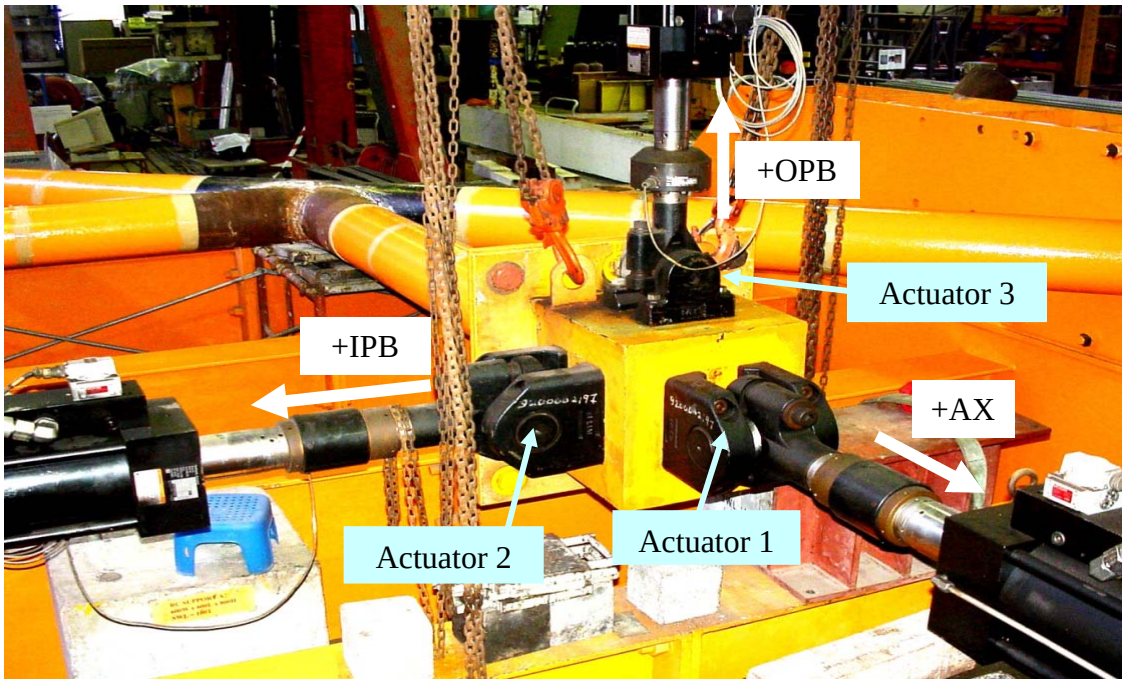


Figure 3.2 Actuators and loading directions

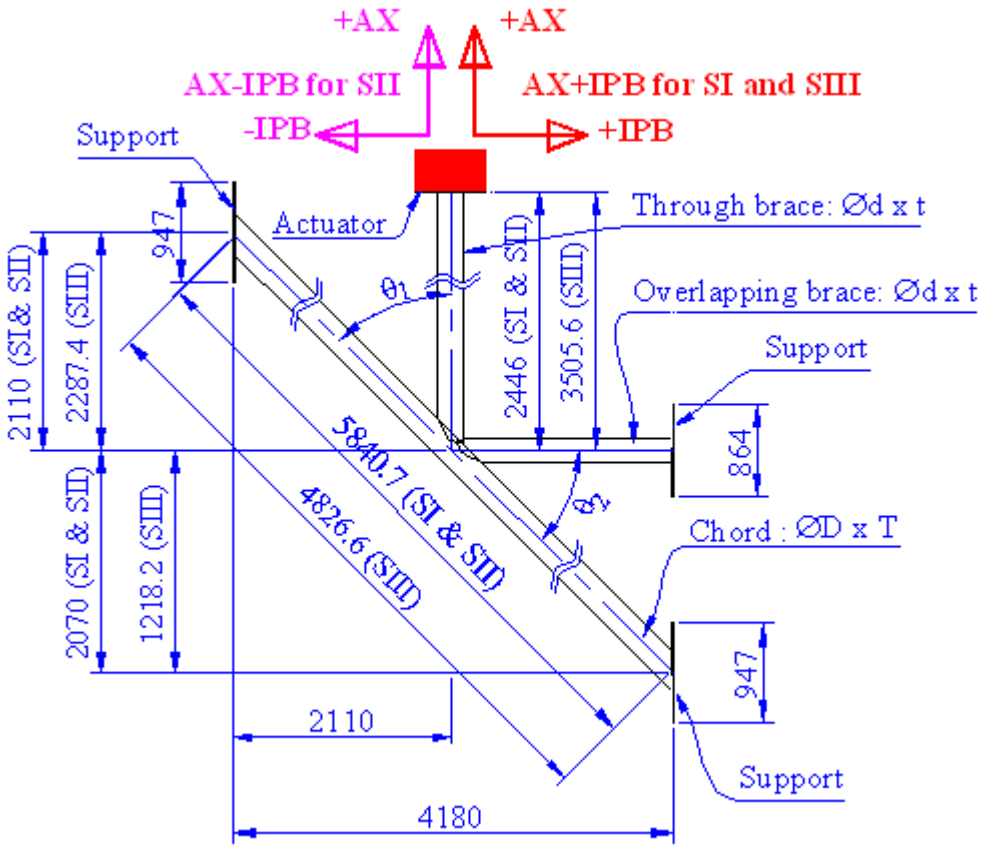


Figure 3.3 Dimensions and configuration of the specimens

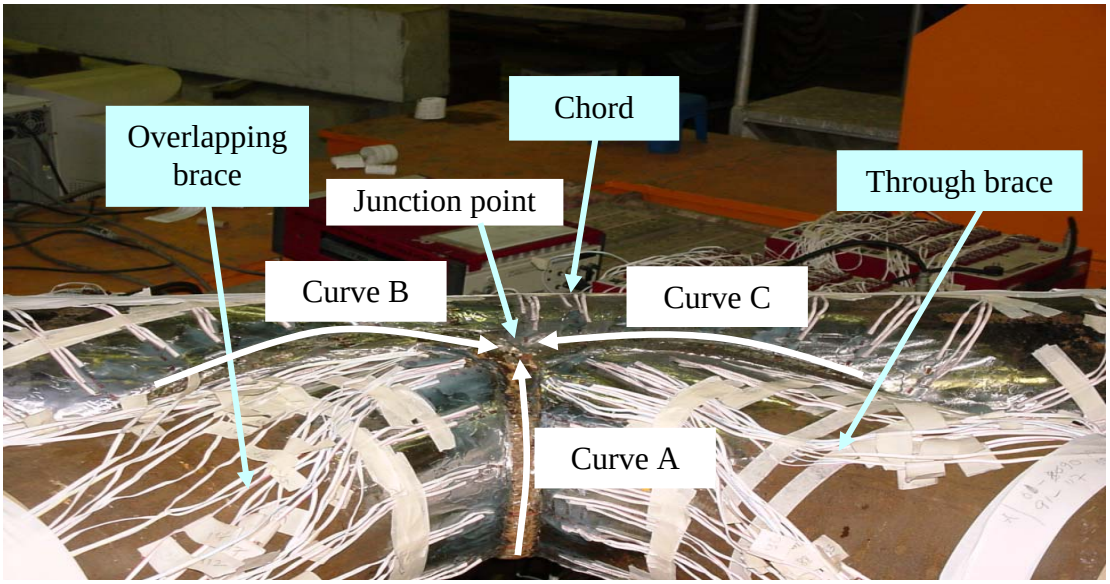


Figure 3.4 Close up view of the partially overlapped CHS K-joint and the three welding curves

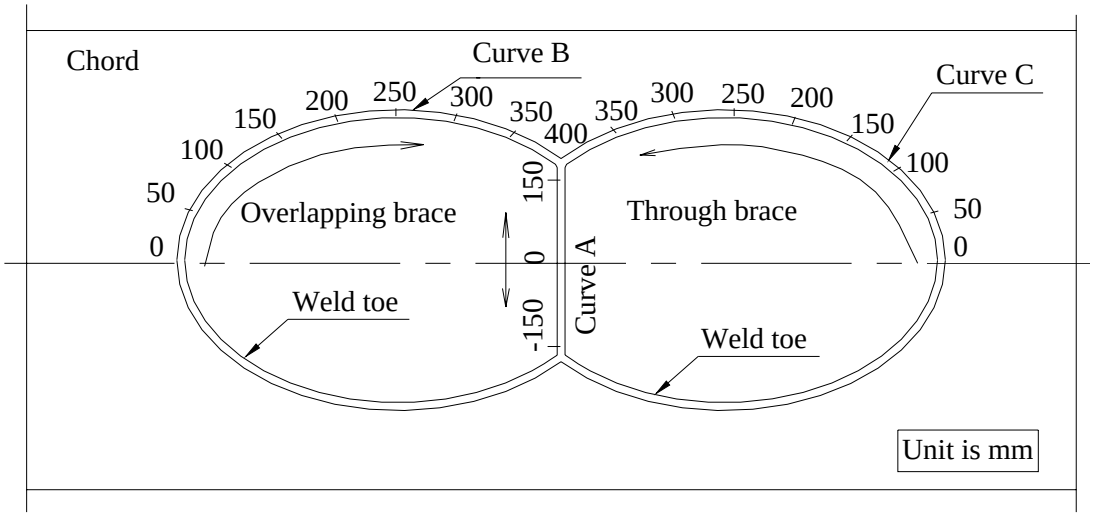


(a) Plan view of the intersection

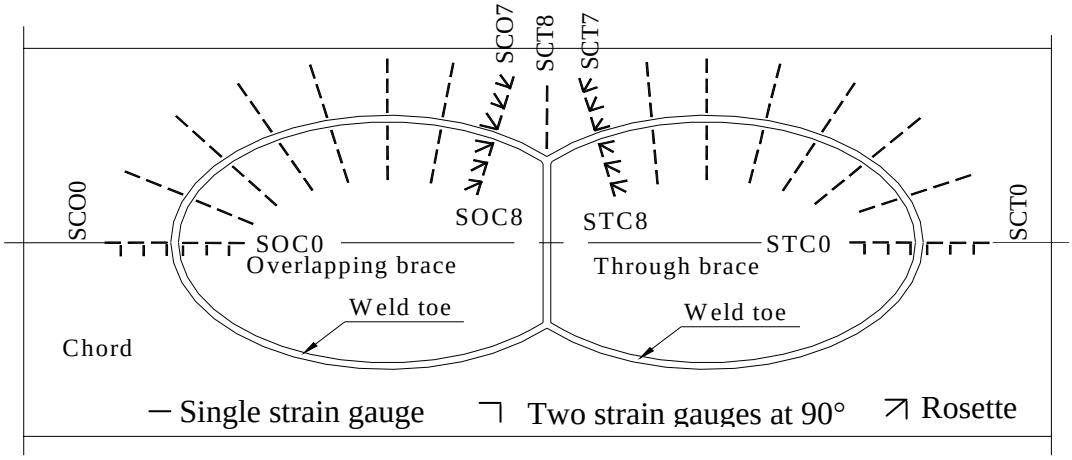


(b) Strain gauges locations on chord and braces, Specimen SI and SII

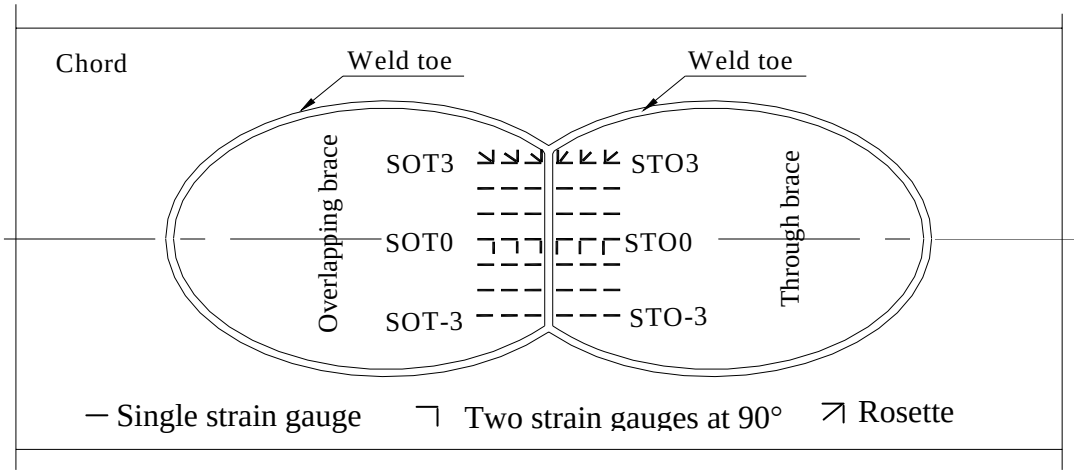


(c) Strain gauges locations on through and overlapping braces, Specimens SI and SII

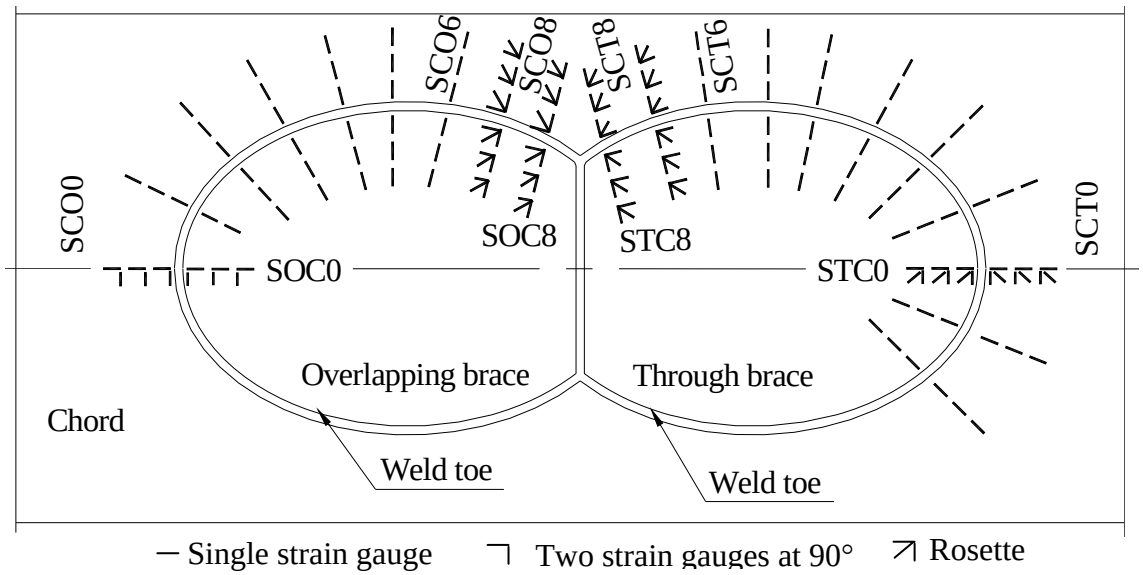


(d) Strain gauges locations on chord and braces, Specimen SIII

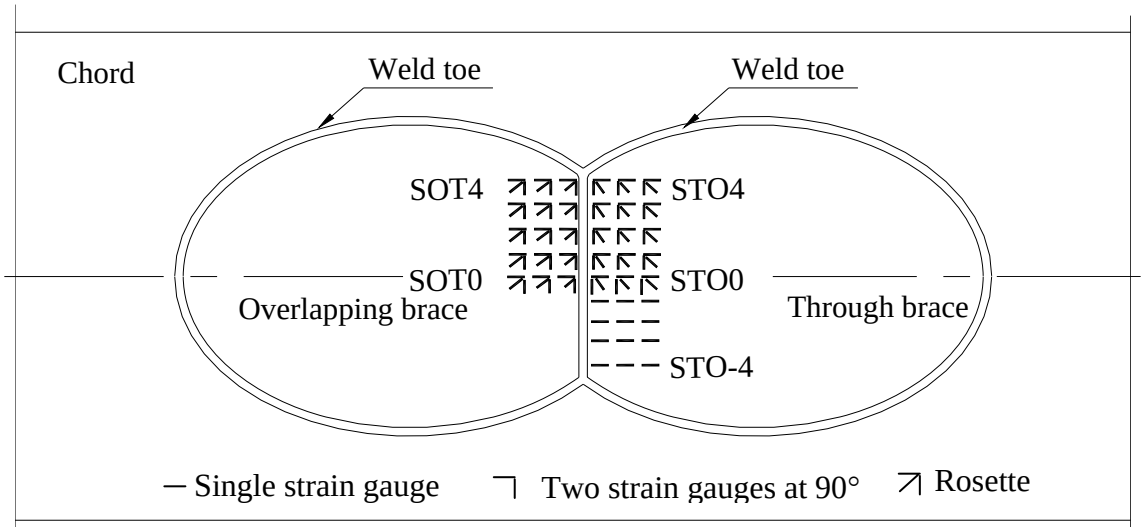


(e) Strain gauges locations on through and overlapping braces, Specimen SIII

Figure 3.5 Strain gauges locations for specimens

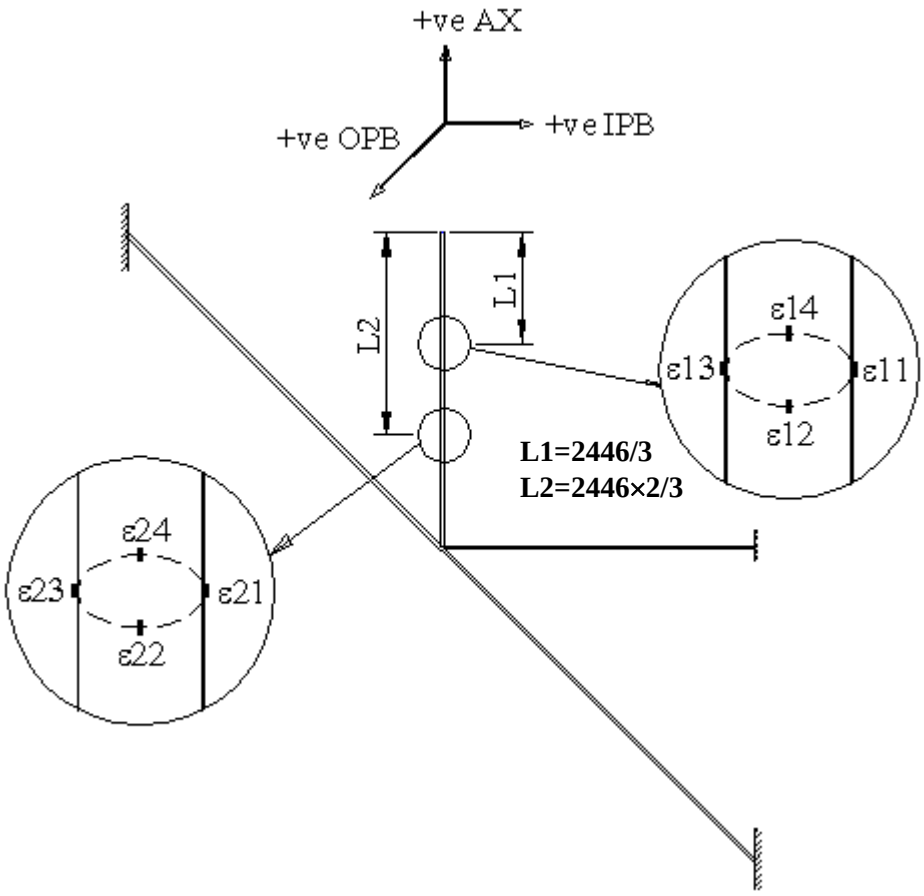


Figure 3.6 Eight strain gauges at the midway of the through brace

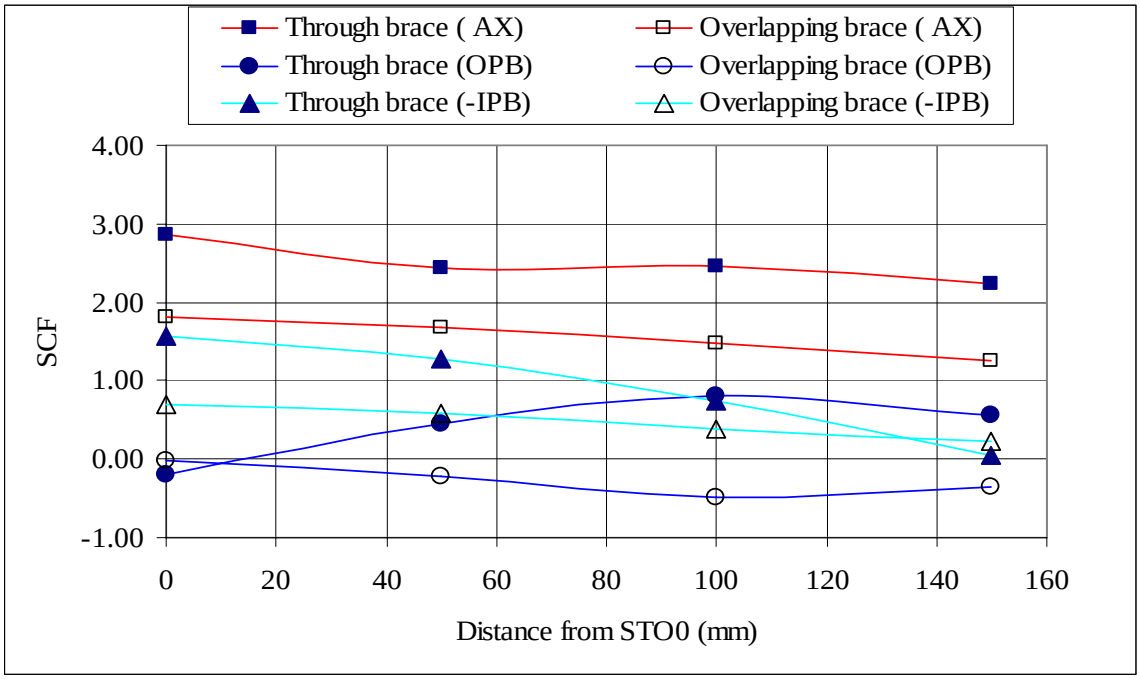


(a) Curve A

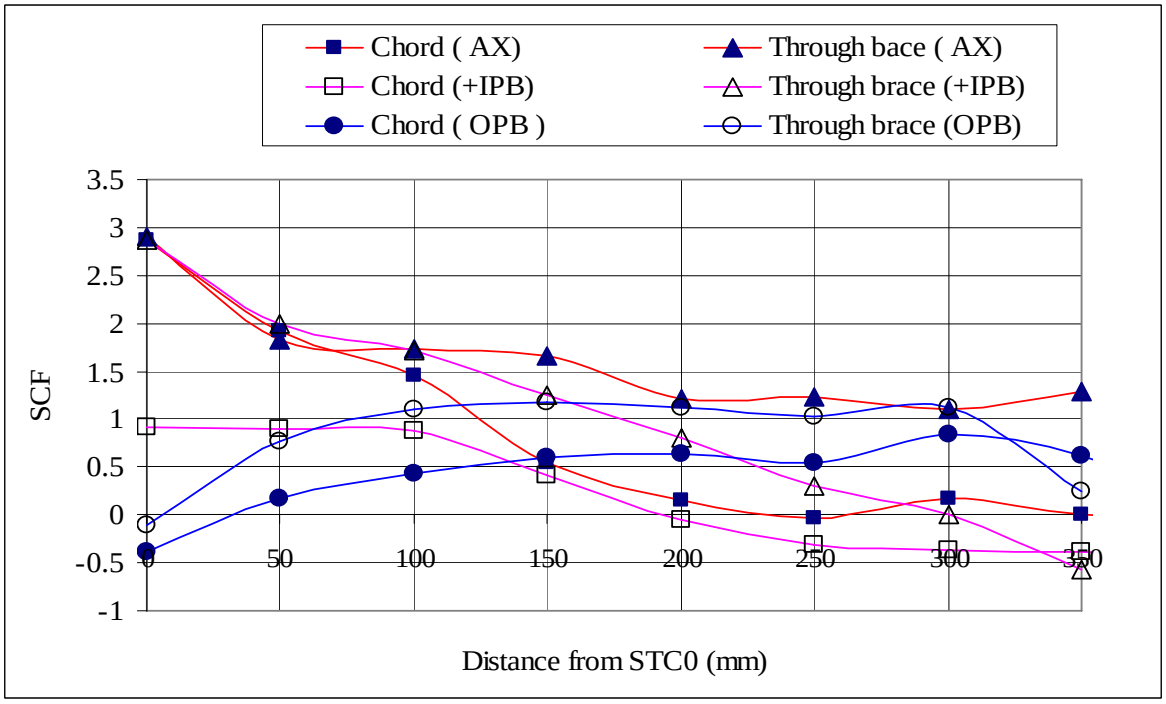


(b) Curve C

Figure 3.7 Variations of SCFs along the welding Curves A and C of Specimens SI and SII

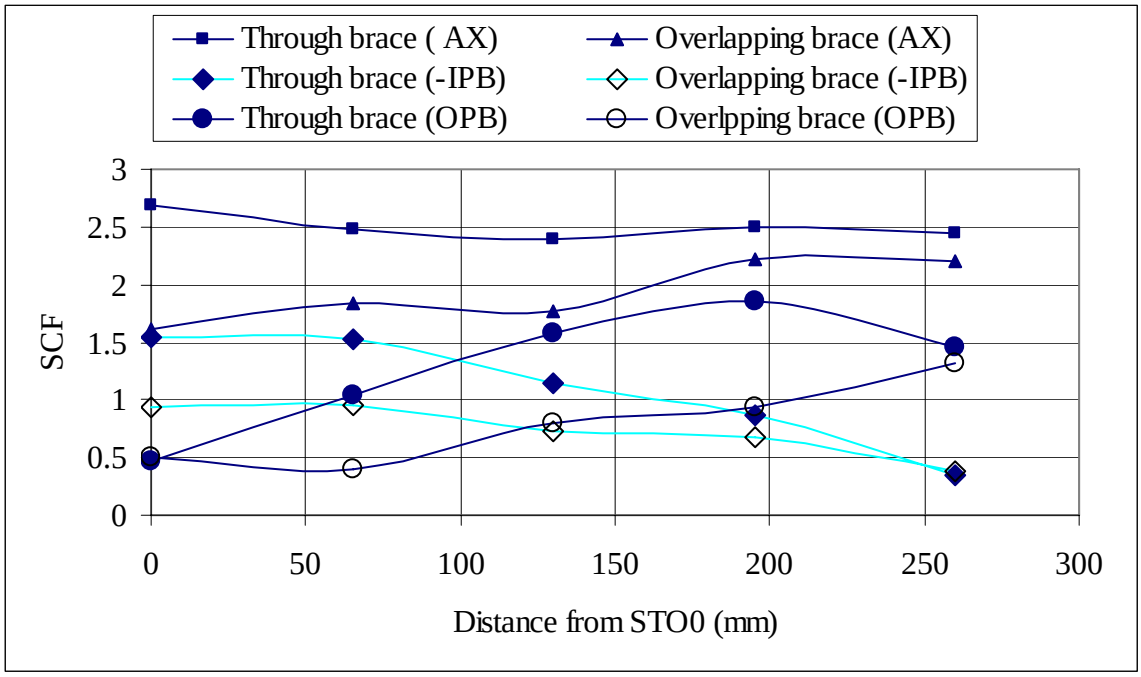


(a) Curve A

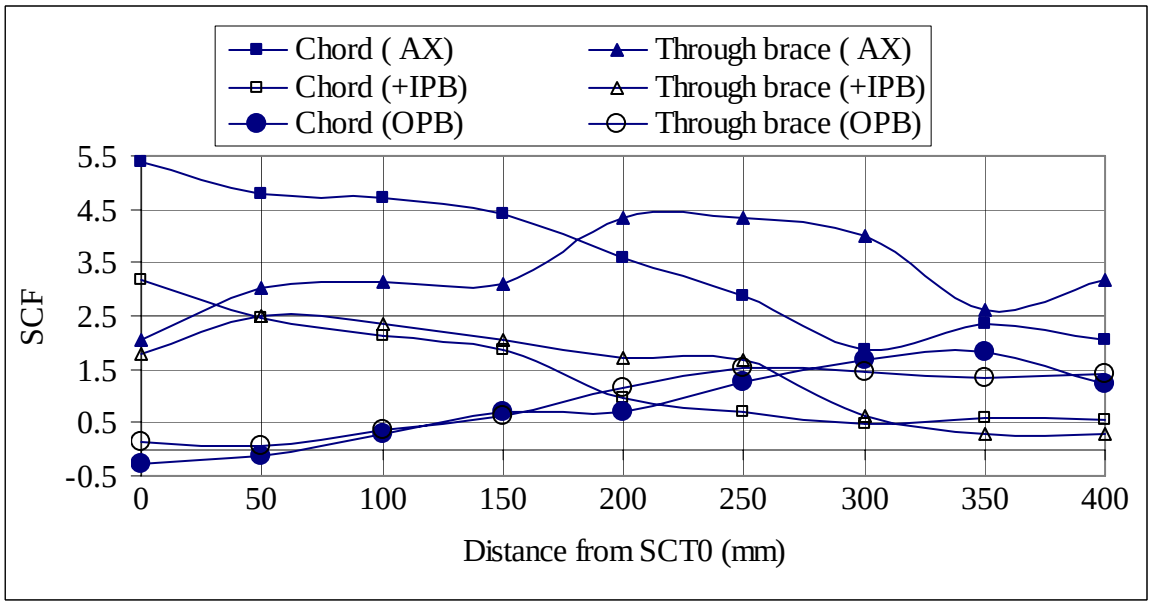


(b) Curve C

Figure 3.8 Variations of SCFs along the welding Curves A and C of Specimen SIII

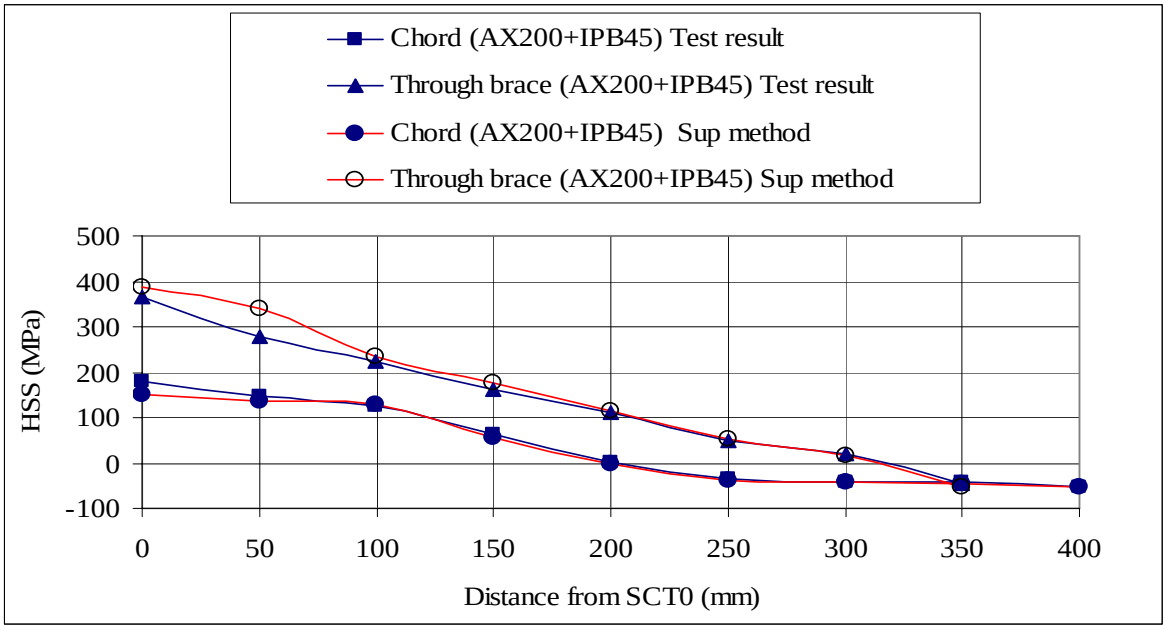


(a) Results for Specimens SI and SII, Curve C

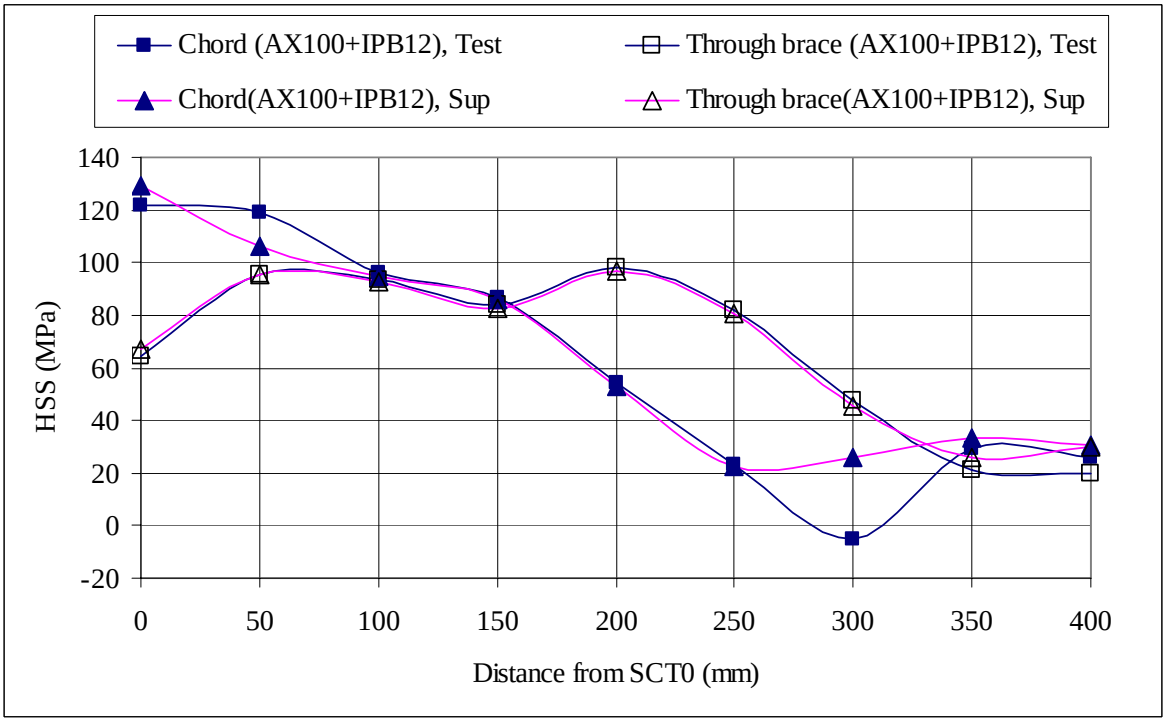


(b) Results for Specimen SIII, Curve C

Figure 3.9 Comparison of HSS obtained from test and superposition method

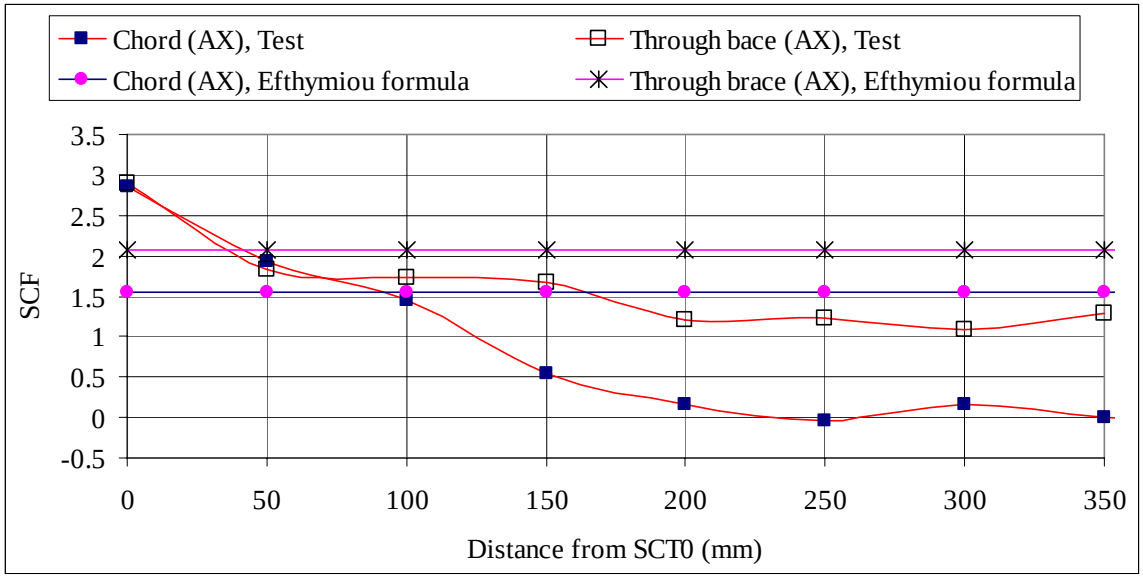


(a) Curve C, AX loading

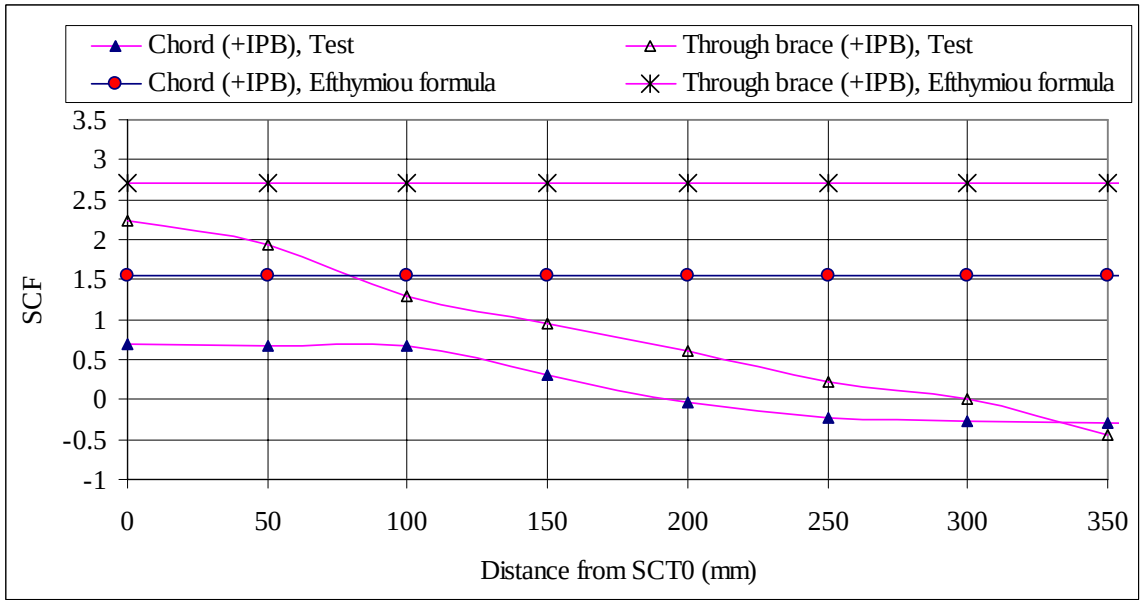


(b) Curve C, +IPB loading

Figure 3.10 Comparison of SCF variations obtained from test and Efthymiou's formulae, Specimens SI and SII

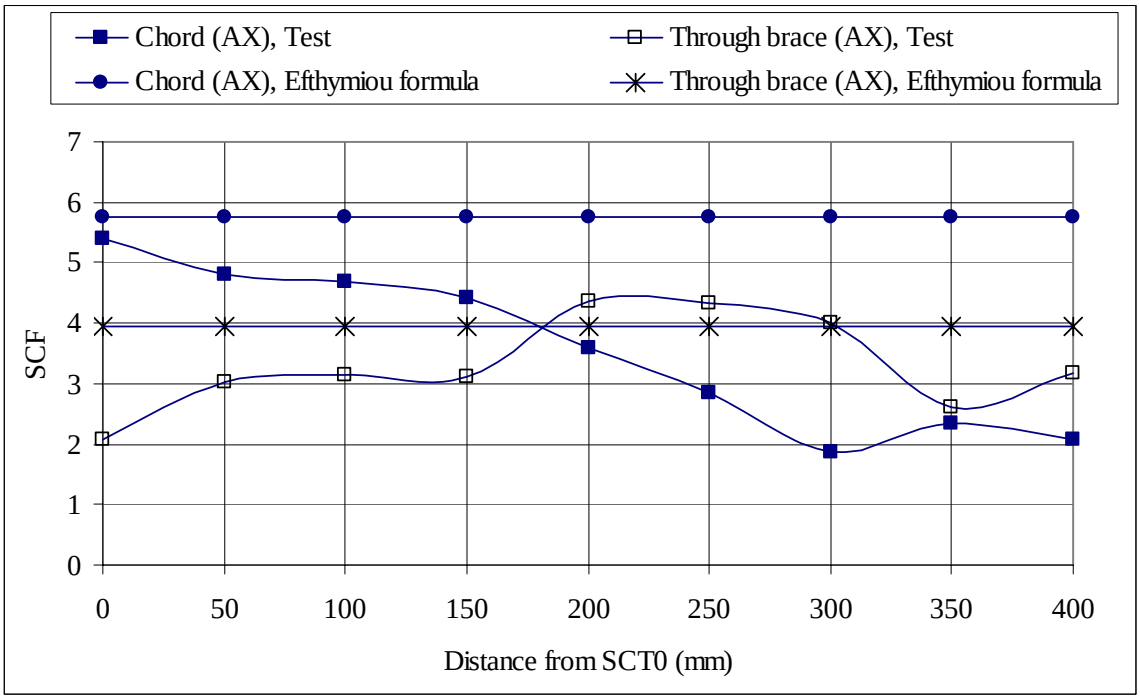


(a) Curve C, AX loading

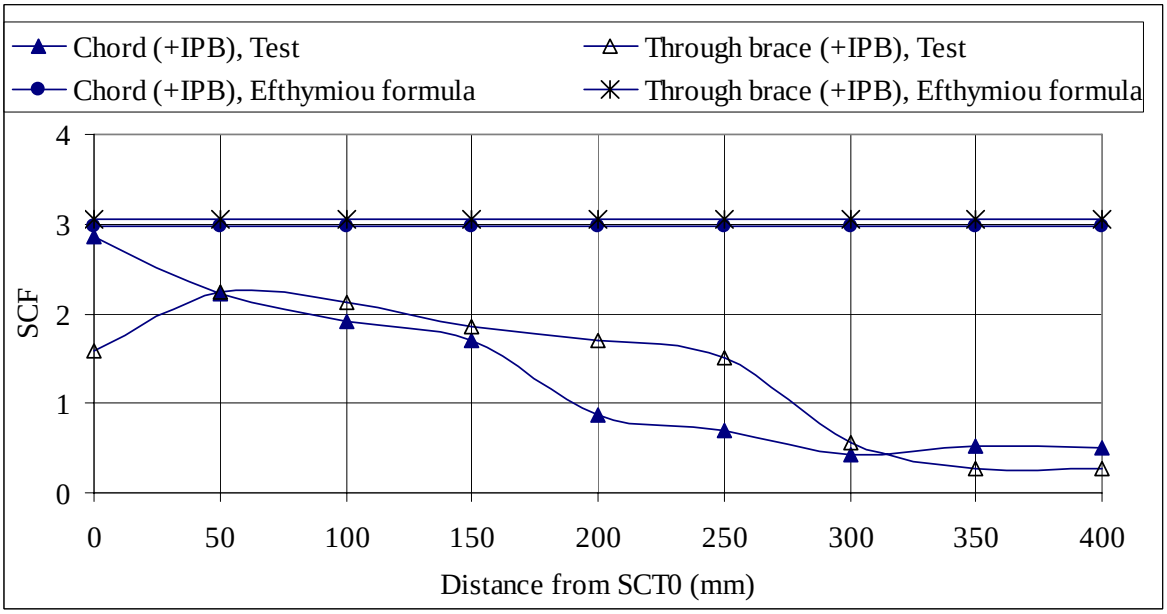


(b) Curve C, +IPB loading

Figure 3.11 Comparison of SCF variations obtained from test and Efthymiou's formulae, Specimen SIII

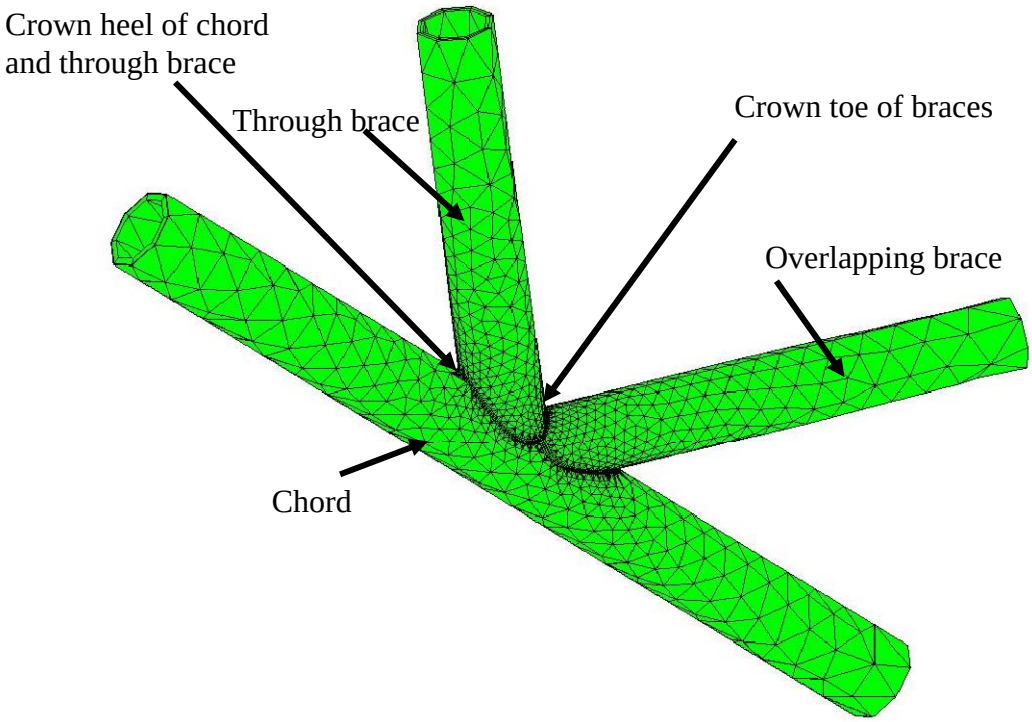


(a) Mesh for Specimens SI and SII

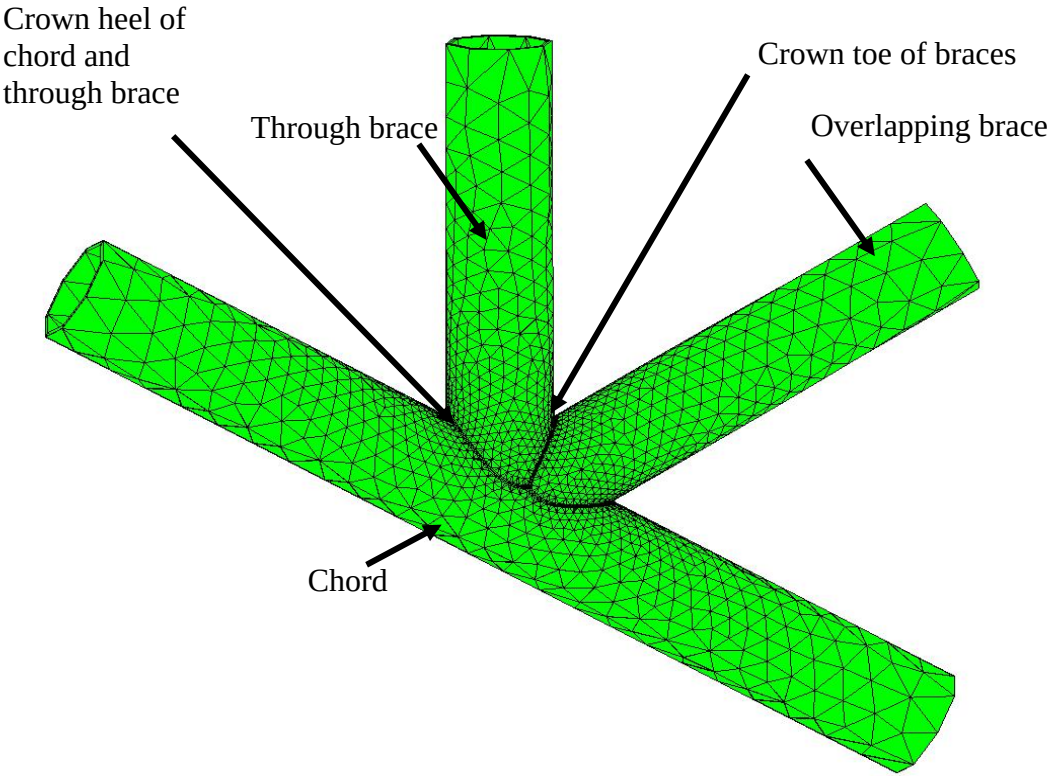


(b) Mesh for Specimen SIII

Figure 3.12 Finite element meshes used in the numerical modeling of the specimens

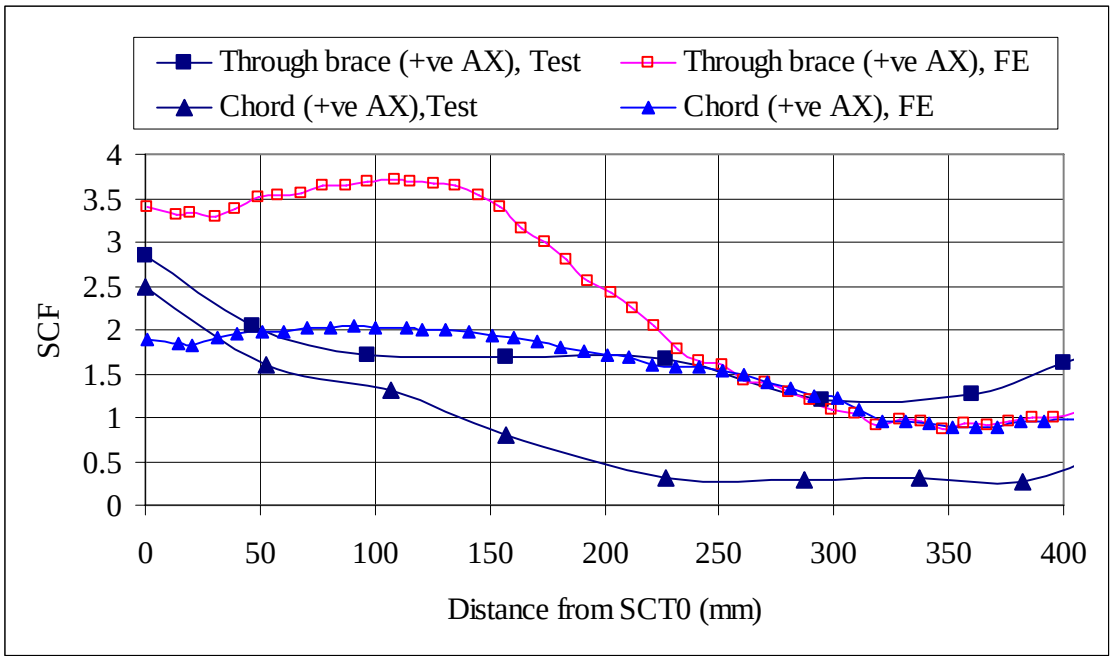


(a) Curve C, +ve AX loading

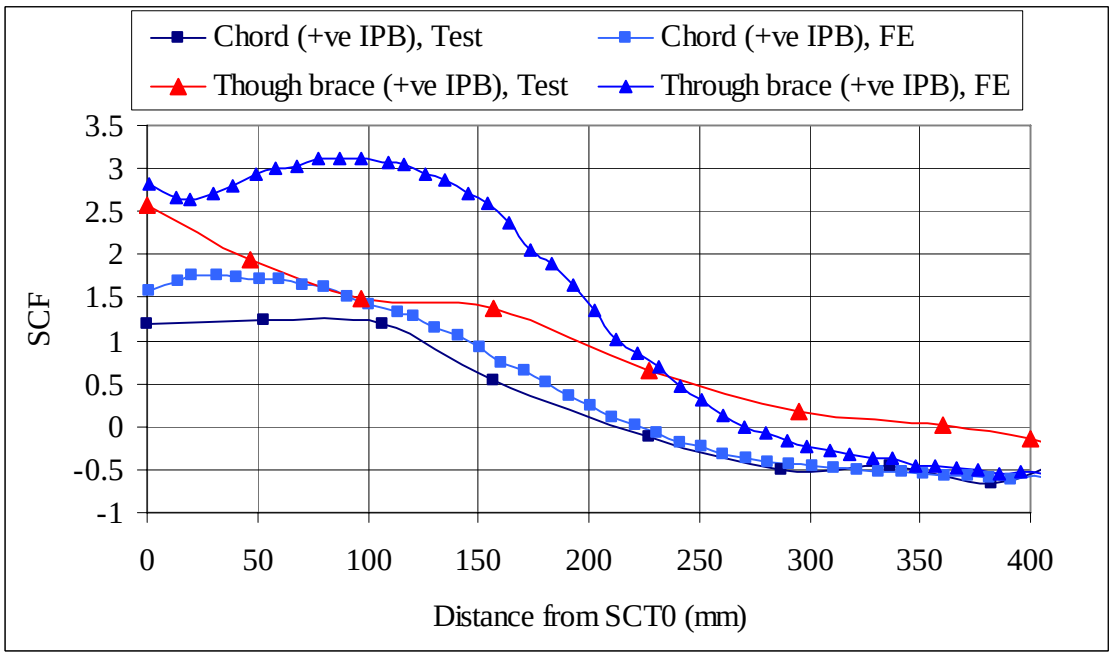


(b) Curve C, +ve IPB loading

Figure 3.13 Comparison of SCF variations obtained from test and FE analysis, Specimen SI (+ve AX and +ve IPB)

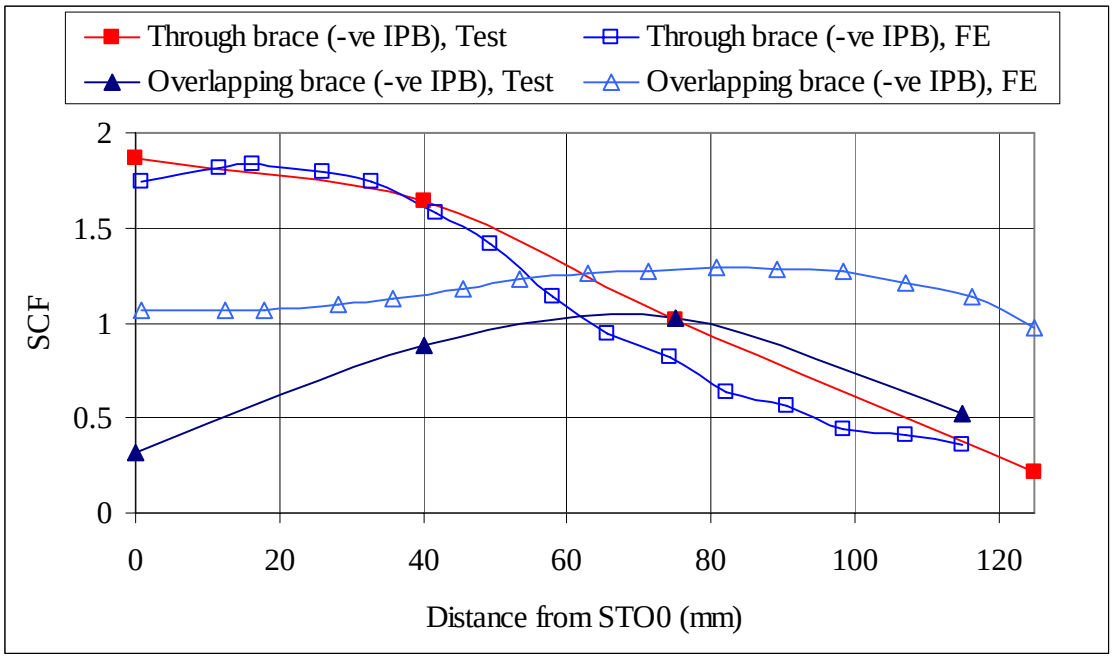


(a) Curve C, -ve IPB loading

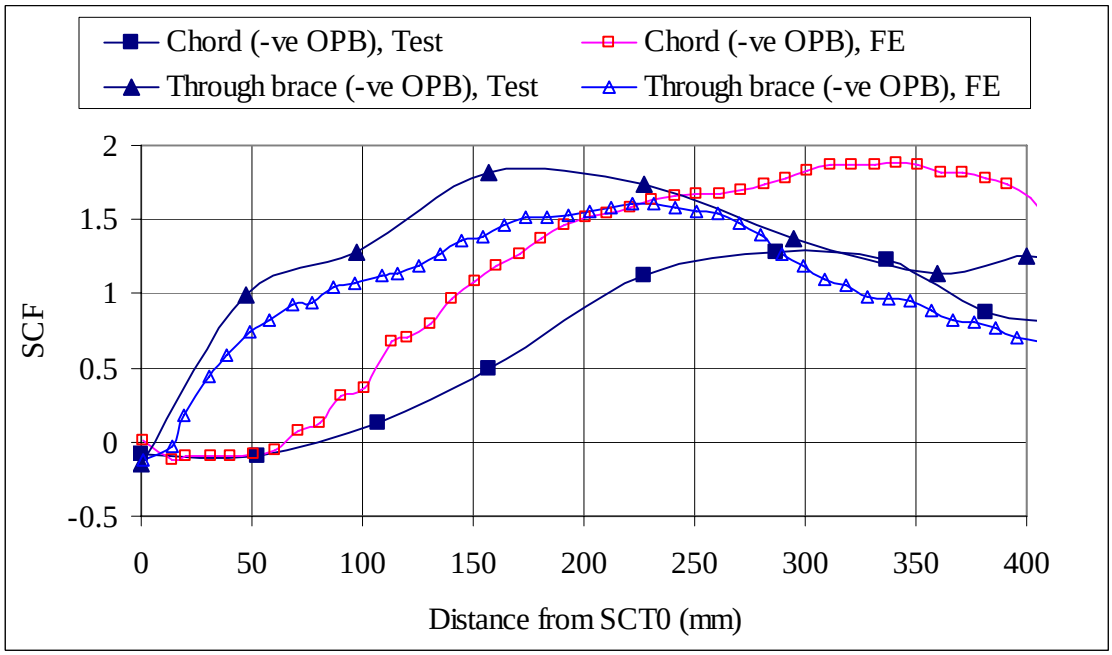


(b) Curve C, -ve OIPB loading

Figure 3.14 Comparison of SCF variations obtained from test and FE analysis, Specimen SI (-ve IPB and –ve OPB)

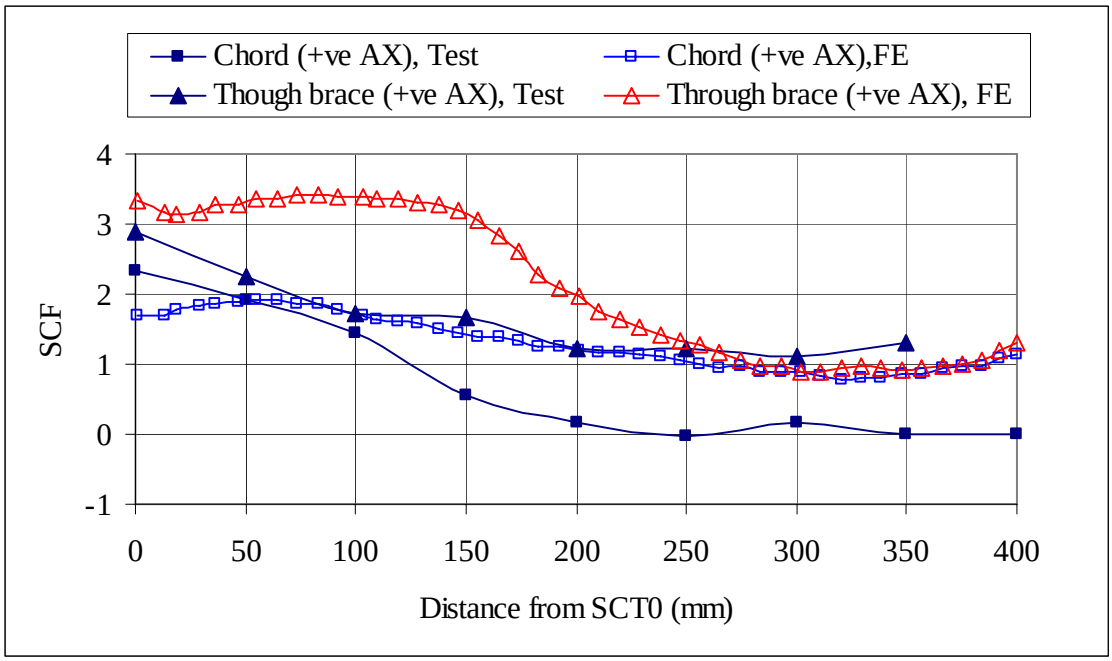


(a) Curve C, +ve AX loading

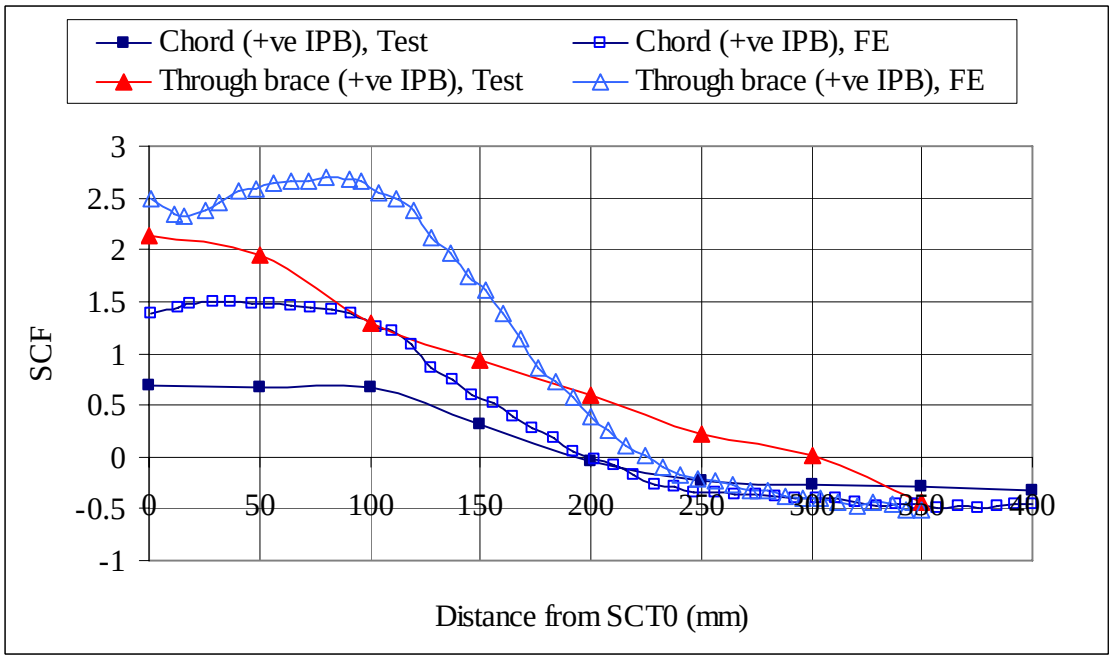


(b) Curve C, +ve IPB loading

Figure 3.15 Comparison of SCF variations obtained from test and FE analysis, Specimen SII (+ve AX and +ve IPB)

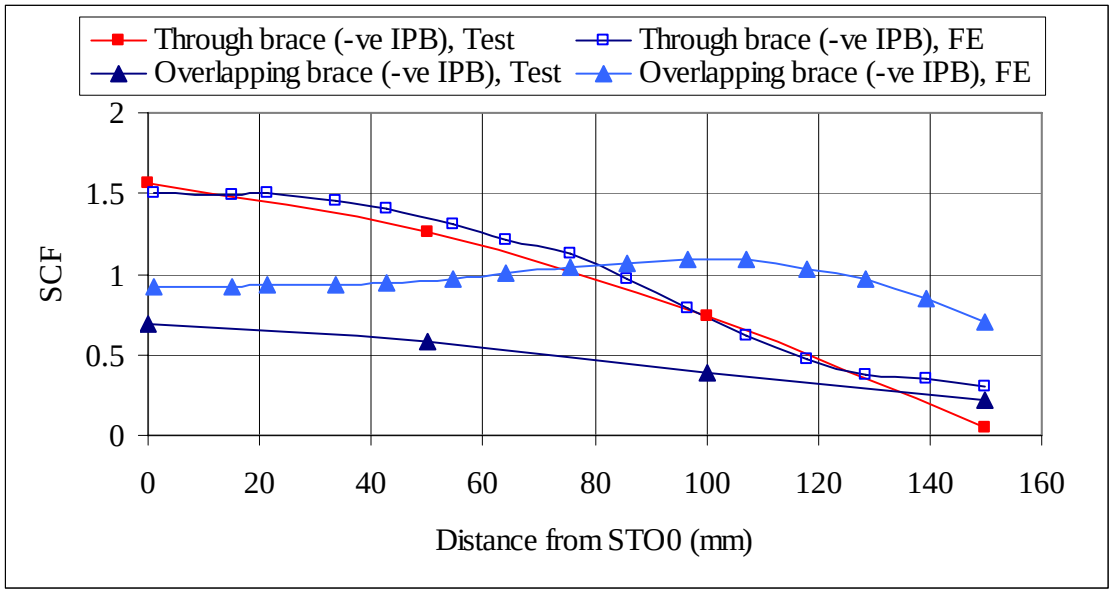


(a) Curve C, -ve IPB loading

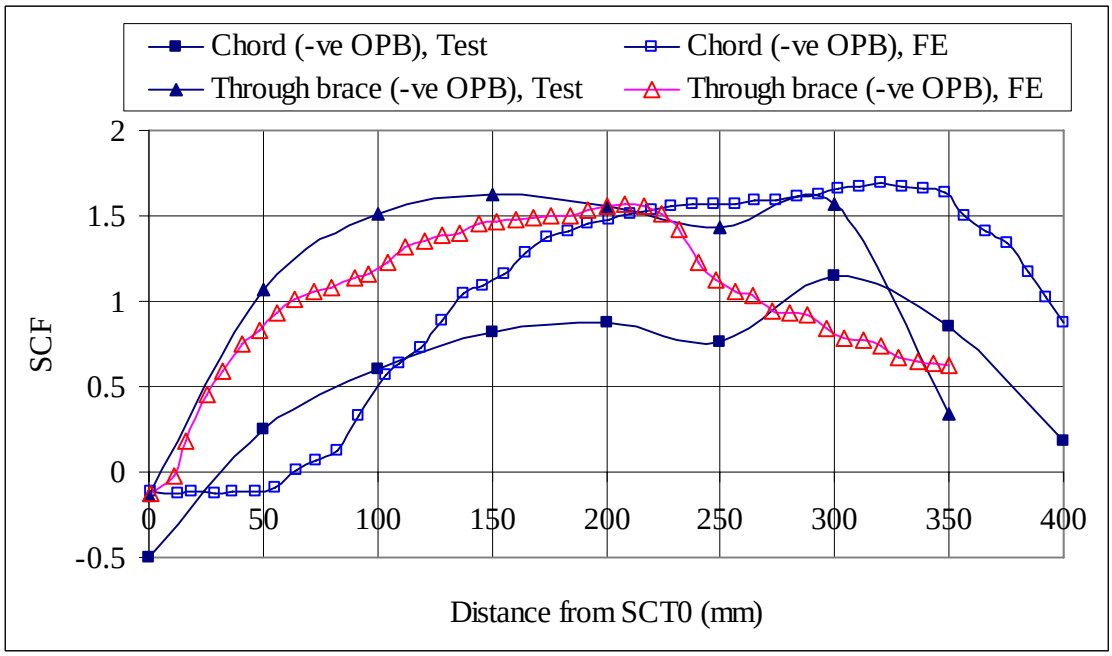


(b) Curve C, -ve OIPB loading

Figure 3.16 Comparison of SCF variations obtained from test and FE analysis, Specimen SII (-ve IPB and –ve OPB)

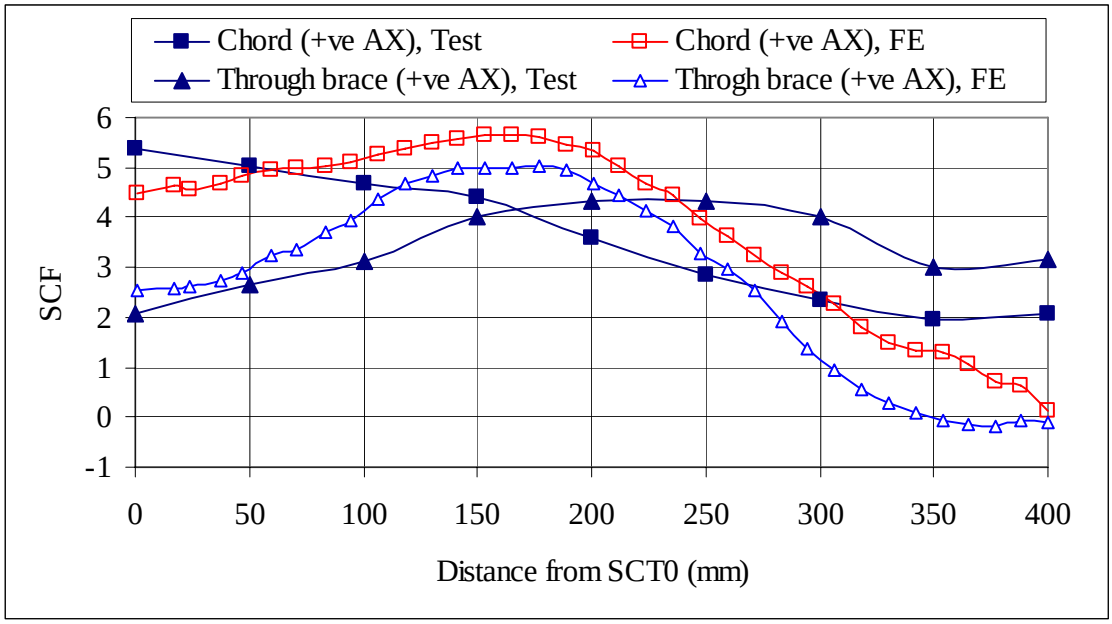


(a) Curve C, +ve AX loading

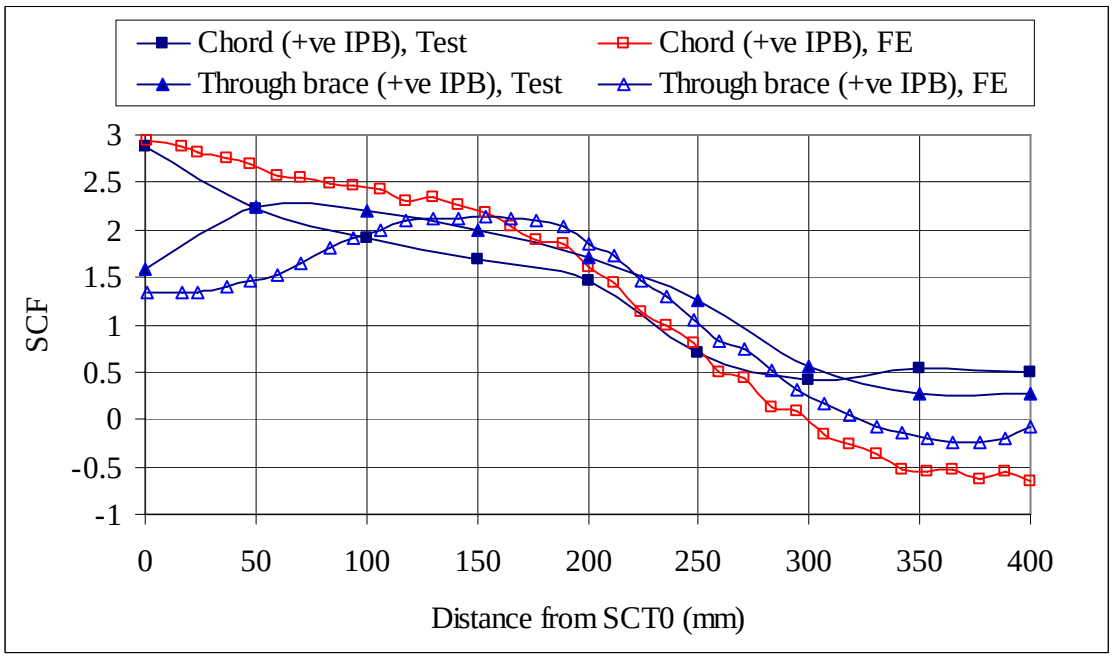


(b) Curve C, +ve IPB loading

Figure 3.17 Comparison of SCF variations obtained from test and FE analysis, Specimen SIII (+ve AX and +ve IPB)

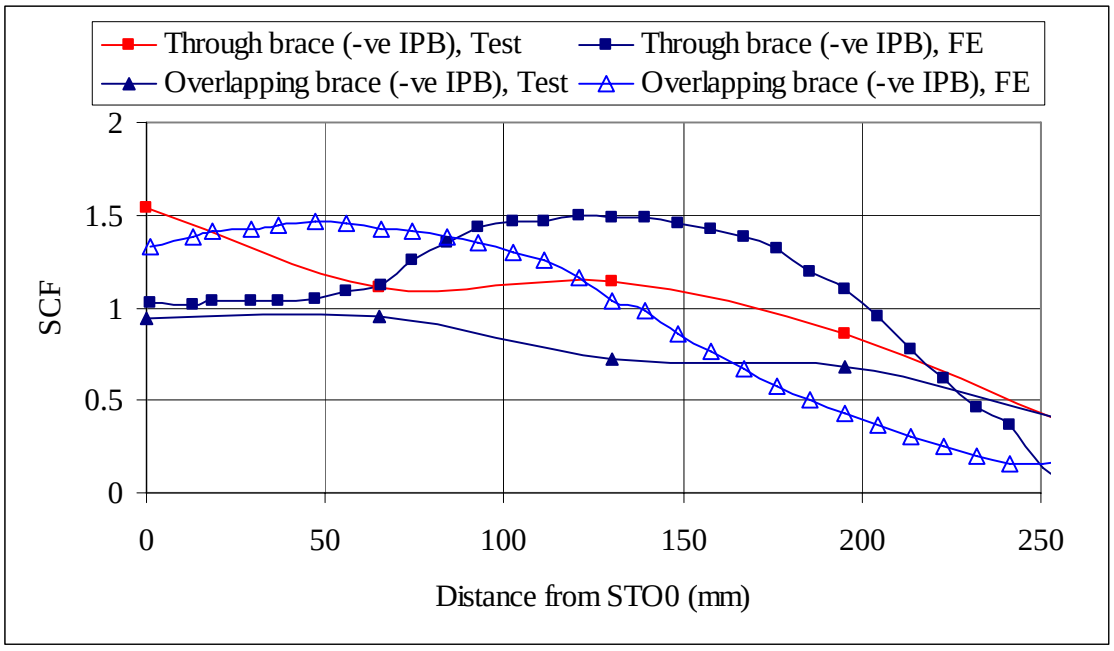


(a) Curve C, -ve IPB loading

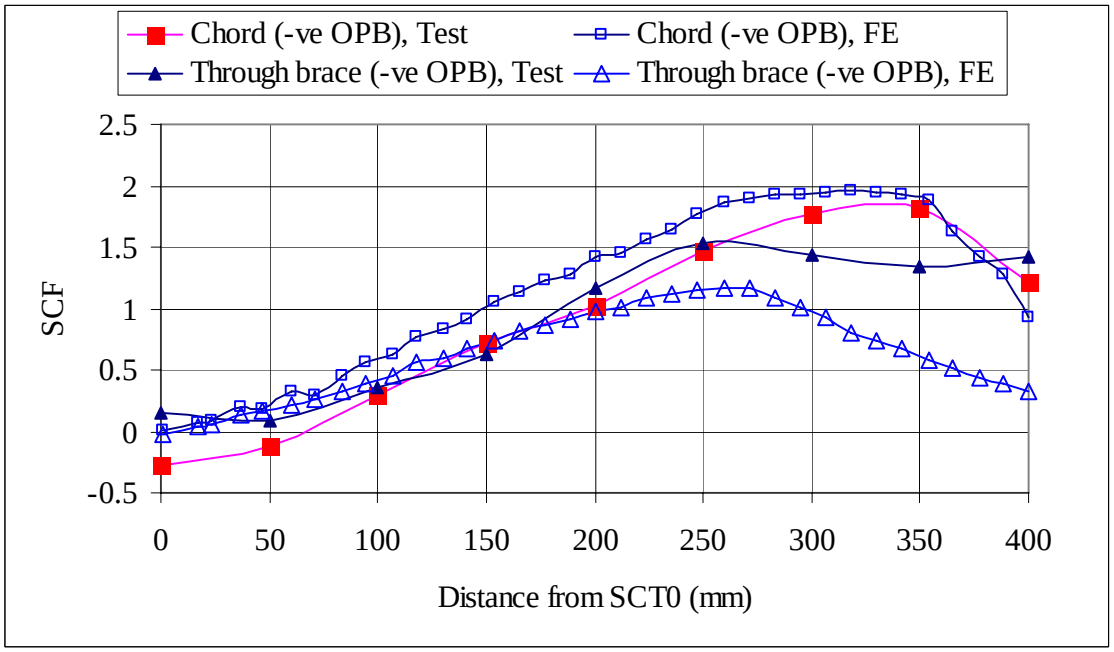


(b) Curve C, -ve OIPB loading

Figure 3.18 Comparison of SCF variations obtained from test and FE analysis, Specimen SIII (-ve IPB and –ve OPB)

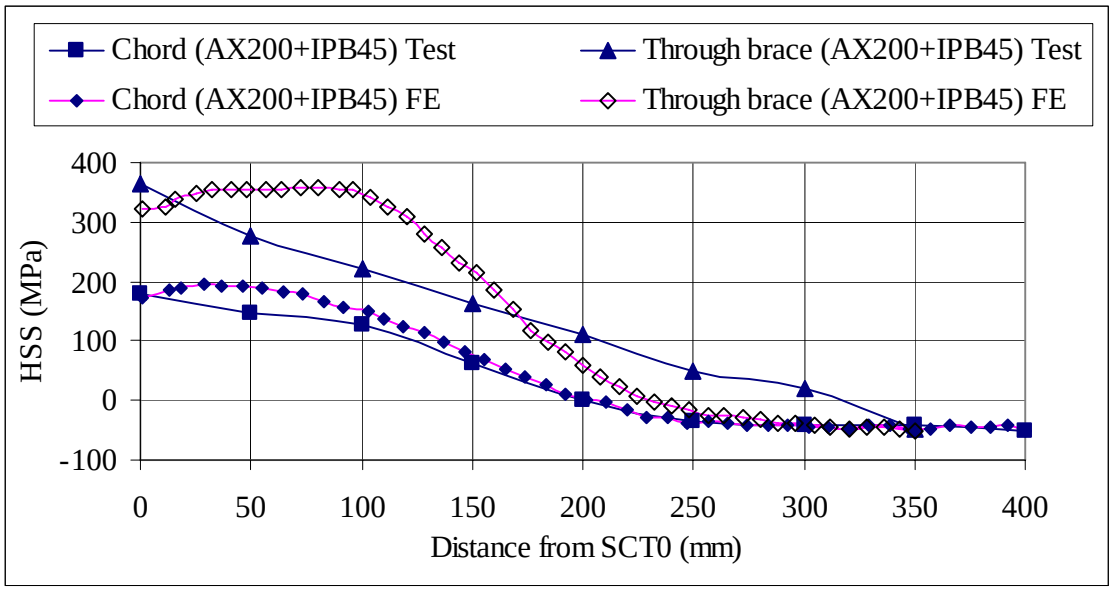


(a) Results for Specimens SI, Curve C

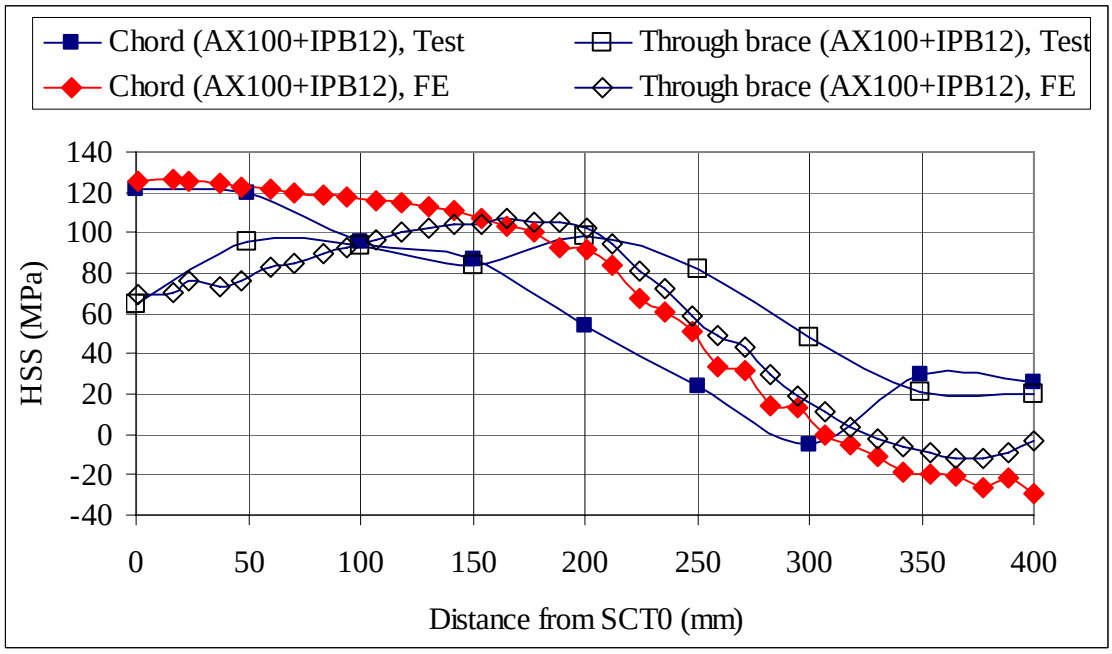


(b) Results for Specimen SIII, Curve C

Figure 3.19 Comparison of HSS obtained from test and FE analyses

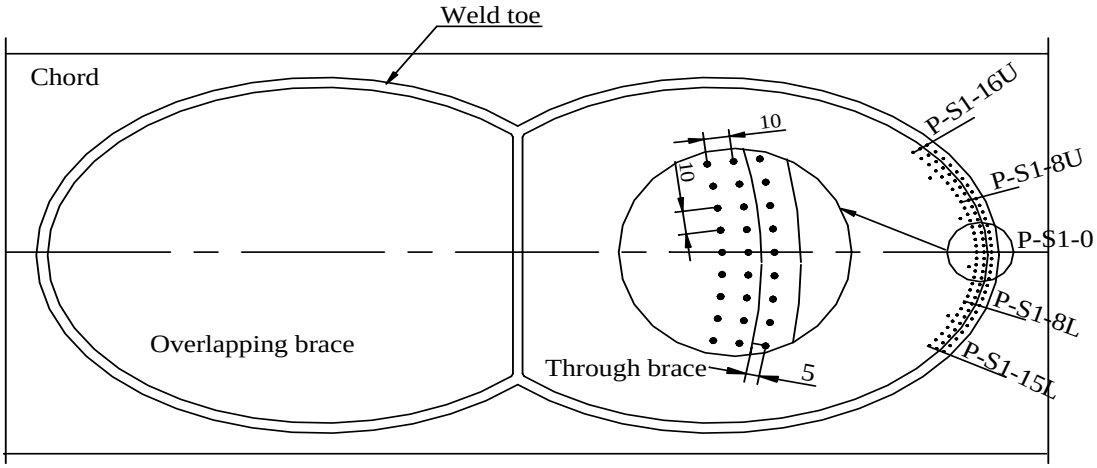


(a) Plan of probe location at the crown heel of the through brace of Specimen SI

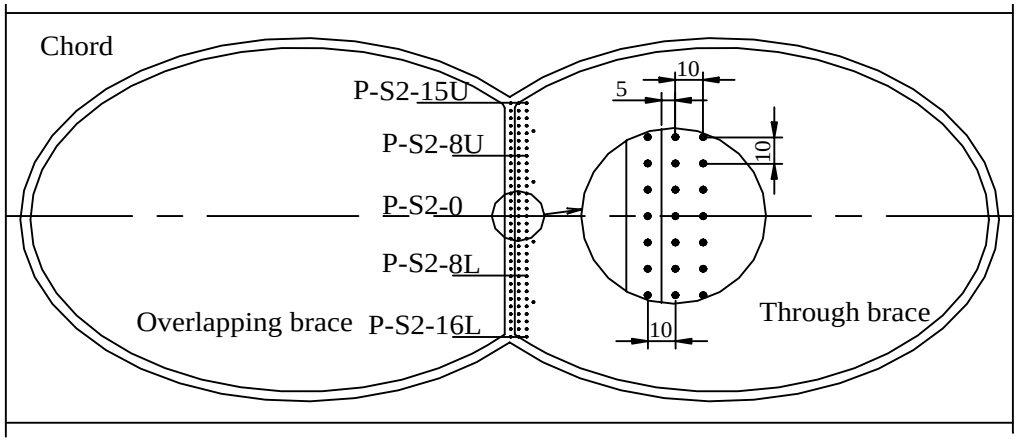


(b) Plan of probe location at the crown toe of the through brace surface of Specimen SII

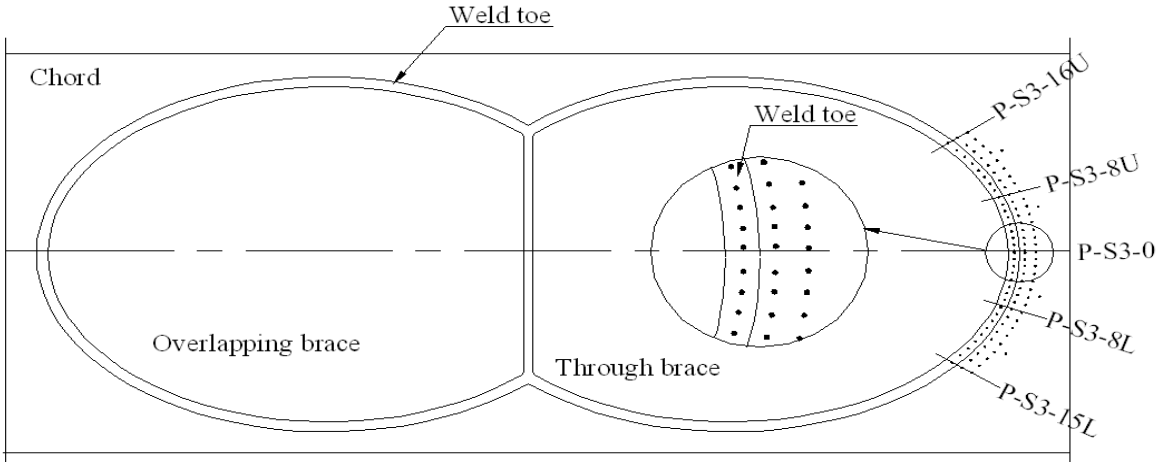


(a) Plan of probe location at the crown heel of the chord of Specimen SIII

Figure 3.20 Plans of probes locations

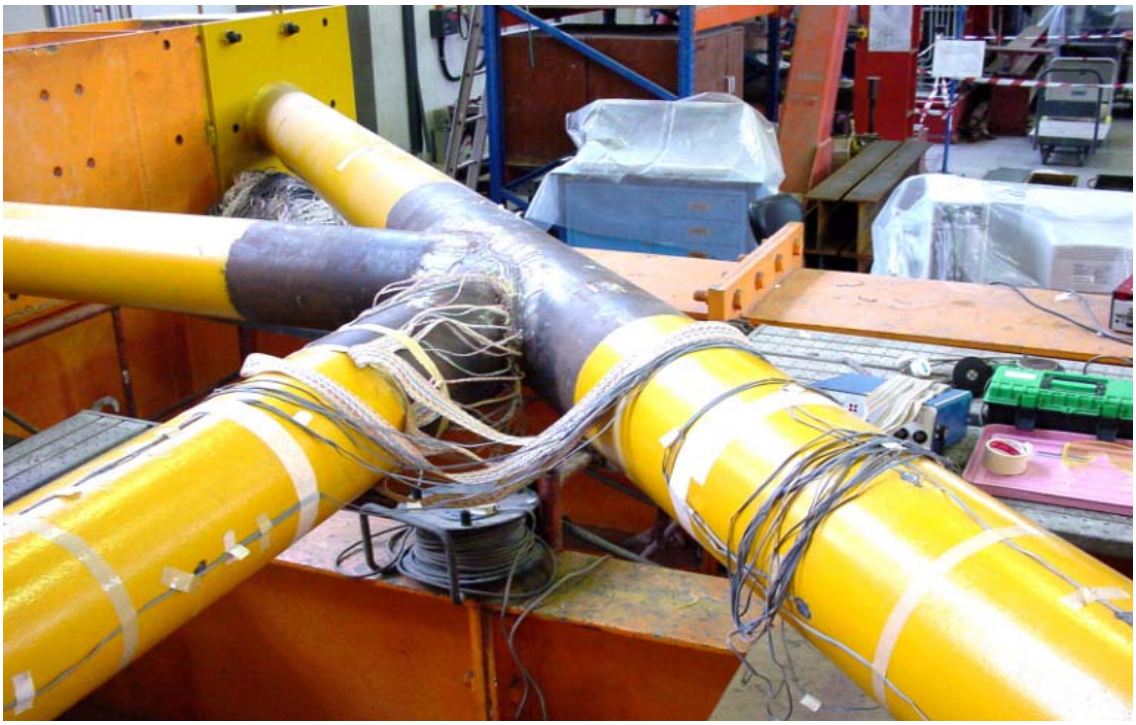

(a) Typical general view of probes and the connecting cables

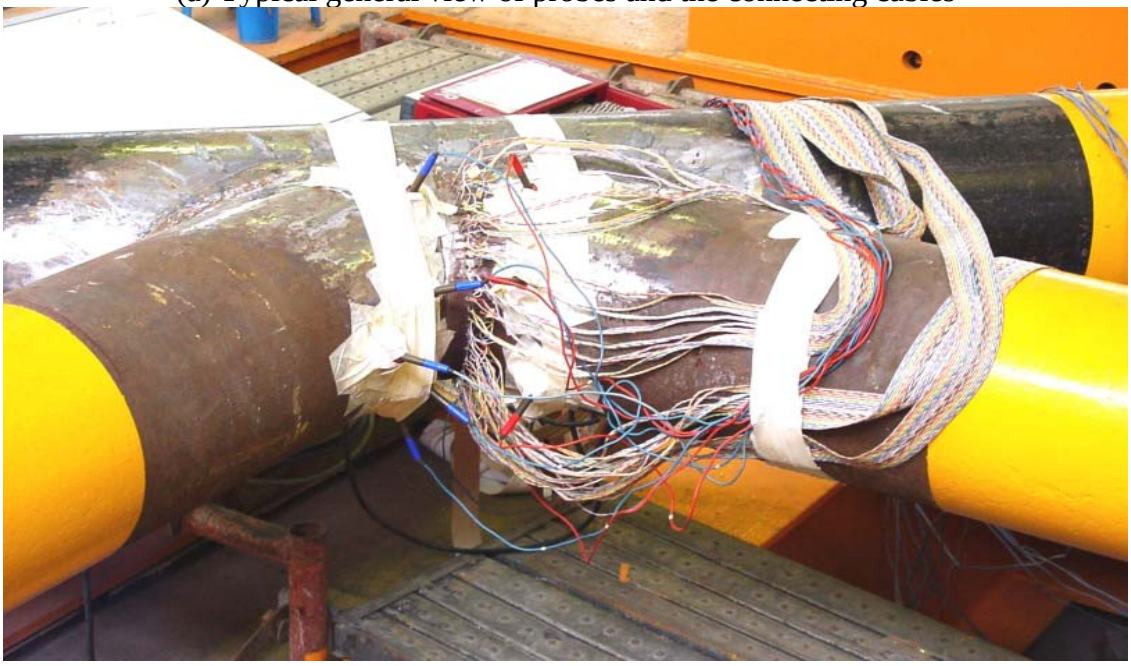

(b) Close view of probes and the connecting cables

Figure 3.21 Typical views of probes sitting.

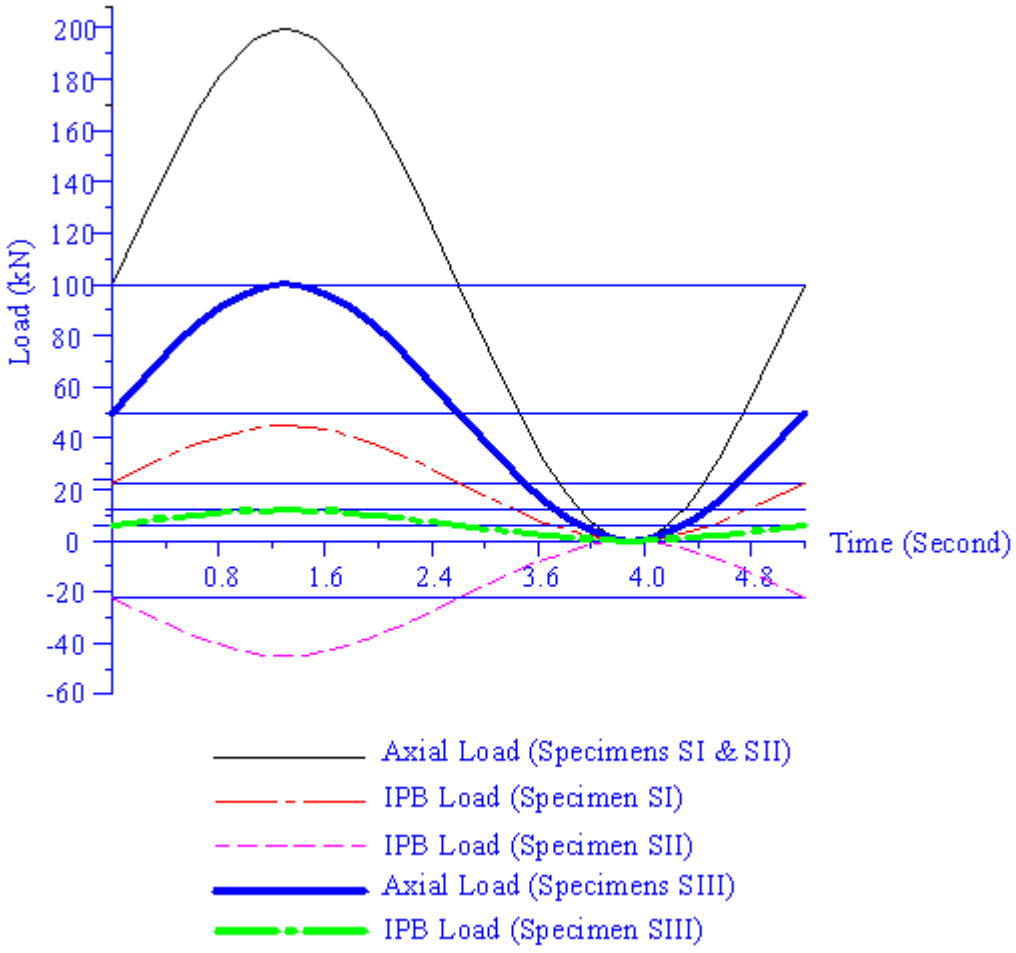


Figure 3.22 Sinusoidal amplitude loads of AX and IPB used in the fatigue tests


(a) Close-up view and opened surface crack at crown heel of through brace of Specimen SI

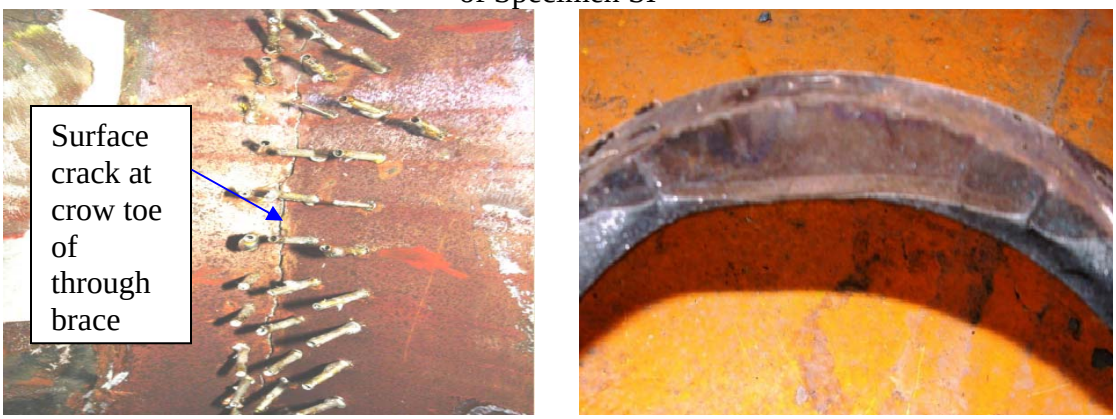


(b) Close-up view and opened surface crack at crown toe of through brace of Specimen SII


(c) Close-up view and opened surface crack at crown heel of the chord of Specimen SIII

Figure 3.23 Actual surface cracks of partially overlapped CHS K-joints

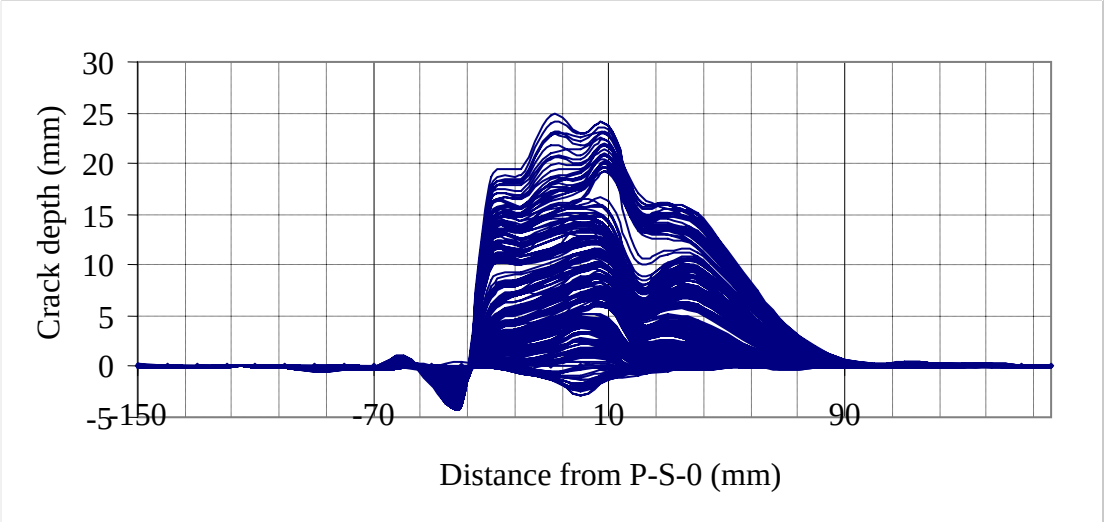


a) ACPD crack development of partially overlapped CHS K-joint, Specimen SI

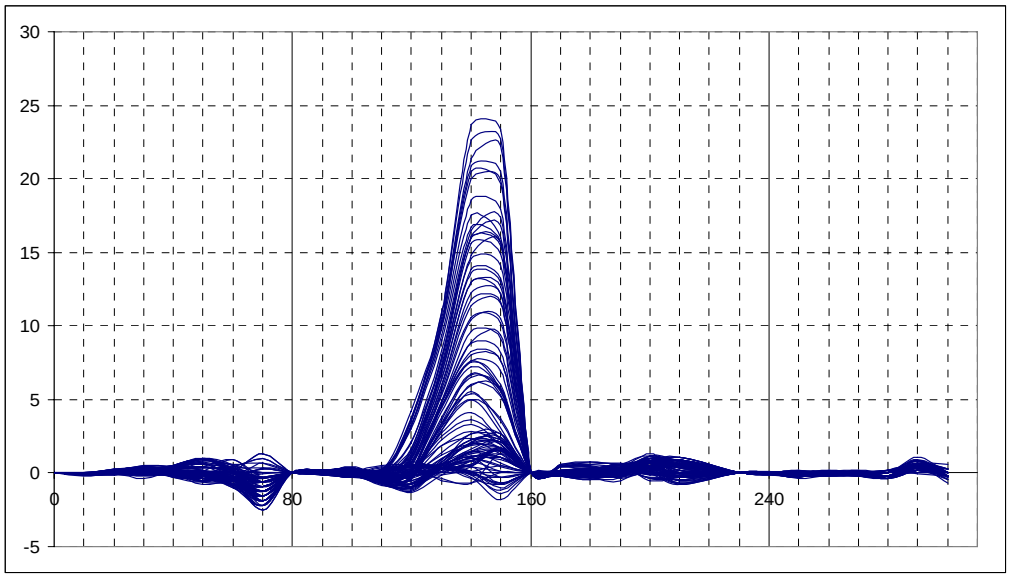


b) ACPD crack development of partially overlapped CHS K-joint, Specimen SII

Figure 3.24 ACPD crack development of partially overlapped CHS K-joints

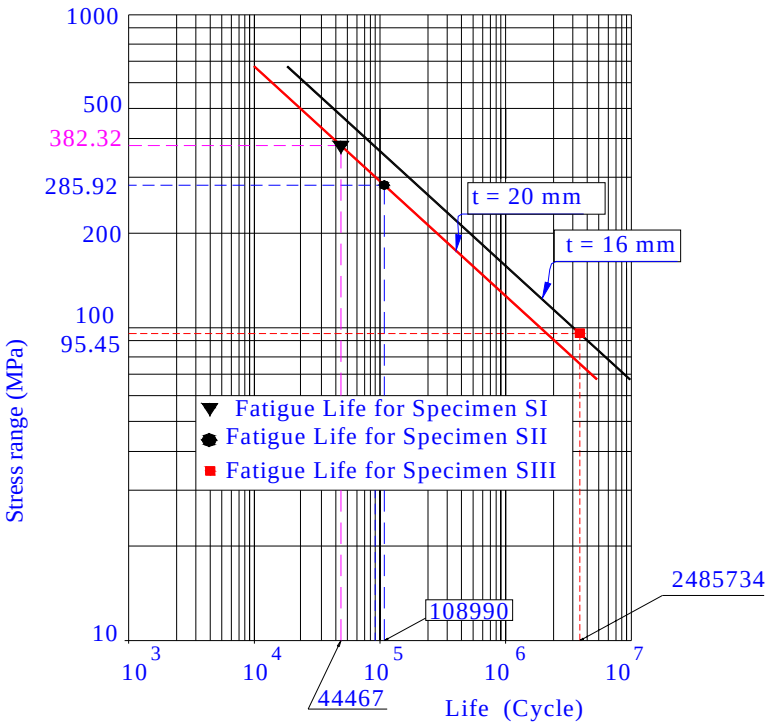


a) Fatigue life based on S-N curve for through braces of Specimens SI, SII and SIII

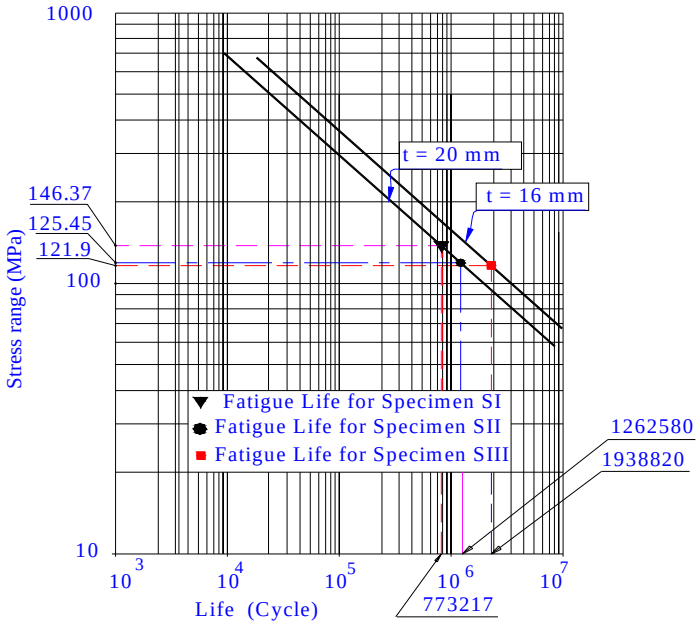


b) Fatigue life based on S-N curve for chords of Specimens SI, SII and SIII

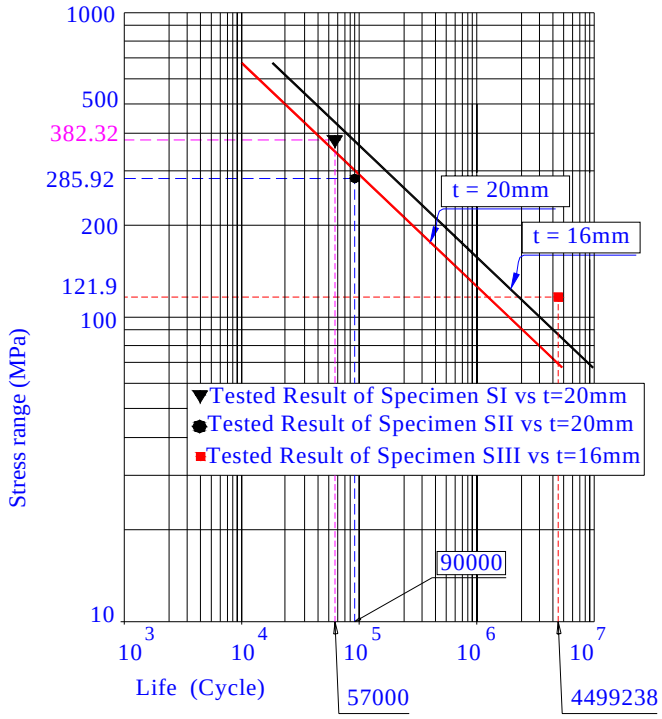


c) Tested fatigue results of Specimens SI, SII and SIII comparing with S-N curves

Figure 3.25 Fatigue results comparing with S-N curves

# *CHAPTER 4*
# *PARAMETRIC STUDY OF SCF FOR PARTIALLY OVERLAPPED CHS K-JOINTS*

## 4.1 INTRODUCTION

The stress distribution at the chord and the brace intersection of a partially overlapped CHS K-joint is complex and non-uniform. Hence, it is almost impossible to obtain the analytical solutions of the stress distribution at the joint intersection. To determine the stress distribution at the tubular joint, two methods are usually used. They are the experimental investigation and the FE method. The experimental investigation of a full-scale specimen with practical size of weld is the most appropriate method to determine the stress concentration of any type of tubular joint. However, experimental investigation is too expensive due to the high cost of fabricating a large capacity test rig and specimens, especially when it comes to studying the partially overlapped CHS K-joints with various geometrical parameters and load conditions. As a result, the FE method becomes the most widely used technique for modelling tubular joint to determine the stress distribution. In the current study, three full-scale partially CHS K-joints tested have been carried out for a purpose of verifying the FE model in predicting the SCF results.

In this chapter, the influence of geometrical parameters on the SCF of partially overlapped CHS K-joints is investigated. The partially overlapped CHS K-joints are subjected to AX and IPB. All the FE models are generated by using a mesh generator developed by Nguyen [65]. For all FE models, the boundaries, loading conditions and material properties are assigned as the tested specimens as described in Chapter 3. The analyses have been conducted by using the FE program ABAQUS [70].

In addition, in this chapter parametric SCF equations are also developed for fatigue

design of partially overlapped CHS K-joints as a first attempt to achieve the time and cost savings. Although the FE mesh generator developed by Nguyen [65] could successfully be used as a reliable numerical tool for modelling and analyzing partially overlapped CHS K-joints with various geometrical properties and load conditions, the use of such method in normal day-to-day design office operation still seems to be unfeasible as at least 90 minutes are needed for data preparation, running and post processing to get a complete set of SCF values for one partially overlapped CHS K-joint. In addition, the users are needed to be familiar with ABAQUS [70] and all those procedures related to the FE mesh generator.

## 4.2 MESH GENERATION FOR PARTIALLY OVERLAPPED CHS K-JOINTS

A mesh generator developed by Nguyen [65] has been used in the current research to carry out a large scale parametric study. A detail about mesh generation procedure for partially overlapped CHS K-joints can be found in [65]. Hence, in this study only a short summary is given. In this mesh generation procedure, a surface mesh is firstly created with different element size densities which are used in different parts of the joint to accurately model the geometry for the connection. The whole structure is divided into several zones. An adaptive surface mesh generator [78] was applied to discretize these zones into surface meshes as shown in Figure 4.1. During the discretization of all zones, triangular elements are mainly generated (Figure 4.1a), while the quadrilateral elements are used at where the welding is applied the corresponding CHS as to connect the respective zones (Figure 4.1b).

The surface mesh is converted into a solid mesh by connecting corresponding nodes on respective boundary surfaces using an algorithm to relate the nodal connectivity [79]. The entire joint is divided into four sub-spaces: the outer space (Space 1) and the inner space (Space 2) for the chord, the through brace (Space 3) and the overlapping brace (Space 4) as shown in Figure 4.2b.

Finally, the weld profile is added into the extruded solid mesh to form mesh with welding as shown in Figure 4.2c. The common area of all the welds is filled up by tetrahedron elements as shown in Figure 4.2d. As mentioned earlier in Chapter 3, the FE modelling models created were verified to be accurate and reliable. As a result, a parametric study using the proposed techniques can be carried out with confidence.

## 4.3 RANGE OF GEOMETRICAL PARAMETERS AND LOAD CASES

### 4.3.1 Range of Geometrical Parameters

In this current study, the range of geometrical parameters has been taken within the range of validity available for partially overlapped CHS K-joints subjected to static loading [80] since so far there no range and no formula for partially overlapped CHS K-joints subjected to cyclic loading is given in the CIDECT guides [5]. The ranges of the current study are shown in Table 4.1. Note that due to time limitation of the current study, only partially overlapped CHS K-joint having through brace and overlapping brace with same diameters and the same intersecting angles between chord and brace are considered.

The numbers of numerical cases analyzed in this study are also tabulated in Table 4.1. Basically, five parameters ($\theta$, Ov,$\beta$, $\gamma$ and $\tau$) are included in the parametric study. Therefore, the total numbers of the numerical models are equal to $5 \times 5 \times 7 \times 5 \times 4 = 3500$. From the last column of Table 4.1, it can be seen that the intervals of $\tau$ for each $\gamma$ are different. This is because they are selected to tidy to the CHS dimensions commonly used in practice. These ranges of study are used for creating a set of new regression equations and new method which is based on interpolation method and would be described in Chapter 5.

It is important to note that the number is manageable for two reasons: (i) Automatic mesh generation program were special created (by the PhD works of another student) and (ii) Special management Marco program were also created to organize the results. In fact, for interpolation method applied more databases are needed and welcome. The more data be supplied, the high accurate results can be obtained. However, due to time limitation 3500 models are the scope of the current research.

### 4.3.2 Load Cases

The load cases were selected to reflect all possible loads happened in reality. Due to the geometry asymmetry of partially overlapped CHS K-joints, loads were applied in both through brace and overlapping brace. Six different basic load cases were used in this study, namely the AX11, IPB11 and the IPB12 load cases applied at the end of through brace and the AX21, IPB21 and the IPB22 load cases applied at the end of overlapping brace of each model, as shown in Figure 4.2.

## 4.4 VARIATION OF SCF WITH RESPECT TO $\beta$

### 4.4.1 Variation of SCFs with respect to $\beta$ and $\gamma$

In this section, the variation of the SCF for partially overlapped CHS K-joints is studied by varying the parameters $\beta$ (from 0.4 to 1.0 in step of 0.1) and $\gamma$ (6.83, 8.53, 11.38 and 17.06). It is observed that the trends of the SCF curves of $\beta$ versus $\gamma$ are similar for the AX11 and the AX21 load cases. In addition, the trends of the SCF curves of $\beta$ versus $\gamma$ are similar for the IPB11, IPB12, IPB21 and the IPB22 load cases. Therefore, in further descriptions for the SCF curves of $\beta$ versus $\gamma$, the AX11 and the AX21 load cases are combined together and are represented by the AX11 load case only. Similarly, the IPB11, IPB12, IPB21 and the IPB22 load cases are also combined together and are represented by the IPB11 load case only. The SCF curves of $\beta$ versus $\gamma$

for the AX11 and the IPB11 load cases are shown in Figures 4.4 and 4.5, respectively. The following results from these figures are specifically noted.

*AX load cases (AX11 and AX21)*

- The maximum SCFs for the chord and the braces occur at the saddle of the sections.
- Values of SCF increase with the increase of $\gamma$.
- In general, values of SCF slightly decrease with the increase of $\beta$.

*IPB load cases (IPB11, IPB12, IPB21 and IPB22)*

- The maximum SCFs for the chord and the braces occur at the crown heel of the sections.
- Values of SCF increase with the increase of $\gamma$.
- In general, values of SCF slightly decrease with the increase of $\beta$.

### 4.4.2 Variation of SCFs with respect to $\beta$ and $\tau$

In this section, the variation of the SCF for partially overlapped CHS K-joints is studied by varying the parameters $\beta$ (from 0.4 to1.0 with step of 0.1) and $\tau$ (0.24, 0.32, 0.48, 0.64, 0.8 and 1.00). It is observed that the trends of the SCF curves of $\beta$ versus $\tau$ are similar for the AX11 and the AX21 load cases. In addition, the trends of the SCF curves of $\beta$ versus $\tau$ are similar for the IPB11, IPB12, IPB21 and the IPB22 load cases. Therefore, in further descriptions for the SCF curves of $\beta$ versus $\tau$, the AX11 and the AX21 load cases are combined together and are represented by the AX11 load case only. Similarly, the IPB11, IPB12, IPB21 and the IPB22 load cases are also combined together and are represented by the IPB11 load case only. The SCF curves of $\beta$ versus $\tau$ for the AX11 and the IPB11 load cases are shown in Figures 4.6 and 4.7, respectively. The following results from these figures are specifically noted.

*AX load cases (AX11 and AX21)*

- The maximum SCFs for the chord and the braces occur at the saddle of the sections.
- Values of SCF increase with the increase of $\tau$.
- In general, values of SCF slightly decrease with the increase of $\beta$.

*IPB load cases (IPB11, IPB12, IPB21 and IPB22)*

- The maximum SCFs for the chord and the braces occur at the crown heel of the sections.
- Values of SCF increase with the increase of $\tau$.
- In general, values of SCF slightly decrease with the increase of $\beta$.

## 4.5 VARIATION OF SCF WITH RESPECT TO $\theta$

### 4.5.1 Variation of SCFs with respect to $\theta$ and $\gamma$

In this section, the variation of the SCF for partially overlapped tubular joints is studied by varying the parameters $\theta$ (30º, 40º, 45º, 50º, 60º) and $\gamma$ (5.46, 8.53, 11.38). It is observed that the trends of the SCF curves of $\theta$ versus $\gamma$ are similar for the AX11 and the AX21 load cases. In addition, the trends of the SCF curves of $\theta$ versus $\gamma$ are similar for the IPB11, IPB12, IPB21 and the IPB22 load cases. Therefore, in further descriptions for the SCF curves of $\theta$ versus $\gamma$, the AX11 and the AX21 load cases are combined together and are represented by the AX11 load case only. Similarly, the IPB11, IPB12, IPB21 and the IPB22 load cases are also combined together and are represented by the IPB11 load case only. The SCF curves of $\theta$ versus $\gamma$ for the AX11 and the IPB11 load cases are shown in Figures 4.8 and 4.9, respectively. The following results from these figures are specifically noted.

*AX load cases (AX11 and AX21)*

- The maximum SCFs for the chord and the braces occur at the saddle of the sections.
- Values of SCF increase with the increase of $\gamma$.
- Values of SCF slightly increase with the increase of $\theta$.

*IPB load cases (IPB11, IPB12, IPB21 and IPB22)*

- The maximum SCFs for the chord and the braces occur at the crown heel of the sections.
- Values of SCF increase with the increase of $\gamma$.
- In general, values of SCF slightly increase with the increase of $\theta$.

### 4.5.2 Variation of SCFs with respect to $\theta$ and $\tau$

In this section, the variation of the SCF for partially overlapped CHS K-joints is studied by varying the parameters $\theta$ (40º, 45º, 50º, and 60º) and $\tau$ (0.24, 0.32, 0.48, 0.64, 0.8 and 1.00). It is observed that the trends of the SCF curves of $\theta$ versus $\tau$ are similar for the AX11 and the AX21 load cases. In addition, the trends of the SCF curves of $\theta$ versus $\tau$ are similar for the IPB11, IPB12, IPB21 and the IPB22 load cases. Therefore, in further descriptions for the SCF curves of $\theta$ versus $\tau$, the AX11 and the AX21 load cases are combined together and are represented by the AX11 load case only. Similarly, the IPB11, IPB12, IPB21 and the IPB22 load cases are also combined together and are represented by the IPB11 load case only. The SCF curves of $\theta$ and $\tau$ for the AX11 and the IPB11 load cases are shown in Figures 4.10 and 4.11, respectively. The following results from these figures are specifically noted.

*AX load cases (AX11 and AX21)*

- The maximum SCFs for the chord and the braces occur at the saddle of the sections.
- Values of SCF increase with the increase of $\tau$.
- Values of SCF slightly increase with the increase of $\theta$.

*IPB load cases (IPB11, IPB12, IPB21 and IPB22)*

- The maximum SCFs for the chord and the braces occur at the crown heel of the sections.
- Values of SCF increase with the increase of $\tau$.
- In general, values of SCF slightly increase with the increase of $\theta$.

## 4.6 VARIATION OF SCF WITH RESPECT TO Ov

### 4.6.1 Variation of SCFs with respect to Ov and $\gamma$

In this section, the variation of the SCF for partially overlapped tubular joints is studied by varying the parameters Ov (25, 40, 50, 60 and 75%) and $\gamma$ (5.46, 8.53 and 11.38). It is observed that the trends of the SCF curves of Ov versus $\gamma$ are similar for the AX11 and the AX21 load cases. In addition, the trends of the SCF curves of Ov versus $\gamma$ are similar for the IPB11, IPB12, IPB21 and the IPB22 load cases. Therefore, in further descriptions for the SCF curves of Ov versus $\gamma$, the AX11 and the AX21 load cases are combined together and are represented by the AX11 load case only. Similarly, the IPB11, IPB12, IPB21 and the IPB22 load cases are also combined together and are represented by the IPB11 load case only. The SCF curves of Ov versus $\gamma$ for the AX11 and the IPB11 load cases are shown in Figures 4.12 and 4.13, respectively. The following results from these figures are specifically noted.

*AX load cases (AX11 and AX21)*

- The maximum SCFs for the chord and the braces occur at the saddle of the sections.
- Values of SCF increase with the increase of $\gamma$.
- In general, values of SCF slightly decrease with the increase of Ov.

*IPB load cases (IPB11, IPB12, IPB21 and IPB22)*

- The maximum SCFs for the chord and the braces occur at the crown heel of the sections.
- Values of SCF increase with the increase of $\gamma$.
- In general, values of SCF slightly decrease with the increase of Ov.

### 4.6.2 Variation of SCFs with respect to Ov and $\tau$

In this section, the variation of the SCF for partially overlapped CHS K-joints is studied by varying the parameters Ov (25, 40, 50, 60 and 75%) and $\tau$ (0.24, 0.32, 0.64 and 1.00). It is observed that the trends of the SCF curves of Ov versus $\tau$ are similar for the AX11 and the AX21 load cases. In addition, the trends of the SCF curves of Ov versus $\tau$ are similar for the IPB11, IPB12, IPB21 and the IPB22 load cases. Therefore, in further descriptions for the SCF curves of Ov versus $\tau$, the AX11 and the AX21 load cases are combined together and are represented by the AX11 load case only. Similarly, the IPB11, IPB12, IPB21 and the IPB22 load cases are also combined together and are represented by the IPB11 load case only. The SCF curves of Ov and $\tau$ under the AX11 and the IPB11 load cases are shown in Figures 4.14 and 4.15, respectively. The following results from these figures are specifically noted.

*AX load cases (AX11 and AX21)*

- The maximum SCFs for the chord and the braces occur at the saddle of the sections.

- Values of SCF increase with the increase of $\tau$.
- In general, values of SCF decrease with the increase of Ov.

*IPB load cases (IPB11, IPB12, IPB21 and IPB22)*

- The maximum SCFs for the chord and the braces occur at the crown heel of the sections.
- Values of SCF increase with the increase of $\tau$.
- In general, values of SCF decrease with the increase of Ov.

From the all above-mentioned investigation of the geometrical parameters, it is found that all parameters: $\beta$, $\theta$, Ov, $\gamma$ and $\tau$ have a large impact on the SCF values of partially overlapped CHS K-joints subjected to the AX and the IPB load cases. It is observed that the SCF values increase generally with the increase of $\gamma$, $\tau$ and $\theta$, but as Ov or $\beta$ increases, the SCF values decrease. Therefore, all these parameters have been taken into account in formation of the SCF regression equations.

## 4.7 SCF DATABASE GENERATED FROM NUMERICAL MODELS

The SCF results obtained from these 3500 models are employed to create a database. The Figure 4.16 shows part of the database and its storage format. In this database, the geometrical parameters ($\theta$, Ov, $\beta$, $\gamma$ and $\tau$) are complied together with the maximum SCF values occurred on the weld toe of the chord and the braces for all the 6 loading cases: AX11, IPB11, IPB12, AX21, IPB21 and IPB22 (see Figures 4.3 and 4.17b). As shown in Figure 4.17b, there are totally 16 peak SCFs from each partially overlapped CHS K-joint model, 6 data from the through brace, 6 data from the overlapping brace and 4 data from the chord. The total numbers of data are therefore $16 \times 3500 = 56000$ SCF values. By properly using this database, the four combined load cases, namely AX11+IPB11, AX11+IPB12, AX21+IPB21 and AX21+IPB22, could be studied.

The 16 peak SCF values listed in Table 4.2 and Figures 4.16 and 4.17, e.g. AX11tA, AX11oA, AX11tC, AX11cC and etc, were named following their load cases name, member name and curves name. The locations of the Curves A, B and C are shown in Figure 4.17. Curve A is along the weld toe between through brace and overlapping brace, Curve B is along the weld toe between overlapping brace and chord, and finally Curve C is along between through brace and chord. Members of partially overlapped K-joint are chord "c", through brace "t" and overlapping brace "o". For example, AX11cC is the maximum SCF under AX11 on the weld toe of chord along Curve C, and AX11tC is the maximum SCF under AX11 on the weld toe of through brace along Curve C (see more details in Table 4.2 and Figures 4.16 and 4.17). It can be seen from Table 4.2 and these figures, for the AX11 load case four SCFs (AX11tA, AX11oA, AX11tA and AX11cC) are recorded, even though the AX11tA and the AX11oA are not the maximum SCF values for the AX11 load case. Similarly, from the AX21 load case four SCFs (AX21oA, AX21tA, AX22oB and AX22cB) are recorded, even though the AX21oA and the AX21tA are also not the maximum SCF values for the AX21 load case (see Figure 4.17). Their SCF values are recorded as their values will be useful to improve the accuracy of the estimation for the HSS of some combined load cases (e.g. AX11+IPB12 and AX21+IPB22).

## 4.8 PARAMETRIC REGRESSION ANALYSIS

A non-linear regression curve fitting program, DataFit [81], is adopted in the current study for the development of SCF parametric equations. In each parametric equation, five parameters, namely F1, F2, F3, F4 and F5, are involved. The parameter F1 takes into account the influence of overlap ratio of CHS K joint. The parameter F2 considers the influence of intersecting angle between the chord and the brace. F3 considers influence of brace to chord diameter ratio. F4 considers the influence of chord radius to wall thickness ratio and F5 considers the influence of brace to chord wall thickness ratio. The regression models are expressed as:

$$SCF_{brace} = F1_b + F2_b + F3_b + F4_b + F5_b + f_b \quad (4.1)$$

$$SCF_{chord} = F1_c + F2_c + F3_c + F4_c + F5_c \quad (4.2)$$

where $F1_b = a_b \times Ov$, $F2_b = b_b \times \theta$, $F3_b = c_b \times \beta$, $F4_b = d_b \times \gamma$, $F5_b = e_b \times \tau$, $F1_c = a_c \times Ov$, $F2_c = b_c \times \theta$, $F3_c = c_c \times \beta$, $F4_{bc} = d_c \times \gamma$ and $F5_c = e_c \times \tau$. Coefficients: $a_b$, $b_b$, $c_b$, $d_b$, $e_b$, $f_b$, $a_c$, $b_c$, $c_c$, $d_c$ and $e_c$ are obtained from the Data Fit analysis results.

All these functions of the above parameters are included in the regression models. The regression models and the SCF obtained from FE analysis are input as data into the fitting program DataFit [81]. It should be noted that DataFit utilizes the Levenber-Marquardt method with double precision to perform the non-linear regression analysis. As the regression models are solved, they are automatically sorted according to the best fit criteria of residual sum of squares and the results come out with full regression information. In the present study, the parametric regression equations are derived to predict the maximum SCF at the braces and chord. The equations for each load case are listed in Table 4.4, where there are 16 proposed equations for predicting SCF values in different load cases.

It should be noted that several attempts on adopting the regression models for the parametric equations of partially overlapped CHS K-joint were applied. Firstly, the regression models for the parametric equations of partially overlapped CHS K-joint were adopted similar to the format of Efthymiou SCF parametric equations for partially overlapped K-joint [29]. Secondly, the regression models for the parametric equations of partially overlapped CHS K-joint were adopted similar to the format of DEn SCF parametric equations for the CHS K-joint with gap [26]. Thirdly, the regression models for the parametric equations of partially overlapped CHS K-joint were adopted similar to the format of SCF parametric equations for the rectangular hollow section K-joint with gap found in [82]. It was found that the last attempt provided better results than the first two adopted formats. The SCF values from the first two attempts, however,

turned out to be too conservative when compared with the SCF values from the FE analyses. As a result, the last result was adopted for the parametric equations of partially overlapped CHS K-joint in this chapter.

## 4.9 ASSESSMENT OF THE PROPOSED SCF EQUATIONS

### 4.9.1 P/R Ratio Assessment

The proposed parametric regression SCF equations of this study are assessed against the SCF obtained from the FE analyses of the basic data tabulated in Table 4.1. For this purpose, a program has firstly been developed for calculating the SCFs of partially overlapped CHS K-joints by using the proposed equations based on the *parametric regression method* (PRM). Then, the calculated SCF value obtained from the PRM (referred as the "P" predictions) is compared to the original SCF obtained from the FE analyses (referred as the "R" solutions).

According to the Fatigue Guidance Review Panel recommendation of acceptance criteria for assessment of parametric equations found in [83], the P/R ratio of the joint with different geometrical parameters is concluded, if P/R ratio is equal to unity. The equations are commented to underestimate and overestimate the SCF of the joint if P/R ratios were less and greater than 0.8 and 1.5 respectively.

Table 4.4 shows the detailed assessment information of SCF obtained from the PRM for different loading cases against those obtained from the FE solutions. It is observed that the highest and lowest percentages that fall in the range of $0.8 \leq P/R \leq 1.2$ are 90.28 % and 64.69 %, respectively, with a mean of 74.7 %. However, if compared with the range of acceptance criteria, the highest and lowest percentages that fall in the range of $0.8 \leq P/R \leq 1.5$ are 90.54% and 70.45%, respectively, with a mean of 81.92%. Thus, it could be concluded that the SCFs obtained from the PRM and the SCFs

obtained from the FE analyses results are reasonably accurate.

### 4.9.2 Additional Assessment using Mid-point Models

To evaluate the accuracy of the estimated SCF values obtained from the PRM, 192 numerical mid-point models listed in Table 4.5 are also analyzed. The estimated SCF values obtained from the PRM are compared with the SCF values obtained from the FE solutions with respect to the mid-point models. These mid-point models are created by using geometrical parameters that are corresponding to the mid values of the 3500 models using in the regression analysis. They, to some extend, would able to lead to maximum error for the PRM. For example, the $\beta$ ratios for the mid-point models are 0.45, 0.55, 0.65, 0.75, 0.85 and 0.95, while the $\beta$ ratios for the basic models are 0.4, 0.5, 0.6, 0.7, 0.8, 0.9 and 1.0, and the same principle was applied to other parameters. The relative error ($E_{PRM\text{-}FEM}(SCF)$) between estimated SCF values obtained from the PRM and the FE analyses obtained for the mid-point data tabulated in Table 4.6 is defined as:

$$E_{PRM-FEM}(SCF) = \frac{SCF_{PRM} - SCF_{FEM}}{SCF_{PRM}} \times 100\% \qquad (4.3)$$

where $SCF_{PRM}$ is the SCF value obtained from the PRM, and $SCF_{FEM}$ is SCF value obtained from the FE analyses.

Figures 4.18 to 4.23 and Table 4.6 show the statistics of the numbers of numerical models in different relative error ranges for different loading cases. From these figures and Table 4.6, it is found that the highest and lowest percentages, that fall in the range of $-20\% \le E_{PRM\text{-}FEM}(SCF) \le 20\%$, are 94.08% and 44.74%, respectively, with mean of 79.45%. The PRM appears to be overestimate in the AX11 and the AX21 loading cases with the percentage of errors of 54.61% and 26.32%, respectively.

It is observed that the SCFs for IPB are apparently the most accurate one, both from finite element analyses and experimental tests results. However in Figure 4.20, between

the estimated SCF values obtained from PRM and FE analyses mid-point data. This could be due to the interpolation nature of the PRM. The trend of the PRM seems to be straight line which does not reflect the SCF nature of the partially overlapped CHS K-joints. The PIM and LIM are going to develop to cover the weakness of the PRM.

## 4.10 CONCLUDING REMARKS

The assessment of current proposed parametric equations for partially overlapped CHS K-joints with respect to the basic SCF database of FE models seems to satisfy the criteria of Fatigue Guidance Review Panel. The assessment results seem to confirm the reliability of these equations for predicting the SCF of partially overlapped CHS K-joints under basic load cases. However, it is observed that the SCFs obtained from the PRM do not fit well with the SCF obtained from the FE analyses when it comes to the 192 additional mid-point models which have no contribution in proposing the equations. It seems to be an obvious disadvantage of parametric equations when predicting the SCFs of partially overlapped CHS K-joint.

Table 4.1 Range of geometrical parameters of basic data (3500 models)

| Models | $\theta$ | Ov | $\beta$ | $\gamma$ | $\tau$ |
|---|---|---|---|---|---|
| Case 1 | 30° | 0.25, 0.4, 0.5, 0.6, 0.75 | 0.4, 0.5, 0.6, 0.7, 0.8, 0.9, 1.0 | 17.06 | 0.65, 0.75, 0.85, 1.00 |
| | | | | 11.38 | 0.50, 0.60, 0.80, 1.00 |
| | | | | 8.53 | 0.38, 0.50, 0.75, 1.00 |
| | | | | 6.83 | 0.30, 0.60, 0.80,1.00 |
| | | | | 5.46 | 0.32 , 0.64, 0.80, 1.00 |
| Case 2 | 40° | 0.25, 0.4, 0.5, 0.6, 0.75 | 0.4, 0.5, 0.6, 0.7, 0.8, 0.9, 1.0 | 17.06 | 0.65, 0.75, 0.85, 1.00 |
| | | | | 11.38 | 0.50, 0.60, 0.80, 1.00 |
| | | | | 8.53 | 0.38, 0.50, 0.75, 1.00 |
| | | | | 6.83 | 0.30, 0.60, 0.80,1.00 |
| | | | | 5.46 | 0.32 , 0.64, 0.80, 1.00 |
| Case 3 | 45° | 0.25, 0.4, 0.5, 0.6, 0.75 | 0.4, 0.5, 0.6, 0.7, 0.8, 0.9, 1.0 | 17.06 | 0.65, 0.75, 0.85, 1.00 |
| | | | | 11.38 | 0.50, 0.60, 0.80, 1.00 |
| | | | | 8.53 | 0.38, 0.50, 0.75, 1.00 |
| | | | | 6.83 | 0.30, 0.60, 0.80,1.00 |
| | | | | 5.46 | 0.32 , 0.64, 0.80, 1.00 |
| Case 4 | 50° | 0.25, 0.4, 0.5, 0.6, 0.75 | 0.4, 0.5, 0.6, 0.7, 0.8, 0.9, 1.0 | 17.06 | 0.65, 0.75, 0.85, 1.00 |
| | | | | 11.38 | 0.50, 0.60, 0.80, 1.00 |
| | | | | 8.53 | 0.38, 0.50, 0.75, 1.00 |
| | | | | 6.83 | 0.30, 0.60, 0.80,1.00 |
| | | | | 5.46 | 0.32 , 0.64, 0.80, 1.00 |
| Case 5 | 60° | 0.25, 0.4, 0.5, 0.6, 0.75 | 0.4, 0.5, 0.6, 0.7, 0.8, 0.9, 1.0 | 17.06 | 0.65, 0.75, 0.85, 1.00 |
| | | | | 11.38 | 0.50, 0.60, 0.80, 1.00 |
| | | | | 8.53 | 0.38, 0.50, 0.75, 1.00 |
| | | | | 6.83 | 0.30, 0.60, 0.80,1.00 |
| | | | | 5.46 | 0.32 , 0.64, 0.80, 1.00 |

Table 4.2 Definition of database

| ID | SCF Names | Maximum SCF values: |
|---|---|---|
| 1 | AX11tA | under AX11 load case on the weld toe of through brace along Curve A |
| 2 | AX11oA | under AX11 load case on the weld toe of overlapping brace along Curve A |
| 3 | AX11tC | under AX11 load case on the weld toe of through brace along Curve C |
| 4 | AX11cC | under AX11 load case on the weld toe of chord along Curve C |
| 5 | AX21oA | under AX21 load case on the weld toe of overlapping brace along Curve A |
| 6 | AX21tA | under AX21 load case on the weld toe of through brace along Curve A |
| 7 | AX21oB | under AX21 load case on the weld toe of overlapping brace along Curve B |
| 8 | AX21cB | under AX21 load case on the weld toe of chord along Curve A |
| 9 | IPB11tC | under IPB11 load case on the weld toe of through brace along Curve C |
| 10 | IPB11cC | under IPB11 load case on the weld toe of chord along Curve C |
| 11 | IPB12tA | under IPB12 load case on the weld toe of through brace along Curve A |
| 12 | IPB12oA | under IPB12 load case on the weld toe of overlapping brace along Curve A |
| 13 | IPB21oB | under IPB21 load case on the weld toe of overlapping brace along Curve B |
| 14 | IPB21cB | under IPB21 load case on the weld toe of chord along Curve B |
| 15 | IPB22oA | under AX11 load case on the weld toe of overlapping brace along Curve C |
| 16 | IPB22tA | under IPB22 load case on the weld toe of through brace along Curve A |

Table 4.3 Parametric regression equations for overlapped CHS K-joints

| SCF names | SCF parametric equations |
|---|---|
| AX11tA<br>AX11oA | Though brace SCF:<br>$-0.0205\times Ov - 3.5569 \times \sin(\theta) + 0.4793 \times \beta + 0.096 \times \gamma - 0.9326 \times \tau + 3.61$<br>Overlapping SCF:<br>$1.819 \times Ov - 1.788 \times \sin(\theta) + 2.2778 \times \beta - 0.0735 \times \gamma + 1.76 \times \tau$ |
| AX11tC<br>AX11cC | Through brace SCF:<br>$-2.089 \times Ov + 6.036 \times \sin(\theta) - 1.883 \times \beta + 0.1608 \times \gamma + 1.657 \times \tau - 0.267$<br>Chord SCF:<br>$-2.163 \times Ov + 5.836 \times \sin(\theta) - 1.959 \times \beta + 0.16 \times \gamma + 1.622 \times \tau$ |
| IPB11tC<br>IPB11cC | Through brace SCF:<br>$-1.541 \times Ov + 2.793 \times \sin(\theta) + 1.017 \times \beta + 0.181 \times \gamma - 1.929 \times \tau + 3.66$<br>Chord SCF:<br>$-2.491 \times Ov - 0.458 \times \sin(\theta) - 0.703 \times \beta + 0.35 \times \gamma + 3.625 \times \tau$ |
| IPB12tA<br>IPB12oA | Through brace SCF:<br>$0.255 \times Ov + 5.179 \times \sin(\theta) + 2.002 \times \beta + 0.246 \times \gamma - 0.354 \times \tau - 4.56$<br>Overlapping brace SCF:<br>$0.65 \times Ov - 0.152 \times \sin(\theta) + 2.371 \times \beta + 0.16 \times \gamma + 0.357 \times \tau$ |
| AX21oA<br>AX21tA | Overlapping brace SCF:<br>$3.167 \times Ov - 4.099 \times \sin(\theta) + 2.581 \times \beta + 0.088 \times \gamma - 2.757 \times \tau + 4.944$<br>Through brace SCF:<br>$3.025 \times Ov - 2.252 \times \sin(\theta) + 7.665 \times \beta + 0.333 \times \gamma - 4.111 \times \tau$ |
| AX21oB<br>AX21cB | Overlapping brace SCF:<br>$-3.847 \times Ov + 2.615 \times \sin(\theta) - 2.454 \times \beta + 0.095 \times \gamma + 1.718 \times \tau + 3.181$<br>Chord SCF:<br>$-2.143 \times Ov + 0.859 \times \sin(\theta) - 2.162 \times \beta + 0.489 \times \gamma + 1.614 \times \tau$ |
| IPB21oB<br>IPB21cB | Overlapping brace SCF:<br>$-0.482 \times Ov - 2.042 \times \sin(\theta) + 2.846 \times \beta + 0.242 \times \gamma - 4.327 \times \tau + 7.602$<br>Chord SCF:<br>$-2.192 \times Ov - 1.414 \times \sin(\theta) - 0.197 \times \beta + 0.391 \times \gamma + 3.876 \times \tau$ |
| IPB22oA<br>IPB22tA | Overlapping brace SCF:<br>$2.955 \times Ov + 7.682 \times \sin(\theta) + 3.406 \times \beta + 0.271 \times \gamma - 1.683 \times \tau - 6.189$<br>Through brace SCF:<br>$0.884 \times Ov - 0.229 \times \sin(\theta) + 5.827 \times \beta + 0.398 \times \gamma - 3.871 \times \tau$ |

Table 4.4 Assessment of the proposed SCF regression equations against the SCF obtained from the FE analyses based on ranges of P/R

| Percentage of models in different ranges of P/R (%) | | | | |
|---|---|---|---|---|
| Load Cases | Members | Frequency of occurrence of SCF P/R | | |
| | | < 0.8 | 0.8↔1.2 | >1.2 |
| AX11 | Though brace | 4.17 | 73.88 | 21.94 |
| | Chord | 4.97 | 64.19 | 30.83 |
| AX21 | Overlapping brace | 3.29 | 65.00 | 31.71 |
| | Chord | 3.40 | 69.90 | 26.80 |
| IPB11 | Though brace | 2.57 | 79.77 | 17.66 |
| | Chord | 4.20 | 70.98 | 24.77 |
| IPB12 | Though brace | 3.48 | 78.76 | 17.75 |
| | Overlapping brace | 1.29 | 73.13 | 25.58 |
| IPB21 | Overlapping brace | 1.20 | 77.31 | 20.49 |
| | Chord | 3.23 | 71.88 | 24.89 |
| IPB22 | Overlapping brace | 3.97 | 81.36 | 14.66 |
| | Though brace | 1.09 | 90.28 | 7.63 |

Table 4.5 Range of geometrical parameters of 192 mid-point models

| Models | $\theta$ | Ov | $\beta$ | $\gamma$ | $\tau$ |
|---|---|---|---|---|---|
| Case 1 | 35° | 0.35, 0.45, 0.55, 0.65 | 0.45, 0.55, 0.66, 0.75, 0.85, 0.95 | 13.65 | 0.6, 0.63 |
| | | | | 9.75 | 0.71, 0.86 |
| Case 2 | 55° | 0.35, 0.45, 0.55, 0.65 | 0.45, 0.55, 0.66, 0.75, 0.85, 0.95 | 13.65 | 0.6, 0.63 |
| | | | | 9.75 | 0.71, 0.86 |

Table 4.6 Assessment of the proposed regression SCF equations against the SCF obtained from the FE analyses results based on relative error ($E_{PRM\text{-}FEM}(SCF)$)

| Percentage of models in different ranges of relative error (%) | | | | |
|---|---|---|---|---|
| Load Cases | Members | Frequency of occurrence of SCF relative error (%) | | |
| | | < -20.00 | -20.00 ↔ 20.00 | > 20.00 |
| AX11 | Through brace | 1.97 | 92.11 | 7.24 |
| | Chord | 0.66 | 44.74 | 54.61 |
| AX21 | Overlapping brace | 5.26 | 68.42 | 26.32 |
| | Chord | 9.21 | 85.53 | 5.92 |
| IPB11 | Through brace | 7.89 | 87.50 | 5.26 |
| | Chord | 23.68 | 69.08 | 10.53 |
| IPB12 | Through brace | 5.92 | 88.16 | 5.92 |
| | Overlapping brace | 6.58 | 88.16 | 5.26 |
| IPB21 | Overlapping brace | 8.55 | 85.53 | 5.92 |
| | Chord | 13.03 | 69.21 | 17.76 |
| IPB22 | Overlapping brace | 3.95 | 80.92 | 15.13 |
| | Through brace | 4.61 | 94.08 | 1.32 |

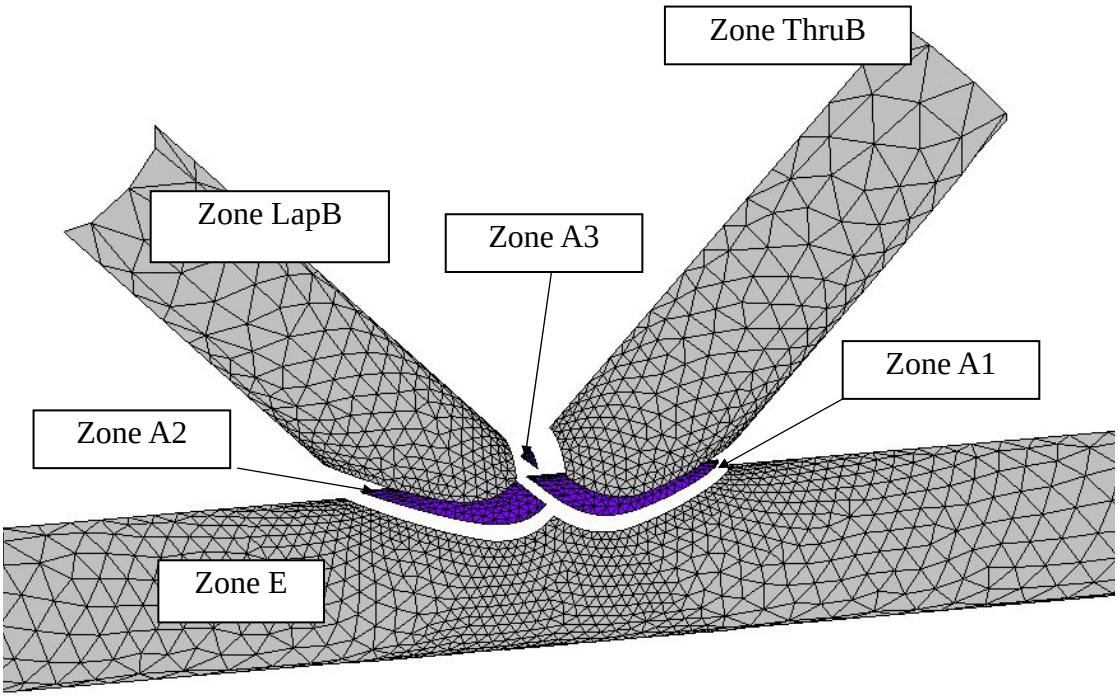


(a) Various Zones in surface mesh extracted from Figure 4.3 [65]

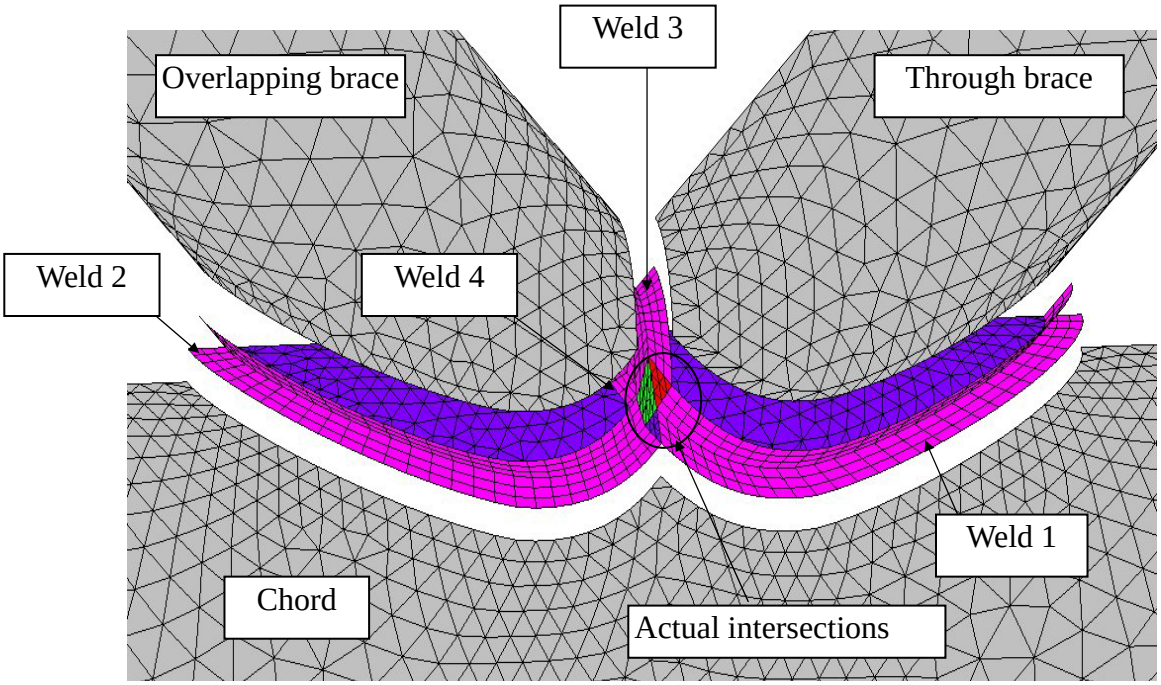


(b) Surface mush with quadrilaterals in weld positions extracted from Figure 4.4 [65]

Figure 4.1 Surface mesh of a partially overlapped CHS K-joint

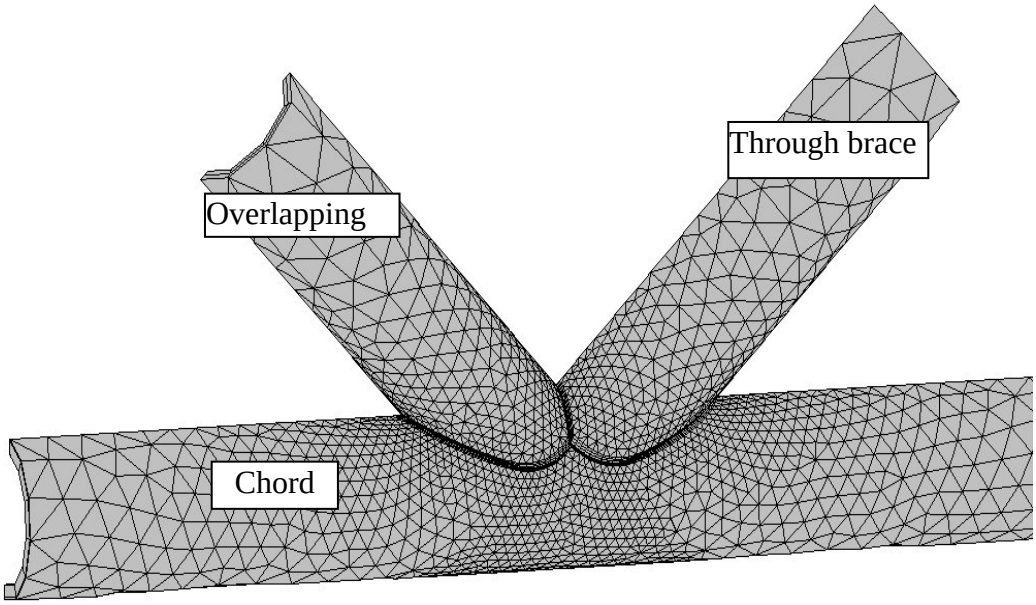


(a) Extruded solid mesh extracted from Figure 4.7 [65]

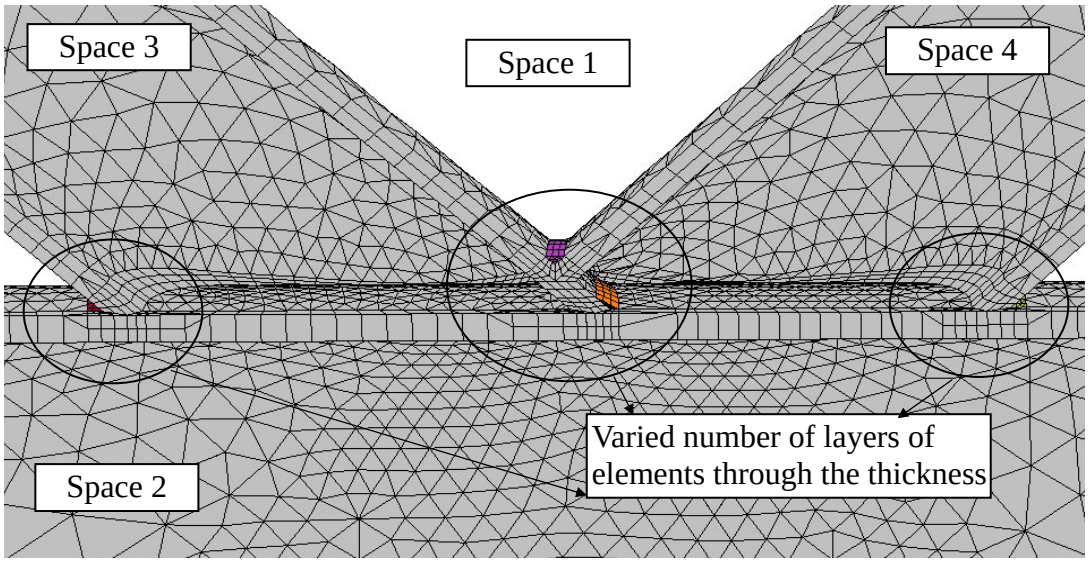


(b) Different number of layers of element along the thickness of the CHS K-joint extracted from Figure 4.8 [65]

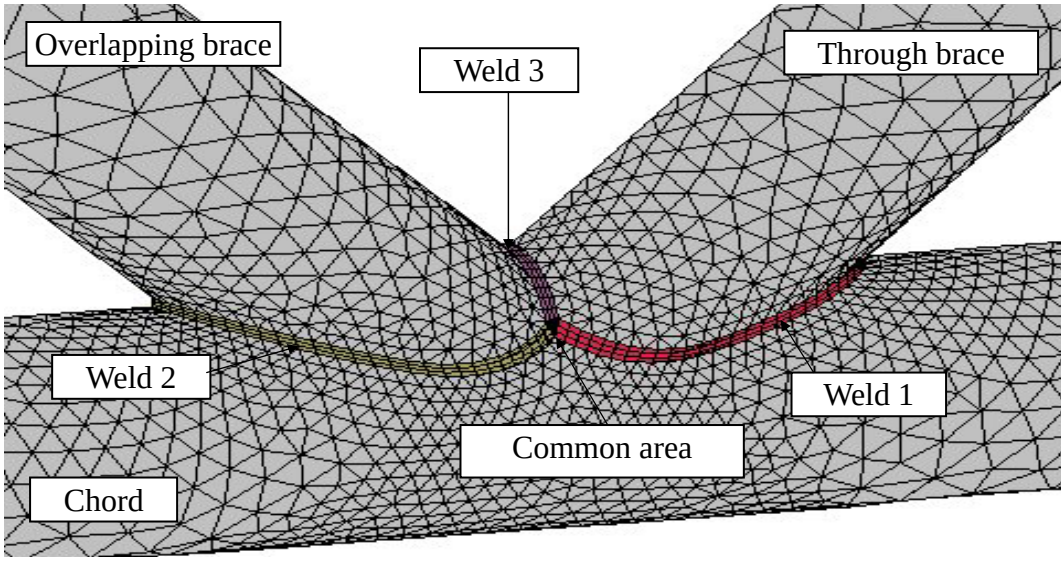


(c) Extruded solid mesh with welding details extracted from Figure 4.9 [65]

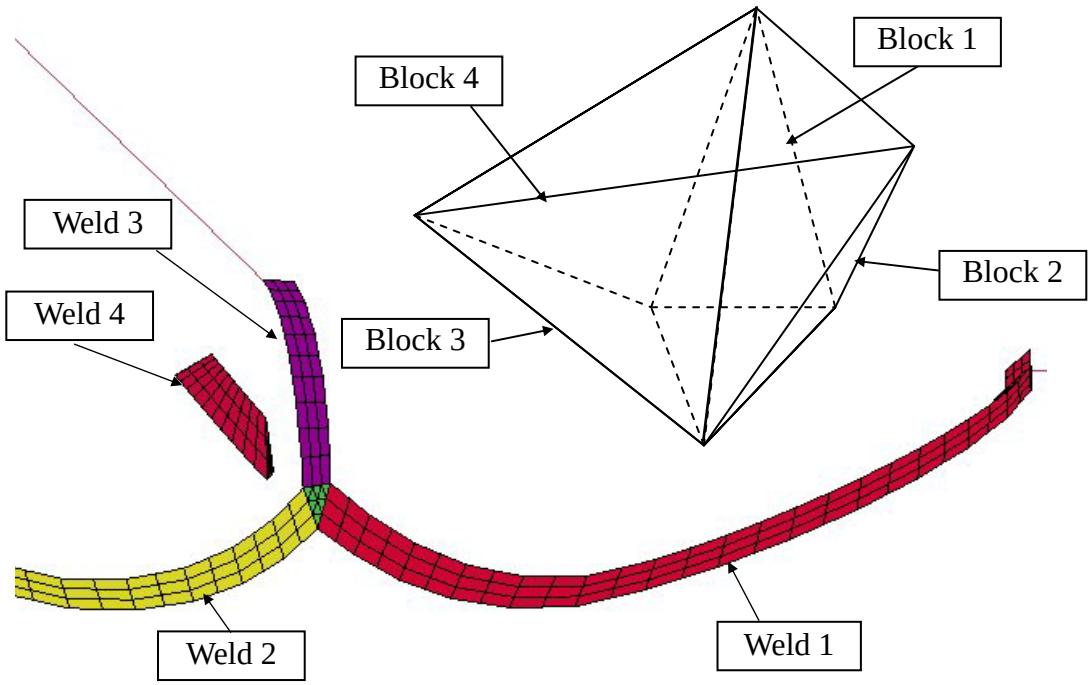


(d) Close up of the common area extracted from Figure 4. 11 [65]

Figure 4.2 Solid mesh of a partially overlapped CHS K-joint

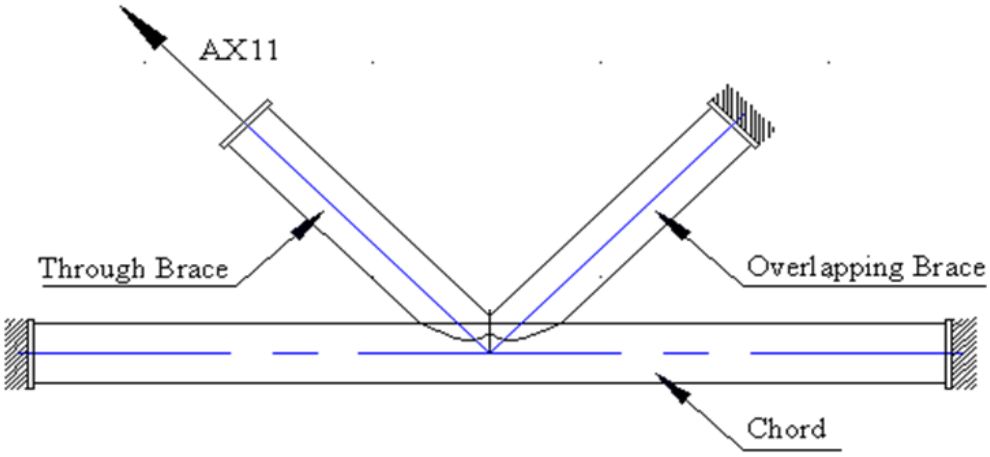


a) Case 1: AX11 load case

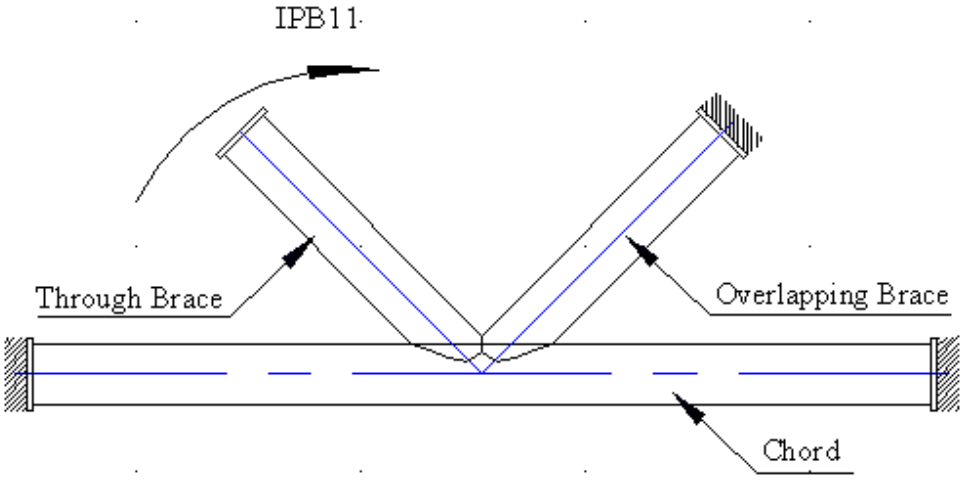


b) Case 2: IPB11 load case

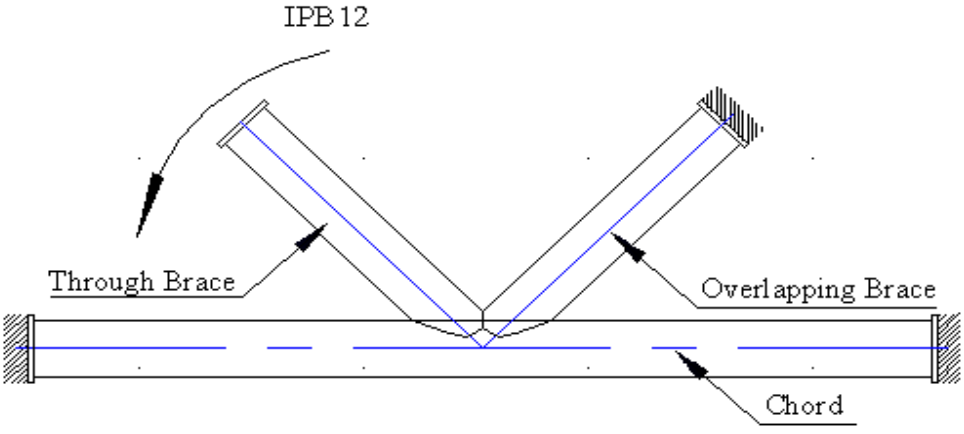


c) Case 3: IPB12 load case

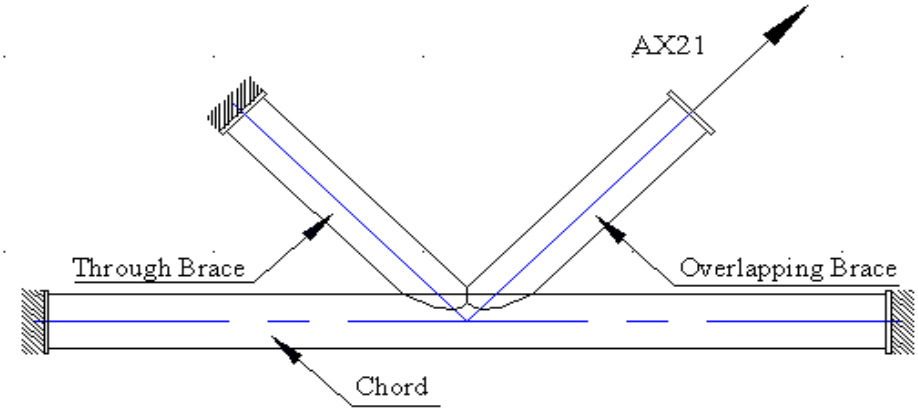


d) Case 4: AX21 load case

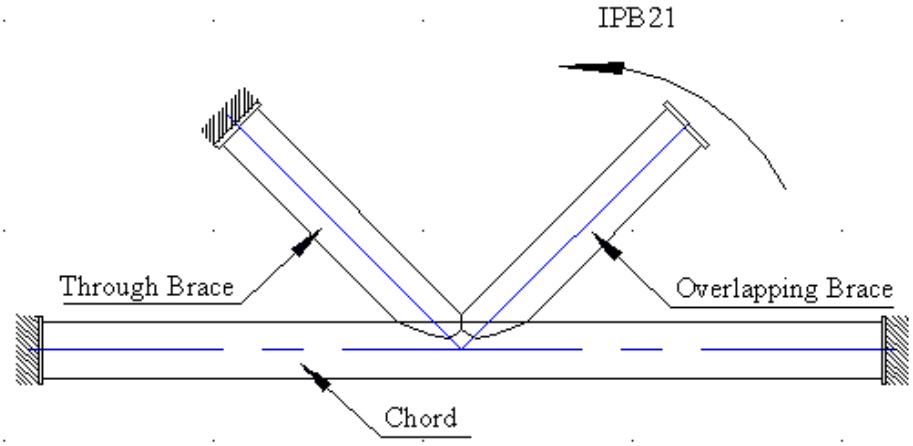


e) Case 5: IPB21 load case

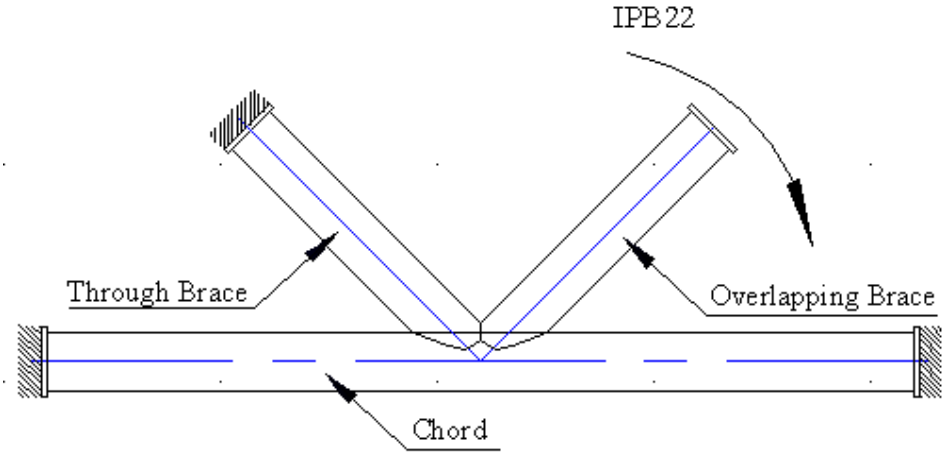


f) Case 6: IPB22 load case

Figure 4.3 Load cases

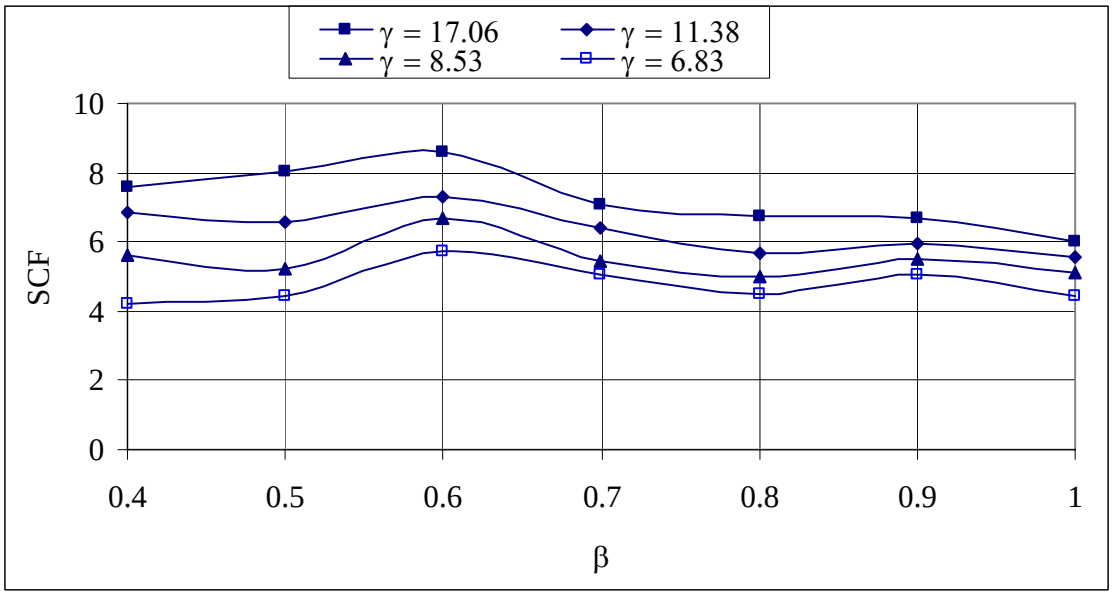


a) Through brace of overlapped CHS K-joint under the AX11 load case

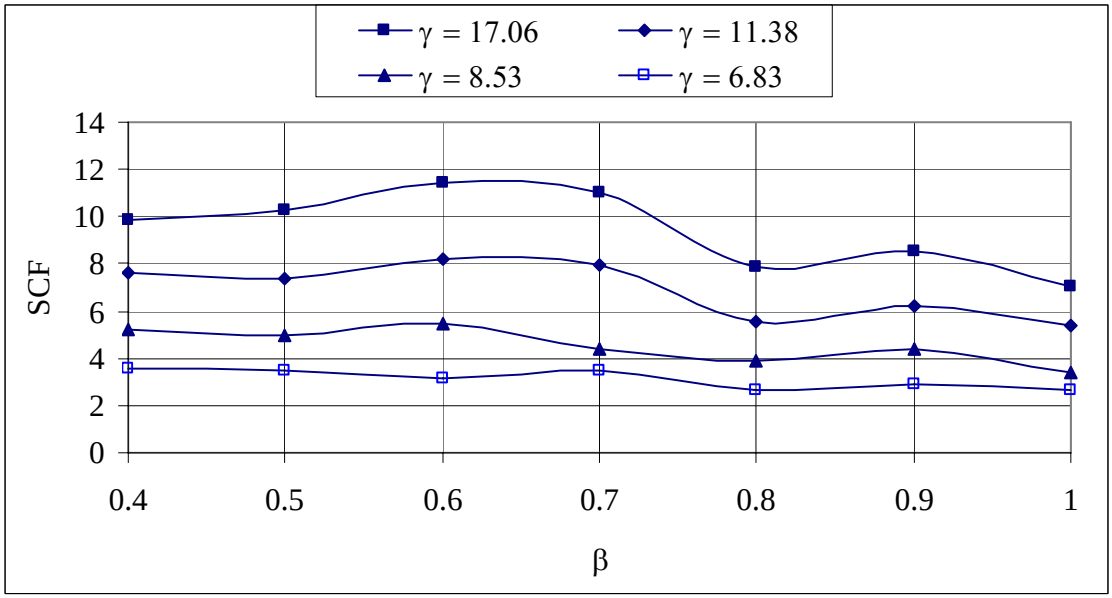


b) Chord of partially overlapped CHS K-joint under the AX11 load case

Figure 4.4 Effects of $\beta$ and $\gamma$ on SCF results for $\theta = 50°$, $\tau = 1$ and Ov = 50% for partially overlapped CHS K-joint under the AX11 load case

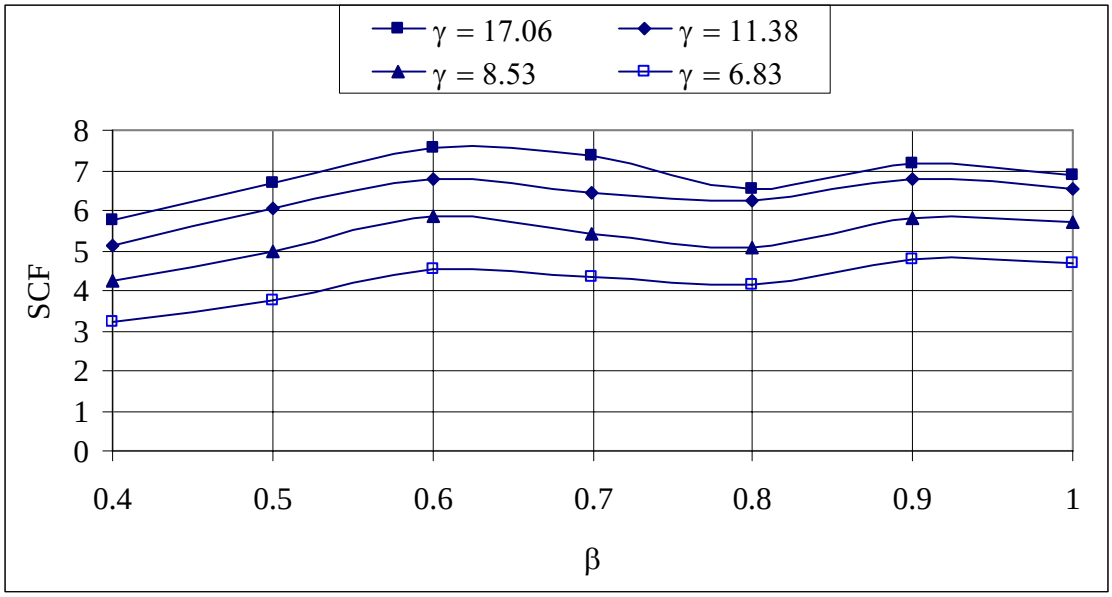


a) Through brace of overlapped CHS K-joint under the IPB11 load case

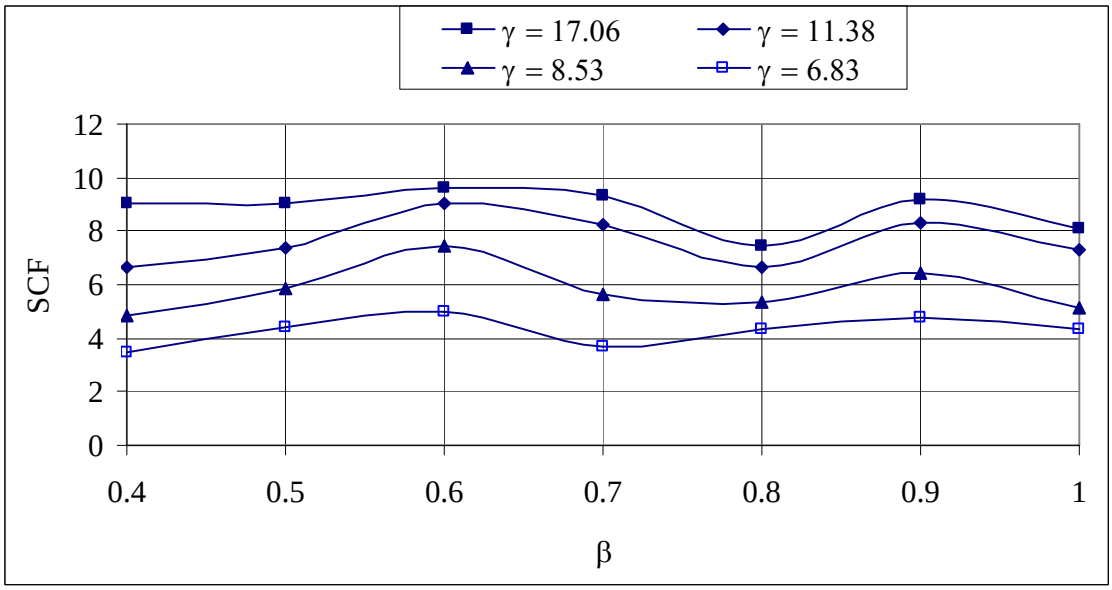


b) Chord of overlapped CHS K-joint under the IPB11 load case

Figure 4.5 Effects of $\beta$ and $\gamma$ on SCF results for $\theta = 50°$, $\tau = 1$ and Ov = 50% for partially overlapped CHS K-joint under the IPB11 load case

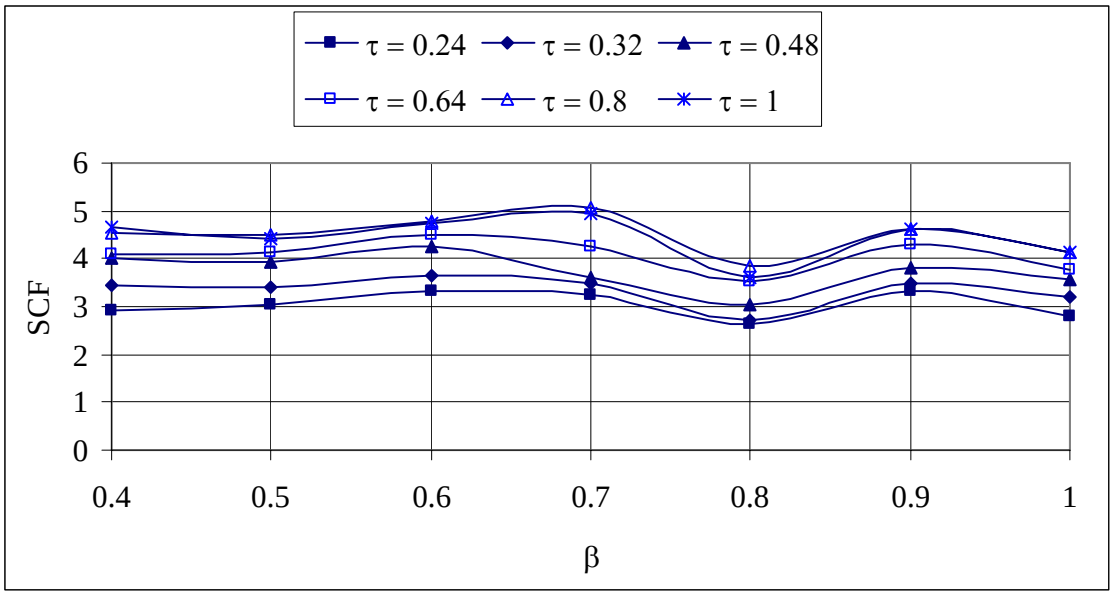


a) Through brace of overlapped CHS K-joint under the AX11 load case

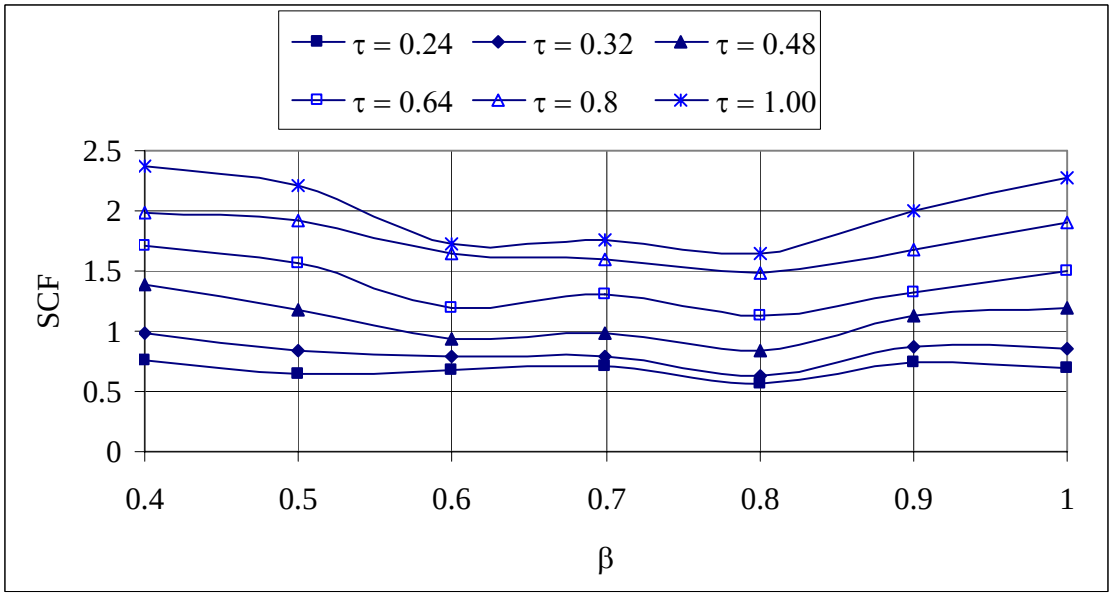


b) Chord of overlapped CHS K-joint under the AX11 load case

Figure 4.6 Effects of $\beta$ and $\tau$ on SCF results for $\theta$ = 50°, γ = 5.46 and Ov = 50% for partially overlapped CHS K-joint under the AX11 load case

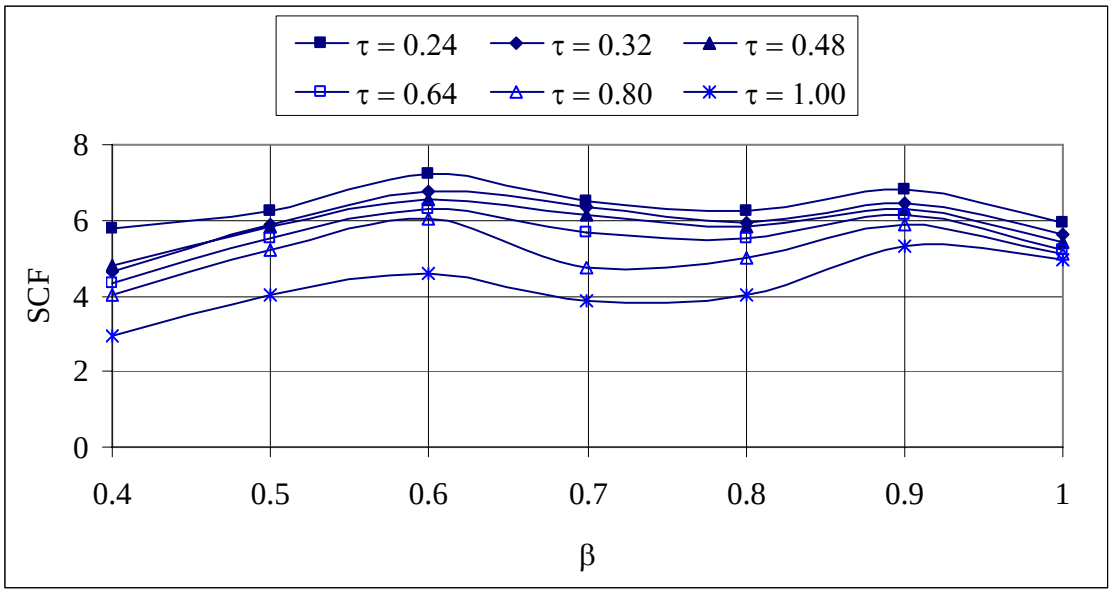


a) Through brace of overlapped CHS K-joint under the IPB11 load case

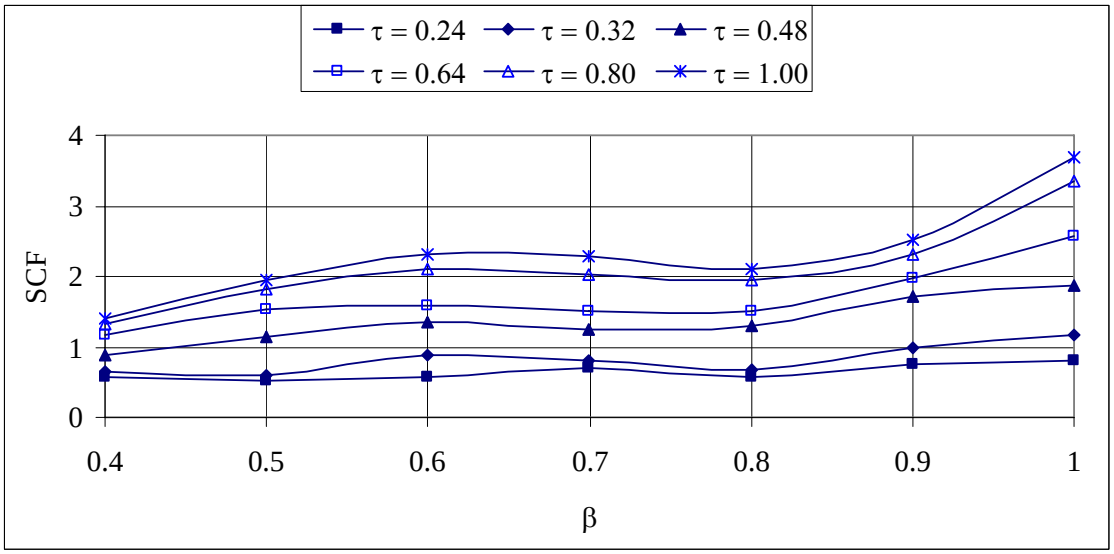


b) Chord of overlapped CHS K-joint under the IPB11 load case

Figure 4.7 Effects of $\beta$ and $\tau$ on SCF results for $\theta$ = 50°, $\gamma$ = 5.46 and Ov = 50% for partially overlapped CHS K-joint under the IPB11 load case

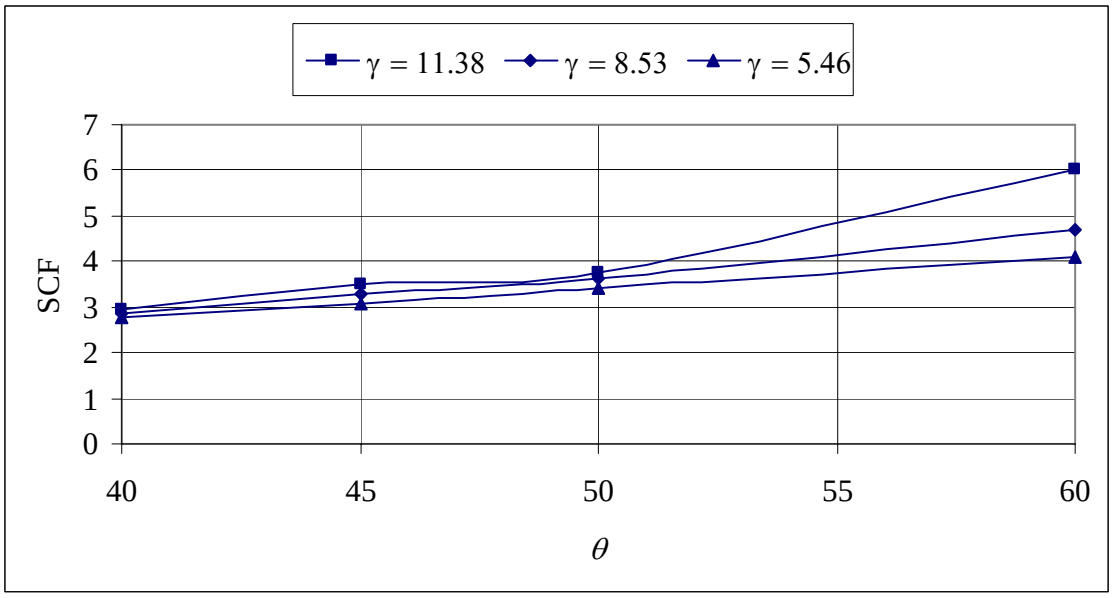


a) Through brace of overlapped CHS K-joint under the AX11 load case

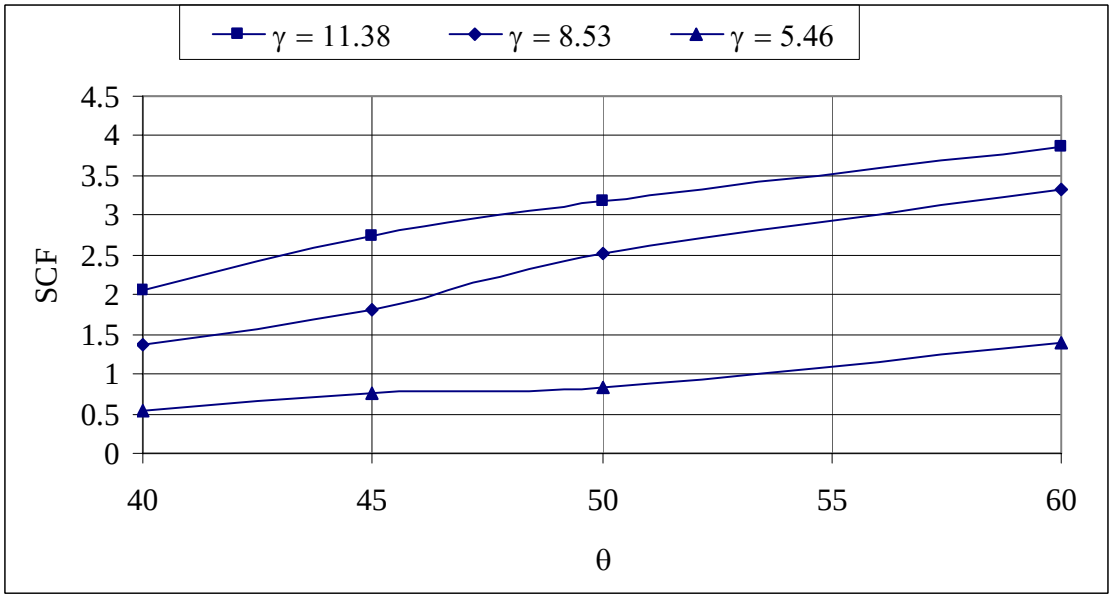


b) Chord of overlapped CHS K-joint under the AX11 load case

Figure 4.8 Effects of $\theta$ and $\gamma$ on SCF results for $\beta$=0.9, $\tau$ = 0.5 and Ov = 50% for partially overlapped CHS K-joint under the AX11 load case

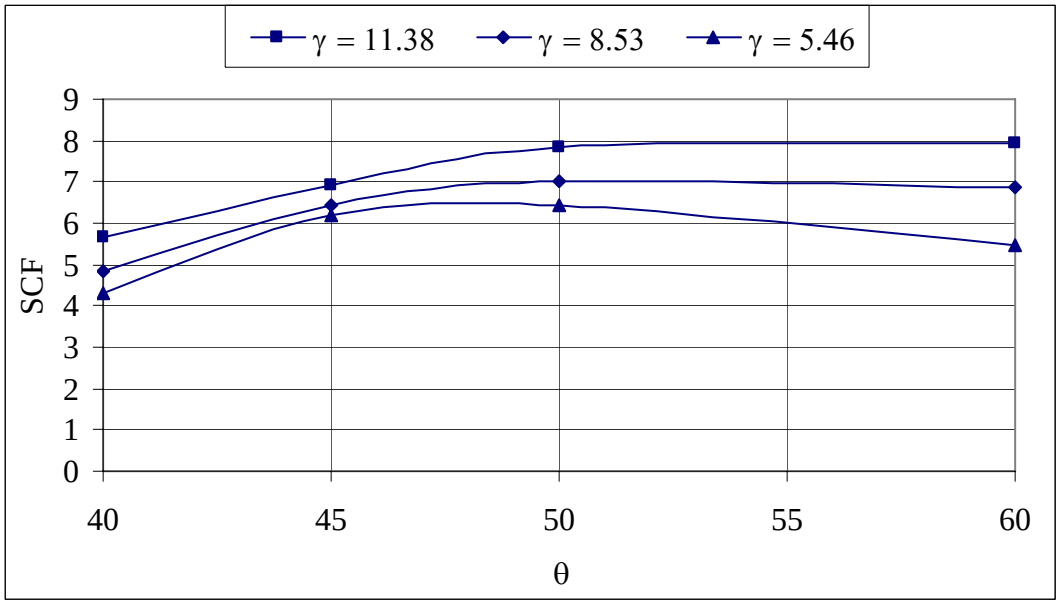


a) Through brace of overlapped CHS K-joint under the IPB11 load case

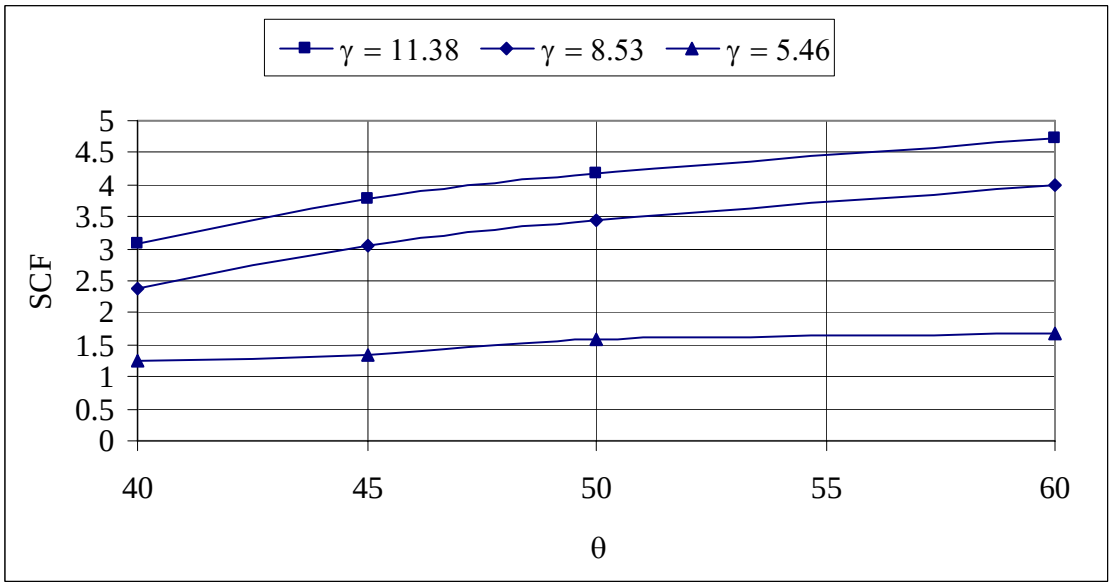


b) Chord of overlapped CHS K-joint under the IPB11 load case

Figure 4.9 Effects of $\theta$ and $\gamma$ on SCF results for $\beta$=0.9, $\tau$ = 0.5 and Ov = 50% for partially overlapped CHS K-joint under the IPB11 load case

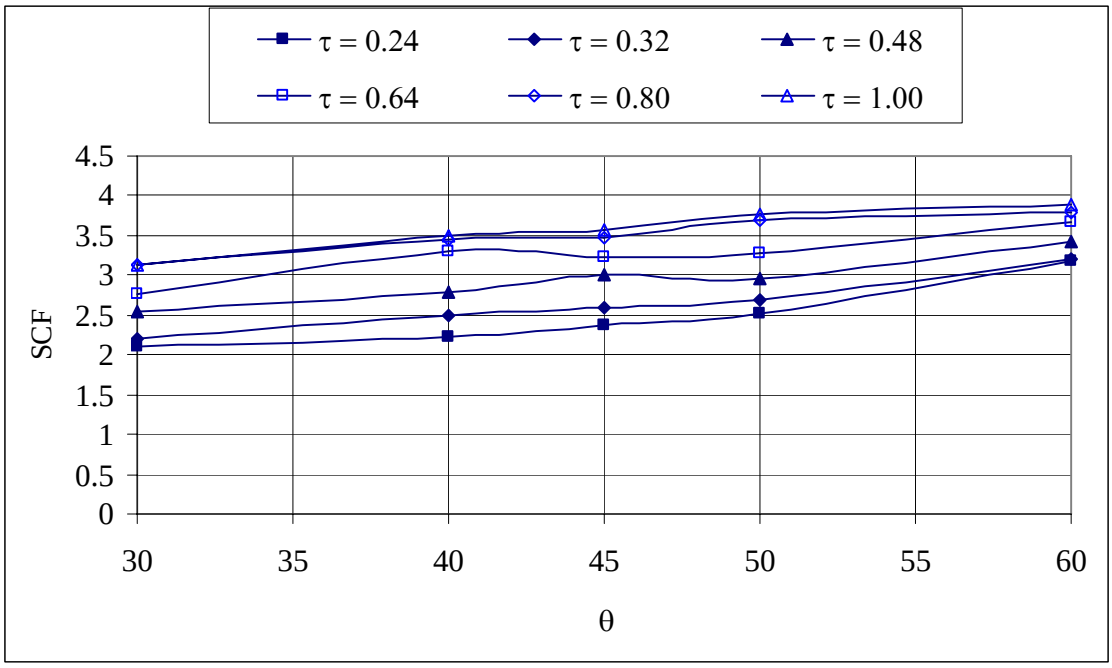


a) Through brace of overlapped CHS K-joint under the AX11 load case

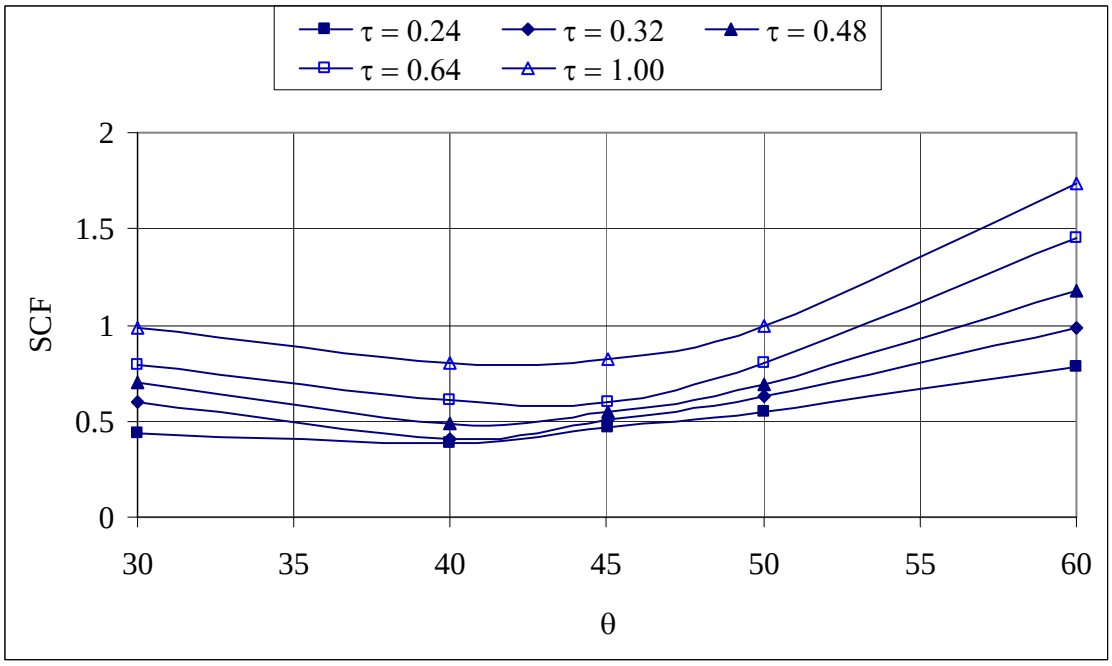


b) Chord of overlapped CHS K-joint under the AX11 load case

Figure 4.10 Effects of $\theta$ and $\gamma$ on SCF results for $\beta$=0.9, $\gamma$= 5.46 and Ov = 50% for partially overlapped CHS K-joint under the AX11 load case

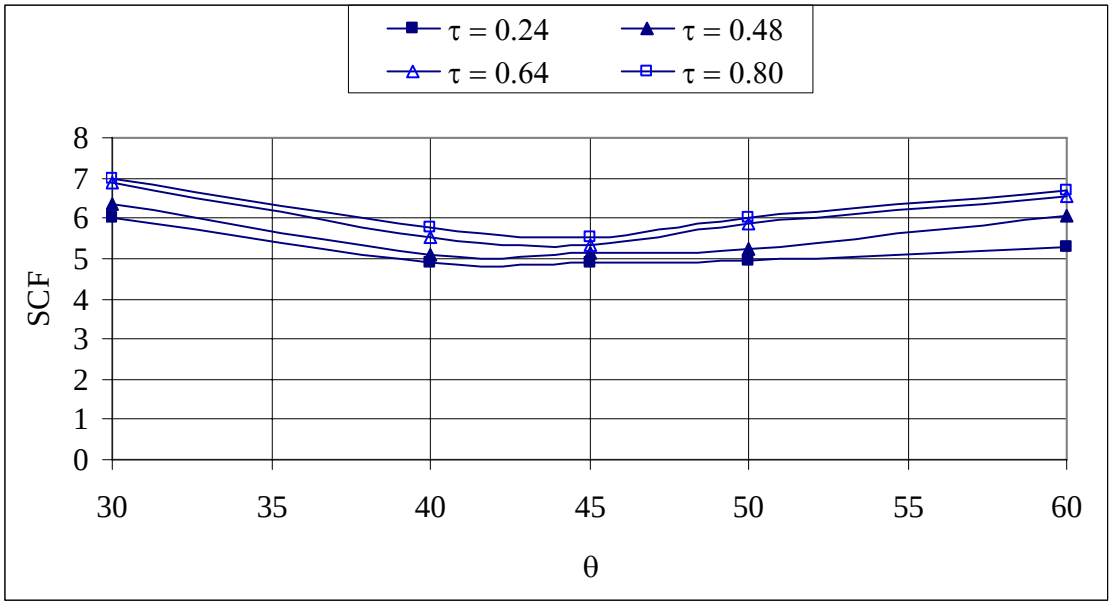


a) Through brace of overlapped CHS K-joint under the IPB11 load case

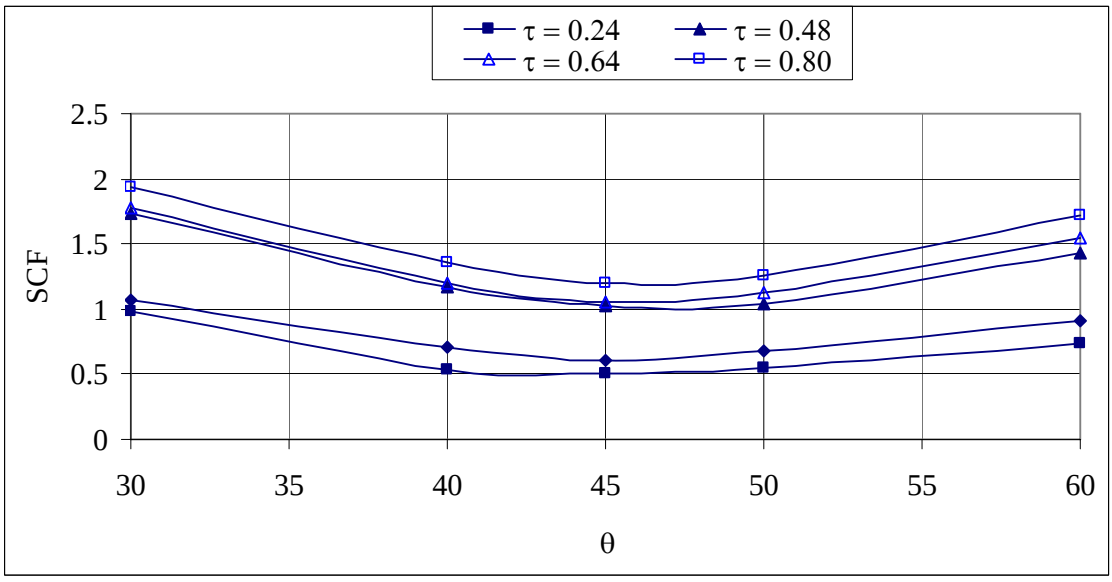


b) Chord of overlapped CHS K-joint under the IPB11 load case

Figure 4.11 Effects of $\theta$ and $\gamma$ on SCF results for $\beta$ =0.9, $\gamma$ = 5.46 and Ov = 50% for partially overlapped CHS K-joint under IPB11 load case

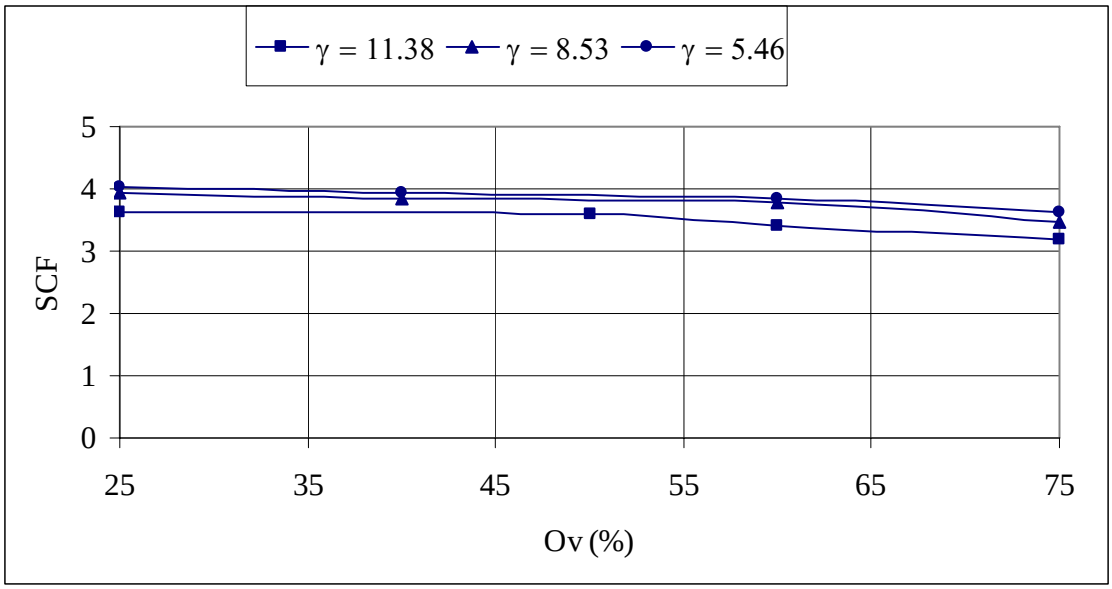


a) Through brace of overlapped CHS K-joint under the AX11 load case

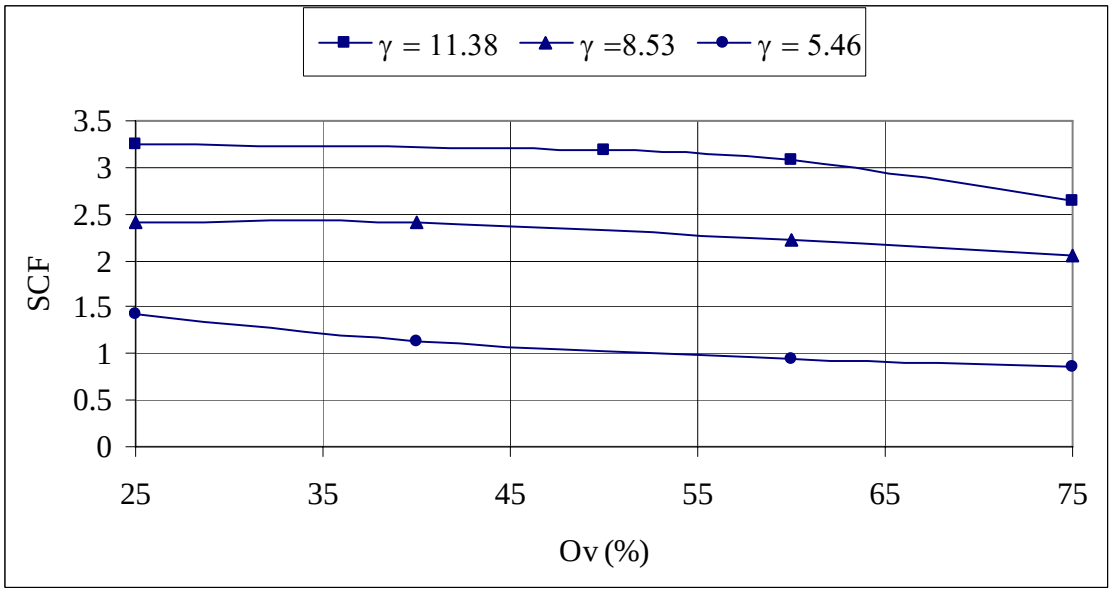


b) Chord of overlapped CHS K-joint under the AX11 load case

Figure 4.12 Effects of Ov and $\gamma$ on SCF results for $\beta$=0.9, $\tau$ = 0.5 and $\theta$ = 50° for partially overlapped CHS K-joint under the AX11 load case

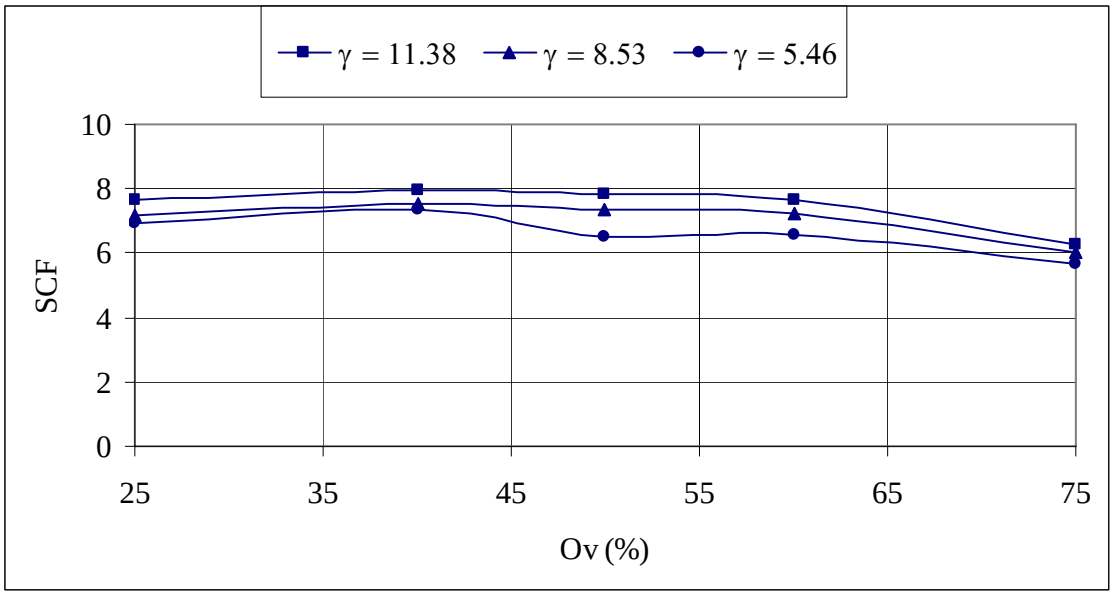


a) Through brace of overlapped CHS K-joint under the IPB11 load case

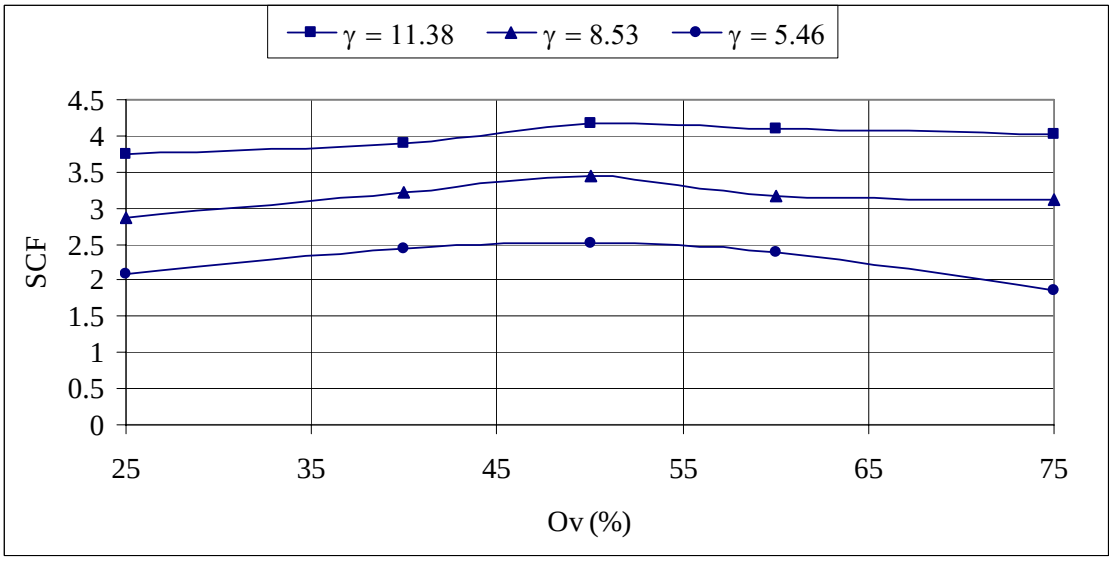


b) Chord of overlapped CHS K-joint under the IPB11 load case

Figure 4.13 Effects of Ov and $\gamma$ on SCF results for $\beta$=0.9, $\tau$ = 0.5 and $\theta$ = 50° for partially overlapped CHS K-joint under the IPB11 load case

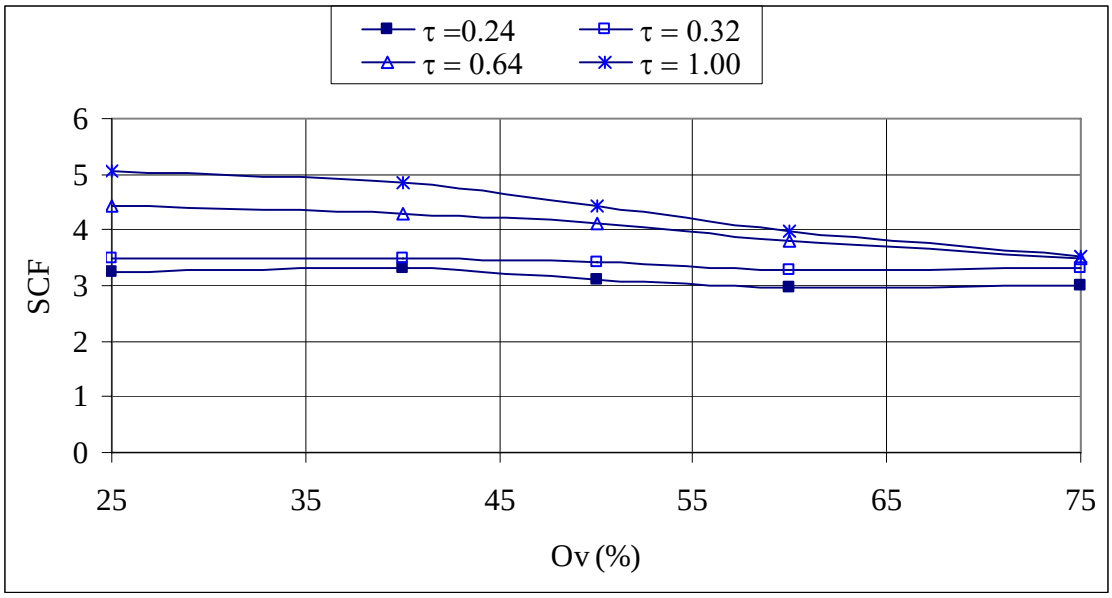


a) Through brace of overlapped CHS K-joint under the AX11 load case

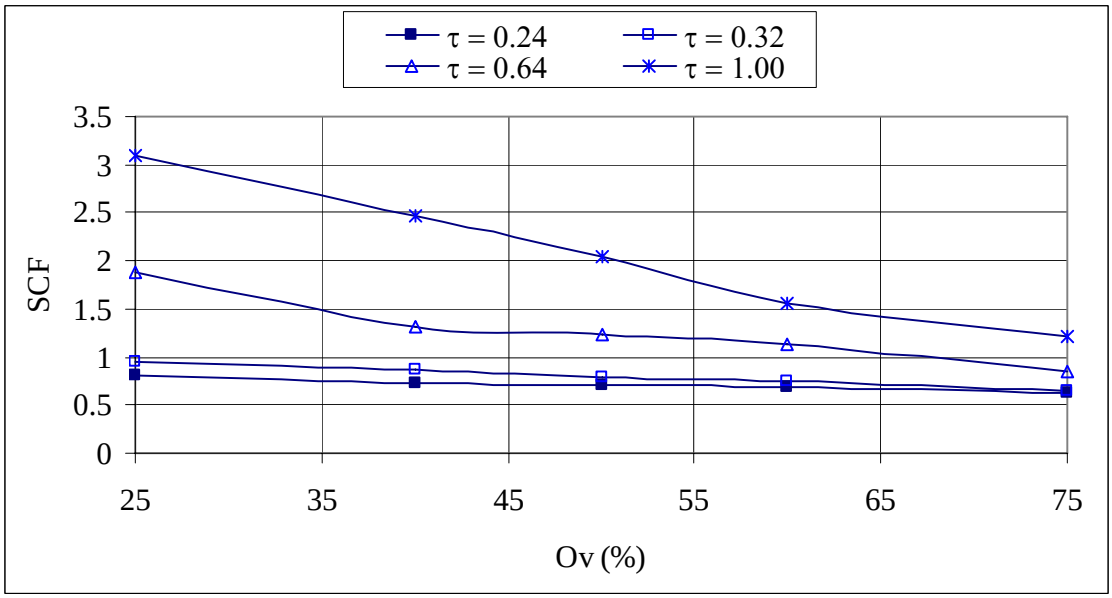


b) Chord of overlapped CHS K-joint under the AX11 load case

Figure 4.14 Effects of Ov and $\tau$ on SCF results for $\beta$=0.9, $\gamma$= 5.46 and $\theta$= 50° for partially overlapped CHS K-joint under the AX11 load case

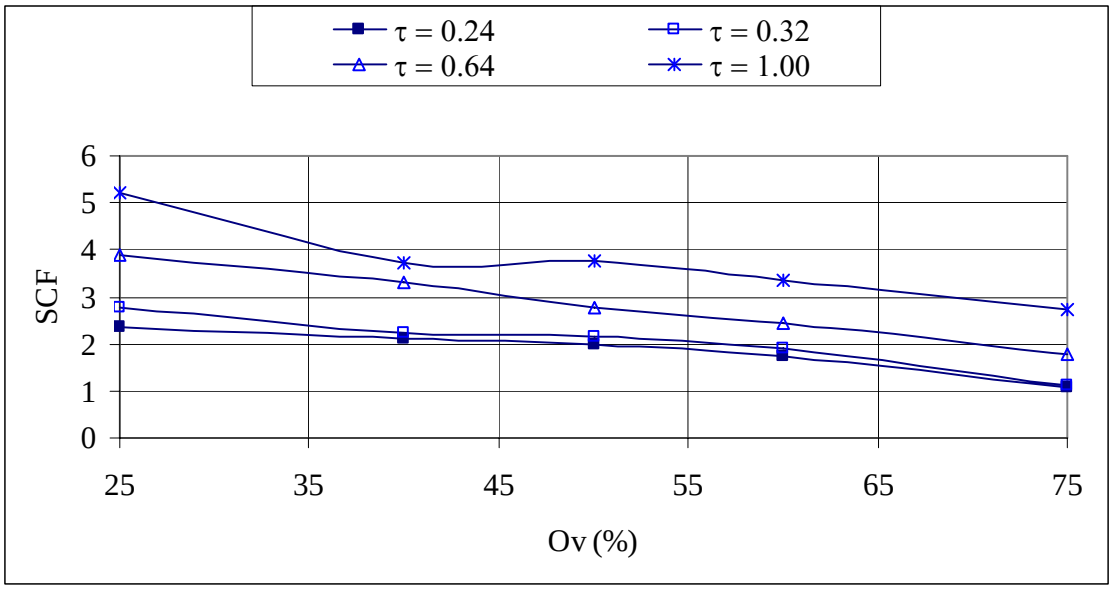


a) Through brace of overlapped CHS K-joint under the IPB11 load case

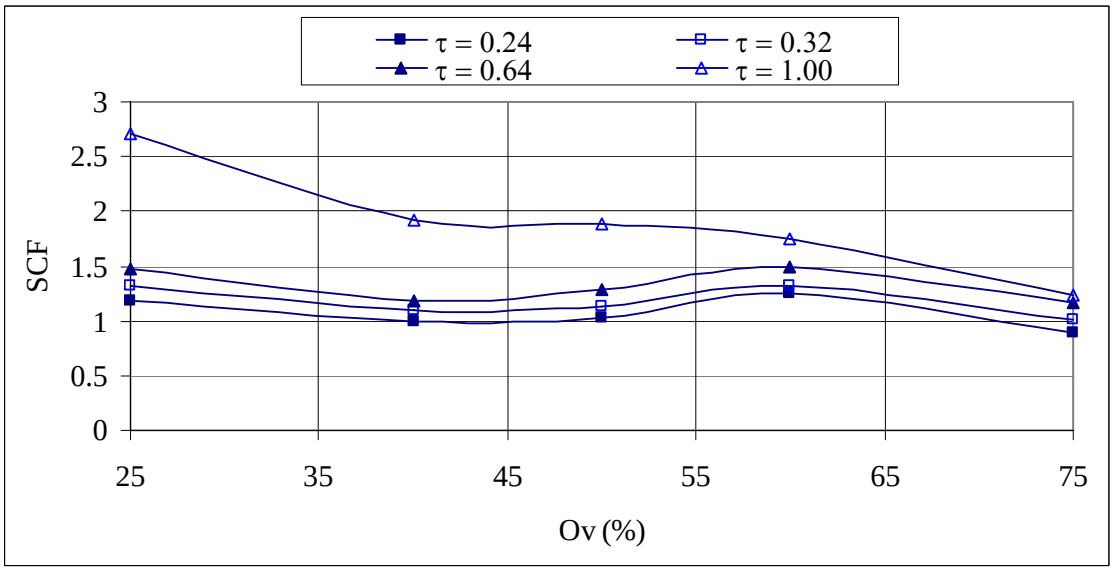


b) Chord of overlapped CHS K-joint under the IPB11 load case

Figure 4.15 Effects of Ov and $\tau$ on SCF results for $\beta$=0.9, $\gamma$= 5.46 and $\theta$= 50° for partially overlapped CHS K-joint under the IPB11 load case

| ID | Ov | $\theta$ | $\beta$ | $\gamma$ | $\tau$ | SCF Values | | | | |
|---|---|---|---|---|---|---|---|---|---|---|
| | | | | | | AX11tA | AXoA | AX11tC | AX11cC | AX21oA |
| 1 | 0.25 | 60.00 | 1.00 | 17.06 | 0.65 | 0.92 | -1.00 | 5.37 | 6.65 | 2.33 |
| 2 | 0.25 | 60.00 | 1.00 | 17.06 | 0.75 | 1.85 | 5.86 | 7.05 | 6.20 | 1.59 |
| 3 | 0.25 | 60.00 | 1.00 | 17.06 | 0.85 | 0.11 | -1.29 | 6.64 | 8.78 | 3.06 |
| 4 | 0.25 | 60.00 | 1.00 | 17.06 | 1.00 | 2.14 | 5.61 | 7.64 | 8.76 | 4.50 |
| 5 | 0.25 | 60.00 | 1.00 | 11.38 | 0.50 | 1.30 | 4.34 | 4.61 | 3.16 | 3.45 |
| 6 | 0.25 | 60.00 | 1.00 | 11.38 | 0.67 | 1.38 | 4.09 | 5.32 | 4.41 | 2.00 |
| 7 | 0.25 | 60.00 | 1.00 | 11.38 | 0.80 | 0.20 | -0.74 | 5.64 | 5.68 | 3.14 |
| 8 | 0.25 | 60.00 | 1.00 | 11.38 | 1.00 | 1.87 | 4.01 | 5.92 | 6.74 | 2.99 |
| 9 | 0.25 | 60.00 | 1.00 | 8.53 | 0.38 | 1.23 | 3.49 | 3.40 | 1.94 | 3.56 |
| 10 | 0.25 | 60.00 | 1.00 | 8.53 | 0.50 | 1.13 | 3.29 | 4.18 | 2.44 | 2.20 |
| 11 | 0.25 | 60.00 | 1.00 | 8.53 | 0.75 | 1.37 | 3.16 | 5.64 | 3.79 | 2.22 |
| 12 | 0.25 | 60.00 | 1.00 | 8.53 | 1.00 | 1.72 | 2.44 | 6.40 | 4.72 | 2.01 |
| 13 | 0.25 | 60.00 | 1.00 | 6.83 | 0.30 | 1.16 | 2.96 | 3.27 | 1.43 | 3.56 |
| 14 | 0.25 | 60.00 | 1.00 | 6.83 | 0.60 | 1.18 | 2.66 | 4.70 | 2.86 | 2.35 |
| 15 | 0.25 | 60.00 | 1.00 | 6.83 | 0.80 | 1.41 | 1.94 | 5.24 | 3.52 | 2.46 |
| 16 | 0.25 | 60.00 | 1.00 | 6.83 | 1.00 | 1.76 | 1.04 | 5.72 | 4.35 | 2.33 |
| 17 | 0.25 | 60.00 | 1.00 | 5.46 | 0.30 | 1.22 | 2.82 | 4.13 | 1.53 | 2.53 |
| 18 | 0.25 | 60.00 | 1.00 | 5.46 | 0.64 | 1.22 | 1.57 | 4.88 | 2.53 | 2.75 |
| 19 | 0.25 | 60.00 | 1.00 | 5.46 | 0.80 | 1.52 | 0.88 | 5.08 | 3.34 | 2.53 |
| 20 | 0.25 | 60.00 | 1.00 | 5.46 | 1.00 | 1.91 | 1.02 | 4.95 | 3.90 | 2.52 |

| SCF Values | | | | | | | | | | |
|---|---|---|---|---|---|---|---|---|---|---|
| AX21tA | AX21oB | AX21cB | IPB11tC | IPB11cC | IPB12tA | IPB21oA | IPB21oB | IPB21cB | IPB22oA | IPB22tA |
| 7.08 | 5.06 | 6.94 | 7.29 | 6.25 | 6.33 | 4.34 | 8.08 | 5.57 | 7.51 | 10.01 |
| 6.04 | 6.80 | 6.39 | 8.75 | 5.81 | 5.90 | 4.19 | 10.57 | 5.54 | 6.88 | 9.65 |
| 6.50 | 6.35 | 9.46 | 8.08 | 8.40 | 5.39 | 5.39 | 8.88 | 7.25 | 6.75 | 9.68 |
| 5.52 | 8.43 | 8.92 | 7.90 | 8.06 | 6.27 | 5.06 | 11.27 | 7.24 | 8.32 | 9.36 |
| 6.20 | 4.16 | 3.10 | 6.33 | 3.05 | 4.28 | 3.12 | 8.55 | 3.57 | 5.91 | 8.30 |
| 5.45 | 5.00 | 3.93 | 7.41 | 4.09 | 4.52 | 3.93 | 9.21 | 4.64 | 6.47 | 7.84 |
| 5.81 | 5.16 | 5.30 | 6.38 | 5.40 | 3.97 | 3.95 | 7.47 | 6.26 | 5.59 | 7.72 |
| 4.62 | 6.34 | 6.34 | 6.38 | 6.35 | 4.70 | 4.41 | 9.31 | 6.96 | 6.84 | 7.56 |
| 6.11 | 3.34 | 1.96 | 5.78 | 2.11 | 3.45 | 2.61 | 7.82 | 2.49 | 5.91 | 7.55 |
| 5.38 | 3.85 | 2.46 | 6.72 | 2.84 | 3.60 | 3.35 | 8.16 | 3.30 | 5.64 | 7.02 |
| 4.59 | 4.81 | 3.36 | 6.98 | 4.61 | 3.63 | 3.74 | 8.08 | 4.74 | 5.70 | 6.62 |
| 3.26 | 6.28 | 4.42 | 6.77 | 5.59 | 4.33 | 3.80 | 6.00 | 6.33 | 6.46 | 5.38 |
| 5.98 | 2.95 | 1.42 | 5.61 | 1.48 | 2.84 | 2.33 | 7.39 | 1.71 | 4.05 | 7.06 |
| 4.56 | 3.93 | 2.50 | 6.63 | 3.40 | 2.99 | 3.34 | 7.17 | 3.52 | 5.04 | 6.02 |
| 3.21 | 5.09 | 3.37 | 6.99 | 4.18 | 3.57 | 4.37 | 8.00 | 4.83 | 5.59 | 4.86 |
| 2.22 | 5.77 | 4.12 | 5.65 | 4.93 | 3.58 | 4.15 | 5.60 | 5.81 | 6.30 | 4.05 |
| 5.20 | 2.93 | 1.27 | 7.21 | 1.61 | 3.10 | 3.20 | 7.63 | 1.55 | 4.89 | 6.12 |
| 3.24 | 4.45 | 2.40 | 6.11 | 2.95 | 2.81 | 3.92 | 7.90 | 3.43 | 4.92 | 4.54 |
| 2.22 | 5.06 | 2.98 | 5.46 | 3.83 | 3.04 | 3.71 | 7.57 | 4.33 | 5.64 | 3.19 |
| 1.42 | 5.27 | 3.91 | 4.71 | 4.28 | 2.68 | 2.85 | 4.58 | 5.41 | 5.41 | 2.54 |

Figure 4.16 Typical SCF values stored in a database

| ID | Ov | $\theta$ | $\beta$ | $\gamma$ | $\tau$ | SCF Values | | | | |
|---|---|---|---|---|---|---|---|---|---|---|
| | | | | | | AX11tA | AXoA | AX11tC | AX11cC | AX21oA |
| 3481 | 0.75 | 30.00 | 0.40 | 17.06 | 0.65 | 4.48 | 2.63 | 3.77 | 4.58 | 4.44 |
| 3482 | 0.75 | 30.00 | 0.40 | 17.06 | 0.75 | 2.56 | 2.31 | 4.81 | 4.57 | 4.82 |
| 3483 | 0.75 | 30.00 | 0.40 | 17.06 | 0.85 | 2.07 | 2.77 | 4.50 | 5.91 | 4.31 |
| 3484 | 0.75 | 30.00 | 0.40 | 17.06 | 1.00 | 2.14 | 2.53 | 5.51 | 6.22 | 4.29 |
| 3485 | 0.75 | 30.00 | 0.40 | 11.38 | 0.50 | 2.37 | 2.51 | 3.18 | 2.25 | 4.46 |
| 3486 | 0.75 | 30.00 | 0.40 | 11.38 | 0.67 | 1.85 | 2.79 | 3.87 | 2.97 | 4.16 |
| 3487 | 0.75 | 30.00 | 0.40 | 11.38 | 0.80 | 2.80 | 3.20 | 4.52 | 4.04 | 3.78 |
| 3488 | 0.75 | 30.00 | 0.40 | 11.38 | 1.00 | 1.30 | 2.89 | 4.20 | 4.24 | 3.39 |
| 3489 | 0.75 | 30.00 | 0.40 | 8.53 | 0.38 | 2.18 | 2.58 | 2.67 | 1.30 | 4.11 |
| 3490 | 0.75 | 30.00 | 0.40 | 8.53 | 0.50 | 1.56 | 2.85 | 3.12 | 1.67 | 4.00 |
| 3491 | 0.75 | 30.00 | 0.40 | 8.53 | 0.75 | 0.94 | 2.98 | 3.14 | 2.39 | 3.22 |
| 3492 | 0.75 | 30.00 | 0.40 | 8.53 | 1.00 | 0.87 | 3.02 | 3.47 | 2.81 | 3.02 |
| 3493 | 0.75 | 30.00 | 0.40 | 6.83 | 0.30 | 2.03 | 2.61 | 2.23 | 0.79 | 3.90 |
| 3494 | 0.75 | 30.00 | 0.40 | 6.83 | 0.60 | 0.93 | 2.99 | 2.43 | 1.38 | 3.05 |
| 3495 | 0.75 | 30.00 | 0.40 | 6.83 | 0.80 | 0.91 | 3.05 | 2.84 | 1.63 | 2.90 |
| 3496 | 0.75 | 30.00 | 0.40 | 6.83 | 1.00 | 0.57 | 3.12 | 2.89 | 1.84 | 3.01 |
| 3497 | 0.75 | 30.00 | 0.40 | 5.46 | 0.30 | 1.32 | 2.86 | 2.23 | 0.61 | 3.77 |
| 3498 | 0.75 | 30.00 | 0.40 | 5.46 | 0.64 | 0.81 | 3.03 | 2.50 | 0.85 | 2.77 |
| 3499 | 0.75 | 30.00 | 0.40 | 5.46 | 0.80 | 0.74 | 3.14 | 2.67 | 1.41 | 3.48 |
| 3500 | 0.75 | 30.00 | 0.40 | 5.46 | 1.00 | 0.41 | 3.21 | 2.68 | 1.26 | 2.84 |

| SCF Values | | | | | | | | | | |
|---|---|---|---|---|---|---|---|---|---|---|
| AX21tA | AX21oB | AX21cB | IPB11tC | IPB11cC | IPB12tA | IPB21oA | IPB21oB | IPB21cB | IPB22oA | IPB22tA |
| 6.92 | 3.60 | 6.32 | 3.87 | 4.44 | 1.75 | 4.10 | 5.84 | 4.73 | 2.93 | 5.77 |
| 6.26 | 3.02 | 6.72 | 3.78 | 4.90 | 2.28 | 3.77 | 7.74 | 5.09 | 3.31 | 5.22 |
| 6.33 | 3.85 | 7.61 | 4.04 | 5.64 | 1.81 | 4.30 | 6.95 | 6.66 | 2.88 | 5.42 |
| 5.59 | 4.05 | 8.28 | 3.89 | 6.15 | 2.22 | 3.96 | 6.18 | 6.65 | 3.89 | 4.80 |
| 5.92 | 2.32 | 3.25 | 3.49 | 2.00 | 1.73 | 3.07 | 8.53 | 2.19 | 2.87 | 4.39 |
| 5.40 | 3.76 | 4.12 | 3.31 | 3.18 | 1.55 | 3.12 | 5.47 | 3.21 | 3.23 | 3.93 |
| 5.31 | 3.02 | 5.07 | 5.94 | 4.00 | 1.22 | 3.38 | 6.68 | 4.87 | 2.14 | 4.03 |
| 4.23 | 3.33 | 5.57 | 3.91 | 4.90 | 1.11 | 3.05 | 6.34 | 5.38 | 1.93 | 3.17 |
| 5.63 | 4.33 | 2.11 | 3.38 | 1.18 | 1.46 | 2.74 | 8.74 | 1.45 | 2.69 | 3.96 |
| 5.18 | 3.28 | 2.28 | 3.44 | 1.58 | 1.24 | 2.71 | 5.01 | 1.73 | 2.91 | 3.46 |
| 4.07 | 2.85 | 3.10 | 3.76 | 2.80 | 0.86 | 2.57 | 6.24 | 2.52 | 1.68 | 2.65 |
| 3.48 | 2.73 | 3.54 | 5.31 | 3.66 | 1.04 | 2.37 | 5.83 | 3.65 | 1.97 | 2.22 |
| 5.40 | 3.76 | 1.49 | 3.40 | 0.77 | 1.32 | 2.56 | 8.74 | 0.97 | 2.60 | 3.70 |
| 3.90 | 2.68 | 1.95 | 3.51 | 1.47 | 0.71 | 2.29 | 6.40 | 1.45 | 1.55 | 2.34 |
| 3.37 | 2.69 | 2.38 | 5.28 | 2.18 | 0.83 | 2.08 | 6.01 | 1.98 | 1.66 | 1.92 |
| 2.58 | 3.50 | 2.91 | 3.02 | 3.83 | -0.21 | 2.48 | 3.50 | 3.63 | 0.78 | 1.38 |
| 4.81 | 2.35 | 0.84 | 3.42 | 0.50 | 0.94 | 2.31 | 4.60 | 0.71 | 2.59 | 2.96 |
| 3.25 | 2.63 | 1.45 | 3.13 | 0.81 | 0.67 | 1.86 | 6.12 | 0.96 | 1.80 | 1.68 |
| 3.36 | 3.41 | 2.21 | 3.43 | 2.93 | -0.27 | 2.53 | 4.42 | 2.79 | 0.81 | 1.86 |
| 2.20 | 3.44 | 2.32 | 2.79 | 3.39 | -0.53 | 2.23 | 3.15 | 3.03 | 0.44 | 0.88 |

Figure 4.16 Typical SCF values stored in a database (Cont'd)

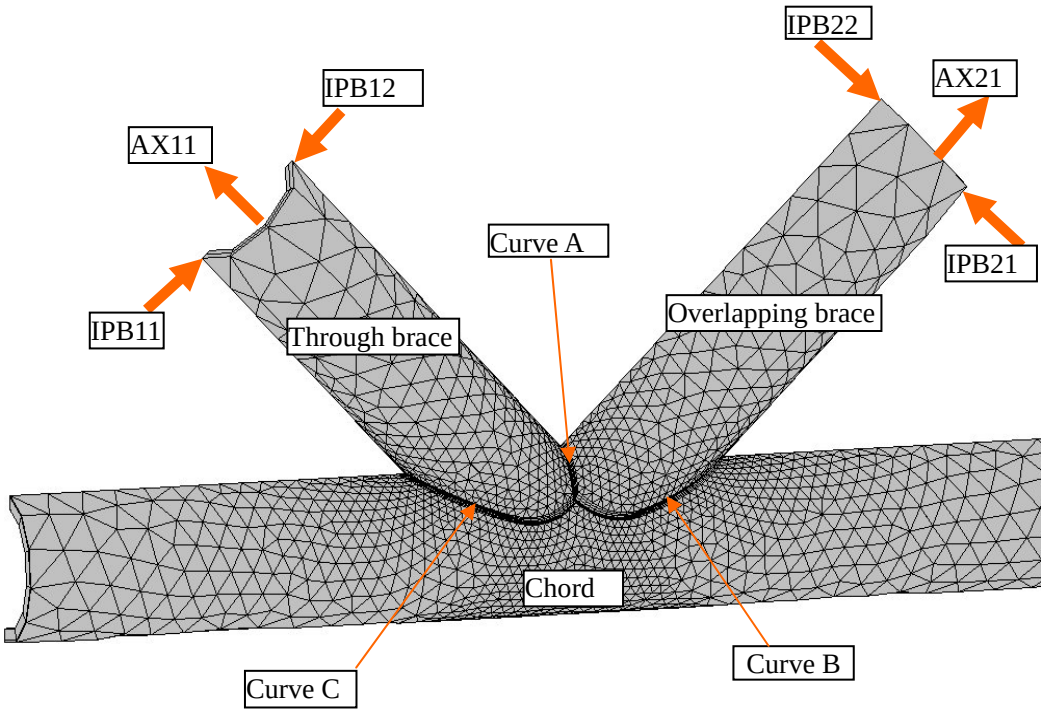


(a) Weld Curves A, B, C and six load cases

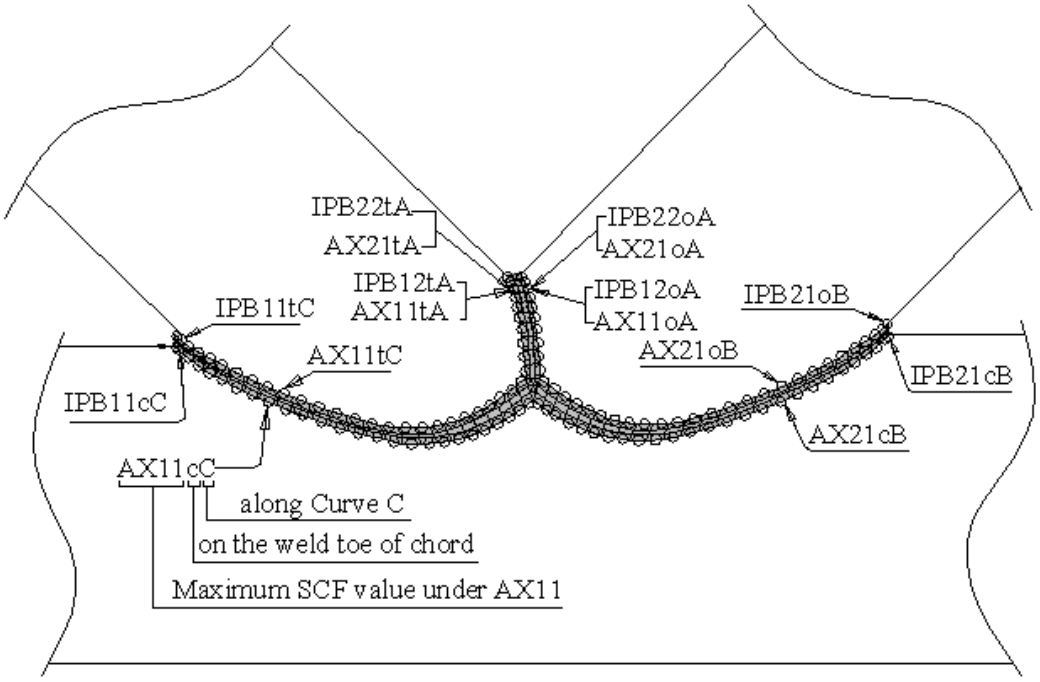


(b) The 16 SCF values locations

Figure 4.17 Three welding Curves A, B and C together with the six load cases and the

16 SCF values locations

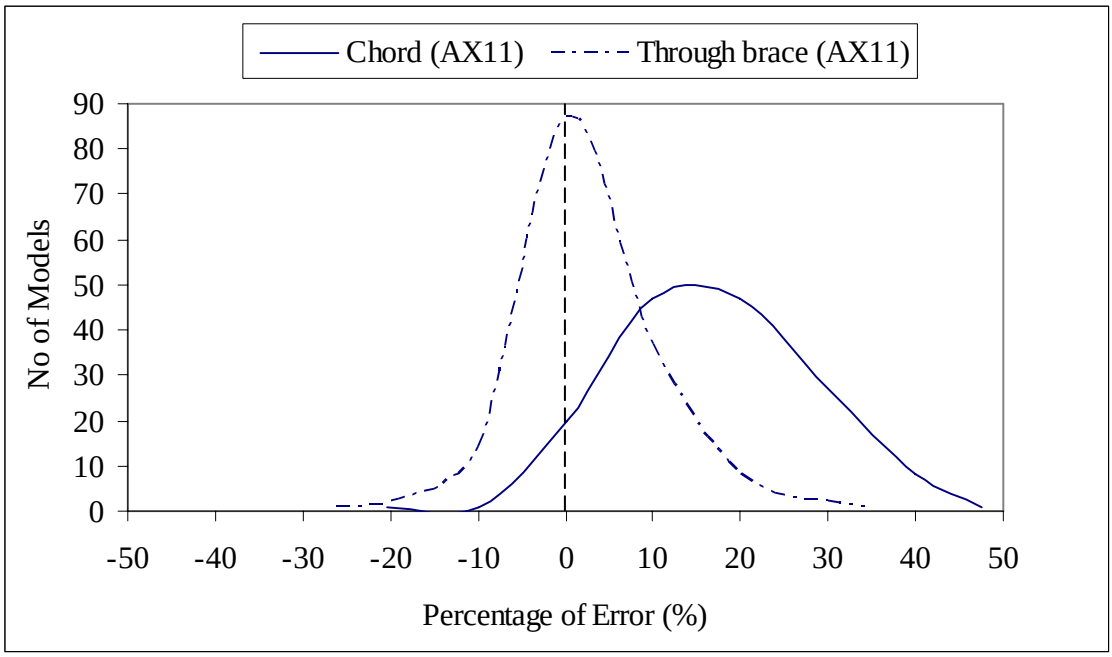


Figure 4.18 Error percentage statistics of numerical models in Table 4.2 for partially overlapped CHS K-joints under the AX11 load case along Curve C

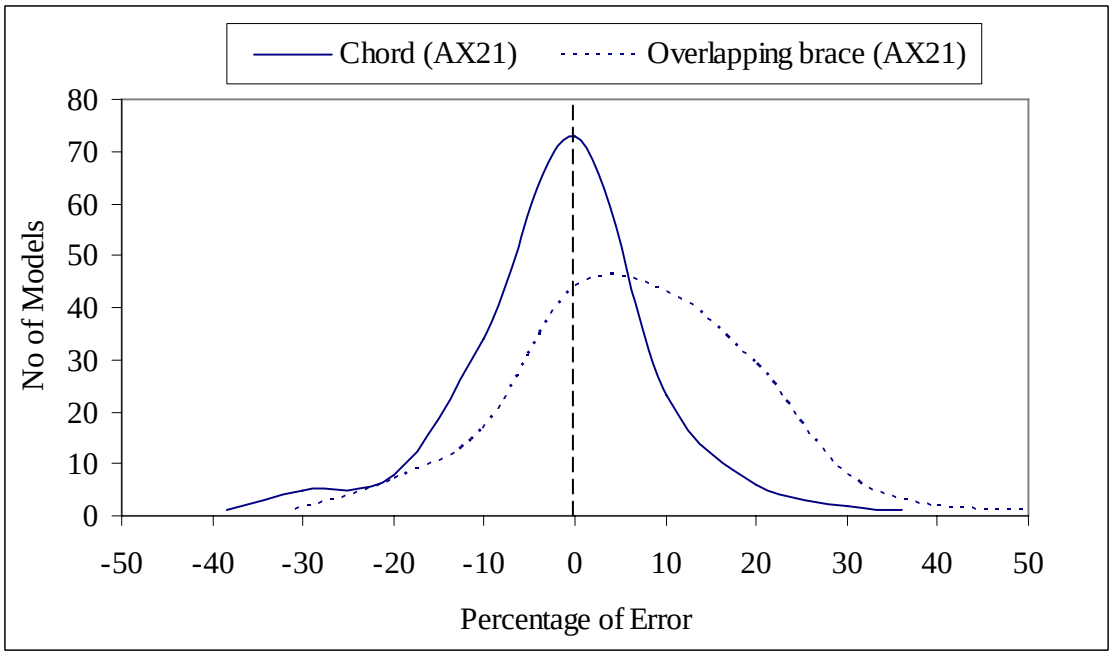


Figure 4.19 Error percentage statistics of numerical models in Table 4.2 for partially overlapped CHS K-joints under the AX21 load case along Curve B

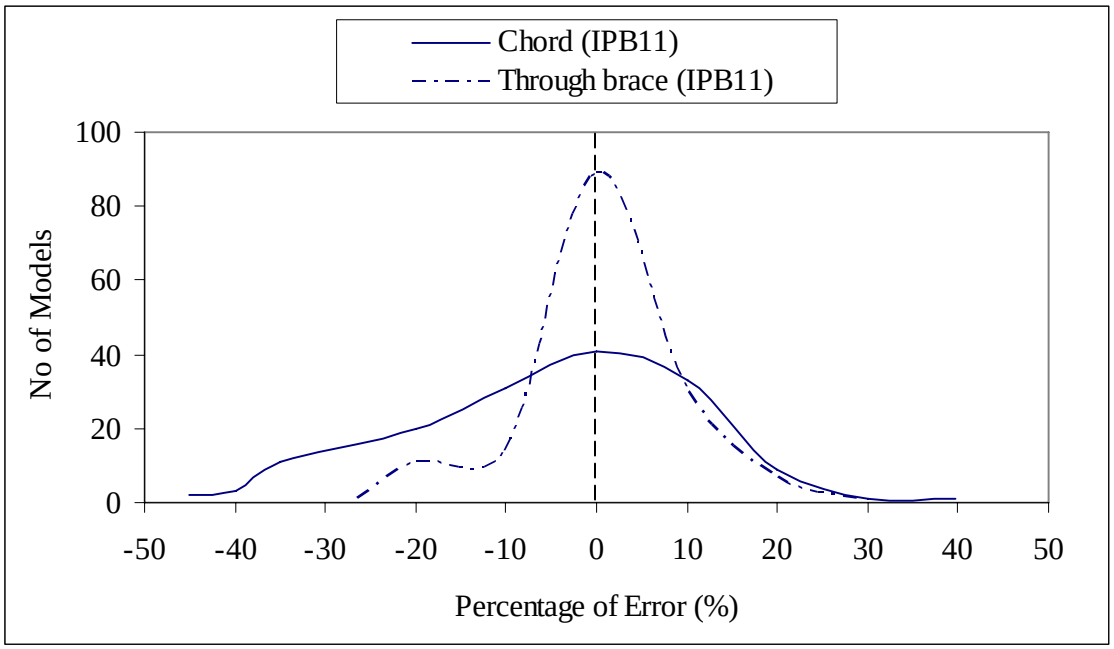


Figure 4.20 Error percentage statistics of numerical models in Table 4.2 for partially overlapped CHS K-joints under the IPB11 load case along Curve C

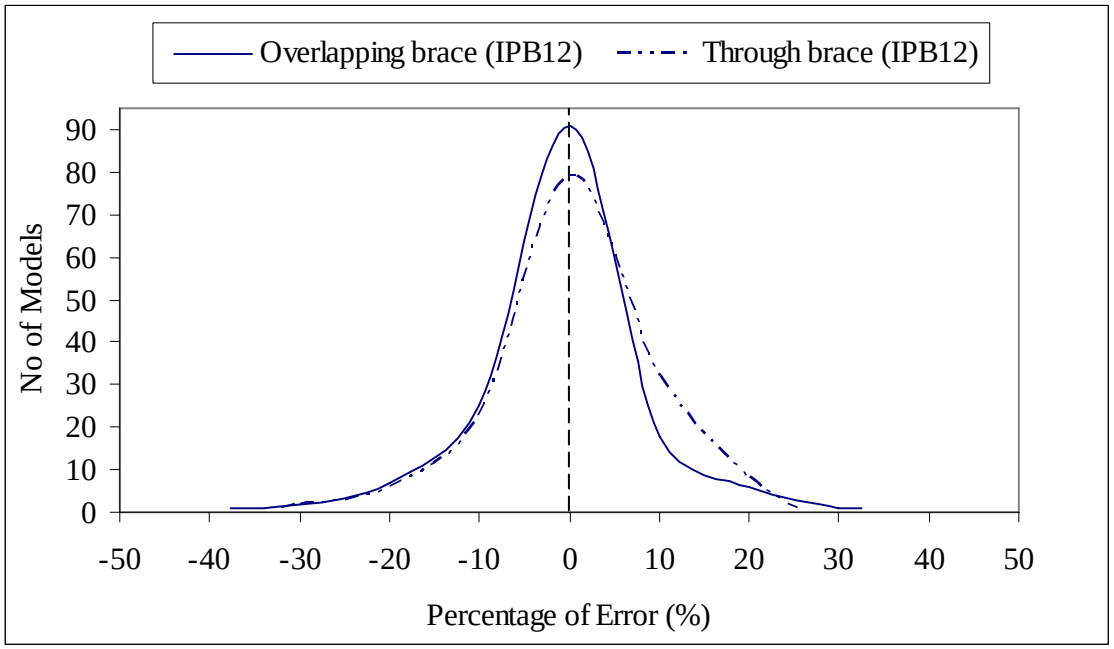


Figure 4.21 Error percentage statistics of numerical models in Table 4.2 for partially overlapped CHS K-joints under the IPB12 load case along Curve A

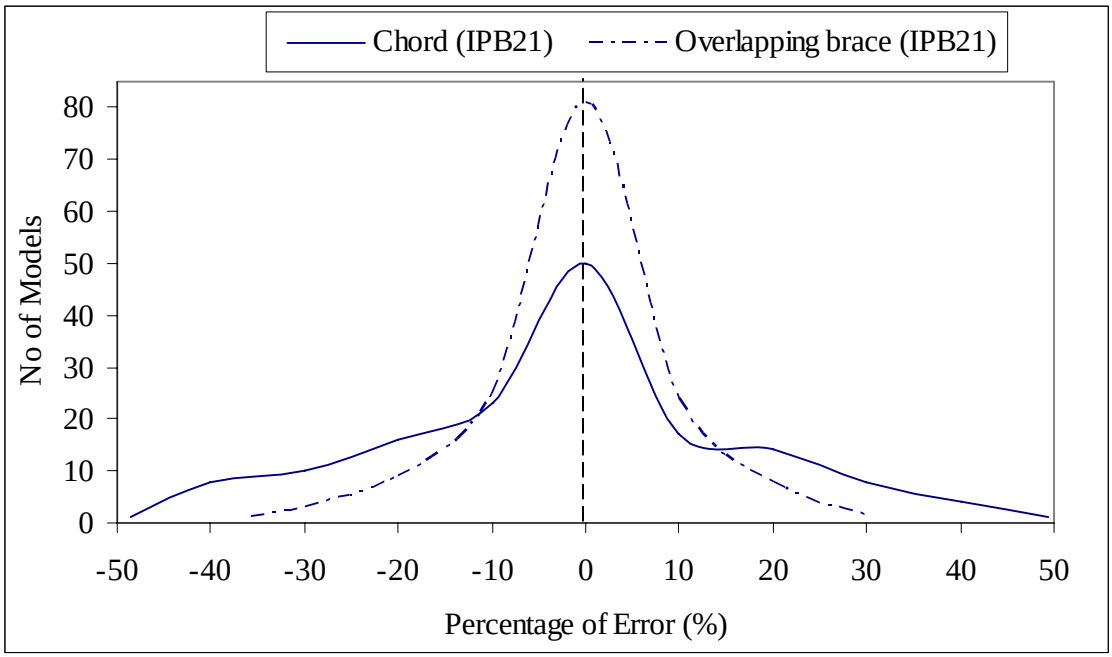


Figure 4.22 Error percentage statistics of numerical models in Table 4.2 for partially overlapped CHS K-joints under the IPB21 load case along Curve B

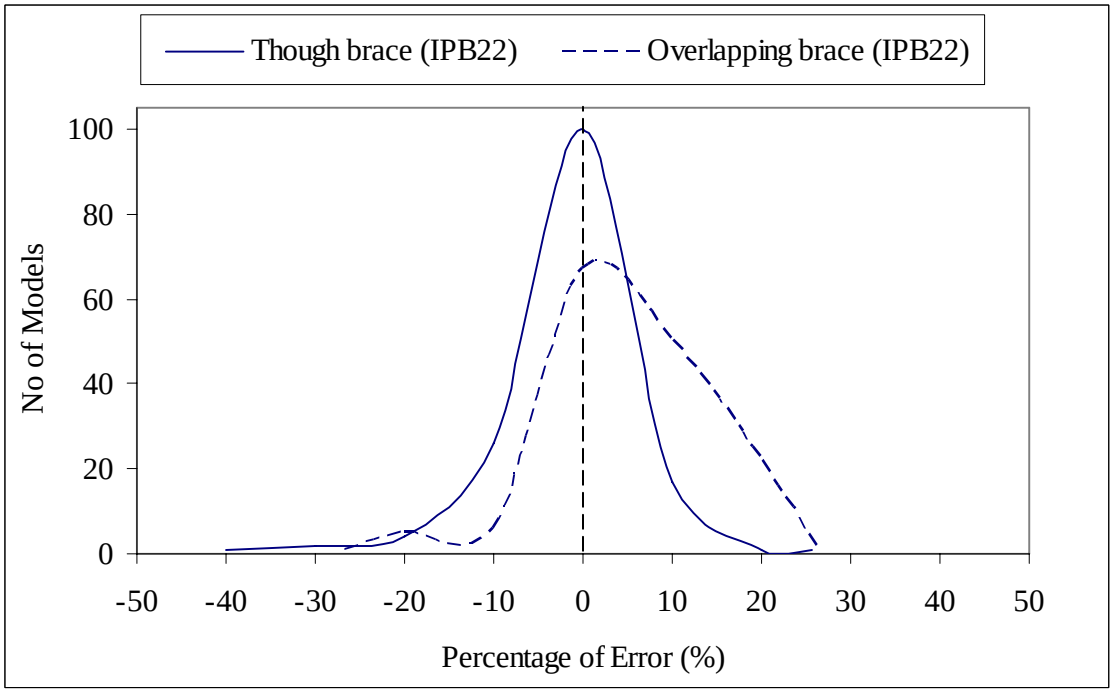


Figure 4.23 Error percentage statistics of numerical models in Table 4.2 for partially overlapped CHS K-joints under the IPB22 load case along Curve A

# *CHAPTER 5*
# *INTERPOLATION METHOD TO CALCULATE SCF VALUES OF PARTIALLY OVERLAPPED CHS K-JOINTS*

## 5.1 INTRODUCTION

In this Chapter, an interpolation method is proposed to estimate the SCF values of partially overlapped CHS K-joints. The interpolation method is not a completely new method as it has been applied to analyze SIFs of tubular gapped K-joints by Shao [53] in his research works. However, it is the first time that this method is applied to estimate SCFs and HSSs of partially overlapped CHS K-joints.

According to the results of the study done by Shao [53], the accuracy of the SIFs obtained from interpolation method is higher than that of SIFs obtained from the proposed parametric equations. The more data, the higher the accuracy of the results can be obtained. Having compared the interpolation method with the proposed equations for tubular T and Y-joints [54 and 55], the interpolation method appears to be more accurate, feasible and practical. Therefore, in the present study the concept of interpolation method has been adopted and extended to create a new tool for predicting the SCF and HSS values for partially overlapped CHS K-joints.

## 5.2 INTERPOLATION METHOD

The main concept of this approach is to combine the results obtained from the numerical parametric studies with the standard interpolation method which is commonly used in FE method [84]. Since the responses of the joints for those identified parameters over some selected ranges were pre-computed at some fixed intervals during the parametric study, a logical way to approximate the variation of the responses can be obtained by using the standard Lagrangian interpolation functions that

are frequently used in the FE analysis. Figure 5.1 shows an example where the variation of the response $\Phi$ is a function of a certain parameter $\xi$ in the range [$\xi_1$, $\xi_8$]. Note that $\Phi$ could be the SCF of the joint or it could be other key responses such as the stress intensity factor (SIF) at the crack tip for a cracked joint. The values of $\Phi$ at the nodes, $\xi_i$, $i$ = 1,.., 8 are already computed during the parametric study and are denoted as $\Phi_i$. If the value of $\Phi$ at a given value of $\xi = \xi_{eval}$ is required, the third interval [$\xi_3$, $\xi_4$] that contains $\xi_{eval}$ is first identified. The approximated value $\tilde{\Phi}(\xi_{eval})$ is then computed as

$$\tilde{\Phi}(\xi_{eval}) = L_1(\xi_{eval})\Phi_3 + L_2(\xi_{eval})\Phi_4 \tag{5.1}$$

In Eqn. (5.1), $L_j(\xi)$, j=1, 2 are the first order Lagrangian interpolation function defined as

$$L_1(\xi) = \frac{\xi_{i+1} - \xi}{\xi_{i+1} - \xi_i}$$
$$L_2(\xi) = \frac{\xi - \xi_i}{\xi_{i+1} - \xi_i}, i = 3 \tag{5.2}$$

For the 2D case, the variation of $\Phi$ is a function of two parameters $\xi^1$ and $\xi^2$ and the desired point ($\xi^1_{eval}, \xi^2_{eval}$) is enclosed by $2^2=4$ nodal points as shown in Figure 5.2. The $i_1$th interval along the $\xi^1$ axis and the $i_2$th interval along the $\xi^2$ axis that enclosing ($\xi^1_{eval}, \xi^2_{eval}$) can be easily identified. The approximated value $\tilde{\Phi}(\xi^1_{eval}, \xi^2_{eval})$ at the desired point can be obtained by extending Equations (5.1) and (5.2) as

$$\tilde{\Phi}(\xi^1_{eval}, \xi^2_{eval}) = \sum_{\alpha_1,\alpha_2=1,2}^{\alpha_1+\alpha_2 \le 4} L^1_{\alpha_1}(\xi^1_{eval}) L^2_{\alpha_2}(\xi^2_{eval}) \Phi_{i_1+\alpha_1-1, i_2+\alpha_2-1} \tag{5.3}$$

where

$$L_1^k\left(\xi^k\right)=\frac{\xi_{i_k+1}^k-\xi^k}{\xi_{i_k+1}^k-\xi_{i_k}^k}$$
$$L_2^k\left(\xi^k\right)=\frac{\xi^k-\xi_{i_k+1}^k}{\xi_{i_k+1}^k-\xi_{i_k}^k}, k=1,2 \quad (5.4)$$

In general, in order to obtain approximation of $\Phi$ with respected to the variation of $M$ selected parameters $\xi^k$, k=1,…., $M$, the above interpolation approach should be extended to the $M$-dimensional space. In this case, the desired point of evaluation $\boldsymbol{\xi}_{eval} = (\xi_{eval}^1, \xi_{eval}^2, ...., \xi_{eval}^M)$ is enclosed by a hyper-rectangle with $2^M$ nodes and $M$ intervals $[\xi_{i_k}^k, \xi_{i_{k+1}}^k]$ such that $\xi_{i_k}^k \le \xi_{eval}^k \le \xi_{i_{k+1}}^k$ for $k$=1,….,$M$. The expression of the approximated value at the point $\boldsymbol{\xi}_{eval}$, $\tilde{\Phi}\left(\boldsymbol{\xi}_{eval}\right)$, is given by

$$\tilde{\Phi}\left(\boldsymbol{\xi}_{eval}\right)=\sum_{\alpha_k=1,2,k=1,..M}^{\sum\alpha_k\le 2M}\left(\prod_{k=1}^{M}L_{\alpha_k}^k\left(\xi_{eval}^k\right)\right)\Phi_{\mathbf{i_k}+\boldsymbol{\alpha_k}-1} \quad (5.5)$$

In Equation (5.5), $\Phi_{\mathbf{i_k}+\boldsymbol{\alpha_k}-1}$ denotes the pre-computed nodal value of $\Phi$ at the node $(\xi_{i_1+\alpha_1-1}^1, \xi_{i_2+\alpha_2-1}^2, ...., \xi_{i_M+\alpha_M-1}^k)$. Note that in Equations (5.1) to (5.5), the number of intervals may not be the same for all parameters and the interval may not be uniform.

## 5.3 DEVELOPMENT OF NEW METHODS

### 5.3.1 Introduction

From the extensive numerical study carried out to access the performance of the above interpolation approach for the prediction of the SIF at the deepest point of surface

cracks for gapped CHS K-joints [53], it was found that this approach has led to more accurate and reliable response predictions with a lower relative error and a smaller error range. As a rule, to implement the interpolation method, there is a need to create a database, where the new method can refer to.

### 5.3.2 SCF Database for New Methods

The SCF results together with the corresponding parameters are stored in a database as discussed earlier in Chapter 4. Two types of database were created and used in conjunction with two slightly different approaches of the interpolation method: the first one is called the *point interpolation method* (PIM), and the second one is called the *line interpolation method* (LIM). The SCF database for the PIM stores only one maximum SCF value from each load case, except for the AX11 and the AX21 load cases where two maximum values are stored. An explanation why that is needed would be described later. The SCF database for the PIM was shown in Figure 4.16 of Chapter 4.

The SCF database for the LIM, in general, stores a set of SCF values along each intersection curve. The data are specially organized in the "Tree structure" format as shown in Figure 5.3 so as to facilitate the searching of the SCF data for the SCF and HSS estimations. There are five levels of sub-folders in the database, including seven $\beta$ sub-folders, five $\theta$ sub-folders, five Ov sub-folders, twenty $\gamma$–$\tau$ sub-folders and eventually eight loading cases SCF data files for each $\gamma$–$\tau$ sub-folder as shown in detailed in Figure 5.3. The eight loading cases SCF data files stored the SCF values belong to different curves as shown in Figure 5.4. As can be seen from Figure 5.3, the eight loading cases are following: AX11A, AX11C, AX21A, AX21B, IPB11C, IPB12A, IPB21B and IPB22A. In addition, each loading case SCF data file stores the information about the SCF values along the weld toe (curve) on both chord and braces under different load cases. For example from Figure 5.4, the AX11C consists from AX11cC and AX11tC which refer to maximum SCF values under AX11 load case on the weld toe of chord and through brace along Curve C, respectively. All these SCF

values were obtained from FE analyses.

In this study, based on the FE meshes used in the FE analyses there are 14 to 25 SCF values recorded along each intersection curve at the weld toe. Each SCF value was calculated based on quadratic extrapolation procedure at the mild point of FE meshes along the intersection (see Figure 5.5).

### 5.3.3 The Point Interpolation Method "PIM"

The PIM has been developed based on the interpolation method using 5D shape functions and the SCF database to estimate the maximum SCF for partially overlapped CHS K-joint within the range of this study. The fact that the method is named *Point Interpolation Method* (PIM) is because its database mainly stored only one maximum SCF value obtained from the FE analysis from each load case. In this method, to estimate the HSS for a partially overlapped K-joint, the SCF values corresponding to the different loading cases are firstly computed based on the data inputted the geometrical properties and load cases together with the interpolation method and SCF database. Once the SCF values for different loading cases are estimated, the HSS is computed based on superposition approach proposed by API RP-2A [33]. The peak hot spot stress is expressed as the following:

$$Peak\ HSS = \left|SCF_{AX} f_{AX}\right| + \left[(SCF_{IPB} f_{IPB})^2 + (SCF_{OPB} f_{OPB})^2\right]^{\frac{1}{2}} \quad (5.6)$$

where $SCF_{AX}$, $SCF_{IPB}$, $SCF_{OPB}$ are SCFs for the AX, the IPB and the OPB loading cases, respectively. $f_{AX}$, $f_{IPB}$ and $f_{OPB}$ are the corresponding nominal stresses provided.

However, since the OPB load case is not considered in this current study, the HSS values for the basic and combined load cases are expressed as:

1. HSS values for basic AX load cases (AX11, AX21)

$$Peak\ HSS_{AX11} = \left|SCF_{AX11} f_{AX1}\right| \tag{5.7}$$

$$Peak\ HSS_{AX21} = \left|SCF_{AX21} f_{AX2}\right|$$

2. HSS values for basic IPB load cases (IPB11, IPB12, IPB21 and IPB22)

$$Peak\ HSS_{IPB11} = \left[SCF_{IPB11} f_{IPB1}\right] \tag{5.8}$$

$$Peak\ HSS_{IPB12} = \left[SCF_{IPB12} f_{IPB2}\right]$$

$$Peak\ HSS_{IPB21} = \left[SCF_{IPB21} f_{IPB3}\right]$$

$$Peak\ HSS_{IPB22} = \left[SCF_{IPB22} f_{IPB4}\right]$$

3. HSS values for combined load case of AX11+IPB11

$$Peak\ HSS_{AX11+IPB11} = \left|SCF_{AX11} f_{AX1}\right| + \left[SCF_{IPB11} f_{IPB1}\right] \tag{5.9}$$

4. HSS values for combined load case of AX11+IPB12

$$Peak\ HSS_{AX11+IPB12} = \left|SCF_{AX11} f_{AX1}\right| + \left[SCF_{IPB12} f_{IPB2}\right] \tag{5.10}$$

5. HSS values for combined load case of AX21+IPB21

$$Peak\ HSS_{AX21+IPB21} = \left|SCF_{AX21} f_{AX2}\right| + \left[SCF_{IPB21} f_{IPB3}\right] \tag{5.11}$$

6. HSS values for combined load case of AX21+IPB22

$$Peak\ HSS_{AX21+IPB22} = \left|SCF_{AX21} f_{AX2}\right| + \left[SCF_{IPB22} f_{IPB4}\right] \tag{5.12}$$

where $SCF_{AX11}$, $SCF_{AX21}$, $SCF_{IPB11}$, $SCF_{IPB12}$, $SCF_{IPB21}$, and $SCF_{IPB22}$ are the maximum SCFs for the AX11, AX21, IPB11, IPB12, IPB21 and IPB22 loading cases, respectively. $f_{AX1}$, $f_{AX2}$, $f_{IPB1}$, $f_{IPB2}$, $f_{IPB3}$ *and* $f_{IPB4}$ are the nominal stresses for the AX11, AX21, IPB11, IPB12, IPB21 and IPB22 load cases, respectively.

Figure 5.6 shows the basic concept of the PIM on how it calculates the HSS for a partially overlapped CHS K-joint subjected to combined load case of AX+IPB. The HSS value of the combined load case is determined by summing up of maximum HSS value from each load case. From Figure 5.6, the ***A*** value is the maximum HSS value under AX load case and the ***B*** value is the maximum HSS value under IPB load case. Then, the ***A+B*** value is considered as maximum HSS value under combined load case AX+IPB.

Figure 5.7 shows the maximum HSS value obtained for a partially overlapped CHS K-joint subjected to the combined load case of AX11 (100 kN) +IPB11 (12 kN.m). The geometrical properties of the partially overlapped K-joint are following: $\theta = 60°$, Ov = 0.25, $\beta = 0.4$, $\gamma = 11.38$ and $\tau = 0.8$. Based on Equation 5.9, the HSS value of combined load case is summing up the maximum HSS of the AX11 load case (Figure 5.7 (a)) with the maximum HSS of the IPB11 load case (Figure 5.7 (b)). It is observed that the difference of the HSS value obtained from the PIM against the HSS value obtained from the FE analyses is 5.3%. Such a high accuracy is due to (i) both in the AX and the IPB load cases the maximum HSSs occur on the Curve C, (ii) the maximum positions of them are not far from each other, (iii) the variation of the SCFs between these locations are not big. Obviously, if these three conditions are not true, for example under combined loading case of AX11+IPB12, the estimated SCF error could be high.

For the case when the HSS value from each basic load case occurs in different curves (e.g. the combined load case of AX11+IPB12), in the current implementation of the PIM there is an arrangement to avoid unreasonable overestimations by selecting the most appropriate HSS value for summation. Now take the case of AX11+IPB12 as an example, the maximum HSS value from the AX11 load case occurs on the Curve C, while for the IPB12 load case it occurs on the Curve A. These two curves are in opposite side to one another (see Figure 5.4).

Figure 5.8 shows how to avoid the overestimation of the HSS value when the joint is

subjected to the combined load case of AX11 (100 kN) +IPB12 (12 kN.m). The geometrical properties of the partially overlapped CHS K-joint are the following: $\theta$ = 60°, Ov = 0.25, $\beta$ = 0.4, $\gamma$ = 11.38 and $\tau$ = 0.8. The HSS value of this case is obtained by summing up the maximum HSS value of IPB12 load case along curve A (Figure 5.8) with the corresponding HSS of AX11 load case along curve A (AX11A in Figure 5.9(a)), but not with the higher HSS value of AX11 load case along curve C (AX11C in Figure 5.9(b)). However, if based on concept of Equation 5.6 the maximum HSS of combined load case of AX11+IPB12 should have been summing up the maximum HSS of IPB12 load case (along Curve A) with the maximum HSS of the AX11 load case (AX11C in Figure 5.9(b) along Curve C). Obviously, this would have made the results too conservative as shown in Figure 5.10. It is observed that the difference of HSS value obtained from the Equation 5.6 with HSS value obtained from FE analysis is 25.03%. At the same time, the difference of HSS value obtained from the current PIM with HSS value obtained from the same FE analysis is only 0.64%. This example shows that the overestimation of HSS value can be solved in some degree.

However, as the HSS of each load case could be located at different positions in general, this will undoubtedly lead to overestimation of the real peak stress value. This was proven by Pang & Lee [34] in their study on tubular T-joints. Hence, a better method is needed and this leads to the development of the PIM.

### 5.3.4 The Line Interpolation Method "LIM"

As mentioned earlier, Equation (5.6) is simply summing up the products of the nominal stress due to each load type and the corresponding maximum SCFs which are obtained either from the saddle or the crown, depends on where the maximum occurred. This will make the results conservative because in general as the HSS caused by each basic load could be located at different positions. Therefore, the sum of the HSS from Equation (5.6) will overestimate the peak stress value. This had been proven by Pang and Lee [34] in their study on tubular T-joints. To avoid this disadvantage, Gulati et al.

[35] had suggested superimposing the stress distributions from each of basic load modes to obtain the HSS. Subsequently, a new equation was proposed as follow:

$$\sigma(\varphi) = K_A(\varphi) f_{AX} + K_{Bi}(\varphi) f_{IPB} + K_{Bo}(\varphi) f_{OPB} \quad (5.13)$$

where $K_A(\varphi)$, $K_{Bi}(\varphi)$, $K_{Bo}(\varphi)$ specify the stress concentration factors (SCFs) around the intersection of joint subjected to AX, IPB and OPB respectively. $f_{AX}$, $f_{IPB}$ and $f_{OPB}$ are the corresponding nominal stresses.

The position and value of the HSS can be determined from Equation (5.13) if $K_A(\varphi)$, $K_{Bi}(\varphi)$, $K_{Bo}(\varphi)$ can be explicitly provided. However, the explicit expressions were not provided in the literature. Chang and Dover [1] suggested that $K_A(\varphi)$, $K_{Bi}(\varphi)$, $K_{Bo}(\varphi)$ can be obtained using equations of Hellier et al. [36] for tubular T and Y-joints. Yeoh et al. [37] verified this method by conducting a test on a tubular T-joint and found that stress distributions obtained by superposition method of Equation (5.13) compared well with the results obtained directly from the full-scale test. Soh and Soh [38] also studied the superposition method by conducting a test on tubular K-joint and found the results from this method agreed well with experimental results. Although this method can provide more accurate information of hot spot stress, it is still not easy to be applied in practice because the accuracy of the HSS from Equation (5.13) depends on the accurate expressions of $K_A(\varphi)$, $K_{Bi}(\varphi)$, $K_{Bo}(\varphi)$.

Therefore, in the present study a new tool is suggested to predict the HSS values which base on Equation (5.13). The created database is able to provide all positions and $K_A(\varphi)$, $K_{Bi}(\varphi)$, $K_{Bo}(\varphi)$ along the intersection of partially overlapped K-joints.

Since in the current research, the OPB load case is not considered in this current study, the HSS values for the basic and combined load cases are expressed as:

1. HSS values for basic AX load cases (AX11, AX21)

$$\sigma_{AX11}(\varphi) = K_{A1i}(\varphi) f_{AX1} \tag{5.14}$$

$$\sigma_{AX21}(\varphi) = K_{A2i}(\varphi) f_{AX2}$$

2. HSS values for basic IPB load cases (IPB11, IPB12, IPB21, and IPB22)

$$\sigma_{IPB11}(\varphi) = K_{B1i}(\varphi) f_{IPB1} \tag{5.15}$$

$$\sigma_{IPB12}(\varphi) = K_{B2i}(\varphi) f_{IPB2}$$

$$\sigma_{IPB21}(\varphi) = K_{B3i}(\varphi) f_{IPB3}$$

$$\sigma_{IPB22}(\varphi) = K_{B4i}(\varphi) f_{IPB4}$$

3. HSS values for combined load case of AX11+IPB11

$$\sigma_{AX11+IPB11}(\varphi) = K_{A1i}(\varphi) f_{AX1} + K_{B1i}(\varphi) f_{IPB1} \tag{5.16}$$

4. HSS values for combined load case of AX11+IPB12

$$\sigma_{AX11+IPB12}(\varphi) = K_{A1i}(\varphi) f_{AX1} + K_{B2i}(\varphi) f_{IPB2} \tag{5.17}$$

5. HSS values for combined load case of AX21+IPB21

$$\sigma_{AX21+IPB21}(\varphi) = K_{A2i}(\varphi) f_{AX2} + K_{B2i}(\varphi) f_{IPB3} \tag{5.18}$$

6. HSS values for combined load case of AX21+IPB22

$$\sigma_{AX21+IPB22}(\varphi) = K_{A2i}(\varphi) f_{AX2} + K_{B2i}(\varphi) f_{IPB4} \tag{5.19}$$

where $K_{A1i}(\varphi)$, $K_{A2i}(\varphi)$, $K_{B1i}(\varphi)$, $K_{B2i}(\varphi)$, $K_{B3i}(\varphi)$ *and* $K_{B4i}(\varphi)$ specify the stress concentration factors (SCFs) around the intersection of joint subjected to AX11, AX21, IPB11, IPB12, IPB21 and IPB22, respectively; $f_{AX1}$, $f_{AX2}$, $f_{IPB1}$, $f_{IPB2}$, $f_{IPB3}$, $f_{IPB4}$ are the corresponding nominal stresses, respectively.

The LIM has been developed based on the interpolation method using the 5D shape functions and the SCF database shown in Figure 5.3 to generate HSS value for partially overlapped CHS K-joint within the range of this study. The fact that the method is named as the "*Line Interpolation Method* (LIM)" is because the database stored a set of SCF values along the intersection curves (lines) obtained from FE analyses for each load case (Figures 5.4 and 5.5). The LIM has the same working principle as the PIM, but the difference is that the HSS of combined load case obtained from the PIM is based on Equations 5.7 – 5.12, meaning summing up the products of the HSS value due to each load type, which are in general correspondingly to different locations. The HSS of combined load case obtained from the LIM is based on Equations 5.14 to 5.19, which are accurate based on the superposition principle.

The basic concept of LIM is that the maximum HSS of the combined load case is computed from the summation of the variations between the two basic load cases along the weld toe. As shown in Figure 5.11, the HSS values from points *1, 2, 3,.., n* under the basic load case AX are denoted as a(1), a(2), a(3),…, a(n) and the HSS values from points *1, 2, 3,…, n* under the basic load case IPB are denoted as b(1), b(2), b(3),…, b(n). The final HSS value for the combined load case at each point is computed by summing up the HSS from these two basic load cases in the form of a(1)+b(1), a(2)+b(2), a(3)+b(3),…,a(n)+b(n). Finally, the maximum HSS value of combined load case AX+IPB is obtained from these series of HSS sums. As can be seen from Figure 5.11, the maximum value of a(1)+b(1) is considered as the maximum HSS value for the combined load case AX+IPB.

Figure 5.12 shows an example of the LIM on how to obtain the HSS value for a partially overlapped CHS K-joint subjected to the combined load case AX11 (100 kN)+IPB11 (12 kN.m). The geometrical properties of the partially overlapped CHS K-joint are the following: $\theta$ = 60°, Ov = 0.25, $\beta$ = 0.4, $\gamma$ = 11.38 and $\tau$ = 0.8. The maximum HSS value of the combined load case of AX11+IPB11 is obtained from the series of the HSS sums of the two basic load cases AX11 (100 kN) (Figure 5.12 (a))

and IPB (12 kN.m) (Figure 5.12 (b)) at each point along the intersection curve C. It is observed that the difference of HSS value obtained from the LIM against HSS obtained from the FE analyses is 2.01%. It is worth to note that the LIM could predict the HSS value well fit with the HSS value obtained from FE analyses.

## 5.4 VALIDATION OF SCF AND HSS USING THE NEW METHODS

### 5.4.1 Validation of SCF obtained from the PIM

To validate the accuracy and reliability of the PIM, the SCF values obtained from the PIM are compared with the SCF values obtained from the FE analyses based on the 192 additional mid-point models which are tabulated in Table 4.5. The relative error between the estimated SCF values from the PIM and the FE analyses with respect to the 192 additional mid-point data tabulated is defined as:

$$E_{PIM-FEM}(SCF) = \frac{SCF_{PIM} - SCF_{FEM}}{SCF_{PIM}} \times 100\% \tag{5.20}$$

where $SCF_{PIM}$ is the SCF value estimated from the PIM, and $SCF_{FEM}$ is the SCF value obtained from the 192 additional FE analyses.

Figures 5.13 to 5.18 and Table 5.1 show the distribution of numerical models in different error percentage ranges under different load cases. From these figures and Table 5.1, it is observed that most models are within the range of -20% ≤ Error ≤ 20% with a maximum, a minimum percentages and a mean of 99.35%, 96.08% and 99.05 %, respectively. Thus, it could be concluded that the SCF values obtained from the PIM fit well with the SCF values obtained from the FE analyses.

### 5.4.2 Error Comparison of SCF using the PIM and the PRM

The accuracy and reliability of SCFs obtained from the PIM can be also evaluated by comparing the relative errors with the PRM as discussed earlier in Chapter 4. The relative error distributions of the SCFs for the two methods against the SCFs obtained from the FE analyses are plotted in Figures 5.19 to 5.24. These figures illustrate the comparison between the two methods for partially overlapped CHS K-joints under different basic loading cases. It could be seen in Table 5.1 that the PIM produced better results than the PRM. Most models are within the error range of -20% to 20%. The mean of models in the range when using the PIM is 99.05%, while the mean for the same range when using the PRM is only 79.45%. Hence, it could be concluded that the PIM is more accurate than the PRM.

### 5.4.3 Error Comparisons of HSS obtained from the LIM, the PIM and the PRM

Three methods for predicting the HSS for the 192 additional mid-point models, given in Table 4.5, subjected to the combined load cases: AX11 (100 kN) +IPB11 (12 kN.m), AX11 (100 kN) +IPB12 (12 kN.m), AX21 (100 kN) +IPB21 (12 kN.m) and AX21 (100 kN) +IPB22 (12 kN.m) loading employed to comparing the accuracies of the LIM, the PIM and the PRM.

The relative errors of the estimated HSS values from the LIM, the PIM and the PRM against the FE analyses are defined as:

$$E_{LIM-FEM}(HSS) = \frac{HSS_{LIM} - HSS_{FEM}}{HSS_{LIM}} \times 100\% \tag{5.21}$$

$$E_{PIM-FEM}(HSS) = \frac{HSS_{PIM} - HSS_{FEM}}{HSS_{PIM}} \times 100\% \tag{5.22}$$

$$E_{PRM-FEM}(HSS) = \frac{HSS_{PRM} - HSS_{FEM}}{HSS_{PRM}} \times 100\% \tag{5.23}$$

where $HSS_{LIM}$ is the HSS value estimated from the LIM, $HSS_{PIM}$ is the HSS value estimated from the PIM, $HSS_{PRM}$ is the HSS value estimated from the PRM and $HSS_{FEM}$ is the HSS value obtained from the FE analyses.

Figures 5.25 to 5.28 together with Table 5.2 show the comparison of relative error distributions of the HSS values obtained from the LIM, the PIM and the PRM against the HSS values obtained from FE analyses. It is observed that the LIM produces better HSS results in the context that more numerical models are in the error range of -20% to 20%. The means of models for the LIM, the PIM and the PRM in the error range are 96.56%, 95.00% and 88.88 %, respectively. It is observed that the LIM has an advantage in terms of predicting HSS values over the PIM, let alone the PRM.

It is also important to note that the advantage of using the LIM to the PIM and the PRM can be seen when the basic load cases have their peak HSS positions located at very different positions. Figures 5.29 to 5.31 show how the FEM works with combined load case AX21 (100 kN) +IPB21 (6 kN.m). The geometrical properties of the partially overlapped CHS K-joint are following: $\theta$ = 35°, Ov = 0.35, $\beta$ = 0.65, $\gamma$ = 10.92 and $\tau$ = 0.504. The peak HSS under basic load case AX21 (100 kN) occurs at the point 103.89 mm from crown heel of the joint, while the peak HSS under basic load case IPB21 (6 kN.m) occurs at the point 6.06 mm from the crown heel of the joint. Then, the peak HSS under combined load case AX21 (100 kN) +IPB21 (6 kN.m) occurs at the point 43.29 mm from the crown heel of the joint. From Figure 5.32 and Table 5.3, note that the relative errors for the LIM, the PIM and the PRM under combined load case AX21 (100 kN) + IPB21 (6 kN.m) are 5.12%, 35.93% and 42.54%, respectively. With the same geometrical properties of partially overlapped K-joint, Figure 5.33 shows the combined load case AX21 (100 kN) +IPB21 (12 kN.m). From Figure 5.33 and Table 5.3, note that the relative errors for the LIM, the PIM and the PRM under the load case are 1.35%, 25.33% and 34.24%, respectively. It is observed that the relative errors for the LIM, the PIM and the PRM in different load cases are changed even though the joint properties remain the same. However, it should be noted that the relative error for

the LIM still remains the smallest one when compared to that for the PIM and the PRM. Thus, it could be concluded that the LIM is the best one in predicting HSS value when compared with the PIM and the PRM.

## 5.5 IMPLEMENTATION OF THE PIM AND THE LIM

The above interpolation procedure is applied for predicting the SCF and HSS values for partially overlapped CHS K-joints in this study. In order to facilitate the user to compute the predicted value using Equation 5.5, an interactive program which allows user input the dimensional of the joint, as well as the loading applied to it, was developed. As mentioned earlier in Chapter 4, the 5 parameters, namely $\theta$, Ov, $\beta$, $\gamma$ and $\tau$ have a major impact on determining SCF values for partially overlapped CHS K-joint. Therefore, the interpolation approach with these 5 parameters was applied. Based on interpolation approach the desired point of evaluation is enclosed by hyper-quadrilateral with $2^5$ = 32 nodes and used to interpolate the SCF values of the given partially overlapped CHS K-joint model. The detailed format of the 5D shape functions are showed in Appendix B.

A program has been developed based on the interpolation method. Figure 5.34 shows the screen shot of the user input interface of the program. Input data include geometrical parameters and loading components.

1) Geometrical parameters:

$d_1$ = diameter of chord,

$t_1$ = thickness of chord,

$d_2$ = diameter of brace,

$t_1$ = thickness of brace,

$\theta$ = intersecting angle between chord and brace and

Ov = overlap ratio.

2) Loading components:

$P_1$ = tension axial load on the through brace,

$M_1$ = positive in-plane bending on the through brace,

$M_2$ = negative in-plane bending on the through brace,

$P_2$ = tension axial load on the through brace,

$M_3$ = positive in-plane bending on the overlapping brace and

$M_4$ = negative in-plane bending on the overlapping brace.

Once the input data are filled up, they are then saved in a text file names by the user. Alternatively, the inputs can also be prepared in Microsoft Office Excel. This method of creating the input file is useful especially when it comes to multiple analyses of partially overlapped CHS K-joints.

After the input data are all defined, the interactive program allows the user to choose method of calculation (the PIM or the LIM). The PIM can be used to estimate SCF and then used the estimated SCF values to compute the HSS values of any partially overlapped CHS K-joint, whereas the LIM can be used directly to predict the HSS values of partially overlapped CHS K-joint. Once the program is executed, the results of HSS values can be displayed through the user output interface of the program as shown in Figure 5.35. In addition, if needed, the user could also save the results into an output file for future reference. Note that this interactive program also allows the user to specify multiple joints and loading configurations through an input file so that the user would be able to conduct a fast what-if analysis conveniently. In the current implementation, a maximum number of 65000 partially overlapped CHS K-joints cases could be handle by this program at a time.

The total storage size needed to store all programs together with database for the PIM and the LIM is approximately 900 KB and 30Mbytes, respectively. Therefore, the program and the database needed could be easily stored and launched from a portable flash drive. Furthermore, the speed of the program is also very fast such that a multiple run involving 100 joint configurations could be completed within 2.30 and 2.15

minutes for the PIM and the LIM, respectively, on a low end PC.

## 5.6 CONCLUDING REMARKS

From the above discussions on the interpolation and the regression methods, it is clear that the interpolation method has some important advantages over the regression method.

1. It is observed that the accuracy of SCFs obtained from the PIM is better than the PRM.

2. The accuracy of HSSs obtained from the LIM is better than the PIM and the PRM.

3. In the PIM and the LIM, the SCF value or HSS value for each model is actually determined by only several numerical models adjacent to the calculated model only, unlike in the PRM where the SCF or HSS is determined by the whole set of data to form the regression equations. This could be a reason that makes the interpolation methods better than the regression method.
Given the efficiency of this new and workable approach based on interpolation method, it is worth to put an effort and time to analyze as many models as possible. It is obvious that these two new methods (the PIM and the LIM) have an advantage over the conventional regression method.

4. The interactive program allows the users to choose PIM and LIM easily, and is friendly to users.

Table 5.1 Assessment of the SCF values obtained from the PIM and the PRM against the SCF values obtained from the FE analyses based on relative error

| Percentage of models in different ranges of relative error (%) | | | | | |
|---|---|---|---|---|---|
| Methods | Load Cases | Members | Frequency of occurrence of SCF error (%) | | |
| | | | < -20.00 | -20.00 ↔ 20.00 | > 20.00 |
| PIM | AX11 | Through brace | - | 99.35 | 0.65 |
| | | Chord | - | 99.35 | 0.65 |
| | AX21 | Overlapping brace | 1.96 | 96.08 | 1.96 |
| | | Chord | - | 99.08 | 0.65 |
| | IPB11 | Through brace | - | 99.35 | 0.65 |
| | | Chord | 0.65 | 99.35 | 0.65 |
| | IPB12 | Through brace | - | 99.35 | 0.65 |
| | | Overlapping brace | - | 99.35 | 0.65 |
| | IPB21 | Overlapping brace | - | 99.35 | 0.65 |
| | | Chord | - | 99.35 | 0.65 |
| | IPB22 | Overlapping brace | - | 99.35 | 0.65 |
| | | Through brace | - | 99.35 | 0.65 |
| PRM | AX11 | Through brace | 1.97 | 92.11 | 7.24 |
| | | Chord | 0.66 | 44.74 | 54.61 |
| | AX21 | Overlapping brace | 5.26 | 68.42 | 26.32 |
| | | Chord | 9.21 | 85.53 | 5.92 |
| | IPB11 | Through brace | 7.89 | 87.50 | 5.26 |
| | | Chord | 23.68 | 69.08 | 10.53 |
| | IPB12 | Through brace | 5.92 | 88.16 | 5.92 |
| | | Overlapping brace | 6.58 | 88.16 | 5.26 |
| | IPB21 | Overlapping brace | 8.55 | 85.53 | 5.92 |
| | | Chord | 13.03 | 69.21 | 17.76 |
| | IPB22 | Overlapping brace | 3.95 | 80.92 | 15.13 |
| | | Through brace | 4.61 | 94.08 | 1.32 |

Table 5.2 Assessment of the HSS results obtained from the LIM, the PIM and the PRM against the HSS obtained from the FE analyses based on relative error

| Percentage of models in different ranges of relative error (%) | | | | | |
|---|---|---|---|---|---|
| Methods | Load Cases | Members | Frequency of occurrence of HSS error (%) | | |
| | | | < -20.00 | -20.0 ↔ 20.0 | > 20.00 |
| LIM | AX11(100 kN) +IPB11(12 kN.m) | Through brace | - | 96.05 | 3.95 |
| | | Chord | 0.63 | 98.05 | 1.32 |
| | AX11(100 kN) +IPB12(12 kN.m) | Overlap brace | 0.66 | 96.71 | 2.63 |
| | | Chord | 0.66 | 98.03 | 1.97 |
| | AX21(100 kN) +IPB21(12 kN.m) | Through brace | 0.65 | 96.73 | 2.61 |
| | | Chord | 0.61 | 97.08 | 2.31 |
| | AX21(100 kN) +IPB22(12 kN.m) | Through brace | 0.65 | 95.42 | 3.92 |
| | | Overlap brace | 0.65 | 97.39 | 1.96 |
| PIM | AX11(100 kN) +IPB11(12 kN.m) | Through brace | 0.66 | 92.76 | 6.58 |
| | | Chord | 1.32 | 96.71 | 1.97 |
| | AX11(100 kN) +IPB12(12 kN.m) | Overlap brace | 0.66 | 96.05 | 3.29 |
| | | Chord | - | 96.71 | 3.29 |
| | AX21(100 kN) +IPB21(12 kN.m) | Through brace | 0.65 | 96.73 | 2.61 |
| | | Chord | 0.65 | 88.24 | 11.11 |
| | AX21(100 kN) +IPB22(12 kN.m) | Through brace | 0.65 | 95.42 | 3.92 |
| | | Overlap brace | 0.65 | 97.39 | 1.96 |
| PRM | AX11(100 kN) +IPB11(12 kN.m) | Through brace | 3.27 | 95.42 | 1.31 |
| | | Chord | 10.46 | 79.74 | 9.80 |
| | AX11(100 kN) +IPB12(12 kN.m) | Overlap brace | 3.27 | 89.54 | 7.19 |
| | | Chord | 7.19 | 87.58 | 5.23 |
| | AX21(100 kN) +IPB21(12 kN.m) | Through brace | 3.27 | 95.42 | 1.31 |
| | | Chord | 10.46 | 71.24 | 18.30 |
| | AX21(100 kN) +IPB22(12 kN.m) | Through brace | 0.61 | 96.73 | 2.61 |
| | | Overlap brace | 3.92 | 95.42 | 0.65 |

Table 5.3 Comparison of the HSS results obtained from the PRM, the PIM and the LIM against the HSS obtained from the FE analyses

| Load cases | Methods | Relative Error (%) |
|---|---|---|
| AX100+IPB6 | PRM | 42.54 |
| | PIM | 35.93 |
| | LIM | 5.12 |
| AX100+IPB12 | PRM | 34.24 |
| | PIM | 25.33 |
| | LIM | 1.35 |

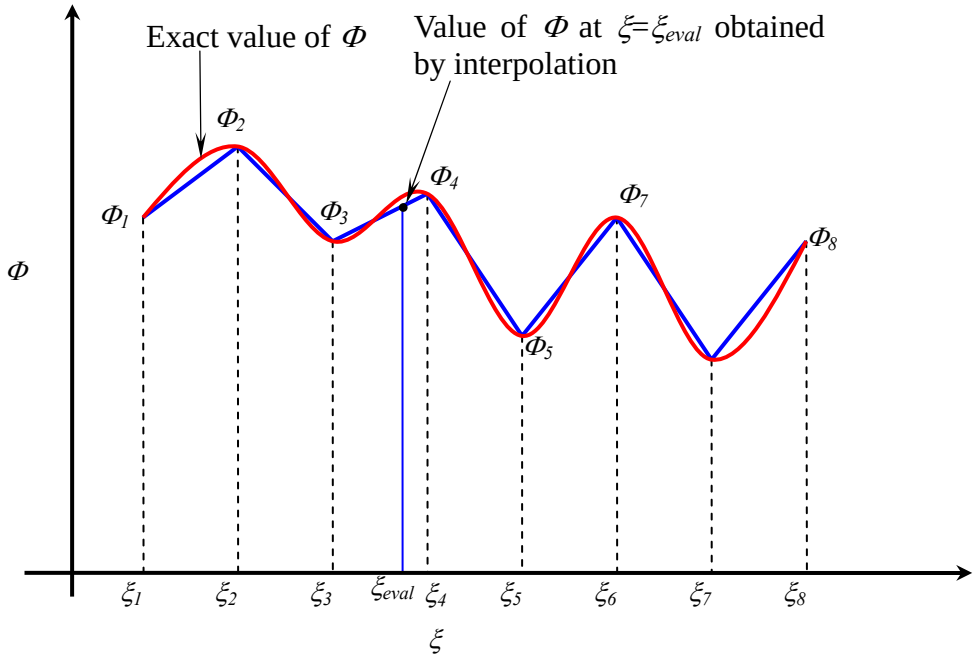


Figure 5.1 Approximation of Φ for the single parameter (1D) case

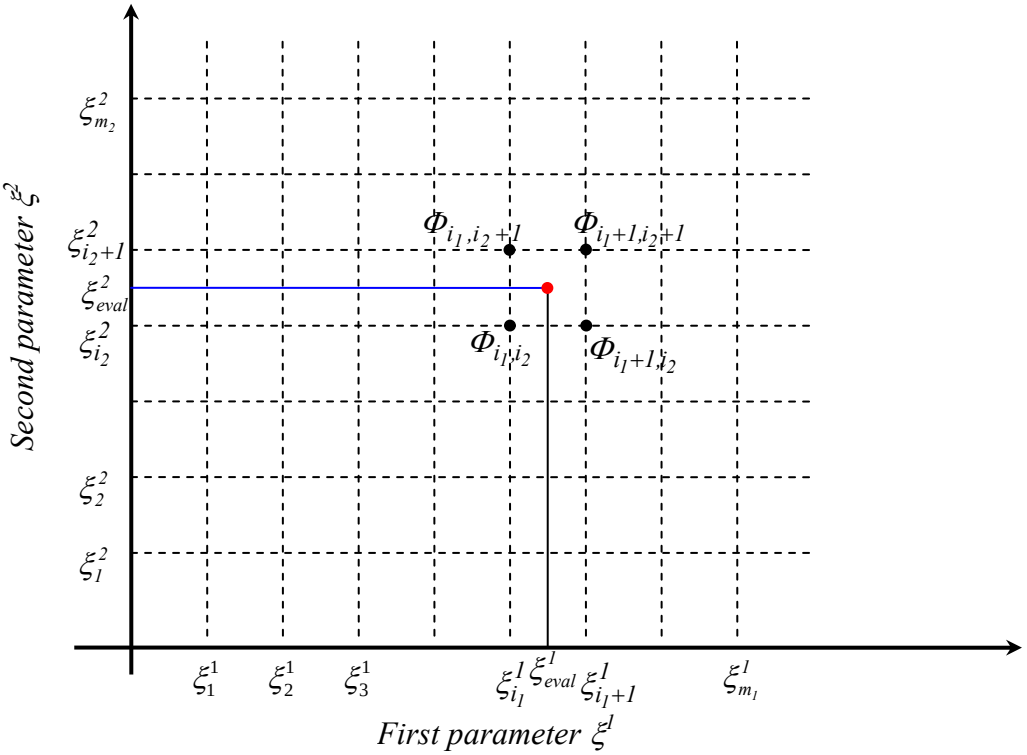


Figure 5.2 Approximation of Φ for the two parameters (2D) case

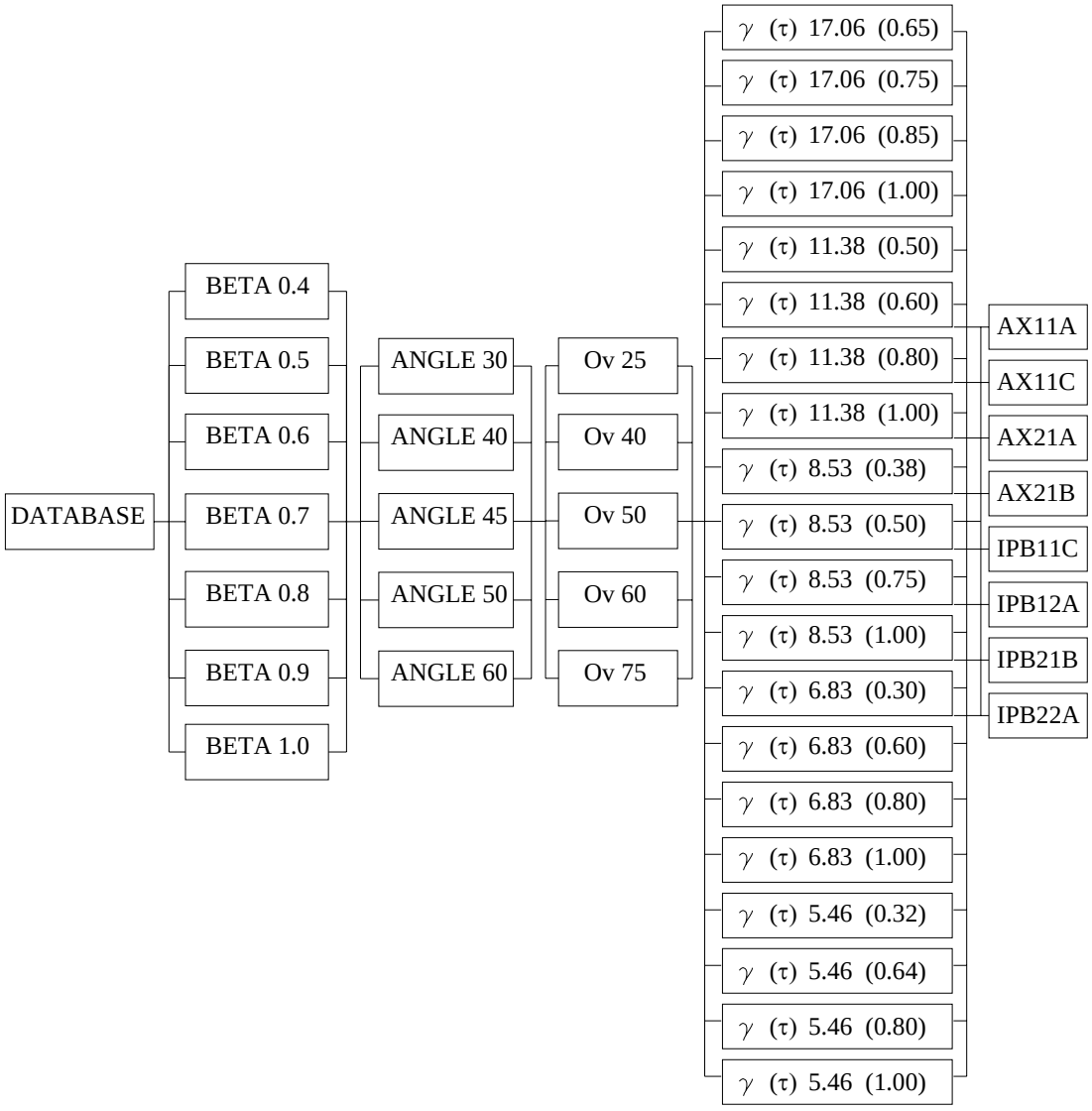


Figure 5.3 SCF database for the LIM

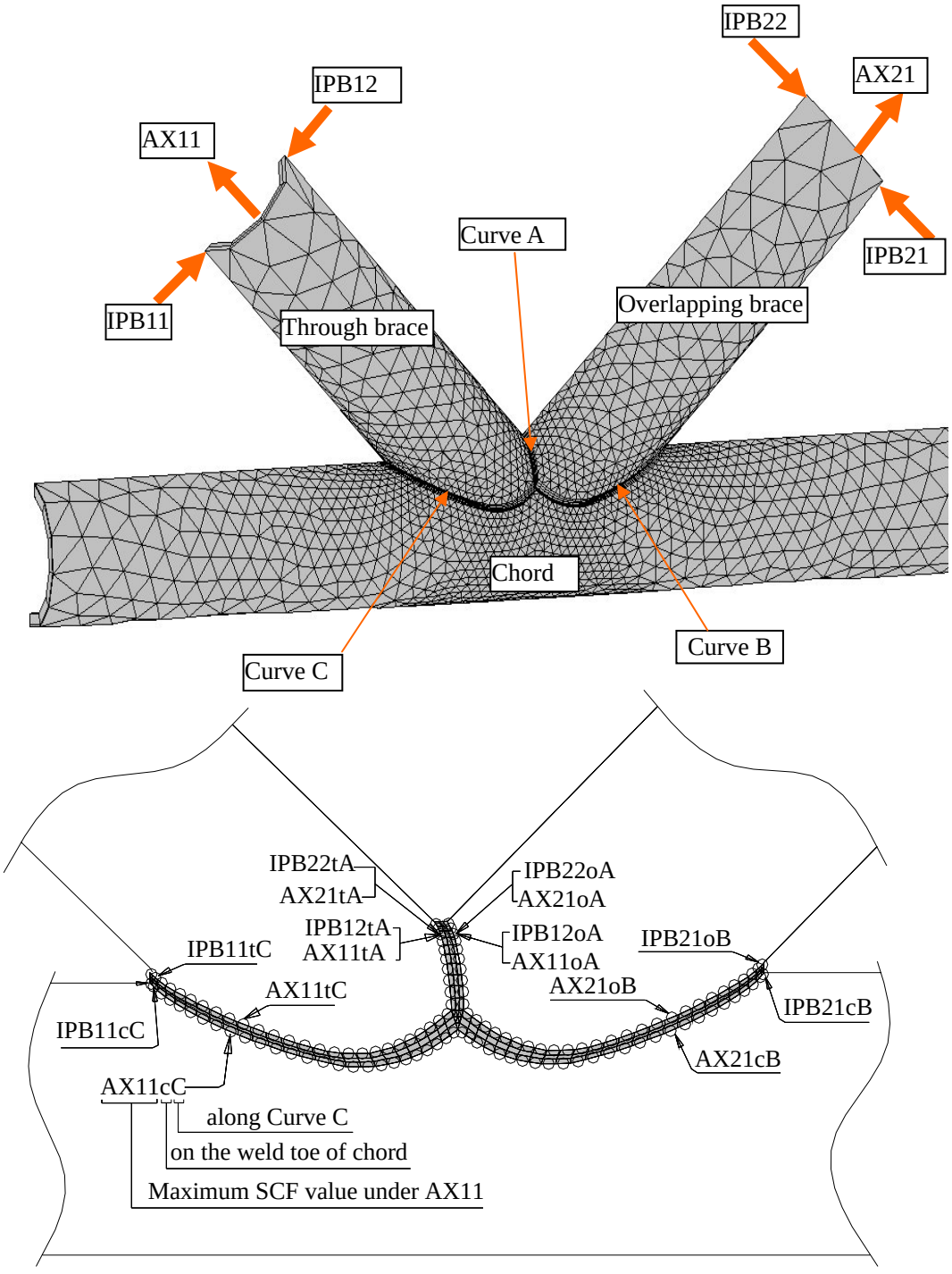


Figure 5.4 Eight loading cases SCF data files names under different load cases on the weld toe along Curves A, B and C

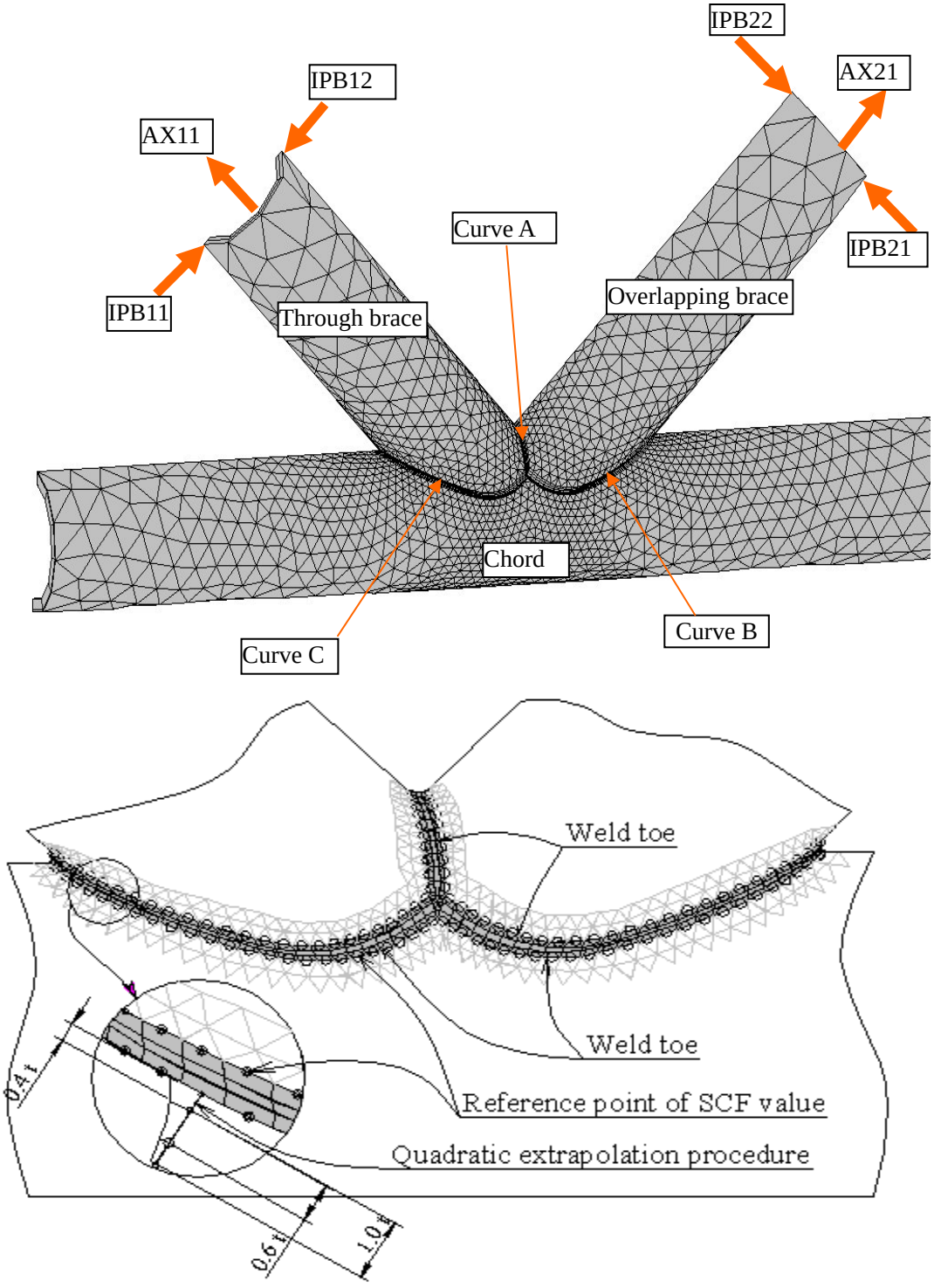


Figure 5.5 SCF reference point along weld toe Curves A, B and C under different load cases

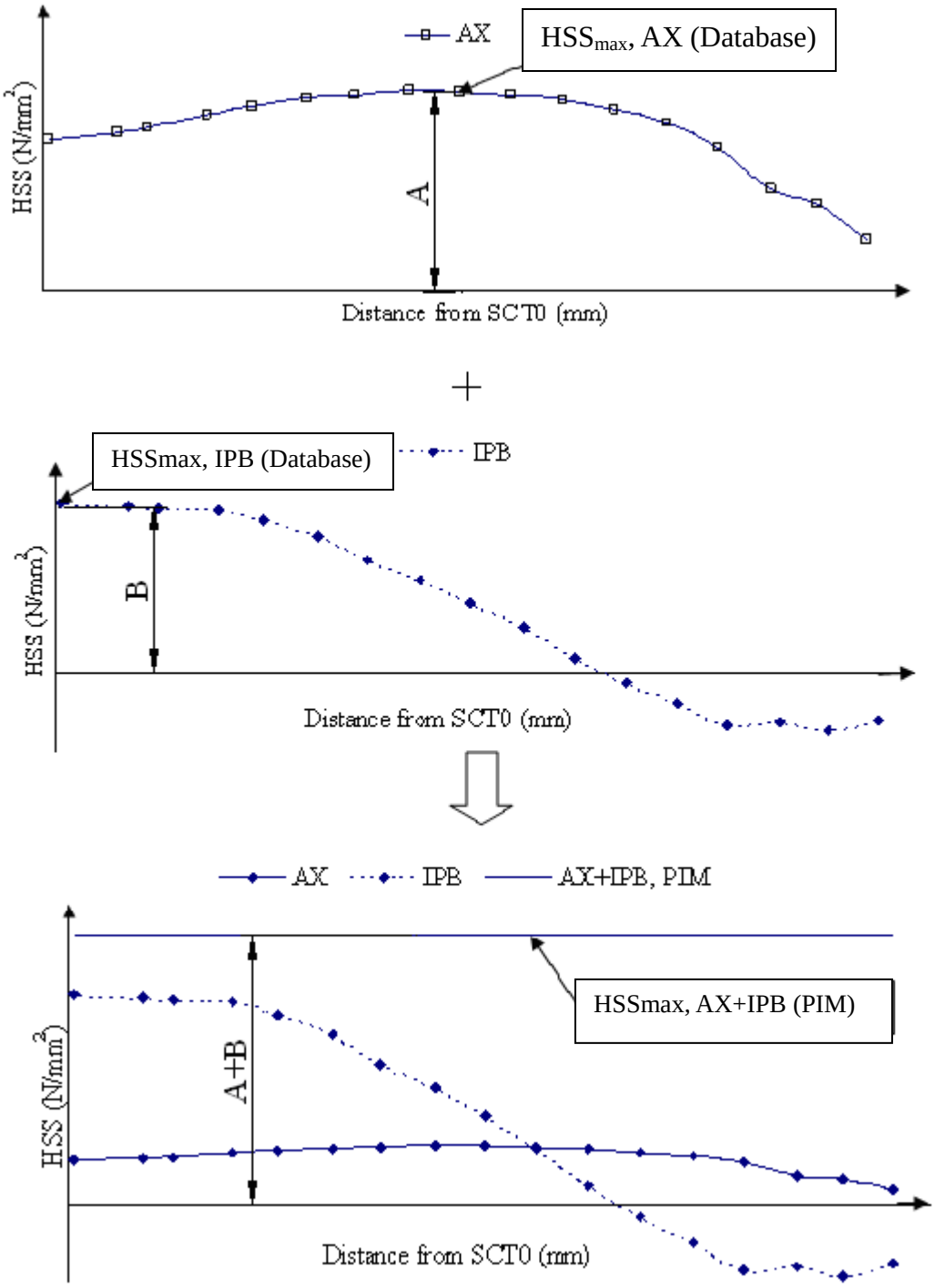


Figure 5.6 Common concept of estimated HSS values obtained from the PIM

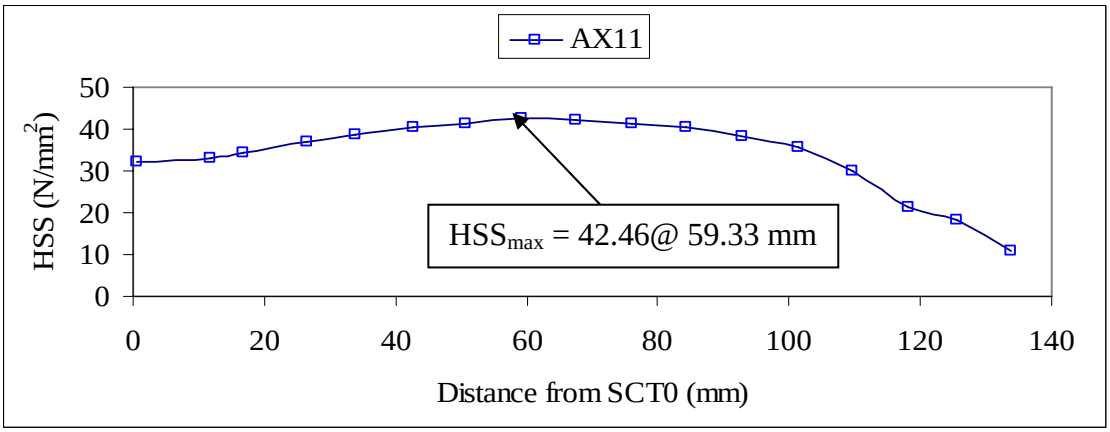


a) Maximum HSS under basic load case AX11 (100 kN) along Curve C

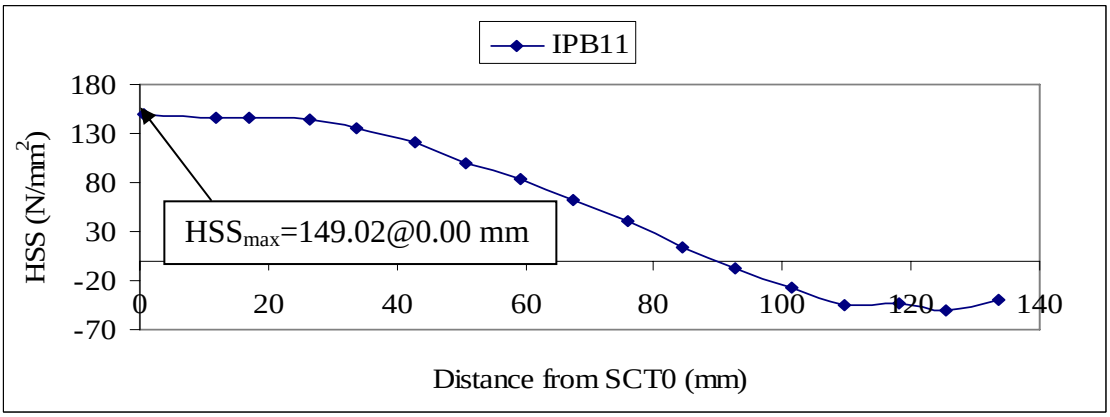


b) Maximum HSS under basic load case IPB11 (12 kN.m) along Curve C

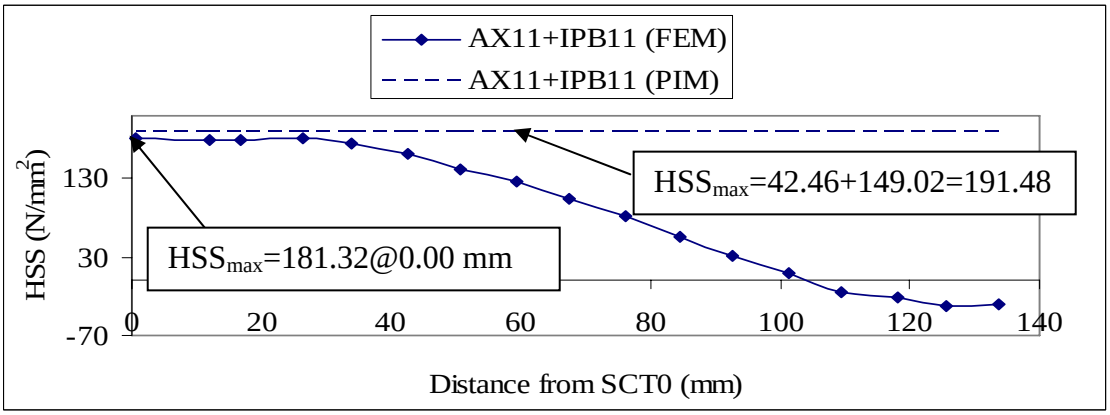


c) Maximum HSS under combined load case AX11 (100 kN) +IPB11 (12 kN.m) along Curve C

Figure 5.7 Maximum HSS under combined load case AX11 (100 kN) +IPB11 (12 kN.m) obtained from the FE analyses and the PIM

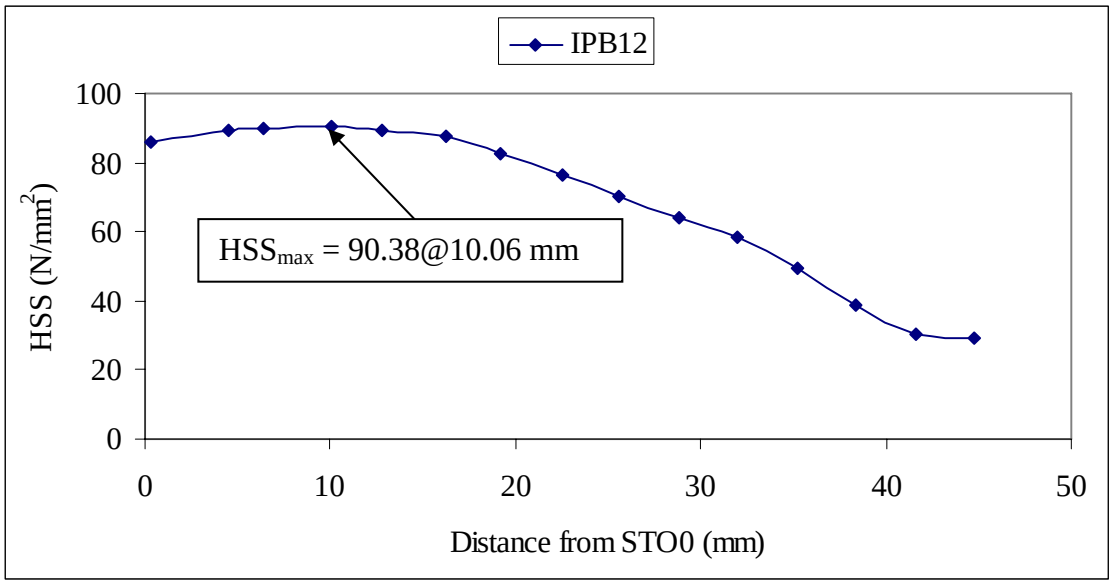


Figure 5.8 HSS result of partially overlapped CHS K-joint subjected to basic load case IPB12 (12 kN.m) along Curve A

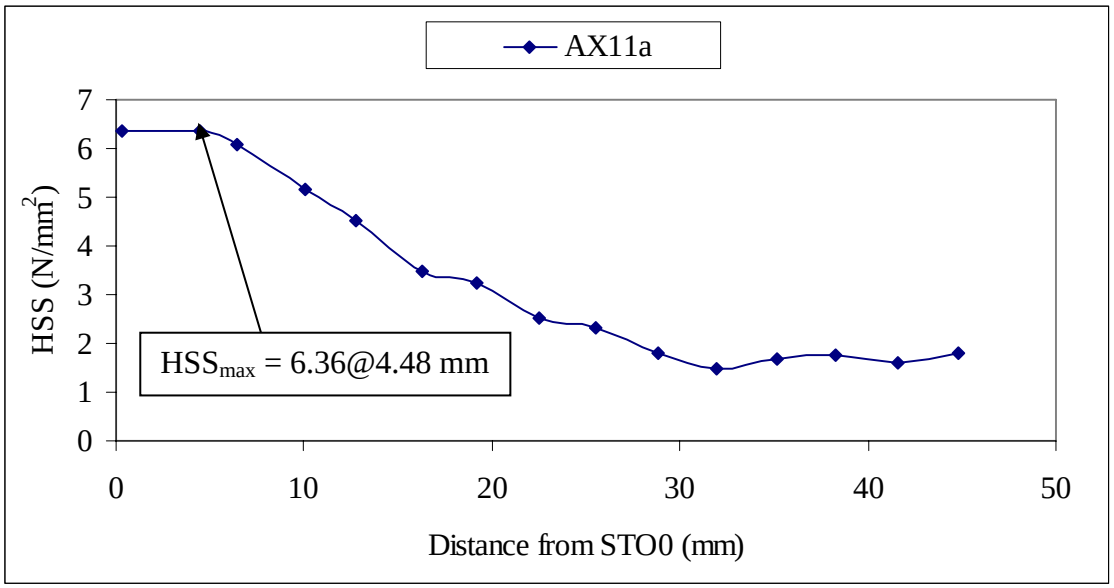


a) HSS under load case AX11 (100 kN) along Curve A

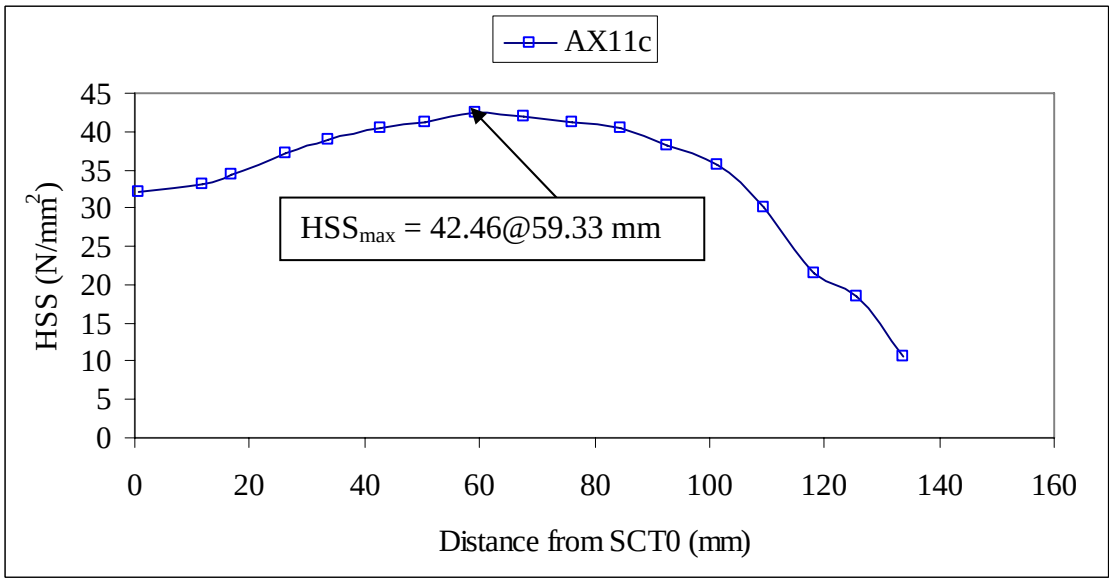


b) HSS under load case AX11 (100 kN) along Curve C

Figure 5.9 HSS result of partially overlapped CHS K-joint subjected to basic load case AX11 (AX=100 kN)

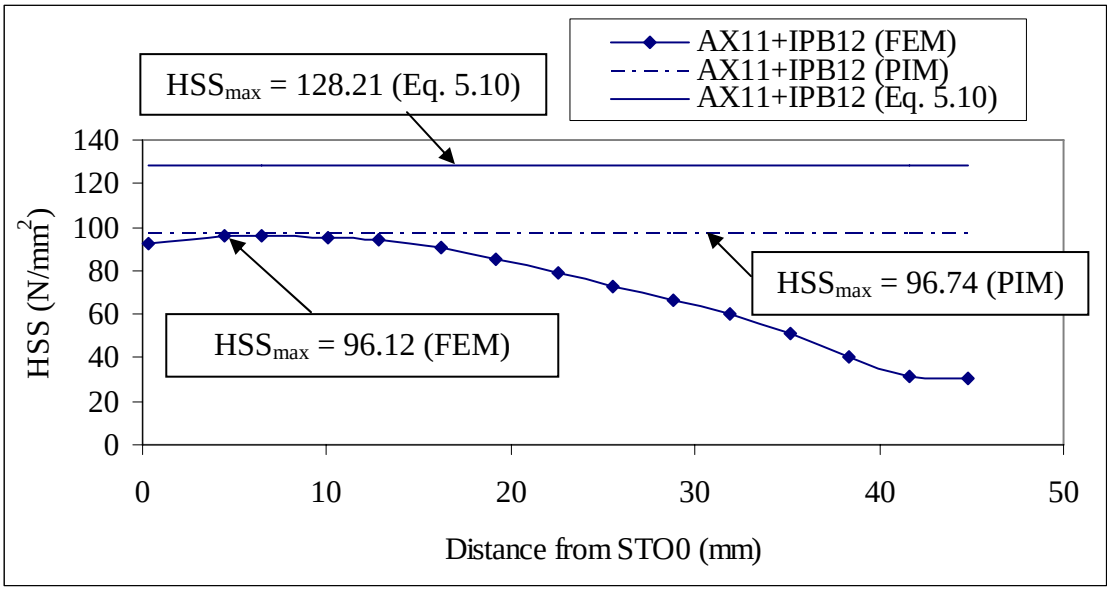


Figure 5.10 HSS result of partially overlapped CHS K-joint subjected to combined load case AX11 (100 kN) + IPB12 (12 kN.m) along Curve A

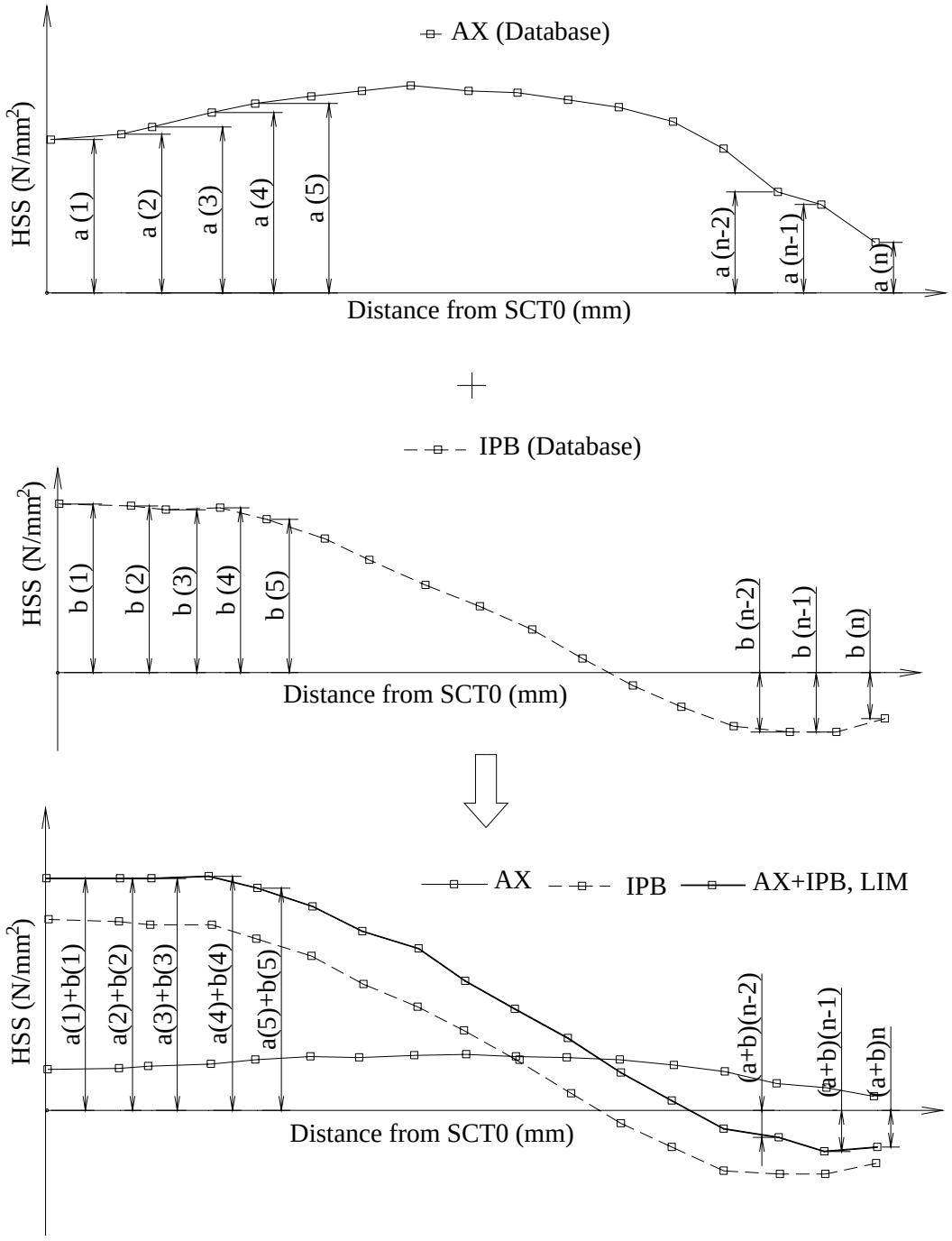


Figure 5.11 Common concept of estimated HSS values obtained from the LIM

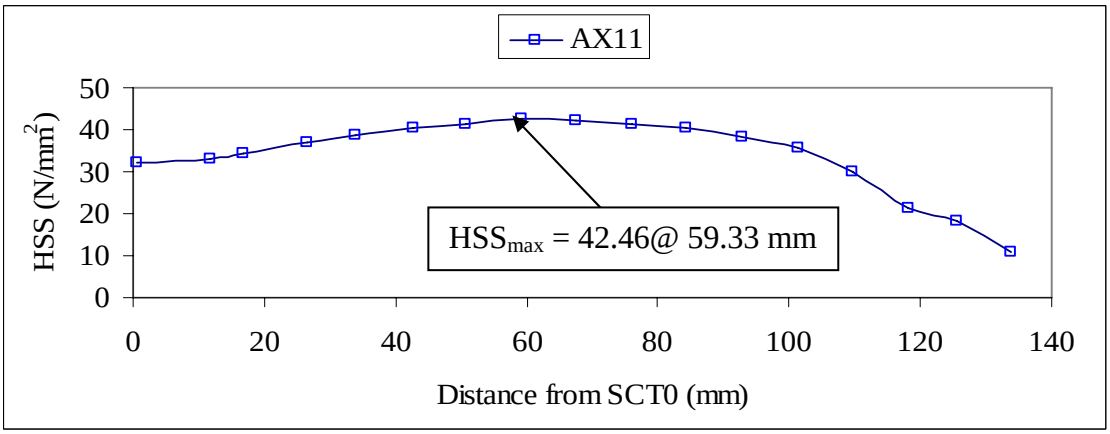


a) HSS under basic load case AX11 (100 kN) along Curve C

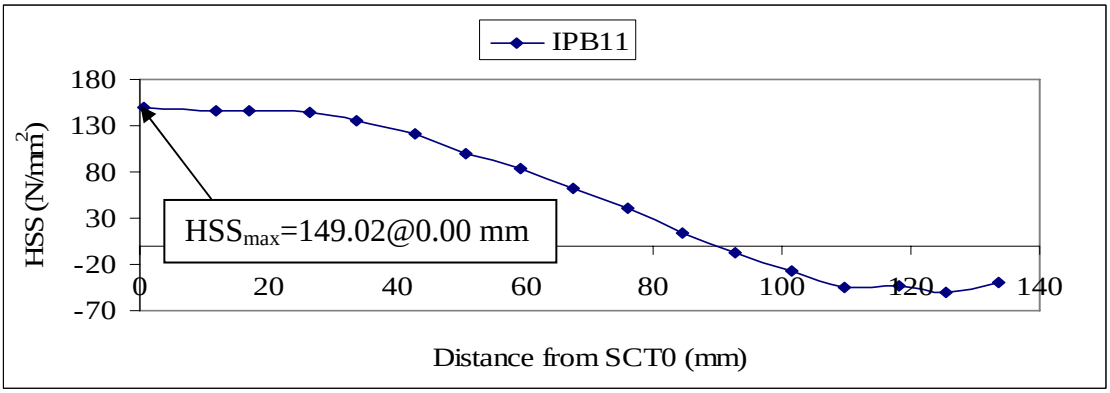


b) HSS under basic load case IPB11 (12 kN.m) along Curve C

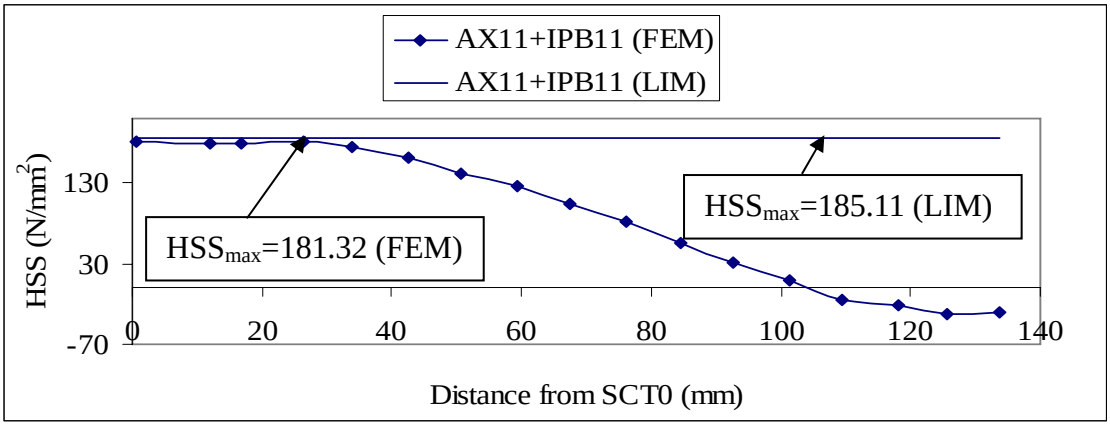


c) Maximum HSS under combined load case AX11 (100 kN) and IPB11 (12 kN.m) along Curve C

Figure 5.12 Maximum HSS under combined load case AX11 (100 kN) and IPB11 (12 kN.m) obtained from the FE analyses and the LIM

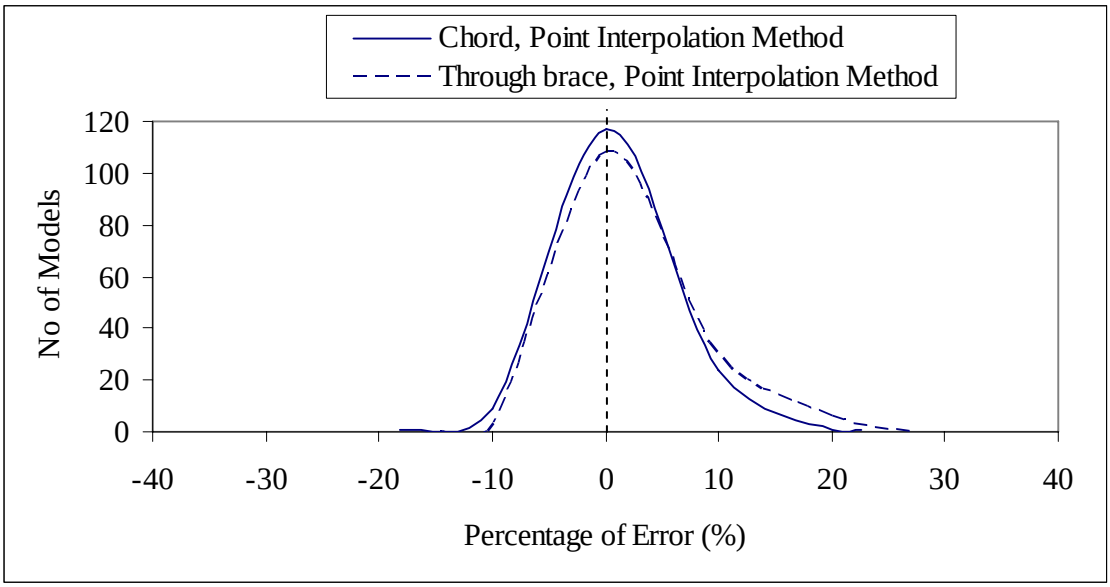


Figure 5.13 Percentage errors between the SCF values obtained from the PIM and the FE analyses under basic load case AX11 (100 kN) along Curve C

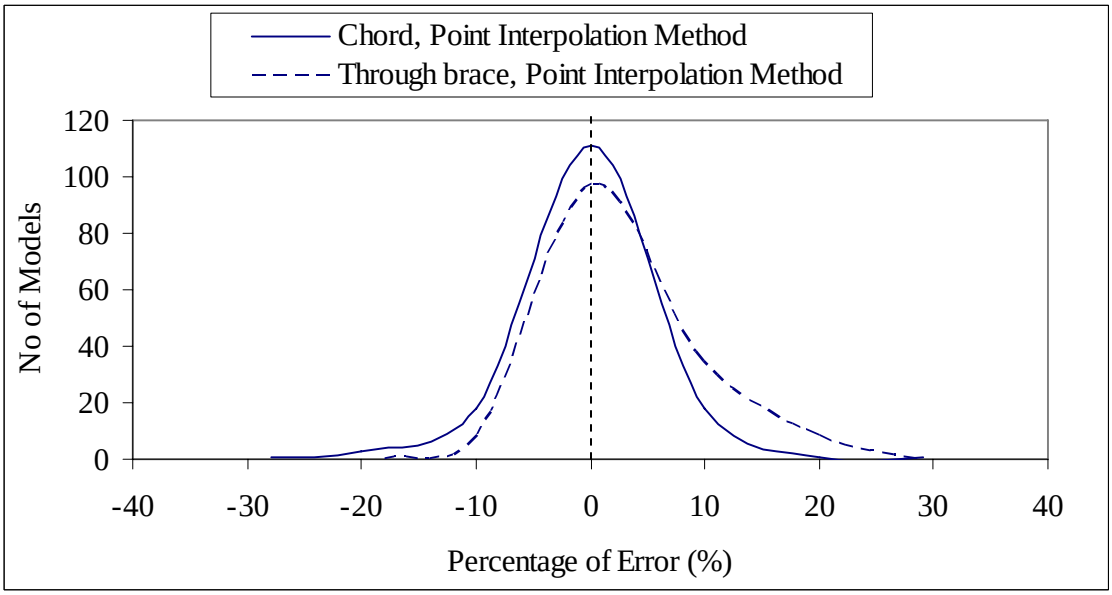


Figure 5.14 Percentage errors between the SCF values obtained from the PIM and the FE analyses under basic load case IPB11 (12 kN.m) along Curve A

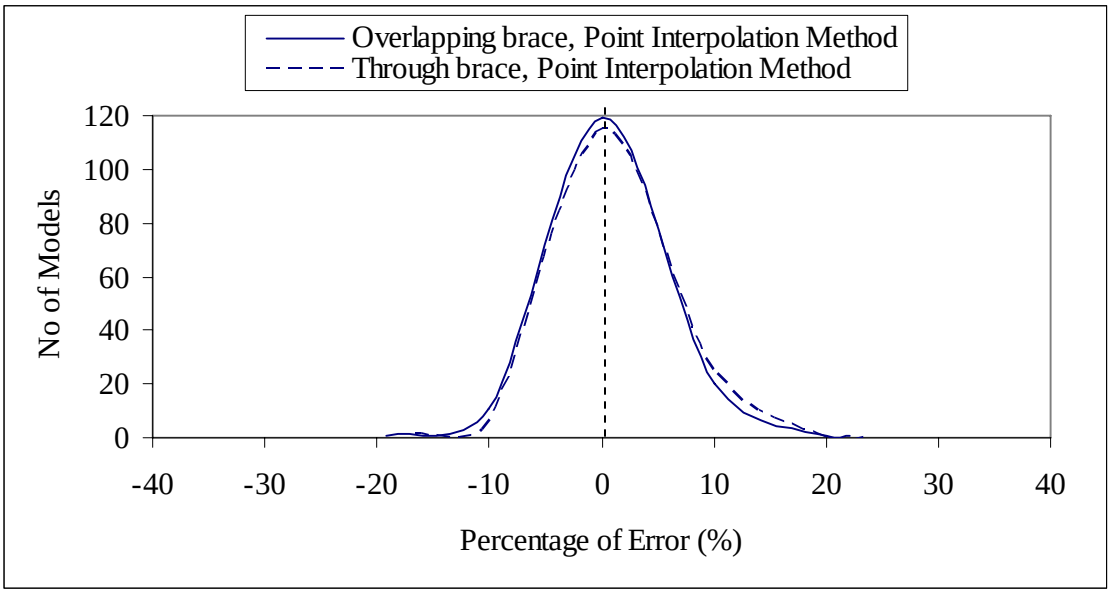


Figure 5.15 Percentage errors between the SCF values obtained from the PIM and the FE analyses under basic load case IPB12 (12 kN.m) along Curve A

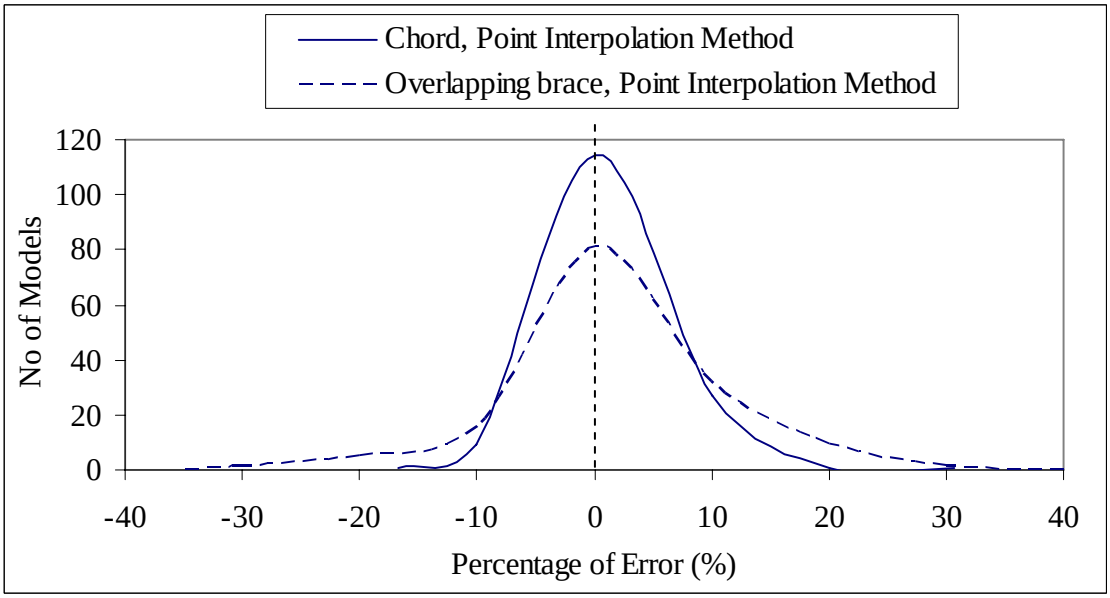


Figure 5.16 Percentage errors between the SCF values obtained from the PIM and the FE analyses under basic load case AX21 (100 kN) along Curve B

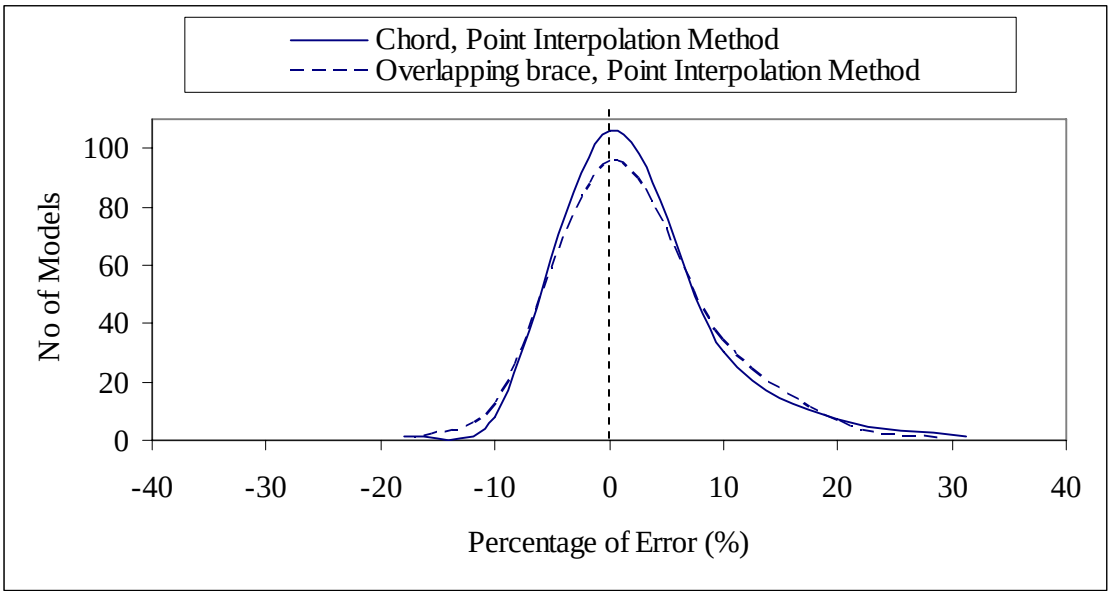


Figure 5.17 Percentage errors between the SCF values obtained from the PIM and the FE analyses under basic load case IPB21 (12 kN.m) along Curve B

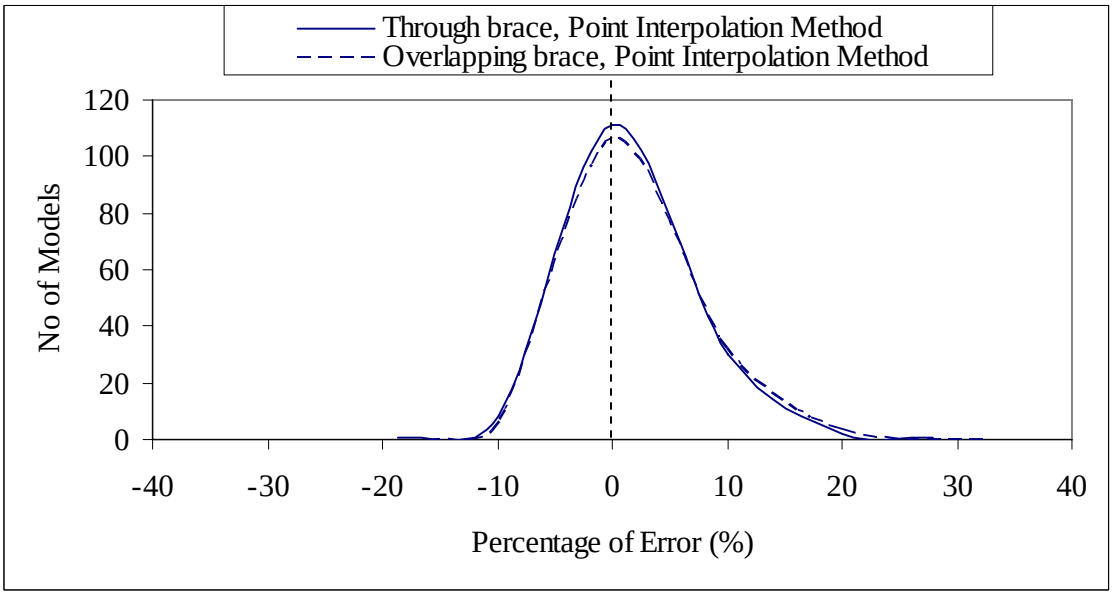


Figure 5.18 Percentage errors between the SCF values obtained from the PIM and the FE analyses under basic load case IPB22 (12 kN.m) along Curve A

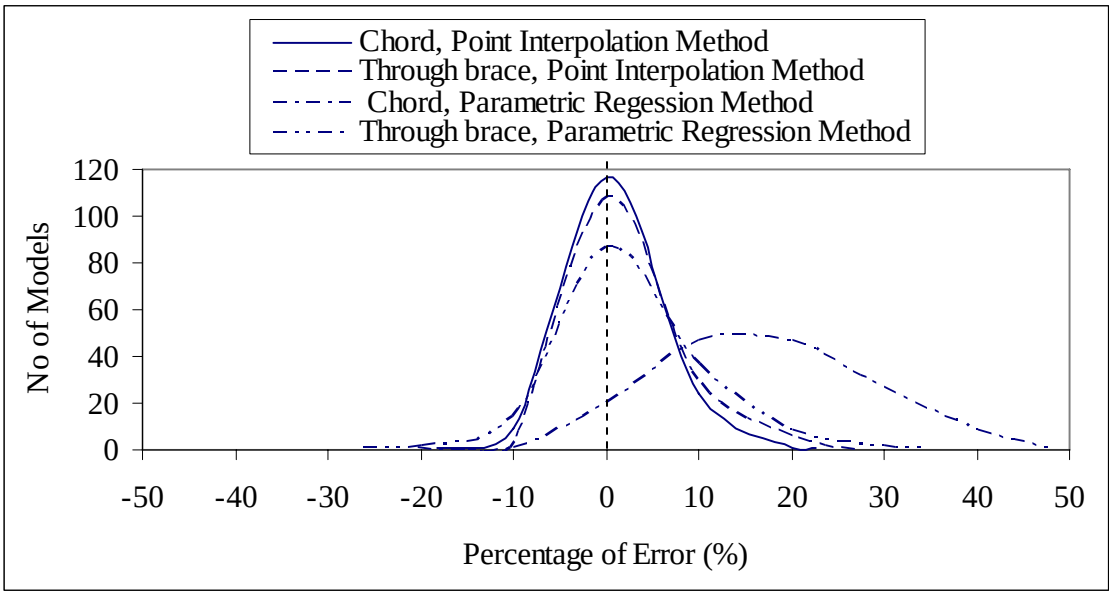


Figure 5.19 Percentage errors between the SCF values obtained from the PIM and the PRM under basic load case AX11 (100 kN.m) along Curve C

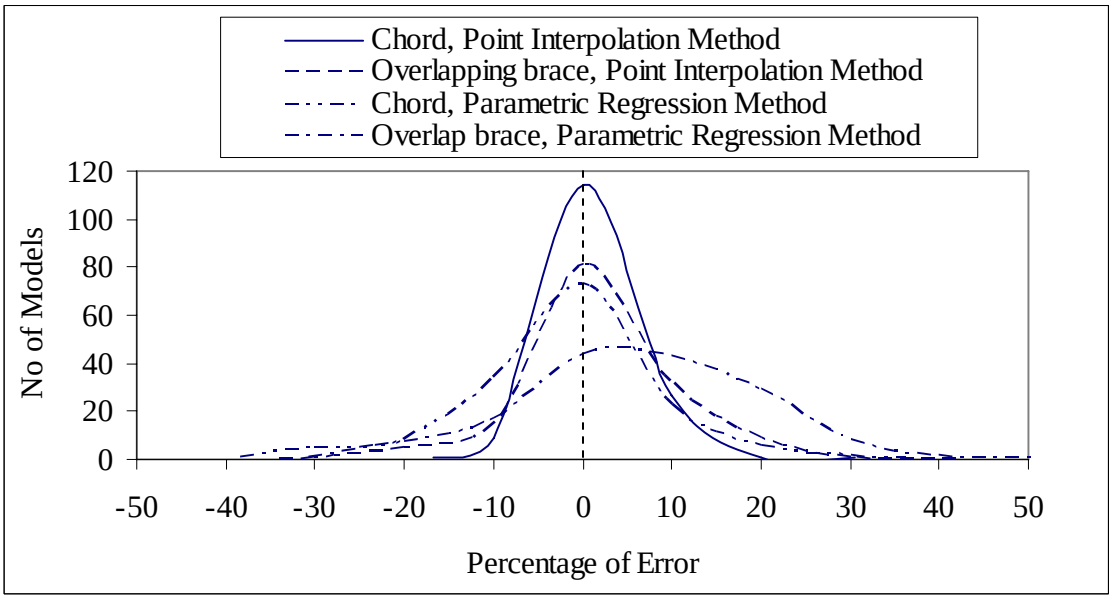


Figure 5.20 Percentage errors between the SCF values obtained from the PIM and the PRM under basic load case IPB11 (12 kN.m) along Curve A

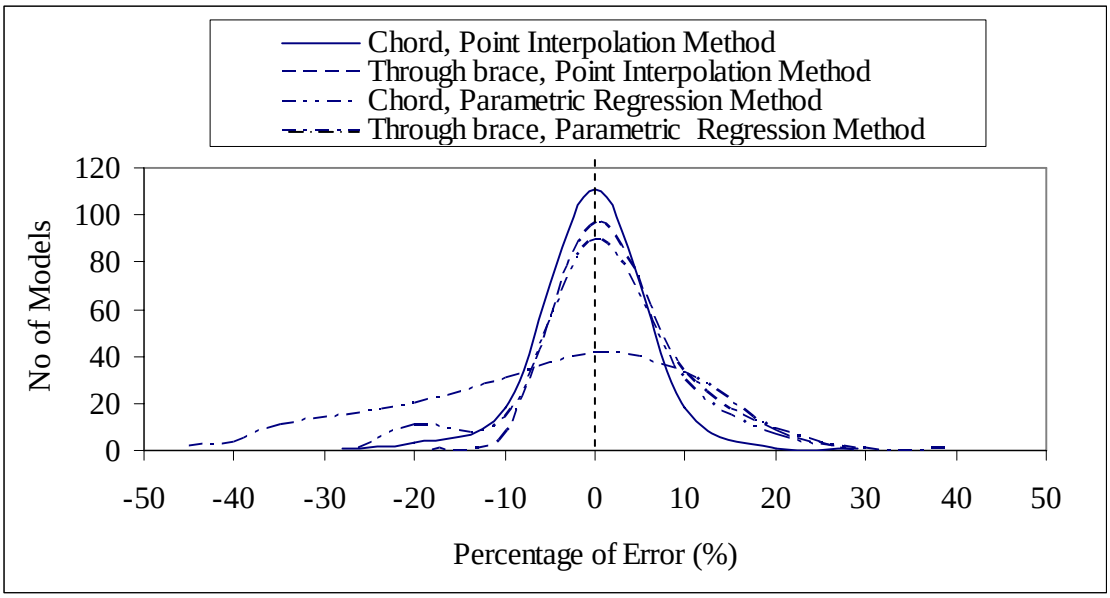


Figure 5.21 Percentage errors between the SCF values obtained from the PIM and the PRM under basic load case IPB12 (12 kN.m) along Curve A

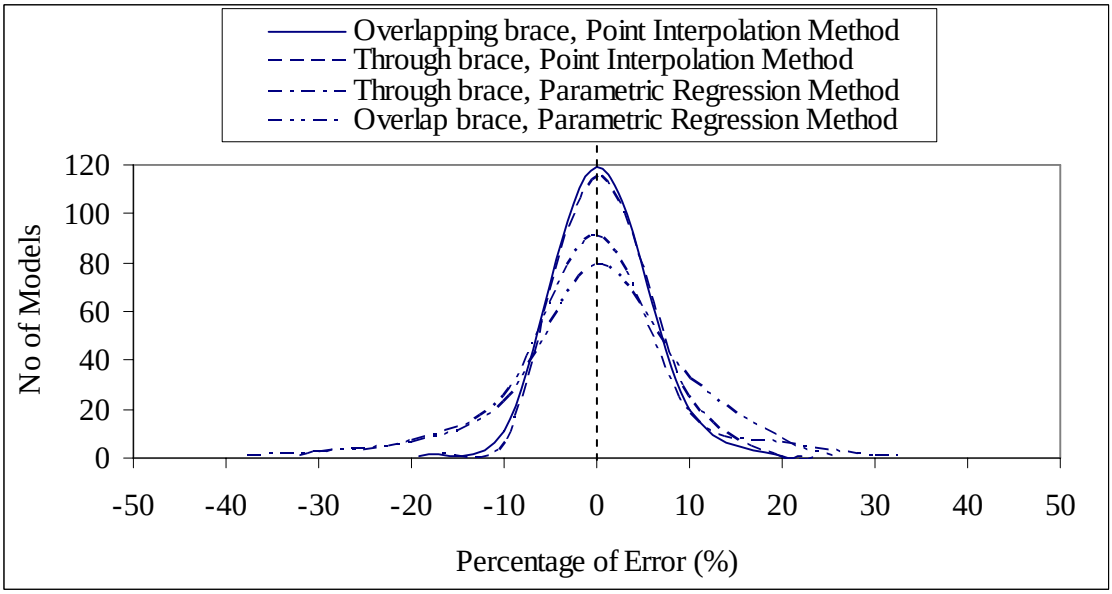


Figure 5.22 Percentage errors between the SCF values obtained from the PIM and the PRM under basic load case AX21 (100 kN) along Curve B

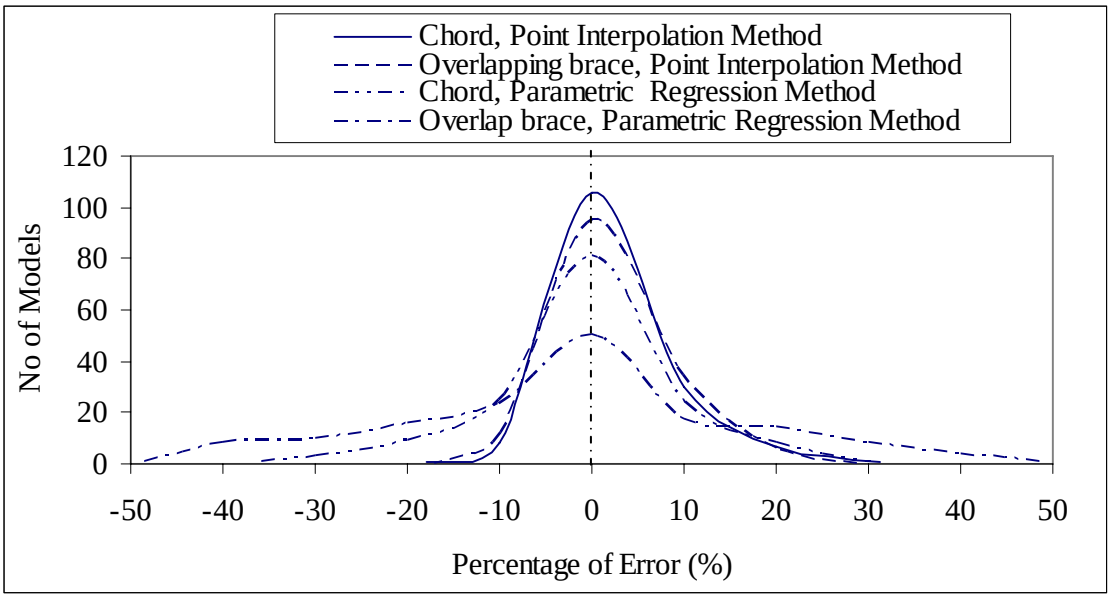


Figure 5.23 Percentage errors between the SCF values obtained from the PIM and the PRM under basic load case IPB21 (12 kN.m) along Curve B

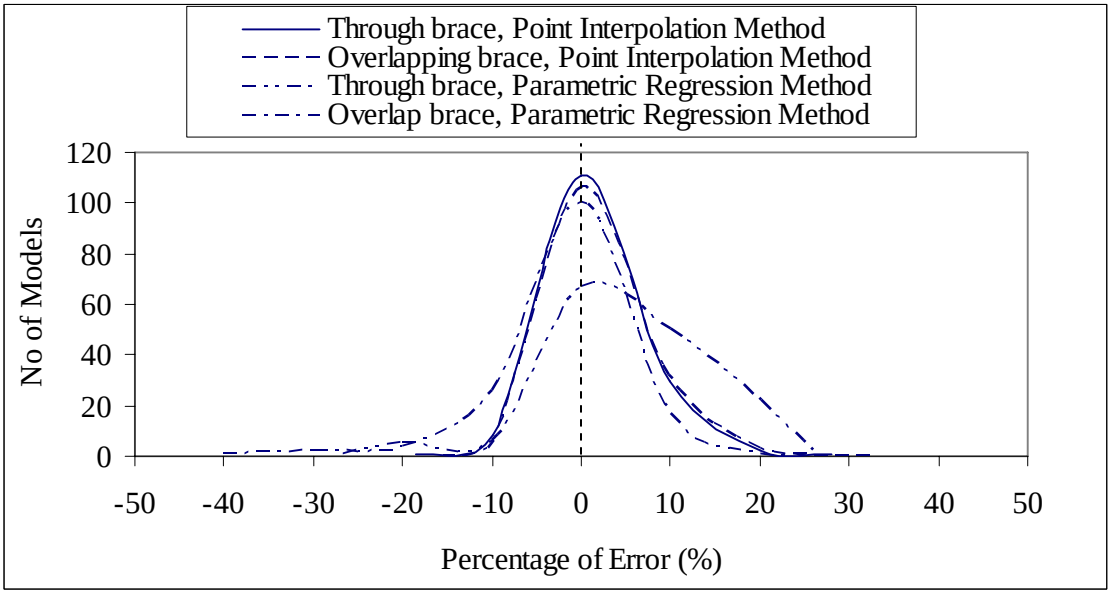


Figure 5.24 Percentage errors between the SCF values obtained from the PIM and the PRM under basic load case IPB22 (12 kN.m) along Curve A

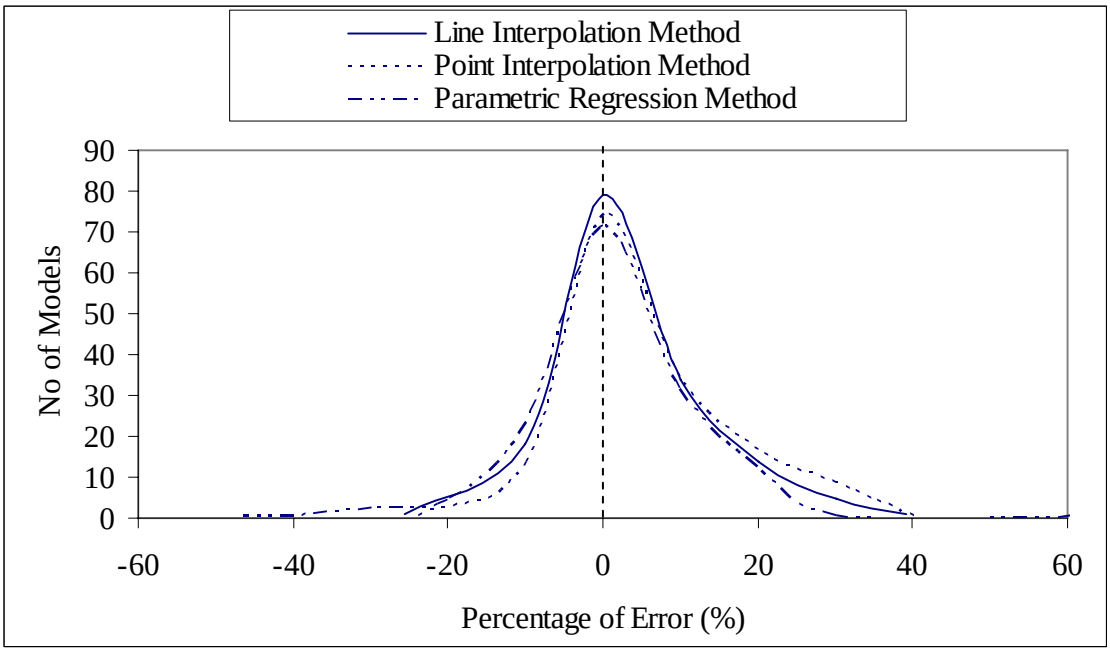


a) Through brace

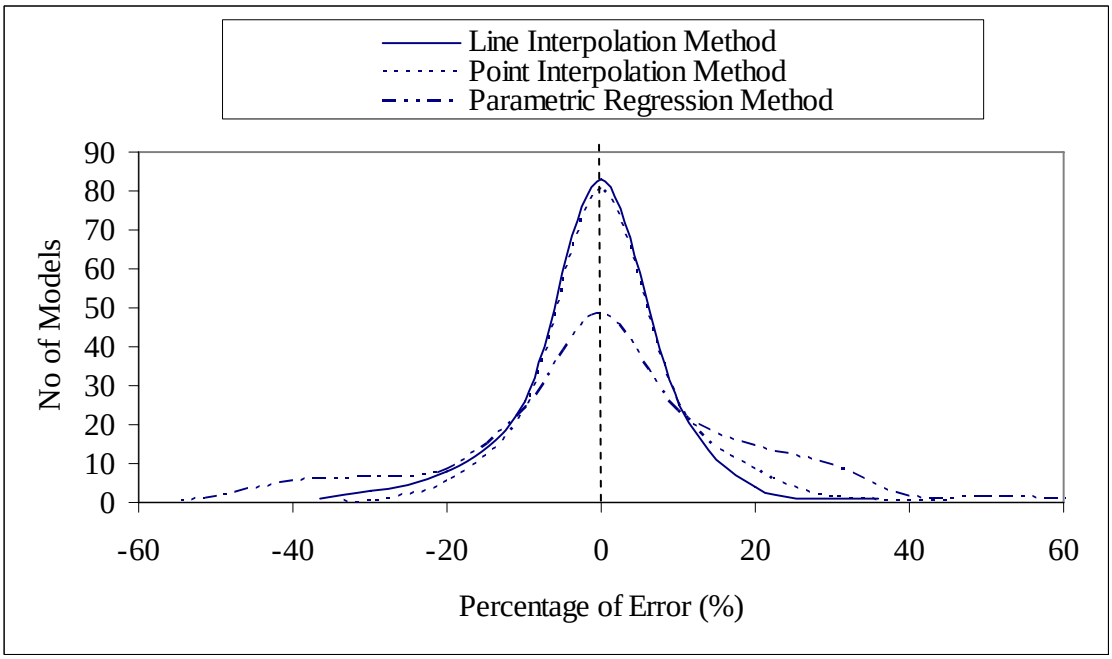


b) Chord

Figure 5.25 Percentage errors between the HSS values obtained from the LIM, the PIM and the PRM under combined load of AX11 (100 kN) and IPB11 (12 kN.m) along Curve C

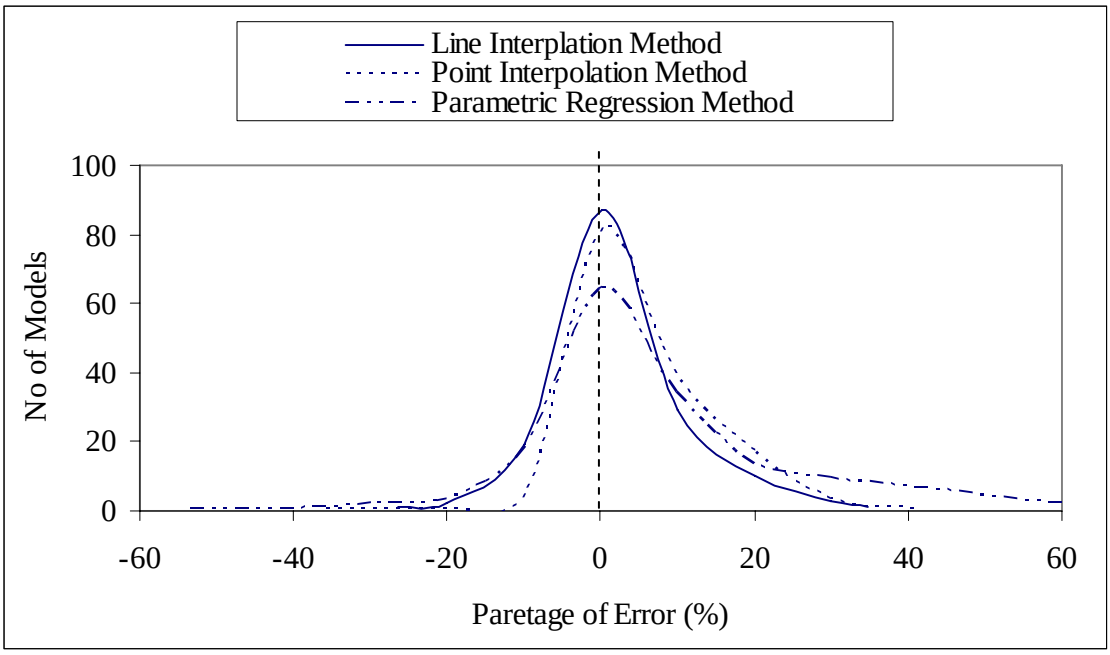


a) Through brace

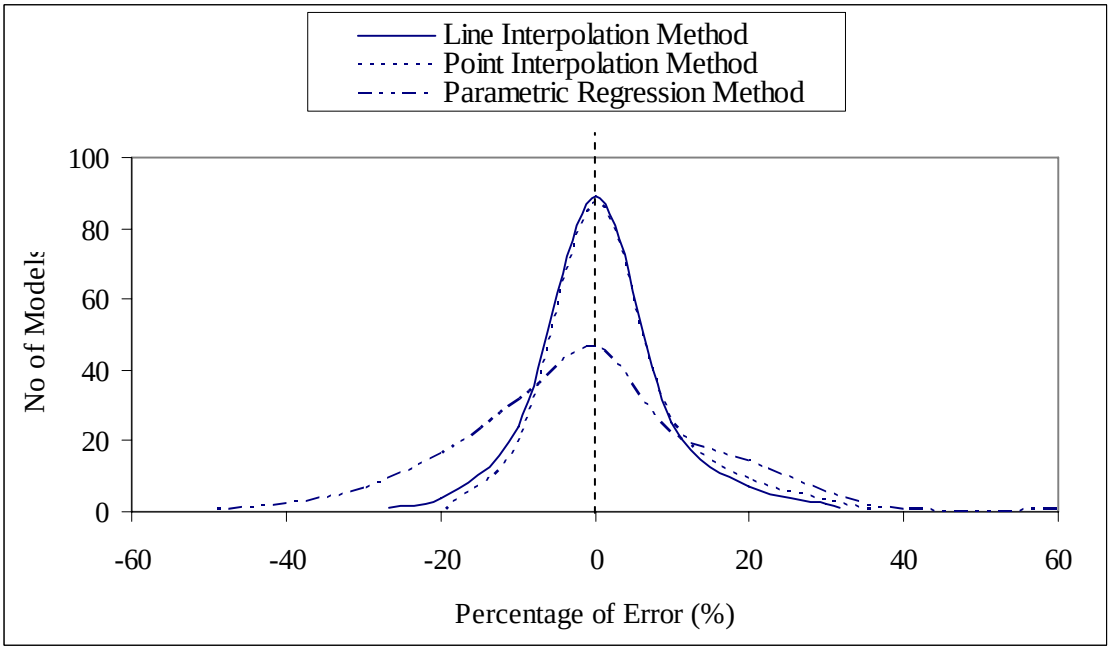


b) Overlapping brace

Figure 5.26 Percentage errors between the HSS values obtained from the LIM, the PIM and the PRM under combined load of AX11 (100 kN) and IPB12 (12 kN.m) along Curve A

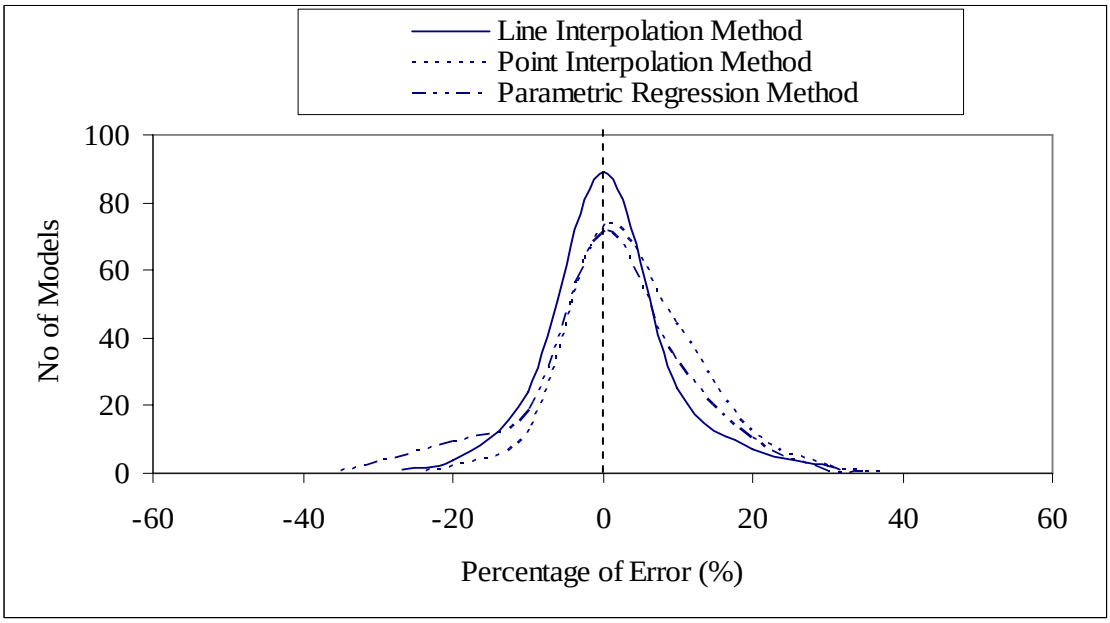


a) Overlapping brace

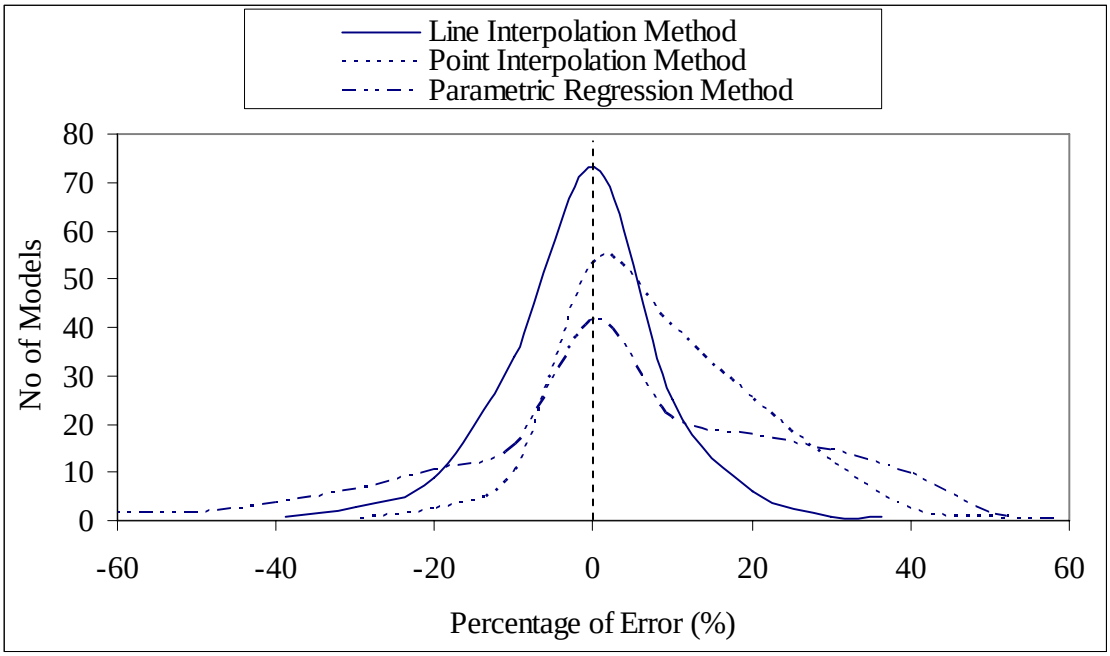


b) Chord

Figure 5.27 Percentage errors between the HSS values obtained from the LIM, the PIM and the PRM under combined load of AX21 (100 kN) and IPB21 (12 kN.m) along Curve B

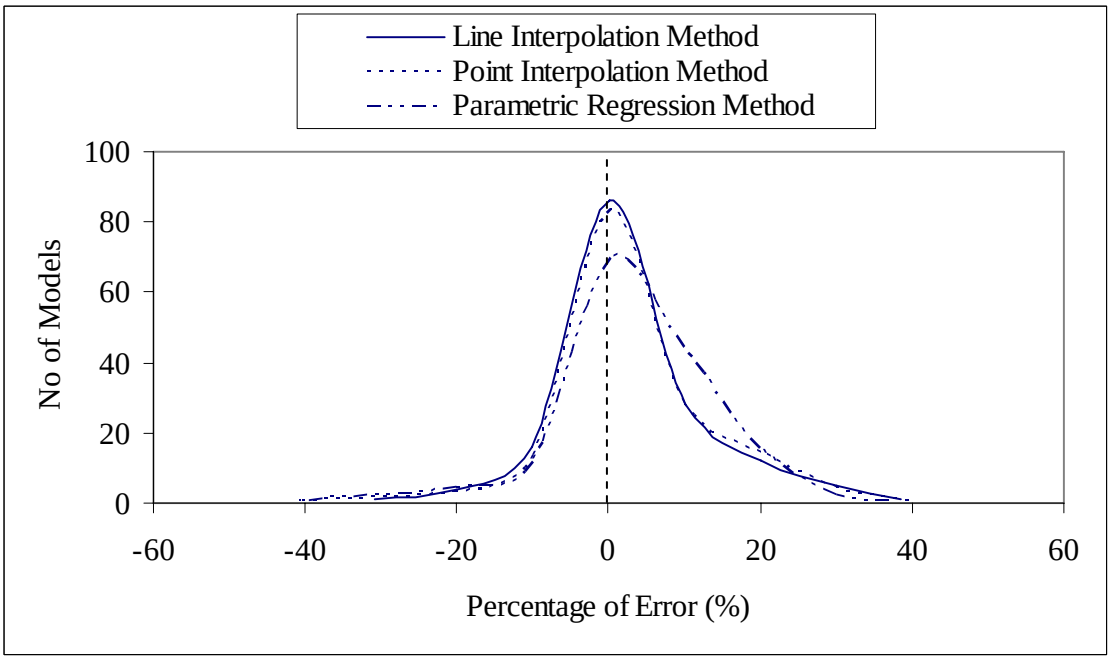


a) Overlapping brace

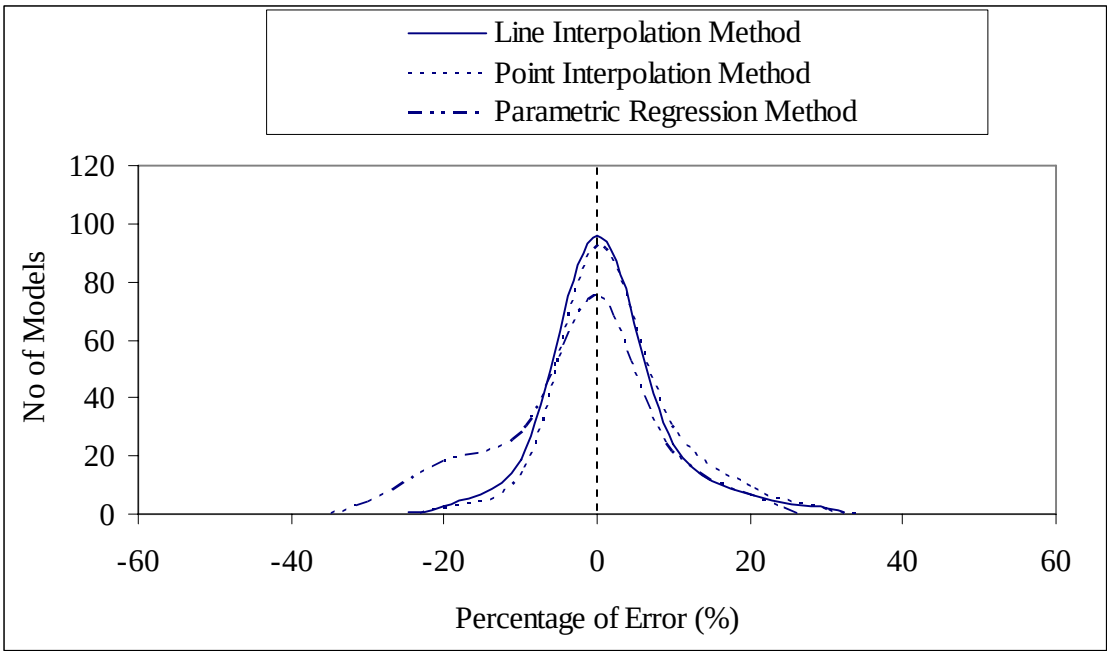


b) Through brace

Figure 5.28 Percentage errors between the HSS value obtained from the LIM, the PIM and the PRM under combined load of AX21 (100 kN) and IPB22 (12 kN.m) along Curve A

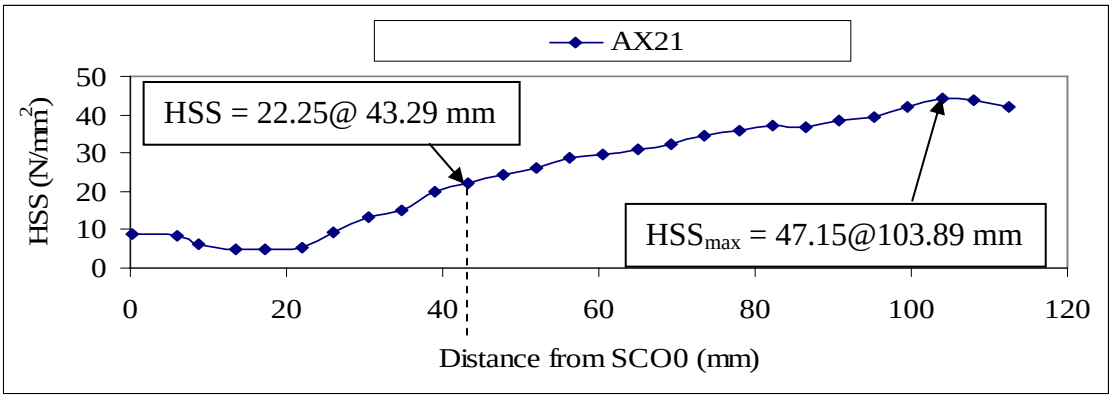


Figure 5.29 HSS obtained from the FE analyses under basic load case AX21 (100 kN) along Curve B

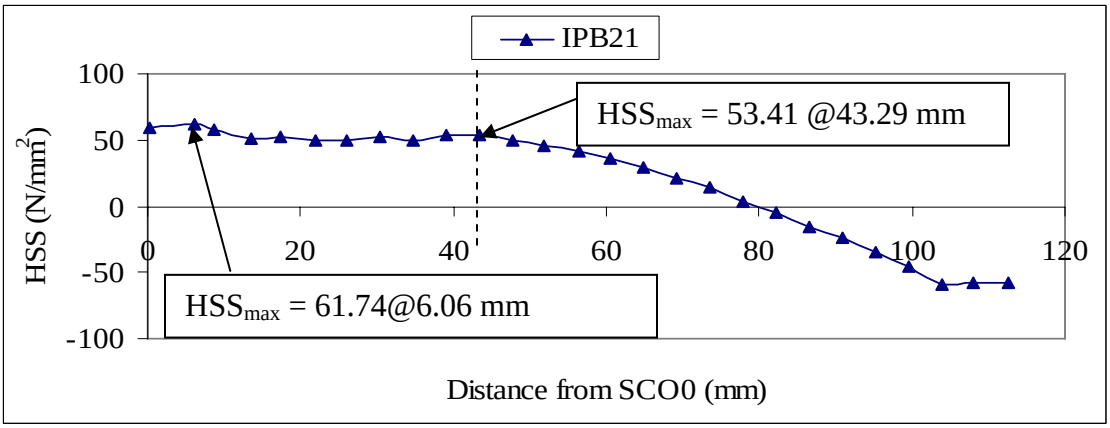


Figure 5.30 HSS obtained from the FE analyses results under basic load case IPB21 (6 kN) along Curve B

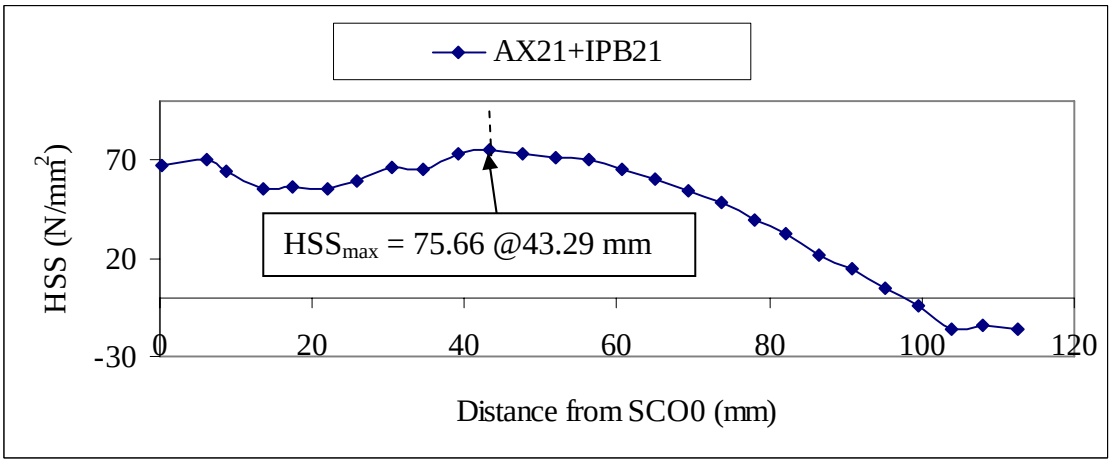


Figure 5.31 HSS obtained from the FE analyses under combined load case AX21 (100 kN) and IPB21 (6 kN.m) along Curve B

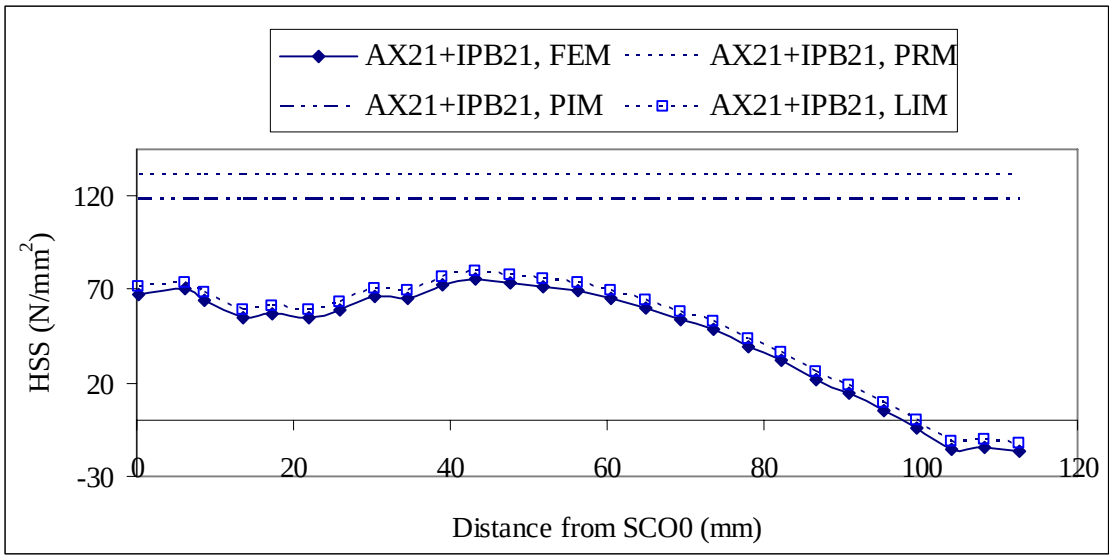


Figure 5.32 Comparison of HSS obtained from the FE analyses with the HSS obtained from the PRM, the PIM and the LIM under combined AX21 (100 kN) and IPB21 (6 kN.m) along Curve B

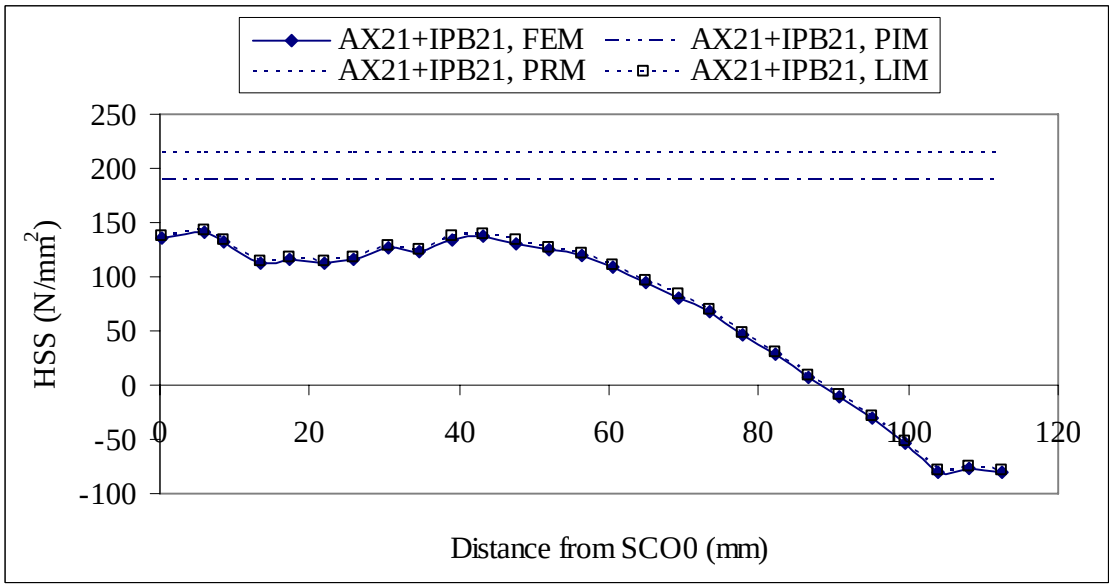


Figure 5.33 Comparison of HSS obtained from the FE analyses with the HSS obtained from the PRM, the PIM and the LIM under combined AX21 (100 kN) and IPB21 (12 kN.m) along Curve B

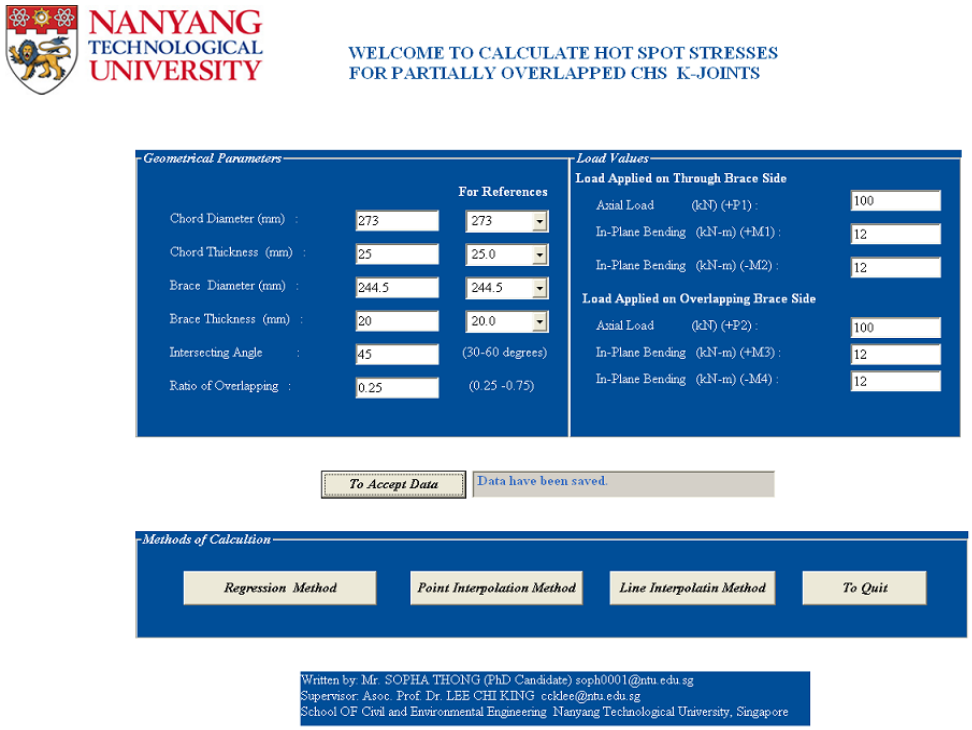


Figure 5.34 Screen input for the interactive program

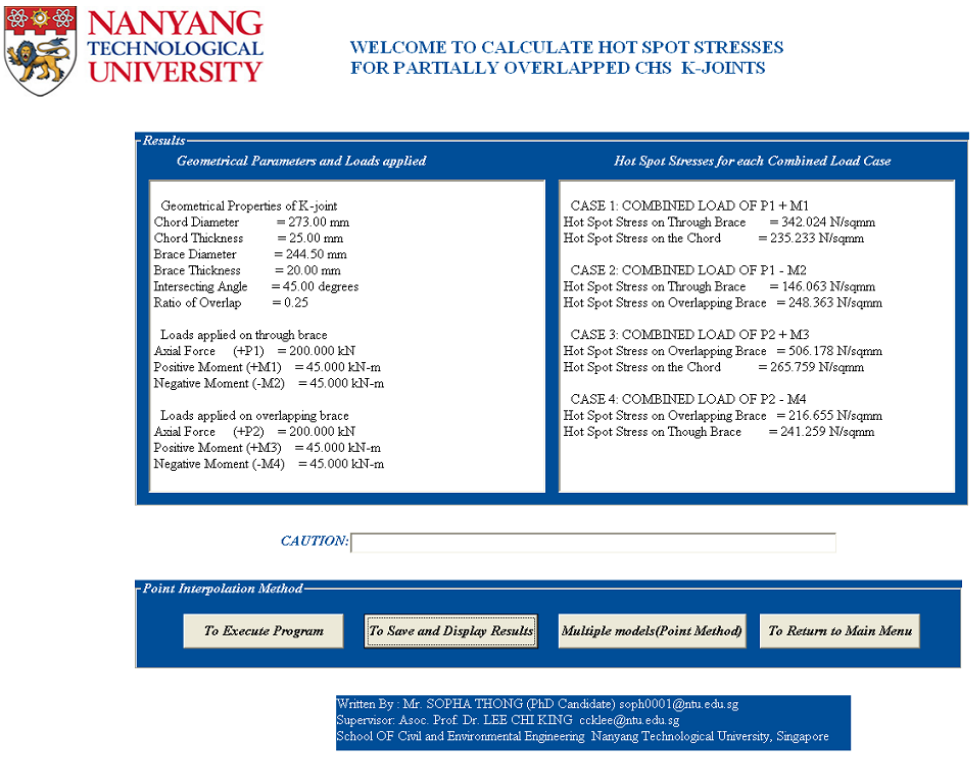


Figure 5.35 Typical output screen for the interactive program

# *CHAPTER 6*
# *A BRIEF COMPARISON OF FATIGUE PERFORMANCE BETWEEN GAPPED AND PARTIALLY OVERLAPPED CHS K-JOINTS*

## 6.1 INTRODUCTION

Due to the ease of fabrication and the existence of many direct calculation methods to assess the joint capacity, simple gapped K-joint is one of the widely used connection types for the construction of offshore steel jackets. However, when the brace to chord diameters ratio is higher than 0.7, the gapped K-joint may not be able to be fabricated due to the limited range of validity of many design codes [27] and then a partially overlapped joint may be necessary instead. In general, a partially overlapped CHS K-joint may have a higher fabrication cost due to the more complex intersection profile, but having said that the partially overlapped CHS K-joint may have a higher residual capacity due to its optimized load transfer pattern. Recently, in a case study comparing the costs of three K-joints design options [4], it was found that after having considered the material based on ultimate strength and fabrication costs, the partially overlapped joint is the cheapest option, with the fabrication cost actually being significantly cheaper than that of the alternative gapped joint. However, in the past, very few research works were carried out to study and compare the fatigue behaviour between the gapped and the partially overlapped CHS K-joints.

Bouwkamp [56 and 57] observed that the ultimate load of partially overlapped CHS K-joints could be twice that of the gapped joints and the SCFs of overlapped CHS K-joints could be decreased by 34.8% when compared with gapped CHS K-joints having the same parameters and properties. Fessler et al. [62] also reported that the HSS along the joint could be reduced as much as 40%-45% by adopting an overlapped joint design. Moe [32] performed the stress analysis based on the fatigue tests of overlapped CHS K-

joints and overlapped CHS K(N)-joint subjected to balanced axial load. According to Moe [32], the stress analysis revealed that the hot spots were located on the brace side. The subsequent fatigue tests showed that this caused a brace failure, which in its initial stage started from the hot spots, but which developed significantly different from previously observed chord failures in the gapped CHS K-joints.

It is important to note that the brace failure mode was also observed in the current study as earlier mentioned in Chapter 3. It seems that the brace failure mode in the partially overlapped CHS K-joints might be more critical than previously observed chord failure due to the acceleration of the crack development from relatively short surface crack, which to some extent may reduce the time in-service for possible crack detection. Furthermore, it seems that this mode of failure may lead to somewhat shorter fatigue life compared with the chord failure as usually happened in the gapped CHS K-joints due to the usual thinner thickness of the brace.

In this chapter, the SCF and HSS values predicted by the new proposed method are compared with SCF and HSS values predicted by parametric SCF equations for the gapped CHS K-joints. In addition, fatigue life predictions of gapped and partially overlapped CHS K-joints are compared to one another so as to investigate which type of K-joints would gain better fatigue performance.

## 6.2 PARAMETRIC SCF EQUATIONS FOR SIMPLE CHS JOINTS

Parametric SCF equations for simple CHS joints have been developed since long time ago by many researchers. The Kuang equations [85] for T-, Y-, K- and KT-joints configurations utilise a modified thin-shell FE program specifically designed to analyse tubular connections. The tubular connections were modelled without a weld fillet, and the stresses were measured at the mid-section of the member wall.

The equations by Wordsworth and Smedley [86, 87] have been developed as part of the UK Offshore Steels Research Project (UKOSRP). First, equations for T-, X- and Y-joints have been presented by Wordsworth and Smedley [85] for axial load, in-plane bending and out of-plane bending in terms of joint parameters $\beta$, $\gamma$, $\tau$ and $\upsilon$. In a later publication, parametric equations for unstiffened, gapped CHS K- and KT-joints have been proposed by Wordsworth [87]. The equations were based on acrylic model tests, and constituted the basis for various design guidelines and specifications such as the International Institute of Welding [88] guidelines.

Efthymiou and Durkin [29] presented a complete set of SCF equations in terms of joint parameters for the design of T-, Y- and K- tubular joints under axial load, in-plane moment and out-of-plane moment. The equations were based on numerical results obtained by program PMBSHELL developed by Liaw et al. [89]. Efthymiou [90] introduced the 'influence function' concept, which takes into account the so-called 'carry-over' effect in multi-brace joints, i.e. the stress concentration in the neighborhood of a brace weld, due to a load in another brace.

The latest SCF equations are the work of Smedley and Fisher [12]. The work, sponsored by the UK Department of Energy, was aimed at developing SCF parametric equations for uni-planar joints (T-, Y-, K-, X- and KT-joints), which later had been named to DEn parametric SCF equations. The DEn parametric SCF equations were based on extensive test data based on steel and acrylic specimens. This investigation took into account the effects of weld profile, the additional stresses caused by chord bending and the effects of chord length. Reference and carry-over loading conditions were also considered. The DEn parametric SCF equations for gapped CHS K-joints are shown in Table 6.1. The parametric SCF equations have been compared to the parametric SCF equations derived by Kuang, Wordsworth/Smedley and Efthymiou/Durkin by Smedley and Fisher. It is found that the Kuang equations frequently gave poor estimates of the measures SCFs; the Wordsworth/Smedley equations generally gave a good fit to the data on the chord side but could be

excessively conservative on brace side; and the Efthymiou/Durkin equations gave the best mean fit to the SCF database as a whole but consequently had more joint underestimate.

In fact, there are some other equations were suggested on works done by Karamanos et al. [91], and Zhao et al. [5]. However, these equations have been developed based on just simplifying the previous SCF equations to shorten them and presented in the graphic format. The short form equations with graphs are unsuitable for parametric study. Therefore, in this study the DEn parametric SCF equations have been compared to the new proposed tool for predicting SCFs of any partially overlapped CHS K-joints.

## 6.3 COMPARISON OF SCF BETWEEN GAPPED AND PARTIALLY OVERLAPPED CHS K-JOINTS

In this study, the geometrical parameters of the gapped and the partially overlapped CHS K-joints were specially selected in such a way that if the gapped CHS K-joints were made from the sections, which produce high eccentricity, but still in the range of validity [5]. However, if the corresponding overlapped CHS K-joints were made from the sections, the eccentricity could be reduced to zero. The geometrical parameters of 762 partially overlapped CHS K-joints without eccentricity are summarized in Table 6.2. From Table 2, as can be seen that the $\beta$ values range from 0.68 to 0.91. The Ov values range from 0.25 to 0.45. Four $\theta$ values are included: 45°, 50°, 55° and 60°. The $\gamma$ values range from 5.48 to 16.14. The $\tau$ values range from 0.32 to 1.0. The geometrical parameters of the gapped CHS K-joints are also taken from the same table, but they are made with minimum gap distance. Both the gapped and the overlapped CHS K-joints are applied with the same loads. Then, the calculated maximum SCFs of the gapped CHS K-joints are compared to the maximum SCFs of the partially overlapped CHS K-joints obtained from the PIM calculations.

The relative difference between the maximum SCF values obtained from the proposed the PIM for the partially overlapped CHS K-joints and the gapped CHS K-joints from the DEn parametric SCF equations is defined as the following:

$$D_{Ov-Gap}(SCF) = \frac{SCF_{Ov} - SCF_{Gap}}{SCF_{Ov}} \times 100\% \quad (6.1)$$

where $SCF_{Ov}$ is the SCF value estimated from the proposed the PIM and $SCF_{Gap}$ is the SCF value estimated from the DEn parametric SCF equations. Note that based on Equation 6.1, the benefit of using one of these two types of CHS K-joints can be recognized by the sign of the $D_{Ov\text{-}Gap}\ (SCF)$. A negative value of the $D_{Ov\text{-}Gap}\ (SCF)$ indicates that the partially overlapped CHS K-joint is in favor, while a positive value of $D_{Ov\text{-}Gap}\ (SCF)$ indicates that the gapped CHS K-joint is in favor.

Figures 6.1 to 6.4 illustrate the relative SCF difference between the gapped and partially overlapped CHS K-joints subjected to the basic load cases of AX and IPB. The AX11 and IPB11 load cases were applied at the end of the through brace and the AX21 and IPB21 load cases were applied at the end of the overlapping brace for the partially overlapped CHS K-joint. However, for the gapped CHS K-joint the AX11 and IPB11 were applied at the end of in any of two braces. The boundary condition was set up as in the parametric study as mentioned earlier in Chapter 4.

From Figures 6.1 to 6.4, it can be seen that in the AX11 and AX21 load cases the SCF values for the partially overlapped CHS K-joints are higher than that for the gapped CHS K-joints on the braces (through brace and overlapping brace), while on the chord are mainly lower than that for the gapped CHS K-joints. The SCF values in the IPB11 and IPB21 load cases for the partially overlapped CHS K-joints are higher than that for the gapped CHS K-joints on both chord and braces. From Figures 6.1 and 6.3, it can be seen that the relative difference of the AX11 and AX21 load cases on the through brace and overlapping brace ranges from 4.30 % to 75.07% with mean of 49.41%, while on

the chord side is from -742.9% to 34.6 % with mean of -138.64%. From the Figures 6.2 and 6.4, it can be seen that the relative difference of IPB11 and IPB21 load case ranges from 30.49% to 69.64% with mean of 56.83% on the through brace and the overlapping brace, while on the chord side from -86.74% to 37.65% with mean of 14.49%.

It seems that the partially overlapped CHS K-joints are good in working in AX load case, and the gapped CHS K-joints are good in working in IPB load case. However, if based on SCF values alone it seems too early to conclude which type of K-joints is the best, since chord and braces of CHS K-joints have different thicknesses. Therefore, to have a clear figure of an advantage of these two types of CHS K-joints, their HSS values are compared.

## 6.4 COMPARISON OF HSS BETWEEN GAPPED AND PARTIALLY OVERLAPPED CHS K-JOINTS

A comparison between the gapped and the partially overlapped CHS K-joints in terms of the maximum HSS value was made to investigate which type of K-joints would perform better under the fatigue loadings. The dimensions of the CHS K-joints used in the HSS study were also taken all from Table 6.2. Both gapped and partially overlapped CHS K-joints are subjected to the basic load case of AX11 (200 kN), and the load case of IPB11 (45 kN.m). Note that these two load cases were used in the experimental investigation in Chapter 3. The calculated HSSs of the gapped CHS K-joints were compared with the HSSs of the partially overlapped CHS K-joints obtained from the LIM.

The relative difference between the HSS values obtained from the proposed LIM for the partially overlapped CHS K-joints and from the DEn parametric SCF equations for the gapped CHS K-joints is defined as follow:

$$D_{Ov-Gap}(HSS) = \frac{HSS_{Ov} - HSS_{Gap}}{HSS_{Ov}} \times 100\% \quad (6.2)$$

where $HSS_{Ov}$ is the HSS values estimated from the proposed LIM and $HSS_{Gap}$ is the HSS values estimated from the DEn parametric equations. Note that based on Equation 6.2, the benefit of using one of these two types of CHS K-joints can be recognized by the sign of $D_{Ov\text{-}Gap}(HSS)$. A negative value of the $D_{Ov\text{-}Gap}$ $(HSS)$ indicates that the partially overlapped CHS K-joint is in favor, while a positive value of the $D_{Ov\text{-}Gap}$ $(HSS)$ indicates that the gapped CHS K-joint is in favor.

From the HSS comparison results between the gapped and the partially overlapped CHS K-joints subjected to the basic load of AX11 = 200 kN, it is observed that all maximum HSSs occur on the chord side for the gapped CHS K-joints, while 79.40% of the partially overlapped CHS K-joints the maximum HSSs occur on the through brace and overlapping brace side. From Figure 6.5, it is observed that the partially overlapped CHS K-joints subjected to AX11 load case gain more benefit than the gapped CHS K-joints. 88.65% gapped CHS K-joints failed earlier than the partially overlapped K-joints. Only 11.35% of partially overlapped CHS K-joints having braces with $\gamma$ value higher than 12, failed earlier than gapped CHS K-joints. It could be concluded that the maximum HSSs mainly occur on the through brace or overlapping brace sides for the partially overlapped CHS K-joints, while for the gapped CHS K-joints maximum HSSs mainly occur on the chord sides.

From the maximum HSS comparison results between the gapped and the partially overlapped CHS K-joints subjected to the basic load of IPB11 = 45 kN.m, note that the maximum HSSs occur on the chord and brace sides with a proportion of 84.12% and 15.88%, respectively, for the gapped CHS K-joints, while for the partially overlapped CHS K-joints, the maximum HSSs occur on chord and brace sides with a proportion of 23.36% and 76.64%, respectively. From Figure 6.6, it is observed that the gapped CHS K-joints subjected to the IPB11 load case gain more benefit than the partially

overlapped CHS K-joints. All partially overlapped CHS K-joints involved in the range of study failed earlier than the gapped CHS K-joints. It could be attributed to the fact that the partially overlapped CHS K-joints are stiffer than the gapped CHS K-joints. As a result, the maximum HSSs very often occur on the braces of partially overlapped CHS K-joints which are usually thinner than the chords.

To have some idea what would happen with these two types CHS K-joints when it comes to combined load case, the dimensions of the CHS K-joints from Table 6.2 subjected to combined load cases of (i) AX11 = 200 kN and IPB11 = 10 kN.m; and (ii) AX11 = 200 kN and IPB11 = 25 kN.m; and eventually (iii) AX11 = 200 kN and IPB11 = 45 kN.m are compared in terms of the maximum HSS values. It goes without saying that if the load amounts were set different from the mentioned above, definitely the percentage of the failed joints would be different from the results below. Nevertheless, it is believed that these load amounts would give some trends on the failure for both types of joints.

For the case that the gapped and partially overlapped CHS K-joints subjected to combined load of AX11 = 200 kN and IPB11 = 10 kN.m, it was found that the maximum HSSs for the gapped CHS K-joints mainly occur on the chords, while for the partially overlapped CHS K-joints mainly occur on the through brace or overlapping brace. From Figure 6.7, note that the percentages of the gapped and the partially overlapped CHS K-joints failed earlier are 59.32% and 40.68%, respectively.

For the case that the gapped and partially overlapped CHS K-joints subjected to the combined load case of AX11 = 200 kN and IPB11 = 25 kN.m, it was found that the maximum HSSs for the gapped CHS K-joints mainly occur on the chords, while for the partially overlapped CHS K-joints mainly occur on the through brace or overlapping brace. From Figure 6.8, note that the percentages of gapped and partially overlapped CHS K-joints failed earlier are 35.83% and 64.17%, respectively. It is observed that with the increase of IPB, the benefit turned out in favor of the gapped CHS K-joints.

For the case that the gapped and partially overlapped CHS K-joints subjected to combined load of AX11 = 200 kN and IPB11 = 45 kN.m, it was found that the maximum HSSs for the gapped CHS K-joints mainly occur on the chords, while for the partially overlapped CHS K-joints mainly occur on the though brace or overlapping brace. From Figure 6.9, note that the percentages of gapped and partially overlapped CHS K-joints failed earlier are 18.11% and 81.89%, respectively. It is observed that with the increase of IPB, the benefit turned out in favor of the gapped CHS K-joints.

From all above HSS comparisons, it was observed that the difference of HSSs between the gapped and the partially overlapped CHS K-joints were small in some cases. It seemed that it could be mistaken to judge which type of CHS K-joint is better in fatigue performance, since the maximum HSSs occurred in different members with different thicknesses. Therefore, the actual fatigue life prediction could be a better option to get a clearer understanding about the fatigue performance of these two types of CHS K-joints.

## 6.5 COMPARISON OF FATIGUE LIFE BETWEEN GAPPED AND PARTIALLY OVERLAPPED CHS K-JOINTS

Some research works concerning overlapped K-joints have been done by Lalani and Forsyth [31], and Moe [32]. Lalani and Forsyth [31] investigated a series of elastic and fatigue tests on overlapping K(N)-joints. According to their studies, test results indicated that S-N curves approaches would yield a conservative estimate of fatigue life. Another researcher Moe [32] performed the stress analysis based on the fatigue tests of two overlapped K-joints subjected to balanced axial load. It is also noted that the S-N curves are found to be on the conservative side of the test results.

In addition, in this present study three specimens have been investigated on fatigue life as mentioned earlier in Chapter 3. It is also observed that the S-N curves [5] have been

found to be on the conservative side of the test results. Therefore, a comparison of fatigue life prediction of these two types: gapped and overlapped CHS k-joints may give a more accurate prediction in their actual fatigue performance.

The dimensions of the CHS K-joints used to compare the fatigue life are shown in Table 6.3, which is in the same format with Table 6.2, but performs with the chord thicknesses instead of $\gamma$ values. There 14 groups are considered. The chord thicknesses range from 6 mm to 25 mm, and the braces thicknesses range in some groups from 6 mm to 20 mm. Both the gapped and the partially overlapped CHS K-joints are subjected to AX11 and IPB11 load cases with 200 kN and 45 kN.m, respectively. Then, the calculated HSSs of the gapped and the partially overlapped CHS K-joints are considered as values of $\Delta\sigma$ to predict their fatigue life.

The relative difference between the numbers of cycles based on S-N curve [5] obtained from the partially overlapped CHS K-joints and from the gapped CHS K-joints is defined as the follow:

$$D_{Gap-Ov}(FL) = \frac{F_{Gap} - F_{Ov}}{F_{Gap}} \times 100\% \qquad (6.3)$$

where $F_{Gap}$ is the number of cycles based on S-N curve [5] estimated from the HSS value based on DEn parametric equations results, $F_{Ov}$ is the number of cycles based on S-N curve [5] estimated from HSS value obtained from the proposed LIM. Note that based on Equation 6.3, the benefit of using one of these two types of CHS K-joints can be recognized by the sign of the $D_{Gap\text{-}Ov}$ *(FL)*. A negative value of the $D_{Gap\text{-}Ov}$ *(FL)* indicates that the partially overlapped CHS K-joint is in favor, while a positive value of the $D_{Gap\text{-}Ov}$ *(FL)* indicates that the gapped CHS K-joint is in favor.

The fatigue life comparison of the gapped and the partially overlapped CHS K-joints subjected to the basic load of AX11 = 200 kN shows that the partially overlapped CHS

K-joints gain more benefit than their gapped counterparts. From Figure 6.10, it is observed that 92.91% of the gapped CHS K-joints failed earlier than the partially overlapped CHS K-joint. Only 7.09% of partially overlapped CHS K-joints having braces with the $\gamma$ value of more than 12 are failed earlier than the gapped CHS K-joints.

The fatigue life comparison of the gapped and the partially overlapped CHS K-joints subjected to the basic load of IPB11 = 45 kN.m shows that the gapped CHS K-joints gain more benefit than their overlapped counterparts. From Figure 6.11, note that all partially overlapped CHS K-joints involved in this comparison failed earlier than gapped CHS K-joints.

Figure 6.12 shows the fatigue life comparison of gapped and partially overlapped CHS K-joints subjected to combined load of AX11 = 200 kN and IPB11 = 10 kN.m. It is observed that the gapped CHS K-joints failed earlier than their counterparts are 79.92%. Figure 6.13 shows the fatigue life comparison of the gapped and the partially overlapped CHS K-joints subjected to combined load of AX11 = 200 kN and IPB11 = 25 kN.m. Note that the gapped CHS K-joints failed earlier than their counterparts are 43.04%. Figure 6.14 shows the fatigue life comparison of gapped and partially overlapped CHS K-joints subjected to combined load of AX11 = 200 kN and IPB11 = 45 kN.m. Note that the gapped CHS K-joints failed earlier than their counterparts are 21%. It is observed that with the increase of IPB load, the benefit turned out in favor of the gapped CHS K-joints.

From all above comparisons, it is observed that the percentages of failed CHS K-joints in terms of fatigue life are slightly different from the percentage of the maximum HSS comparison. It seems that the fatigue life comparison gives a more accurate prediction, especially where the HSSs occurred in different members with different thicknesses.

## 6.6 DISCUSSIONS AND CONCLUDING REMARKS

In this chapter, the proposed new tool based interpolation method and DEn parametric SCF equations have been compared in terms of SCFs, HSSs and fatigue life between the gapped and the partially overlapped CHS K-joints. The comparison results show that the partially overlapped CHS K-joints are mainly good at working under AX load case, especially where the joints having the braces with $\gamma$ of about 12 and lower. The gapped CHS K-joints are good at working under IPB load case. It is observed that the partially overlapped CHS K-joints subjected to combined load case gain more benefits than their counterparts, especially in the load case of AX combined with IPB load case of lesser than 25 kN.m.

In fact, in design of trusses it is usual practice to assume that the members are pin-ended, although some bending moments will be introduced, mostly due to nodding eccentricities between the centerlines of intersecting members at connections. These moments are normally distributed only to the chord member at a joint, depending on the relative chord stiffness on either side of the joint. In the case where one continuous section is used for either the compression or tension chord, half of the moment is distributed to either side of the joint provided that the joints are spaced at equal panel widths [92]. However, Wardenier [24] and the IIW [10] recommended that these moments can be neglected as far as the joint design is concerned provided the eccentricity associated with them falls within the certain limits stipulated in CIDECT guide [5]. In addition to these moments, secondary bending moments are also introduced into the members due to the end fixities of the members and inherent stiffness of the joints. Packer et al. [93] suggested that these moments can also generally be ignored with respect to design of both members and joints, on the basis that there is adequate deformation and rotation capacity in both the joints and members which allow stresses to be redistributed at the ultimate limit state, or after local yielding of the joints.

Therefore, the partially overlapped K-joints could be regarded as a favorite choice when compared to the gapped CHS K-joints provided that the partially overlapped CHS K-joints have no or small nodding eccentricities within the limits stipulated by CIDECT guide [5].

Table 6.1 DEn parametric SCF equations for gapped CHS K-joints

| Load type | SCF equations |
|---|---|
| AX on one brace only | $SCF_{CS} = 1.18 \times T1_A \times S1_{AB} \times (F1_A or F2_A)$<br>$SCF_{CC} = 1.13 \times T2_A \times S2_{AB} + B0_A \times B1_A$<br>$SCF_{BS} = 1.20 \times T3_A \times S1_{AB} \times (F1_A or F2_A)$<br>$SCF_{CC} = 1.23 \times T4_A \times S2_{AB}$ |
| Balanced AX | $SCF_{CS} = 1.22 \times (T1_A \times S1_{AB} - T1_B S1_{BA} IF1_{AB}) \times (F1_A or F2_A)$<br>$SCF_{CC} = 1.25 \times (T2_A \times S2_{AB} - T2_B \times S2_{BA} IF2_{AB}) + B0_A \times B1_A$<br>$SCF_{BS} = 1.12 \times (T3_A \times S1_{AB} - T3_B \times S1_{BA} IF3_{AB}) \times (F1_A or F2_A)$<br>$SCF_{CC} = 1.26 \times (T4_A \times S2_{AB} - T4_B \times S2_{BA} IF4_{AB})$ |
| IPB on one brace only | $SCF_C = 1.15 \times T7_A$<br>$SCF_B = 1.17 \times T8_A$ |
| Balanced IPB | $SCF_C = 1.15 \times (T7_A + T7_B IF7_{AB})$<br>$SCF_B = 1.16 \times (T8_A + T8_B IF8_{AB})$ |

NOMENCLATURE

$SCF_{CS}$= SCF at the chord saddle

$SCF_{CC}$ = SCF at the chord crown heel

$SCF_C$ = Maximum SCF on the chord side

$SCF_{BS}$ = SCF at the brace saddle

$SCF_{BC}$ = SCF at the brace crown heel

$SCF_B$ = Maximum SCF on the brace side

VALIDITY RANGE

The above equations are generally valid for geometrical parameters within the following limits:

$0.13 \le \beta \le 1.00$

$10.0 \le \gamma \le 35$

$0.25 \le \tau \le 1.00$

$30^\circ \le \theta \le 90^\circ$

$4.0 \le \alpha$

$0.00 \le \zeta \le 1.00$

Table 6.1 DEn parametric SCF equations for gapped CHS K-joints (cont'd)

| | |
|---|---|
| T Factors | $T1 = \tau\gamma^{1.2}\beta(2.12-2\beta)\sin^2\theta$<br>$T2 = \tau\gamma^{0.2}\beta(3.5-2.4\beta)\sin^{0.3}\theta$<br>$T3 = 1+\tau^{0.2}\gamma^{1.3}\beta(0.76-0.7\beta)\sin^{2.2}\theta$<br>$T4 = 2.6\beta^{0.8}\gamma^{(1-0.68\times\beta)}\sin^{(1-\beta^2)}\theta$<br>$T7 = 1.22\tau^{0.8}\beta\gamma^{(1-0.68\times\beta)}\sin^{(1-\beta^3)}\theta$<br>$T8 = 1+\tau^{0.2}\gamma\beta(0.26-0.21\beta)\sin^{1.5}\theta$ |
| S Factors | $S1_{ij} = \left[1-0.4\exp\left(-30x_{ij}^2\left(\frac{\beta_i}{\beta_j}\right)^2\left(\frac{\sin\theta_i}{\gamma}\right)\right)\right]$;<br>$S2_{ij} = \left[1+0.4\exp\left(-2x_{ij}^2\left(\frac{1}{\gamma^{0.5}\sin^2\theta_j}\right)\right)\right]$ |
| IF Factors | $IF1_{ij} = \beta_i(2.13-2\beta_i)\gamma^{0.2}\sin\theta_i\left(\frac{\sin\theta_i}{\sin\theta_j}\right)^P\exp(-0.3x_{ij})$;<br>where P=1 if $\theta_i > \theta_j$ *and* P=5 if $\theta_i < \theta_j$; $IF2_{ij} = (20-8(\beta_i+1)^2)\exp(-3x_{ij})$<br>$IF3_{ij} = \beta_i(2.0-1.8\beta_i)\gamma^{0.2}\sin\theta_i\left(\frac{\beta_{\min}}{\beta_{\max}}\right)\left(\frac{\sin\theta_i}{\sin\theta_j}\right)^P\exp(-0.5x_{ij})$<br>where P=2 if $\theta_i > \theta_j$ *and* P=5 if $\theta_i < \theta_j$; $IF4_{ij} = (-1.5\beta_i)\exp(-x_{ij})$<br>$IF7_{ij} = 1.5\tau_i^{(-2)})\exp(-3x_{ij})$; $IF8_{ij} = \left[40.0(\beta_i-0.75)^2-2.5\right]\exp(-3x_{ij})$<br>where<br>$x_{ij} = 1+(\zeta_{ij}\sin\theta_i/\beta_i)$; $\xi_{ij}$ = *Gap between weld toe of brace i and brace j* |
| B Factors | $B0 = \frac{C\tau(\beta-\tau/(2\gamma))(\alpha/2-\beta/\sin\theta)\sin\theta}{(1-3/(2\gamma))}$; for single axial load<br>$B0 = 0$; *for balanced axial load*<br>$B1 = 1.05+\frac{30\tau^{1.5}(1.2-\beta)\cos^4\theta+0.15}{\gamma}$;<br>C = 0.5 fully fixed chord ends, C = 1. 0 pinned chord ends,<br>C = 0.7 normal assume for structural analysis |
| F Factors | F1, F2, F3 = 1.0 $\alpha \geq 12$<br>$F1 = 1-(0.83\beta-0.56\beta^2-0.02)\gamma^{0.23}\exp(-0.21\gamma^{(-1.16)}\alpha^{2.5})$ $\alpha < 12$<br>$F2 = 1-(1.43\beta-0.97\beta^2-0.03)\gamma^{0.04}\exp(-0.71\gamma^{(-1.38)}\alpha^{2.5})$ $\alpha < 12$<br>$F3 = 1-0.55\beta^{1.8}\gamma^{0.16}\exp(-0.49\gamma^{(-0.89)}\alpha^{1.8})$ $\alpha < 12$ |

Table 6.2 Comparison ranges of geometrical parameters of CHS K-joints (762 K-joints)

| Groups | $\beta$ | Ov | $\theta$ | $\gamma$ | $\tau$ |
|---|---|---|---|---|---|
| Group 1 (D = 355.6 mm) | 0.91 | 0.45 | 60° | 14.82 | 1.00 |
| | | | | 14.22 | 0.8, 0.96, 1.00 |
| | | | | 12.70 | 0.86, 0.89, 1.00 |
| | | | | 12.52 | 0.85, 0.88, 0.99, 1.00 |
| | | | | 11.11 | 0.63, 0.75, 0.78, 0.88, 0.89 |
| | | | | 8.89 | 0.50, 0.60, 0.63, 0.70, 0.80, 1.00 |
| | | | | 7.11 | 0.48, 0.50, 0.56, 0.57, 0.64, 0.8, 1.00 |
| | | 0.37 | 55° | 14.82 | 1.00 |
| | | | | 14.22 | 0.80, 0.96, 1.00 |
| | | | | 12.7 | 0.86, 0.89, 1.00 |
| | | | | 12.52 | 0.85, 0.88, 0.99, 1.00 |
| | | | | 11.11 | 0.63, 0.75, 0.78, 0.88, 0.89 |
| | | | | 8.89 | 0.50, 0.60, 0.63, 0.70, 0.80, 1.00 |
| | | | | 7.11 | 0.48, 0.50, 0.56, 0.57, 0.64, 0.8, 1.00 |
| | | 0.29 | 50° | 14.82 | 1.00 |
| | | | | 14.22 | 0.8, 0.96, 1.00 |
| | | | | 12.7 | 0.86, 0.89, 1.00 |
| | | | | 12.52 | 0.85, 0.88, 0.99, 1.00 |
| | | | | 11.11 | 0.63, 0.75, 0.78, 0.88, 0.89 |
| | | | | 8.89 | 0.50, 0.60, 0.63, 0.70, 0.80, 1.00 |
| | | | | 7.11 | 0.48, 0.50, 0.56, 0.57, 0.64, 0.8, 1.00 |
| Group 2 (D= 273 mm) | 0.9 | 0.36 | 55° | 17.06 | 0.75, 0.79, 1.00 |
| | | | | 13.65 | 0.80, 1.00 |
| | | | | 11.38 | 0.50, 0.53, 0.67, 0.83, 1.00 |
| | | | | 10.92 | 0.50, 0.64, 0.80, 0.96, 1.00 |
| | | | | 9.75 | 0.57, 0.71, 0.86, 0.89, 1.00 |
| | | | | 9.61 | 0.56, 0.85, 0.88, 0.99, 1.00 |
| | | | | 8.53 | 0.38, 0.39, 0.50, 0.63, 0.75, 0.78, 0.88, 0.89, 1.00 |
| | | | | 6.83 | 0.30, 0.32, 0.40, 0.60, 0.63, 0.70, 0.71, 0.80, 1.00 |
| | | | | 5.46 | 0.40, 0.48, 0.50, 0.56, 0.57, 0.64, 0.80 |
| | | | | 15.25 | 0.75, 0.79, 1.00 |
| | | | | 12.23 | 0.80 |
| | | | | 10.19 | 0.50, 0.53, 0.67, 0.83, 1.00 |
| | | | | 9.78 | 0.50, 0.64, 0.8, 0.96, 1.00 |
| | | | | 8.73 | 0.57, 0.71, 0.86, 0.89 |
| | | | | 8.61 | 0.56, 0.85, 0.88 |
| | | | | 7.64 | 0.38, 0.39, 0.50, 0.63, 0.75, 0.78, 0.89, 1.00 |
| | | | | 6.11 | 0.30, 0.32, 0.40, 0.5, 0.6, 0.63, 0.71, 0.80, 1.00 |

Table 6.2 Comparison ranges of geometrical parameters of CHS K-joints (cont'd)

| Groups | $\beta$ | Ov | $\theta$ | $\gamma$ | $\tau$ |
|---|---|---|---|---|---|
| Group 3 (D= 177.8 mm) | 0.95 | 0.25 | 45° | 14.82 | 1.00 |
| | | | | 14.11 | 0.95, 1.00 |
| | | | | 11.11 | 0.63, 0.75, 0.79, 1.00 |
| | | | | 8.89 | 0.60, 0.63, 0.80, 1.00 |
| | | | | 7.41 | 0.50, 0.53, 1.00 |
| | | | | 6.35 | 0.43, 0.45, 0.57, 0.71, 0.86, 0.89, 1.00 |
| Group 4 (D =193.7 mm) | 0.92 | 0.46 | 60° | 16.14 | 1.00 |
| | | | | 15.37 | 0.79 |
| | | | | 12.11 | 0.75, 0.79, 1.00 |
| | | | | 9.69 | 0.50, 0.60, 0.63, 0.80, 1.00 |
| | | | | 8.07 | 0.53, 0.67, 0.83, 1.00 |
| | | | | 7.75 | 0.50, 0.64, 0.80, 0.96, 1.00 |
| | | | | 6.82 | 0.56, 0.70, 0.85, 0.88, 1.00 |
| | | | | 6.05 | 0.50, 0.63, 0.75, 0.78, 0.89 |
| | | 0.38 | 55° | 16.14 | 1.00 |
| | | | | 15.37 | 0.79 |
| | | | | 12.11 | 0.75, 0.79, 1.00 |
| | | | | 9.69 | 0.50, 0.60, 0.63, 0.80, 1.00 |
| | | | | 8.07 | 0.53, 0.67, 0.83, 1.00 |
| | | | | 7.75 | 0.50, 0.64, 0.80, 0.96, 1.00 |
| | | | | 6.82 | 0.56, 0.70, 0.85, 0.88, 1.00 |
| | | | | 6.05 | 0.50, 0.63, 0.75, 0.78, 0.89 |
| | | 0.30 | 50° | 16.14 | 1.00 |
| | | | | 15.37 | 0.79 |
| | | | | 12.11 | 0.75, 0.79, 1.00 |
| | | | | 9.69 | 0.50, 0.6, 0.63, 0.80, 1.00 |
| | | | | 8.07 | 0.53, 0.67, 0.83, 1.00 |
| | | | | 7.75 | 0.50, 0.64, 0.80, 0.96, 1.00 |
| | | | | 6.82 | 0.56, 0.70, 0.85, 0.88, 1.00 |
| | | | | 6.05 | 0.50, 0.63, 0.75, 0.78, 0.89 |
| Group 5 (D = 219.1 mm) | 0.88 | 0.43 | 60° | 13.69 | 0.75, 0.79, 1.00 |
| | | | | 10.96 | 0.50, 0.60, 0.63, 0.80, 1.00 |
| | | | | 9.13 | 0.50, 0.53, 0.67, 0.83, 1.00 |
| | | | | 8.76 | 0.50, 0.64, 0.80, 0.96, 1.00 |
| | | | | 7.71 | 0.42, 0.44, 0.56, 0.70, 0.85, 0.88, 1.00 |
| | | | | 6.85 | 0.38, 0.39, 0.50, 0.63, 0.75, 0.78, 0.89 |
| | | | | 5.48 | 0.30, 0.32, 0.40, 0.50, 0.60, 0.63, 0.71, 0.80 |

Table 6.2 Comparison ranges of geometrical parameters of CHS K-joints (cont'd)

| Groups | $\beta$ | Ov | $\theta$ | $\gamma$ | $\tau$ |
|---|---|---|---|---|---|
| Group 5 (D = 219.1 mm) | 0.88 | 0.35 | 55° | 13.69 | 0.75, 0.79, 1.00 |
| | | | | 10.96 | 0.50, 0.60, 0.63, 0.80, 1.00 |
| | | | | 9.13 | 0.50, 0.53, 0.67, 0.83, 1.00 |
| | | | | 8.76 | 0.50, 0.64, 0.80, 0.96, 1.00 |
| | | | | 7.71 | 0.42, 0.44, 0.56, 0.70, 0.85, 0.88, 1.00 |
| | | | | 6.85 | 0.38, 0.39, 0.50, 0.63, 0.75, 0.78, 0.89 |
| | | | | 5.48 | 0.30, 0.32, 0.40, 0.50, 0.60, 0.63, 0.71, 0.80 |
| | | 0.27 | 50° | 13.69 | 0.75, 0.79, 1.00 |
| | | | | 10.96 | 0.50, 0.60, 0.63, 0.80, 1.00 |
| | | | | 9.13 | 0.50, 0.53, 0.67, 0.83, 1.00 |
| | | | | 8.76 | 0.50, 0.64, 0.80, 0.96, 1.00 |
| | | | | 7.71 | 0.42, 0.44, 0.56, 0.70, 0.85, 0.88, 1.00 |
| | | | | 6.85 | 0.38, 0.39, 0.50, 0.63, 0.75, 0.78, 0.89 |
| | | | | 5.48 | 0.30, 0.32, 0.40, 0.50, 0.60, 0.63, 0.71, 0.80 |
| Group 6 (D = 193.7 mm) | 0.87 | 0.42 | 60° | 16.14 | 1.00 |
| | | | | 15.37 | 0.79 |
| | | | | 12.11 | 0.75, 0.79, 1.00 |
| | | | | 9.69 | 0.50, 0.60, 0.63, 0.8, 1.00 |
| | | | | 8.07 | 0.53, 0.67, 0.83, 1.00 |
| | | | | 7.75 | 0.50, 0.64, 0.80, 0.96, 1.00 |
| | | | | 6.82 | 0.56, 0.70, 0.85, 0.88, 1.00 |
| | | | | 6.05 | 0.50, 0.63, 0.75, 0.78, 0.89 |
| | | 0.34 | 55° | 16.14 | 1.00 |
| | | | | 15.37 | 0.79 |
| | | | | 12.11 | 0.75, 0.79, 1.00 |
| | | | | 9.69 | 0.50, 0.60, 0.63, 0.80, 1.00 |
| | | | | 8.07 | 0.53, 0.67, 0.83, 1.00 |
| | | | | 7.75 | 0.50, 0.64, 0.80, 0.96, 1.00 |
| | | | | 6.82 | 0.56, 0.70, 0.85, 0.88, 1.00 |
| | | | | 6.05 | 0.50, 0.63, 0.75, 0.78, 0.89 |
| | | 0.26 | 50° | 16.14 | 1.00 |
| | | | | 15.37 | 0.79 |
| | | | | 12.11 | 0.75, 0.79, 1.00 |
| | | | | 9.69 | 0.50, 0.60, 0.63, 0.80, 1.00 |
| | | | | 8.07 | 0.53, 0.67, 0.83, 1.00 |
| | | | | 7.75 | 0.50, 0.64, 0.80, 0.96, 1.00 |
| | | | | 6.82 | 0.56, 0.70, 0.85, 0.88, 1.00 |
| | | | | 6.05 | 0.50, 0.63, 0.75, 0.78, 0.89 |

Table 6.2 Comparison ranges of geometrical parameters of CHS K-joints (cont'd)

| Groups | $\beta$ | Ov | $\theta$ | $\gamma$ | $\tau$ |
|---|---|---|---|---|---|
| Group 7 (D = 219.1 mm) | 0.84 | 0.35 | 60° | 16.2 | 1.00 |
| | | | | 13.5 | 0.83, 1.00 |
| | | | | 12.96 | 0.80, 0.96, 1.00 |
| | | | | 11.57 | 0.86, 0.89, 1.00 |
| | | | | 11.40 | 0.85, 0.88, 0.99, 1.00 |
| | | | | 10.12 | 0.50, 0.63, 0.75, 0.78, 0.88, 0.89 |
| | | | | 8.10 | 0.40, 0.50, 0.60 |
| | | | | 6.48 | 0.32, 0.40, 0.48, 0.50 |
| Group 8 (D = 168.3 mm) | 0.83 | 0.40 | 60° | 14.30 | 1.00 |
| | | | | 13.36 | 0.95, 1.00 |
| | | | | 10.52 | 0.75, 0.79, 1.00 |
| | | | | 8.42 | 0.60, 0.63, 0.80 |
| | | | | 7.01 | 0.53, 0.67, 0.83, 1.00 |
| | | | | 6.01 | 0.71,0.86, 0.89, 1.00 |
| | | 0.31 | 55° | 14.30 | 1.00 |
| | | | | 13.36 | 0.95, 1.00 |
| | | | | 10.52 | 0.75, 0.79, 1.00 |
| | | | | 8.42 | 0.60, 0.63, 0.80 |
| | | | | 7.01 | 0.53, 0.67, 0.83, 1.00 |
| | | | | 6.01 | 0.71,0.86, 0.89, 1.00 |
| Group 9 (D = 139.7 mm) | 0.82 | 0.39 | 60° | 11.09 | 0.95, 1.00 |
| | | | | 8.73 | 0.75, 0.79, 1.00 |
| | | | | 6.99 | 0.60, 0.63, 0.80, 1.00 |
| | | | | 5.82 | 0.53, 0.67, 0.83, 1.00 |
| | | 0.30 | 55° | 11.09 | 0.95, 1.00 |
| | | | | 8.73 | 0.75, 0.79, 1.00 |
| | | | | 6.99 | 0.60, 0.63, 0.80, 1.00 |
| | | | | 5.82 | 0.53, 0.67, 0.83, 1.00 |
| Group 10 (D = 177.8 mm) | 0.77 | 0.25 | 55° | 14.82 | 1.00 |
| | | | | 14.22 | 0.80, 0.96, 1.00 |
| | | | | 12.7 | 0.86, 0.89, 1.00 |
| | | | | 12.52 | 0.85, 0.88, 0.99, 1.00 |
| | | | | 11.11 | 0.63, 0.75, 0.78, 0.88, 0.89 |
| | | | | 8.89 | 0.50, 0.60, 0.63, 0.70, 0.80, 1.00 |
| | | | | 7.11 | 0.48, 0.50, 0.56, 0.57, 0.64, 0.8, 1.00 |
| Group 11 (D = 168.3 mm) | 0.73 | 0.31 | 60° | 11.09 | 0.95, 1.00 |
| | | | | 8.73 | 0.75, 0.79, 1.00 |
| | | | | 6.99 | 0.60, 0.63, 0.8, 1.00 |
| | | | | 5.82 | 0.53, 0.67, 0.83, 1.00 |

Table 6.2 Comparison ranges of geometrical parameters of CHS K-joints (cont'd)

| Groups | $\beta$ | Ov | $\theta$ | $\gamma$ | $\tau$ |
|---|---|---|---|---|---|
| Group 12 (D =193.7 mm) | 0.75 | 0.34 | 60° | 16.2 | 0.8,1.00 |
| | | | | 13.5 | 0.83, 1.00 |
| | | | | 12.96 | 0.80, 1.00 |
| | | | | 11.57 | 0.86, 0.89 |
| | | | | 11.40 | 0.85, 0.88 |
| | | | | 10.12 | 0.50, 0.63, 0.75, 0.78 |
| | | | | 8.10 | 0.40, 0.50, 0.60, 0.63, 1.00 |
| | | | | 6.48 | 0.32, 0.40, 0.50, 0.64, 0.80 |
| Group 13 (D = 193.7 mm) | 0.72 | 0.31 | 60° | 16.14 | 1.00 |
| | | | | 15.37 | 1.00 |
| | | | | 12.11 | 0.75, 0.79, 1.00 |
| | | | | 9.69 | 0.60, 0.63, 0.8, 1.00 |
| | | | | 8.07 | 0.50, 0.53, 0.67, 0.83 |
| | | | | 7.75 | 0.48, 0.50, 0.64 |
| | | | | 6.82 | 0.42, 0.44, 0.56, 0.70 |
| | | | | 6.05 | 0.50, 0.63 |
| Group14 (D = 168.3 mm) | 0.68 | 0.26 | 60° | 13.36 | 0.95, 1.00 |
| | | | | 10.52 | 0.75, 0.79, 1.00 |
| | | | | 8.42 | 0.60, 0.63, 0.80 |
| | | | | 7.01 | 0.53, 0.67, 0.83, 1.00 |
| | | | | 6.01 | 0.71,0.86, 0.89, 1.00 |

Table 6.3 Geometrical parameters of K-joints for fatigue life comparison (762 K-joints)

| Groups | $\beta$ | Ov | $\theta$ | $T$ *(mm)* | $\tau = t / T$ |
|---|---|---|---|---|---|
| Group 1 (D = 355.6 mm) | 0.91 | 0.45 | 60° | 12 | 1.00 |
| | | | | 12.5 | 0.80, 0.96, 1.00 |
| | | | | 14 | 0.86, 0.89, 1.00 |
| | | | | 14.2 | 0.85, 0.88, 0.99, 1.00 |
| | | | | 16 | 0.63, 0.75, 0.78, 0.88, 0.89 |
| | | | | 20 | 0.50, 0.60, 0.63, 0.70, 0.80, 1.00 |
| | | | | 25 | 0.48, 0.50, 0.56, 0.57, 0.64, 0.8, 1.00 |
| | | 0.37 | 55° | 12 | 1.00 |
| | | | | 12.5 | 0.8, 0.96, 1.00 |
| | | | | 14 | 0.86, 0.89, 1.00 |
| | | | | 14.2 | 0.85, 0.88, 0.99, 1.00 |
| | | | | 16 | 0.63, 0.75, 0.78, 0.88, 0.89 |
| | | | | 20 | 0.50, 0.60, 0.63, 0.70, 0.80, 1.00 |
| | | | | 25 | 0.48, 0.50, 0.56, 0.57, 0.64, 0.8, 1.00 |
| | | 0.29 | 50° | 12 | 1.00 |
| | | | | 12.5 | 0.8, 0.96, 1.00 |
| | | | | 14 | 0.86, 0.89, 1.00 |
| | | | | 14.2 | 0.85, 0.88, 0.99, 1.00 |
| | | | | 16 | 0.63, 0.75, 0.78, 0.88, 0.89 |
| | | | | 20 | 0.50, 0.60, 0.63, 0.70, 0.80, 1.00 |
| | | | | 25 | 0.48, 0.50, 0.56, 0.57, 0.64, 0.8, 1.00 |
| Group 2 (D = 273 mm) | 0.9 | 0.36 | 55° | 8 | 0.75, 0.79, 1.00 |
| | | | | 10 | 0.80, 1.00 |
| | | | | 12 | 0.50, 0.53, 0.67, 0.83, 1.00 |
| | | | | 12.5 | 0.50, 0.64, 0.80, 0.96, 1.00 |
| | | | | 14 | 0.57, 0.71, 0.86, 0.89, 1.00 |
| | | | | 14.2 | 0.56, 0.85, 0.88, 0.99, 1.00 |
| | | | | 16 | 0.38, 0.39, 0.50, 0.63, 0.75, 0.78, 0.88, 0.89, 1.00 |
| | | | | 20 | 0.30, 0.32, 0.40, 0.60, 0.63, 0.70, 0.71, 0.80, 1.00 |
| | | | | 25 | 0.40, 0.48, 0.50, 0.56, 0.57, 0.64, 0.80 |

Table 6.3 Geometrical parameters of K-joints for fatigue life comparison (cont'd)

| Groups | $\beta$ | Ov | $\theta$ | $T$ *(mm)* | $\tau = t / T$ |
|---|---|---|---|---|---|
| Group 3 (D= 177.8 mm) | 0.95 | 0.25 | 45° | 6 | 1.00 |
| | | | | 6.5 | 0.95, 1.00 |
| | | | | 8 | 0.63, 0.75, 0.79, 1.00 |
| | | | | 10 | 0.60, 0.63, 0.80, 1.00 |
| | | | | 12 | 0.50, 0.53, 1.00 |
| | | | | 14 | 0.43, 0.45, 0.57, 0.71, 0.86, 0.89, 1.00 |
| Group 4 (D =193.7 mm) | 0.92 | 0.46 | 60° | 6 | 1.00 |
| | | | | 6.3 | 0.79 |
| | | | | 8 | 0.75, 0.79, 1.00 |
| | | | | 10 | 0.50, 0.60, 0.63, 0.8, 1.00 |
| | | | | 12 | 0.53, 0.67, 0.83, 1.00 |
| | | | | 12.5 | 0.50, 0.64, 0.80, 0.96, 1.00 |
| | | | | 14.5 | 0.56, 0.70, 0.85, 0.88, 1.00 |
| | | | | 16 | 0.50, 0.63, 0.75, 0.78, 0.89 |
| | | 0.38 | 55° | 6 | 1.00 |
| | | | | 6.3 | 0.79 |
| | | | | 8 | 0.75, 0.79, 1.00 |
| | | | | 10 | 0.50, 0.60, 0.63, 0.80, 1.00 |
| | | | | 12 | 0.53, 0.67, 0.83, 1.00 |
| | | | | 12.5 | 0.50, 0.64, 0.80, 0.96, 1.00 |
| | | | | 14.5 | 0.56, 0.70, 0.85, 0.88, 1.00 |
| | | | | 16 | 0.50, 0.63, 0.75, 0.78, 0.89 |
| | | 0.30 | 50° | 6 | 1.00 |
| | | | | 6.3 | 0.79 |
| | | | | 8 | 0.75, 0.79, 1.00 |
| | | | | 10 | 0.50, 0.60, 0.63, 0.80, 1.00 |
| | | | | 12 | 0.53, 0.67, 0.83, 1.00 |
| | | | | 12.5 | 0.50, 0.64, 0.80, 0.96, 1.00 |
| | | | | 14.5 | 0.56, 0.70, 0.85, 0.88, 1.00 |
| | | | | 16 | 0.50, 0.63, 0.75, 0.78, 0.89 |
| Group 5 (D = 219.1 mm) | 0.88 | 0.43 | 60° | 8 | 0.75, 0.79, 1.00 |
| | | | | 10 | 0.50, 0.60, 0.63, 0.80, 1.00 |
| | | | | 12 | 0.50, 0.53, 0.67, 0.83, 1.00 |
| | | | | 12.5 | 0.50, 0.64, 0.80, 0.96, 1.00 |
| | | | | 14.2 | 0.42, 0.44, 0.56, 0.70, 0.85, 0.88, 1.00 |
| | | | | 16 | 0.38, 0.39, 0.50, 0.63, 0.75, 0.78, 0.89 |
| | | | | 20 | 0.30, 0.32, 0.40, 0.50, 0.60, 0.63, 0.71, 0.80 |

Table 6.3 Geometrical parameters of K-joints for fatigue life comparison (cont'd)

| Groups | $\beta$ | Ov | $\theta$ | $T$ *(mm)* | $\tau = t / T$ |
|---|---|---|---|---|---|
| Group 5 (D = 219.1 mm) | 0.88 | 0.35 | 55° | 8 | 0.75, 0.79, 1.00 |
| | | | | 10 | 0.50, 0.60, 0.63, 0.80, 1.00 |
| | | | | 12 | 0.50, 0.53, 0.67, 0.83, 1.00 |
| | | | | 12.5 | 0.50, 0.64, 0.80, 0.96, 1.00 |
| | | | | 14.2 | 0.42, 0.44, 0.56, 0.70, 0.85, 0.88, 1.00 |
| | | | | 16 | 0.38, 0.39, 0.50, 0.63, 0.75, 0.78, 0.89 |
| | | | | 20 | 0.30, 0.32, 0.40, 0.50, 0.60, 0.63, 0.71, 0.80 |
| | | 0.27 | 50° | 8 | 0.75, 0.79, 1.00 |
| | | | | 10 | 0.50, 0.60, 0.63, 0.80, 1.00 |
| | | | | 12 | 0.50, 0.53, 0.67, 0.83, 1.00 |
| | | | | 12.5 | 0.50, 0.64, 0.80, 0.96, 1.00 |
| | | | | 14.2 | 0.42, 0.44, 0.56, 0.70, 0.85, 0.88, 1.00 |
| | | | | 16 | 0.38, 0.39, 0.50, 0.63, 0.75, 0.78, 0.89 |
| | | | | 20 | 0.30, 0.32, 0.40, 0.50, 0.60, 0.63, 0.71, 0.80 |
| Group 6 (D = 193.7 mm) | 0.87 | 0.42 | 60° | 6 | 1.00 |
| | | | | 8 | 0.79 |
| | | | | 10 | 0.75, 0.79, 1.00 |
| | | | | 12 | 0.50, 0.60, 0.63, 0.80, 1.00 |
| | | | | 12.5 | 0.53, 0.67, 0.83, 1.00 |
| | | | | 14.2 | 0.50, 0.64, 0.80, 0.96, 1.00 |
| | | | | 16 | 0.56, 0.70, 0.85, 0.88, 1.00 |
| | | | | 20 | 0.50, 0.63, 0.75, 0.78, 0.89 |
| | | 0.34 | 55° | 6.3 | 1.00 |
| | | | | 8 | 0.79 |
| | | | | 10 | 0.75, 0.79, 1.00 |
| | | | | 12 | 0.50, 0.60, 0.63, 0.80, 1.00 |
| | | | | 12.5 | 0.53, 0.67, 0.83, 1.00 |
| | | | | 14 | 0.50, 0.64, 0.80, 0.96, 1.00 |
| | | | | 14.2 | 0.56, 0.70, 0.85, 0.88, 1.00 |
| | | | | 16 | 0.50, 0.63, 0.75, 0.78, 0.89 |
| | | 0.26 | 50° | 6.3 | 1.00 |
| | | | | 8 | 0.79 |
| | | | | 10 | 0.75, 0.79, 1.00 |
| | | | | 12 | 0.50, 0.60, 0.63, 0.80, 1.00 |
| | | | | 12.5 | 0.53, 0.67, 0.83, 1.00 |
| | | | | 14 | 0.50, 0.64, 0.80, 0.96, 1.00 |
| | | | | 14.2 | 0.56, 0.70, 0.85, 0.88, 1.00 |
| | | | | 16 | 0.50, 0.63, 0.75, 0.78, 0.89 |

Table 6.3 Geometrical parameters of K-joints for fatigue life comparison (cont'd)

| Groups | $\beta$ | Ov | $\theta$ | $T$ (mm) | $\tau = t / T$ |
|---|---|---|---|---|---|
| Group 7 (D = 219.1 mm) | 0.84 | 0.35 | 60° | 8 | 1.00 |
| | | | | 10 | 0.83, 1.00 |
| | | | | 12 | 0.80, 0.96, 1.00 |
| | | | | 12.5 | 0.86, 0.89, 1.00 |
| | | | | 14 | 0.85, 0.88, 0.99, 1.00 |
| | | | | 14.2 | 0.5, 0.63, 0.75, 0.78, 0.88, 0.89 |
| | | | | 16 | 0.40, 0.50, 0.60 |
| | | | | 20 | 0.32, 0.40, 0.48, 0.50 |
| Group 8 (D = 168.3 mm) | 0.83 | 0.40 | 60° | 6 | 1.00 |
| | | | | 6.3 | 0.95, 1.00 |
| | | | | 8 | 0.75, 0.79, 1.00 |
| | | | | 10 | 0.60, 0.63, 0.80 |
| | | | | 12 | 0.53, 0.67, 0.83, 1.00 |
| | | | | 14 | 0.71,0.86, 0.89, 1.00 |
| | | 0.31 | 55° | 6 | 1.00 |
| | | | | 6.3 | 0.95, 1.00 |
| | | | | 8 | 0.75, 0.79, 1.00 |
| | | | | 10 | 0.60, 0.63, 0.80 |
| | | | | 12 | 0.53, 0.67, 0.83, 1.00 |
| | | | | 14 | 0.71,0.86, 0.89, 1.00 |
| Group 9 (D = 139.7 mm) | 0.82 | 0.39 | 60° | 6.3 | 0.95, 1.00 |
| | | | | 8 | 0.75, 0.79, 1.00 |
| | | | | 10 | 0.60, 0.63, 0.80, 1.00 |
| | | | | 12 | 0.53, 0.67, 0.83, 1.00 |
| | | 0.30 | 55° | 6.3 | 0.95, 1.00 |
| | | | | 8 | 0.75, 0.79, 1.00 |
| | | | | 10 | 0.60, 0.63, 0.80, 1.00 |
| | | | | 12 | 0.53, 0.67, 0.83, 1.00 |
| Group 10 (D = 177.8 mm) | 0.77 | 0.25 | 55° | 12 | 1.00 |
| | | | | 12.5 | 0.80, 0.96, 1.00 |
| | | | | 14 | 0.86, 0.89, 1.00 |
| | | | | 14.2 | 0.85, 0.88, 0.99, 1.00 |
| | | | | 16 | 0.63, 0.75, 0.78, 0.88, 0.89 |
| | | | | 20 | 0.50, 0.60, 0.63, 0.70, 0.80, 1.00 |
| | | | | 25 | 0.48, 0.50, 0.56, 0.57, 0.64, 0.8, 1.00 |
| Group 11 (D = 168.3 mm) | 0.73 | 0.31 | 60° | 6.3 | 0.95, 1.00 |
| | | | | 8 | 0.75, 0.79, 1.00 |
| | | | | 10 | 0.60, 0.63, 0.80, 1.00 |
| | | | | 12 | 0.53, 0.67, 0.83, 1.00 |

Table 6.3 Geometrical parameters of K-joints for fatigue life comparison (cont'd)

| Groups | $\beta$ | Ov | $\theta$ | $T$ (mm) | $\tau = t / T$ |
|---|---|---|---|---|---|
| Group 12 ( D =193.7 mm) | 0.75 | 0.34 | 60° | 10 | 0.80,1.00 |
| | | | | 12 | 0.83, 1.00 |
| | | | | 12.5 | 0.80, 1.00 |
| | | | | 14 | 0.86, 0.89 |
| | | | | 14.2 | 0.85, 0.88 |
| | | | | 16 | 0.50, 0.63, 0.75, 0.78 |
| | | | | 20 | 0.40, 0.50, 0.60, 0.63, 1.00 |
| | | | | 25 | 0.32, 0.40, 0.50, 0.64, 0.80 |
| Group 13 (D = 193.7 mm) | 0.72 | 0.31 | 60° | 6 | 1.00 |
| | | | | 6.3 | 1.00 |
| | | | | 8 | 0.75, 0.79, 1.00 |
| | | | | 10 | 0.60, 0.63, 0.80, 1.00 |
| | | | | 12 | 0.50, 0.53, 0.67, 0.83 |
| | | | | 12.5 | 0.48, 0.50, 0.64 |
| | | | | 14.2 | 0.42, 0.44, 0.56, 0.70 |
| | | | | 16 | 0.50, 0.63 |
| Group14 (D = 168.3 mm) | 0.68 | 0.26 | 60° | 6.3 | 0.95, 1.00 |
| | | | | 8 | 0.75, 0.79, 1.00 |
| | | | | 10 | 0.60, 0.63, 0.80 |
| | | | | 12 | 0.53, 0.67, 0.83, 1.00 |
| | | | | 14 | 0.71,0.86, 0.89, 1.00 |

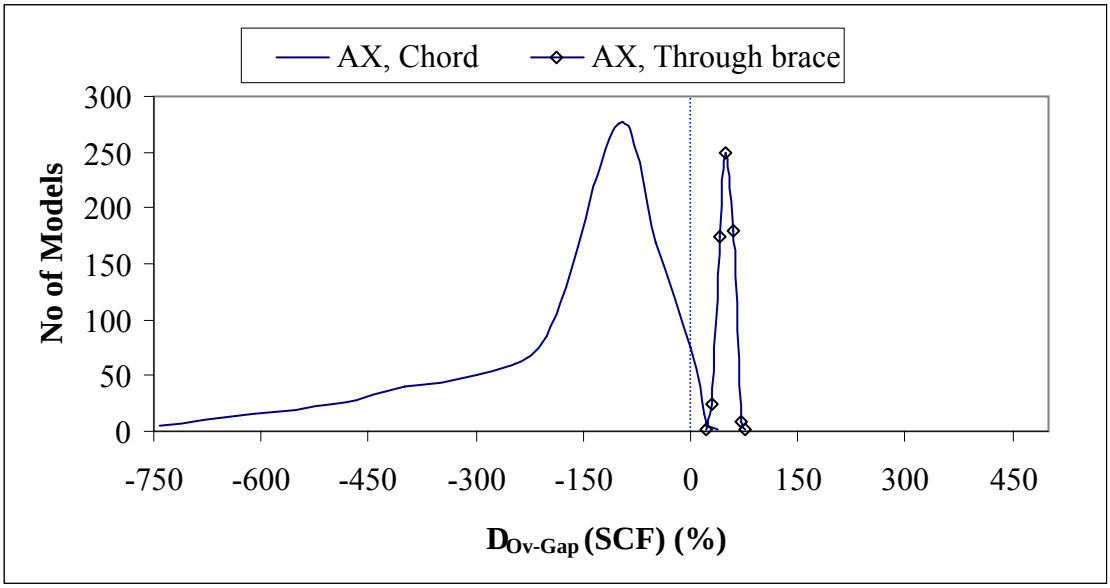


Figure 6.1 SCFs comparison between gapped and partially overlapped CHS K-joints with through brace subjected to AX11 load case

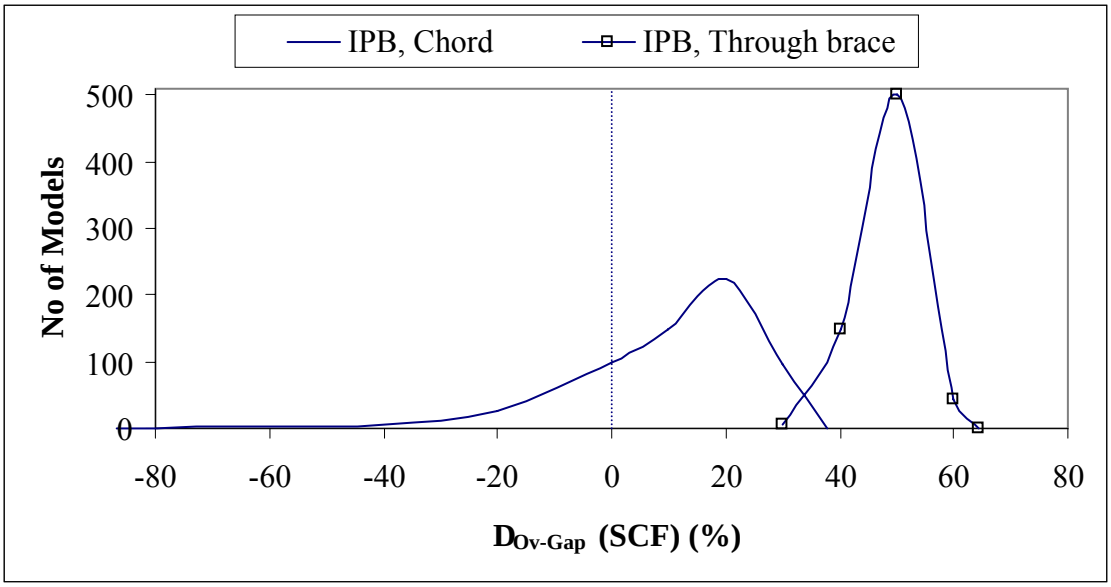


Figure 6.2 SCFs comparison between gapped and partially overlapped CHS K-joints with through brace subjected to IPB11 load case

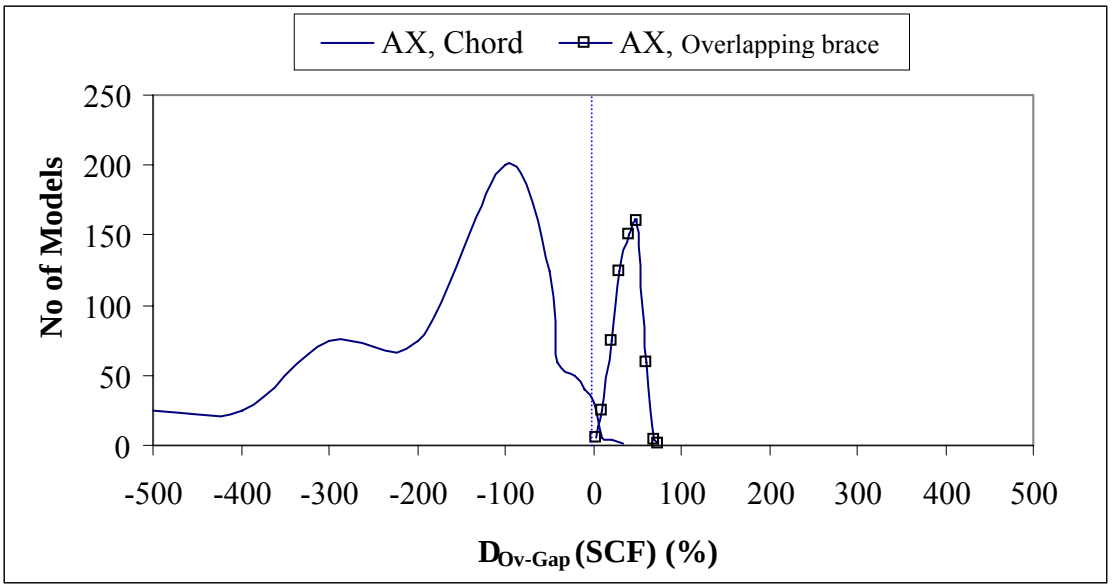


Figure 6.3 SCFs comparison between gapped and partially overlapped CHS K-joints with overlapping brace subjected to AX21 load case

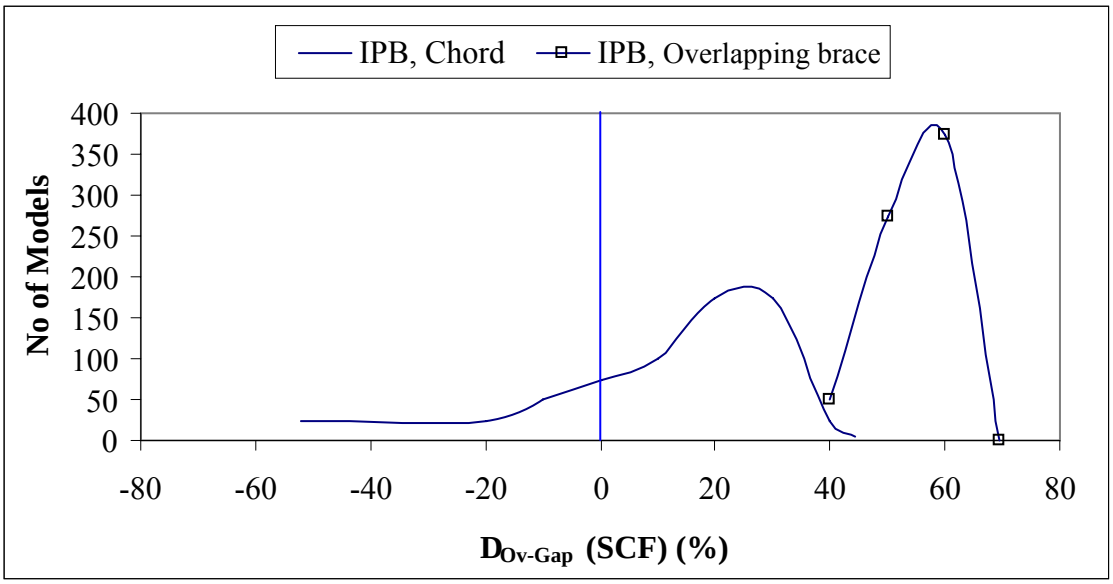


Figure 6.4 SCFs comparison between gapped and partially overlapped CHS K-joints with overlapping brace subjected to IPB21 load case

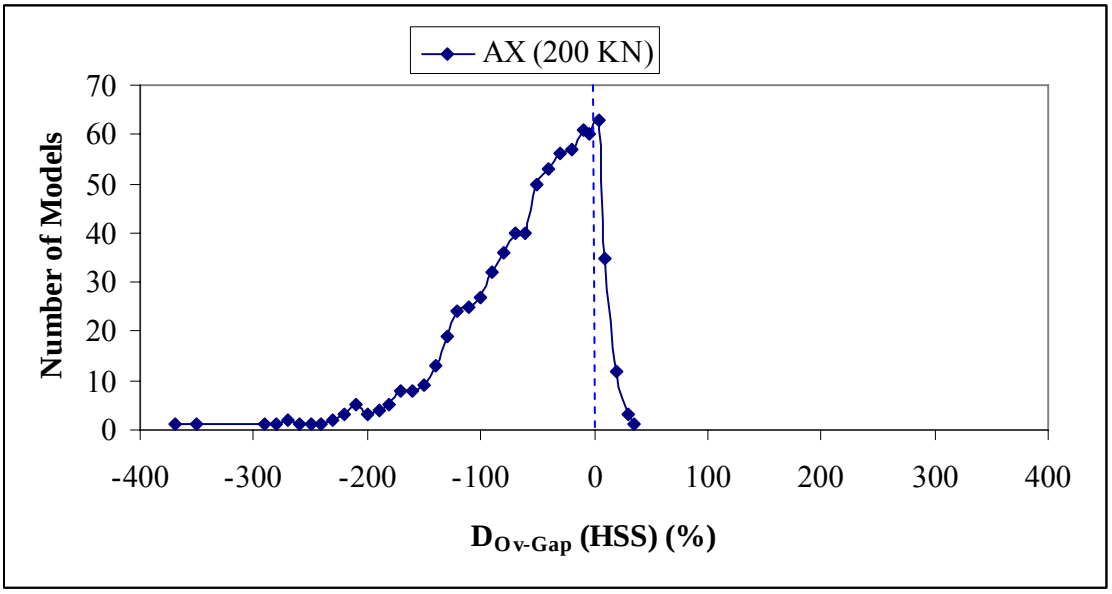


Figure 6.5 HSS comparison between gapped and partially overlapped CHS K-joints with overlapping brace subjected to basic load case AX11 (200 kN)

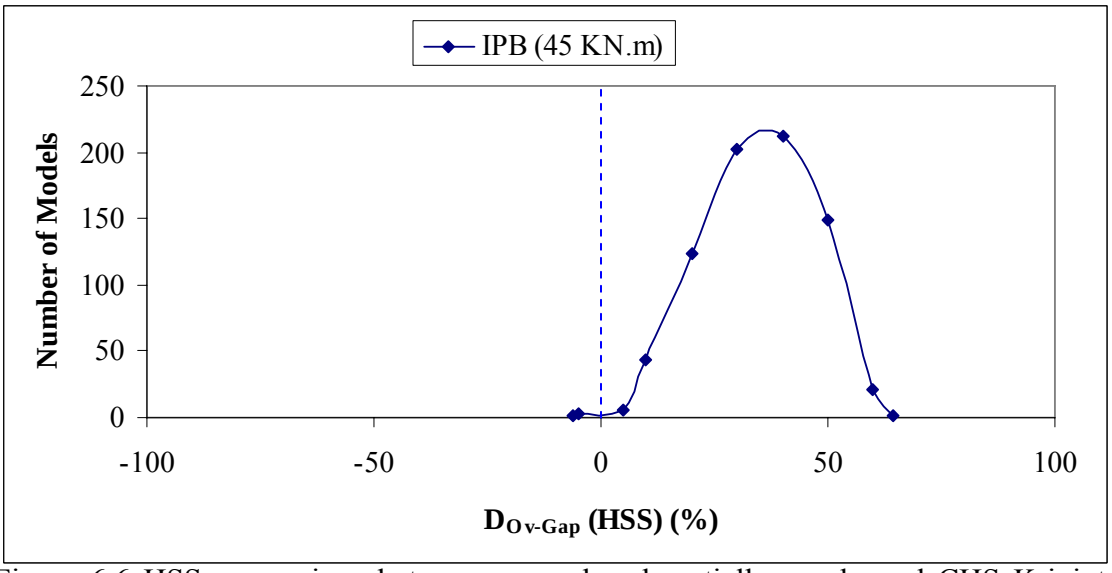


Figure 6.6 HSS comparison between gapped and partially overlapped CHS K-joints with overlapping brace subjected to load case IPB11 (45 kN.m)

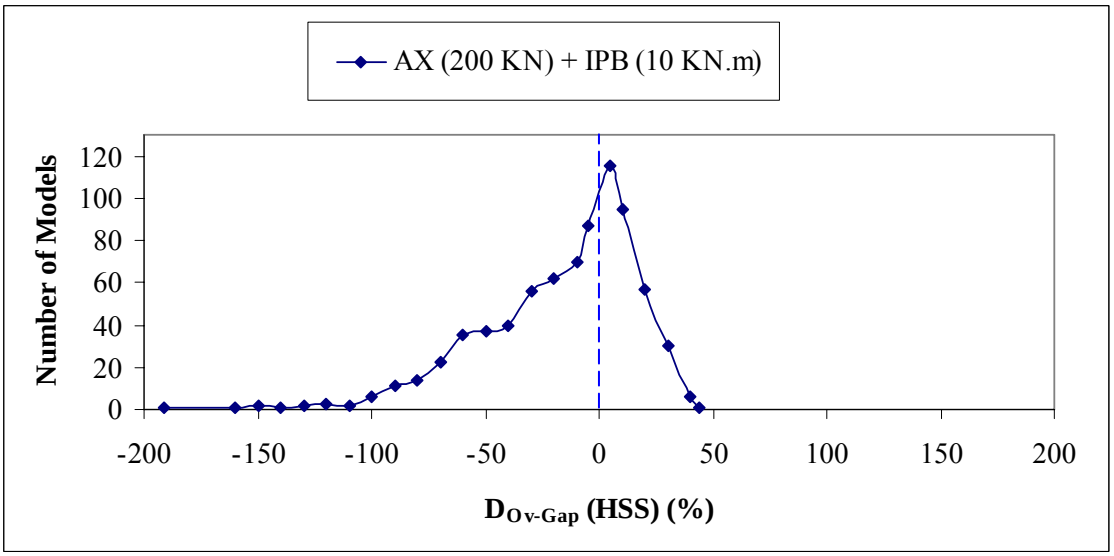


Figure 6.7 HSS comparison between gapped and partially overlapped CHS K-joints with overlapping brace subjected to combined load case AX11 (200 kN) +IPB11 (10 kN.m)

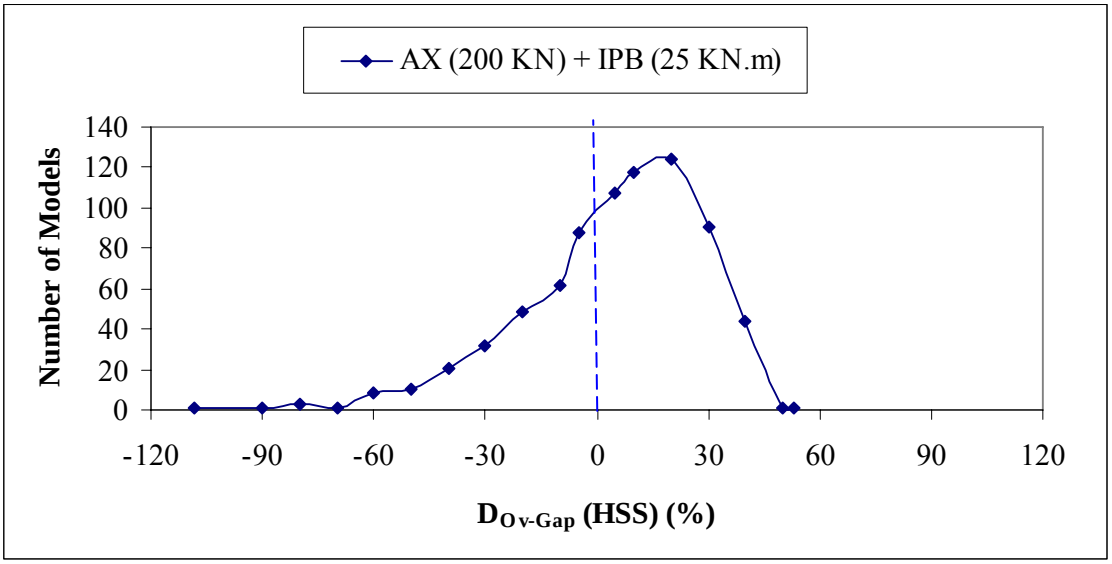


Figure 6.8 HSS comparison between gapped and partially overlapped CHS K-joints with overlapping brace subjected to combined load case AX11 (200 kN) +IPB11 (25 kN.m)

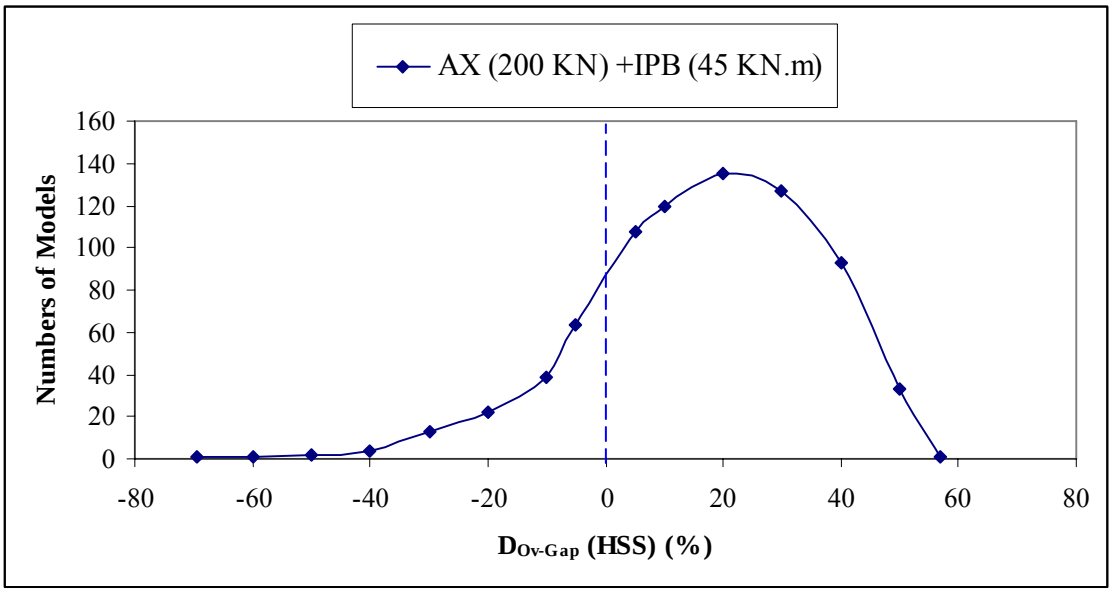


Figure 6.9 HSS comparison between gapped and partially overlapped CHS K-joints with overlapping brace subjected to combined load case AX11 (200 kN) +IPB11 (45 kN.m)

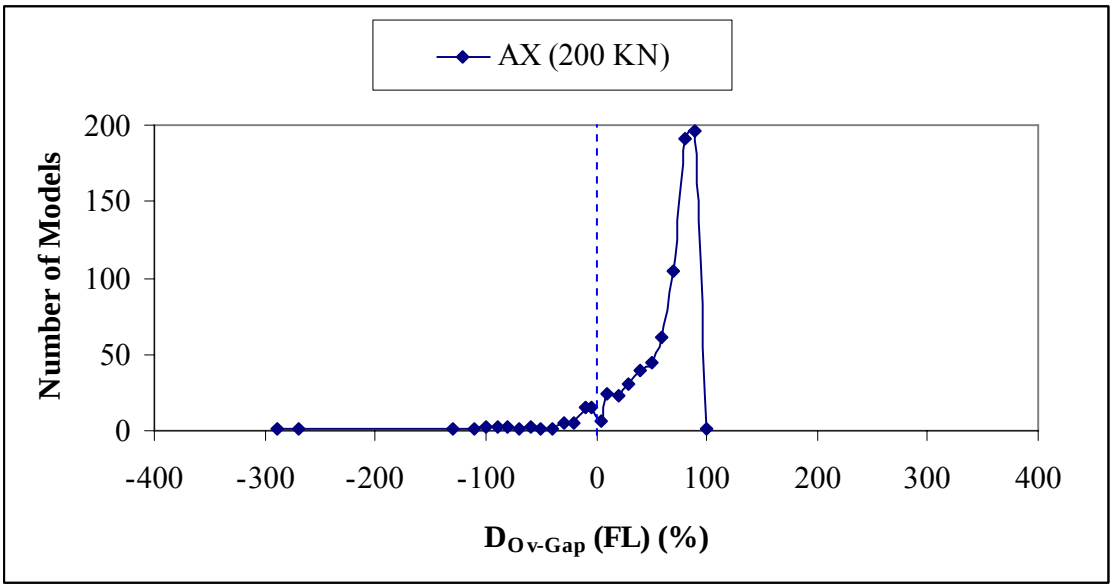


Figure 6.10 Fatigue life comparison between gapped and partially overlapped CHS K-joints with overlapping brace subjected to basic load case AX11 (200 kN)

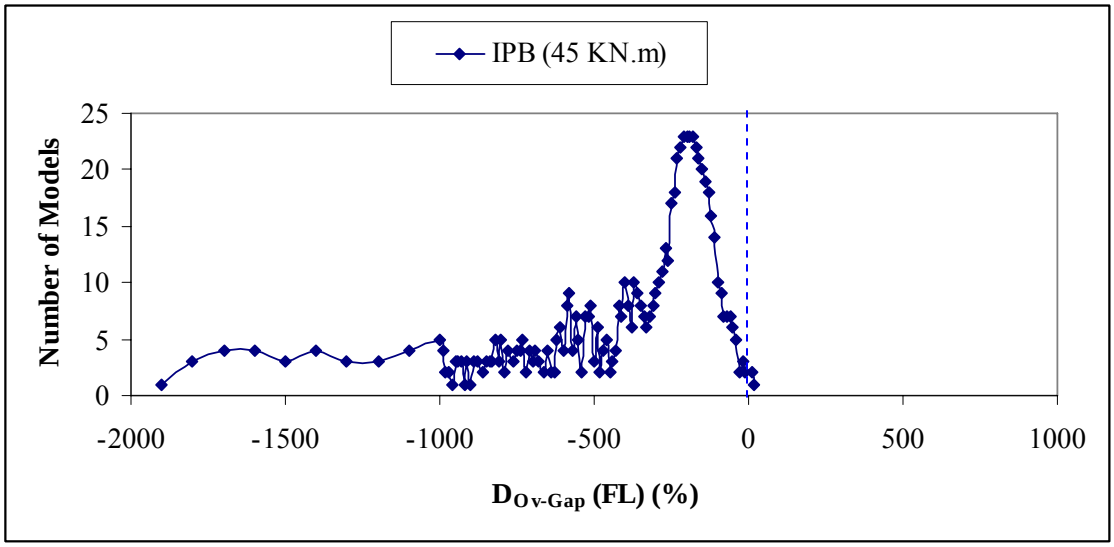


Figure 6.11 Fatigue life comparison between gapped and partially overlapped CHS K-joints with overlapping brace subjected to basic load case IPB11 (45 kN.m)

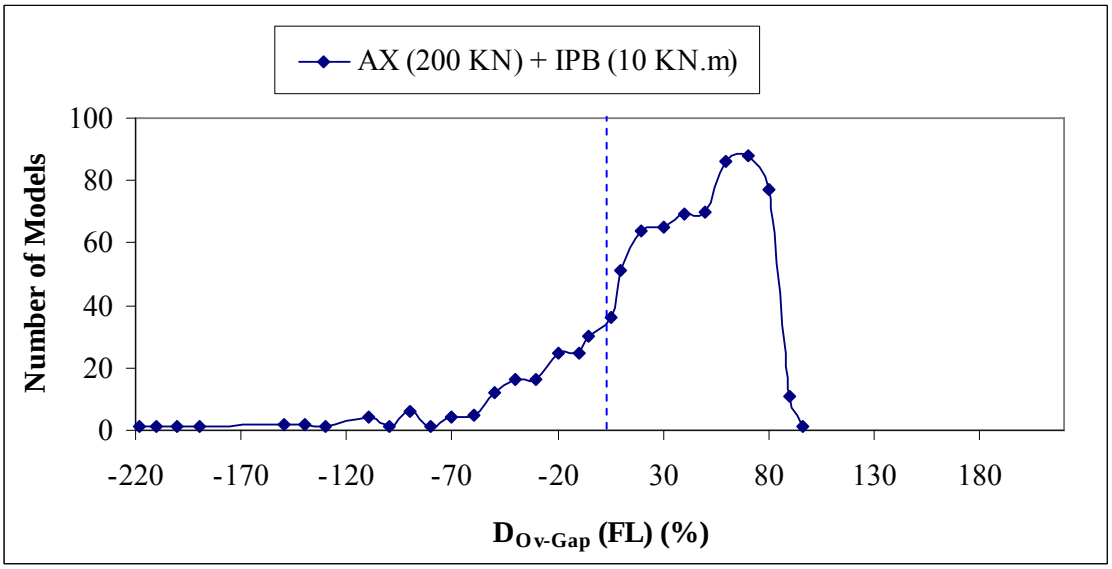


Figure 6.12 Fatigue life comparison between gapped and partially overlapped CHS K-joints with overlapping brace subjected to combined load case AX11 (200 kN) + IPB11 (10 kN.m)

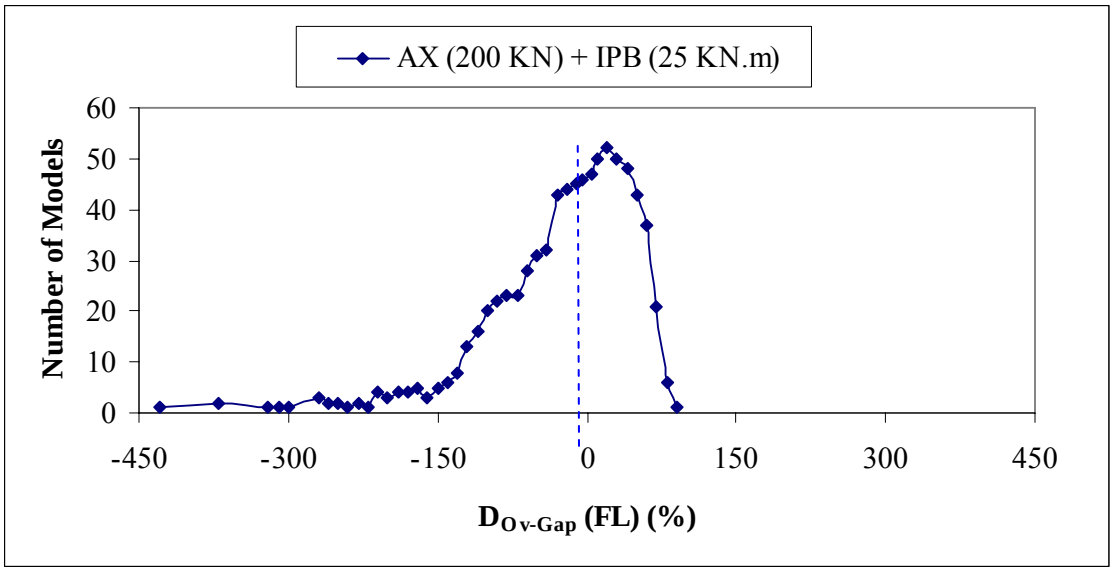


Figure 6.13 Fatigue life comparison between gapped and partially overlapped CHS K-joints with overlapping brace subjected to combined load case AX11 (200 kN) + IPB11 (25 kN.m)

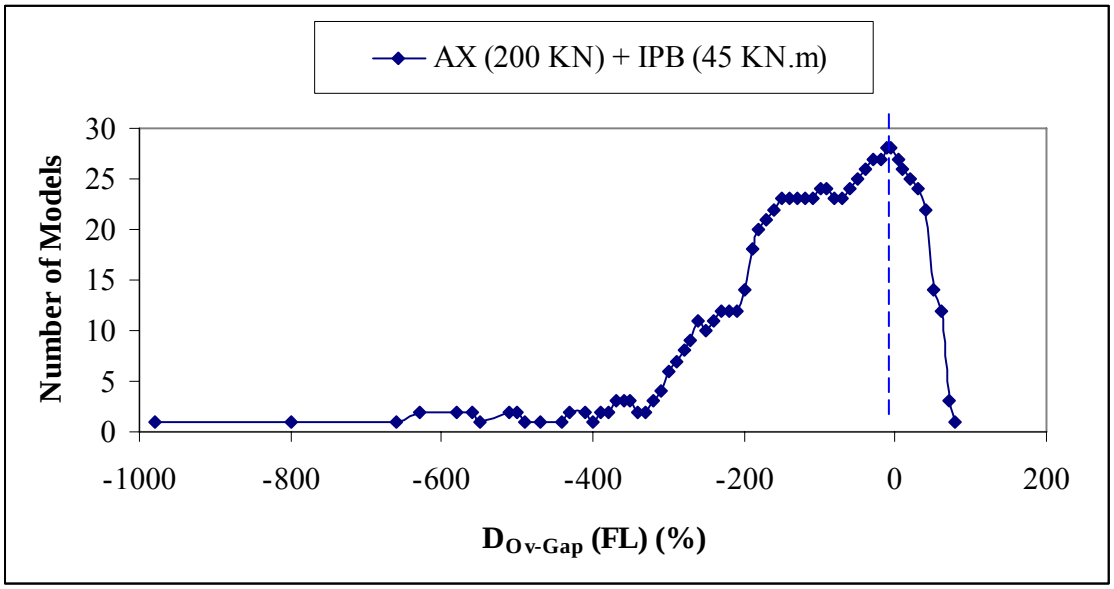


Figure 6.14 Fatigue life comparison between gapped and partially overlapped CHS K-joints with overlapping brace subjected to combined load case AX11 (200 kN) + IPB11 (45 kN.m)

# *CHAPTER 7*
# *CONCLUSIONS AND RECOMMENDATIONS*

## 7.1 CONCLUSIONS

*Experimental Investigation*

In the experimental investigation, a carefully planned experimental study was carried out to investigate the SCF and the HSS distributions along the joint intersection of three full-scale partially overlapped CHS K-joints. The experimental results shown that depending on the geometrical parameters of the partially overlapped K-joints, the maximum SCF could locate on either the brace side or the chord side of the joint.

In addition, the experimental results shown that the Efthymiou formulae [29] were conservative only when the partially overlapped K-joints were subjected to IPB loading, but not for the case of AX loading. Having compared the tests results with the FE modeling based on the mesh generator developed by Nguyen [65], it was found that the mesh generator is reliable. Finally, it was observed that the S-N curves [5] were mainly found to be on the conservative side of the test results.

*Parametric Study*

A parametric study was carried out to investigate the SCF of partially overlapped CHS K-joints. From the parametric study, it was observed that under AX load case the maximum SCF occurred at saddle of chord and braces, while under IPB load case the maximum SCF occurred at crown heel of chord, and at saddle near crown heel of braces. In addition, it was seen that the SCF values increased generally as $\gamma$, $\tau$ and $\theta$ increased, but as Ov or $\beta$ increased the SCF values decreased. Overall, all these parameters had a big impact on SCFs for the partially overlapped CHS K-joints. A

series of parametric equations were proposed for predicting the SCF of partially overlapped CHS K-joints under basic load cases. The equations were developed based on the FE analyses data of 3500 models. The reliability of the proposed SCF parametric equations was verified against the acceptance criteria of Fatigue Guidance Review Panel [83]. The assessment of current proposed parametric equations for partially overlapped CHS K-joints with respect to the basic SCF database of FE models seems to satisfy the criteria of Fatigue Guidance Review Panel. The assessment results seem to confirm the reliability of these equations is reasonable but improvement is certainly needed in order to come up with better SCF/HSS estimation for optional fatigue design.

*Interpolation Method*

The SCF database has been built up based on the 3500 numerical models of partially overlapped CHS K-joints subjected to six basic load cases, namely AX11, IPB11 and IPB12 on the through brace, and AX21, IPB21 and IPB22 on the overlapping brace. The interpolation method has been implemented by developing two new methods, namely the PIM and the LIM, for estimating the SCF and HSS values of any partially overlapped CHS K-joint. For these two methods, there are two types of SCF database stored: the first one for the PIM, and the other one for the LIM. The database for the PIM are stored mainly one maximum SCF value in the table format, while the database for the LIM stores a set of SCF values along the weld toe in a specially design “Tree structure” format. The assessment of these PIM and LIM for partially overlapped CHS K-joints with respect to the additional 192 mid-point FE models shown that these two methods can be used to produce much more reliable and accurate SCF and HSS values than the regression equations.

*Comparison between gapped and partially overlapped CHS K-joints*

A comparison between gapped and partially overlapped CHS K-joints has been done in terms of SCFs, HSSs and fatigue life prediction. The SCF and HSS values for gapped

CHS K-joints based on DEn parametric SCF equations [12] are compared with the SCF and the HSS values for partially overlapped CHS K-joints obtained from the PIM and the LIM. Fatigue life predictions are based on S-N curves [5].

The CHS K-joints have been specially selected in such a way that on the one hand, if gapped CHS K-joints were made from the sections, they would produce high eccentricity, but still in the range of validity [5], and on the other hand, if the overlapped CHS K-joints are made from the sections, the eccentricity can be reduced to zero. 762 gapped and partially overlapped CHS K- joints were subjected to AX, IPB and combined loads of AX and IPB. The gapped CHS K-joints were made with minimum gap distance.

It was observed from the comparison results that the partially overlapped CHS K-joints were mainly in favor on working under the AX load case, especially where the joints having braces with $\gamma$ of 12 and lower. It was also observed that the partially overlapped CHS K-joints subjected to combined load case of the AX with the small IPB, notably less than 25 kN.m, gained more benefits than their counterparts. The gapped CHS K-joints were in favor on working under the IPB load case. However, it should be noted that some researchers [10, 24 and 92] suggested that in the design of trusses it is usually in practice to assume that the members are pin-ended, meaning that bending moment can be ignored. Wardenier [24] and the IIW [10] recommended that bending moment can be neglected as far as the joint design is concerned provided the eccentricity associated with them falls within the certain limits stipulated in CIDECT guide [5]. Packer et al. [92] suggested that these moments can also generally be ignored with respect to design of both members and joints. In this regard, the partially overlapped K-joints could be regarded as a favorite choice when compared to gapped CHS K-joints in terms of fatigue performance.

## 7.2 RECOMMENDATIONS FOR FURTHER RESEARCH WORKS

In order to obtain more complete understanding for the more efficient design of partially overlapped CHS K-joint, the following areas are recommended for future research works.

1. Further fatigue tests on partially overlapped CHS K-joints with other geometries and other loading cases, namely combined load case of AX and OPB are highly recommended.

2. Attentions should be focused on the OPB load case in future parametric study. The OPB load case could also be happened in practice with partially overlapped CHS K-joints, especially in offshore structures.

3. In the parametric study, the cases of different values of the intersecting angles $\theta_1$ and $\theta_2$ should be considered. As in practice, it is possible that the intersecting angles $\theta_1$ and $\theta_2$ are different due to some unexpected limitations in the selection of CHS sizes.

4. Further parametric study on partially overlapped CHS K-joints with other geometries, such as considering the through brace and the overlapping brace having different diameters, is recommended.

5. Extend the current PIM, LIM and their implementation to include more joint types and loading conditions.

# *REFERENCES*

[1] Chang, E. and Dover, W. D. (1999), "Parametric Equations to Predict Stress Distribution along the Intersection of Tubular X and DT-Joints", International Journal of Fatigue, Vol. 21, No. 6, pp. 619-635.

[2] Underwater Engineering Group (1985), Design Guidance on Tubular Joints in Steel Offshore Structures, Report UR33, April, UK.

[3] BOMEL (1992), "Joint industry funded program: analytical and experimental investigation of the behaviour of tubular frames", Final Report, Maidenhead, UK.

[4] Tizani, W.M.K., Yusurf, K.O., Davies, G. and Smith, N.J. (1996), "A knowledge based system to support joint fabrication decision making at the design stage – case study for CHS trusses", Proceeding of the 7th International Symposium on Tubular Structures, Hungary, pp. 483-489.

[5] Zhao, X. L., Herion, S., Packer, J. A., Puthli, R., Sedlacek, G., Wardenier, J., Weynand, K., Wingerde, A. van and Yeomans, N., (2001), Design Guide for Circular and Rectangular Hollow Section Joints Under Fatigue Loading, CIDECT, IIW Doc. TÜV-Verlag Germany.

[6] Department of Energy, DEn (1984), Background to New Fatigue Design Guidance for Steel Welded Joints in Offshore Structures, Report of the Department of Energy Guidance Notes Revision Drafting Panel, Her Majesty's Stationery Office.

[7] Irvine, N. M. (1981), "Review of Stress Analysis Techniques Used in UKOSRP", Proceedings of Conference on Fatigue in Offshore Structural Steels, Institute of Civil Engineers, UK.

[8] American Welding Society, AWS (2000), Structural Welding Code – Steel, ANSI/AWS D1.1-2000, Miami, USA.

[9] van Wingerde, A. M., Packer, J. A. and Wardenier, J. (1996), "New Guidelines for Fatigue Design of HSS Connections", Journal of Structural Engineering, ASCE, USA, Vol. 122, No. 2, pp. 125-132.

[10] International Institute of Welding, IIW (1999), Recommended Fatigue Design Procedure for Welded Hollow Section Joints, IIW Doc. XV-1035-99, XV-E-99-251, XIII-1804-99, Lisbon, Portugal, July, 1999.

[11] Romeijn, A., Puthli, R. S., de Koning, C. H. M. and Wardenier, J. (1992), "Stress and Strain Concentration Factors of Multiplanar Joints Made of Circular Hollow Sections", Proceedings of the 2nd International Offshore and Polar Engineering Conference, San Francisco, USA, ISOPE, pp. 384-393.

[12] Smedley, P. and Fisher, P. (1991), "Stress Concentration Factors for Simple Tubular Joints", Proceedings of the 1st International Offshore and Polar Engineering Conference, Edinburgh, UK, ISOPE, pp. 475-483.

[13] Romeijn, A. and Wardenier J. (1994), "Stress and Strain Concentration Factor of Welded Tubular Joints Caused by Chord Loading", Tubular Structures VI, Grundy, Holgate & Wong (eds), Balkema, Rotterdam, pp. 643-650.

[14] van Wingerde, A. M.(1992), "The fatigue behaviour of T- and X-joints made of square hollow sections". Heron, 37(2), pp. 1-180.

[15] Verheul, A. & Wardenier, J. (1989), "The low cycle fatigue behaviour of axially loaded T-joints between rectangular hollow sections," CIDECT report 7H-89/1-E, Stevin report 25.6.89.22/A1, TNO-IBBC report BI-99-60/63.5.3820, Delft, the Netherlands.

[16] Romeyn, A., Puthli, R. S., de Koning, C. H. M. & Wardenier, J. (1992), "Stress and strain concentration factors of multiplanar joints made of circular hollow sections", Proceedings. International Offshore and Polar Engineering Conference (ISOPE '92), San Francisco, USA, pp. 384-393.

[17] Puthli, R. S., de Koning, C. H. M., Wardenier, J. & Dutta, D.(1986), "A study on strain concentration factors of square hollow section X-joints with brace in tension", Stevin report 6-86-7, TNO-IBBC report BI-86-63/63.5.3820, Delft, The Netherlands.

[18] van Wingerde, A. M., Puthli, R. S., de Koning, C. H. M., Verheul,A., Wardenier, J.& Dutta, D. (1989), "Fatigue strength of welded unstiffened R. H. S. joints in latticed structures and Vierendeel girders. Final Report, Part l: X-

and T-joints", Stevin report 25.6-89-23/A1, TNO-IBBC report BI-89-064/63.5.3820,Delft, The Netherlands.

[19] Puthli, R. S., de Koning, C. H. M., van Wingerde, A. M., Wardenier, J. & Dutta, D. (1989), "Fatigue strength of welded unstiffened R. H. S. joints in latticed structures and Vierendeel girders," Final Report, Part 4: Design Recommendations", Stevin report 25.6-89-37/A1, TNO-IBBC report BI-89-102/63.5.3820, Delft, The Netherlands.

[20] van Wingerde, A. M., Packer, J. A., Wardenier, J., Dutta, D. & Marshall, P.W., (1993), "Proposed revisions for fatigue design of planar welded connections made of hollow structural sections", Proceeding 5th International Symposium on Tubular Structures, Nottingham, UK, pp. 663-72.

[21] Clayton, A. M. and Irvine, N. M. (1978), "Stress Analysis Methods for Tubular Connections", Paper 30, European Offshore Research Seminar, Cambridge, UK.

[22] Gurney T. R. (1979), Fatigue of Welded Structures, 2nd Ed., Cambridge University Press, Cambridge, UK.

[23] Swensson, K., Holdley, P., Yura, J. and Sanders, D. (1986), "Stress Concentration Factors in Double-Tee Joints", Phil M. Ferguson Structural Engineering Laboratory Report 86-1.

[24] Wardenier, J. (1982), Hollow Section Joints, Delft University Press, Delft, The Netherlands.

[25] van Wingerde, A. M., Packer, J. A. and Wardenier, J. (1995), "Criteria for the Fatigue Assessment of Hollow Structural Section Connections", Journal of Constructional Steel Research, Elsevier, pp. 71-115.

[26] Department of Energy (DEn), (1990), Offshore Installations: Guidance on Design and Construction, Department of Energy, London, UK.

[27] EC3, (1992), "Design of steel structures – Part 1.1: General Rules and Rules for Building," ENV 1993-1-1, Eurocode 3, European Committee for Standardisation (CEN).

[28] Almar, N. A. (1985), Fatigue Handbook – Offshore Steel Structures, Published by Tapir, Norge.

[29] Efthymiou, M., and Durkin, S. (1985), "Stress Concentrations in T/Y and Gap/Overlap K-joints", Behavior of Offshore Structures, Elsevier, Amsterdam, Netherlands, pp. 429-440.

[30] Gibstein, M. B. (1987), "Stress Concentration in Tubular K-joints with Diameter Ratio Equal to One", Steel in Marine Structures, Elsevier, Amsterdam, Netherlands, pp. 377-393.

[31] Lalani, M. and Forsyth, P. (1987), "The Fatigue Behavior of Overlapping Joints", Steel in Marine Structures, Elsevier, Amsterdam, Netherlands, pp. 431-443.

[32] Moe, Einar. T. (1987), "Stress Analysis and Fatigue Tests on Overlapped K-joints", Steel in Marine Structures, Elsevier, Amsterdam, Netherlands, pp. 395-404.

[33] American Petroleum Institute, API RP2A-LRFD (1993), Recommended Practice for Planning, Designing and Constructing Fixed Offshore Structures, 1st edition, Washington D.C., USA.

[34] Pang, H.L.J., Lee, C. W., (1995), "Three-dimensional Finite Element Analysis of a Tubular T-joint under Combined Axial and Bending Loading," International Journal of fatigue, Vol. 17, No. 5, pp, 313-320.

[35] Gulati, K. C., Wang, W. J. and Kan, D. K. Y. (1982), "An Analytical Study of Stress Concentration Effects in Multibrace Joints under Combined Loading", Proceedings of the 14th Annual Offshore Technology Conference, OTC 4407, Houston, TX, pp. 337-355.

[36] Hellier, A. K., Connoly, M. P. and Dover, W. D. (1990), "Stress Concentration Factors for Tubular Y- and T-Joints", International Journal of Fatigue, Vol. 12, No. 1, pp. 13-23.

[37] Yeoh, S. K., Soh, A. K. and Soh, C. K. (1995), "Behavior of Tubular T-Joints Subjected to Combined Loadings", Journal of Constructional Steel Research, Vol. 57, No 3, pp. 259-280.

[38] Soh, A. K. and Soh, C. K. (1996), "Stress Concentrations of K Tubular Joints Subjected to Basic and Combined Loadings", Proceedings of Institution, Civil

Engineers Structures & Buildings, No. 11.

[39] Owen, D.R.J. and Fawkes, A.J., (1983), Engineering Fracture Mechanics, Pinerige Press Limited, Swansea, UK.

[40] Monahan, C.C., (1994), "Early Fatigue Crack Growth in Offshore Structure," Ph.D. Thesis, UCL.

[41] Gandhi, P. and Stig Berge (1998), "Fatigue Behaviour of T-Joints: Square Chords and Circular Braces", Journal of Structural Engineering, Vol. 124, No. 4, pp. 399 – 404.

[42] Department of Energy (DEn), (1993), "Background to New Fatigue Design Guidance for steel Joints in Offshore Structures," Internal Report, Department of Energy, London, UK.

[43] Thorpe, T.W. and Sharp, J.V., (1989), "The fatigue performance of tubular joints in air and sea water," MaTSU Report, Harwell Laboratory, Oxfordshire, UK.

[44] Dimitrakis, S. D., Lawrence, F. V. and Mohr, W. C. (1995), "S-N Curves for Welded Tubular Joints", Proceedings of 1995 OMAE, Vol. 3, Materials Engineering, ASME.

[45] van Windgerde, A.M., Packer, J.A., Wardenier, J. and Dutta, D., (1997), "Simplified design graphs for the fatigue design of multiplanar K-joints with gap," CIDECT Report 7R-01/97, University of Toronto, Canada.

[46] van Windgerde, A.M., Packer, J.A., Wardenier, J., (1997), "IIW fatigue rules for tubular joints", IIW International Conference on Performance of Dynamically Loaded Welded Structures, San Francisco, USA, pp 98-107.

[47] van Delft, D. R. V., Noordhoek, C. and de Back, J. (1987), "Evaluation of the European Fatigue Test Data on Large-sized Welded Tubular Joints for Offshore Structures", Offshore Technology Conference, Houston, USA, paper OTC 4999.

[48] Marshall, P.W. (1984), Connections for welded tubular structures, IIW International Conference on Welding of Tubular Structures, Boston, USA, pp. 1-54.

[49] Marshall, P. W. (1992), Design of Welded Tubular Connections – Basic and Use of AWS Code Provisions, Elseviers Science Publishers, Madison Square, New

York, USA.

[50] van Delft, D.R.V., Nookdhoek, C. and de Back, J. (1985), Evalution of European fatigue test data on large-sized welded tubular joints for offshore structures, Offshore Technology Conference, Houston, USA, paper OTC 4999.

[51] Berge, S. and Webster, S.E. (1987), "The size effect on the fatigue behaviour of welded joints," Proceeding, Steel in Marine Structures (SIMS'87), pp. 179-203.

[52] Haagensen, P.J., (1989), "Improvement techniques," Proceedings, International Symposium on the Occasion of the Retirement of Prof. J de Back, Delft, The Netherlands, pp. 77-95.

[53] Shao Y. B., (2005), "Fatigue Behaviour of Uniplanar CHS Gap K-Joints under Axial and In-plane Bending Loads," Ph.D.Thesis, Nanyang Technology University, Singapore.

[54] Chong Rhee, H., Han, S., and Gipson, G. S., (1991), "Reliability of Solution Method and Empirical Formulas of Stress Intensity Factors for Weld Toe Cracks of Tubular Joints," Proceeding of the 10th Offshore Mechanics and Arctic Engineering Conference, ASME, Vol.3, No. B, pp. 441-452.

[55] Huang, Z. W., (2002), "Stress intensity factor of cracked steel tubular T and Y-joints under complex loads", Ph.D. Thesis, Nanyang Technological University, Singapore.

[56] Bouwkamp, J.G. (1961), "Research on Tubular Connections in Structural Work", Welding Research Council Bulletin, USA.

[57] Bouwkamp, J.G. (1964), "Concept of Tubular-Joint Design, Proceedings ASCE", Journal of Structural Division, Vol. 90, ST2, pp. 77-101.

[58] Healy, B. E. and Buitrago, J. (1994), "Extrapolation Procedures for Determining SCFs in Mid-Surface Tubular Joint Models", Proceedings of 6th International Symposium on Tubular Structures, Melbourne, Australia, pp. 651-659.

[59] Dexter, E. M. and Lee, M. M. K. (1999a), "Static Strength of Axially Loaded Tubular K-joints I: Behavior", Journal of Structural Engineering, ASCE, Vol. 125, No. 2, pp. 194-201.

[60] Dexter, E. M. and Lee, M. M. K. (1999b), "Static Strength of Axially Loaded Tubular K-joints II: Ultimate Capacity", Journal of Structural Engineering, ASCE, Vol. 125, No. 2, pp. 202-210.

[61] Dexter, E.M., Lee, M.M.K. and Kirkwood, M.G., (1996), "POCHS K-joints in circular hollow sections under axial loading (an investigation of the factors affecting the static strength using numerical modelling)", Journal of Offshore Mechanics and Artic Engineering, Vol. 118, No. 1, pp.53-61.

[62] Fessler, H., Little, W.J.G. and Shellard, I.J. (1979), "Elastic Stress Due to Axial Loading of Tubular Joints with Overlap", BOSS'79, USA.

[63] Dharmavasan, S. and Seneviratne, L.D., (1986), "Stress analysis of POCHS K-joints", Fatigue and Crack Growth in Offshore Structures, IMechE 1986-2, pp. 17-30.

[64] Lee, C.K., Lie, S.T., Chiew, S.P., Sopha, T. and Nguyen, T.B.N. (2006), "An experimental study on the fatigue behaviour of partially overlapped CHS K-joints", Proceeding of the 8th International conference on steel space composite structures, Kuala Lumpur, pp. 273-279, Malaysia.

[65] Nguyen T. B. N., (2008), "Model and Mesh Generation of Partially Overlapped Circular Hollow Section K-Joints for Fatigue Studies," Ph.D. Thesis, Nanyang Technology University, Singapore.

[66] Lee, C.K., Lie, S.T., Chiew, S.P., Sopha, T. and Nguyen, T.B.N. (2007), "Experimental Studies on Fatigue Behaviour of Partially Overlapped CHS K-joints", International Maritime-Port Technology and Development Conference, Singapore, pp. 280-285.

[67] Lee, C.K., Lie, S.T., Chiew, S.P., Sopha, T. and Nguyen, T.B.N. (2007), "Experimental Studies on Stress Distributions for Partially Overlapped CHS K-joints", The 9th International Conference on Steel, Space and Composite Structures, China, pp. 262-272.

[68] Lee, C.K., Lie, S.T., Chiew, S.P., Sopha, T. and Nguyen, T.B.N., (2007), "On Stress Concentration Factors for Partially Overlapped CHS K-joints by

Experimental Studies", The 5th International Conference on Advance in Steel Structures, Singapore, pp. 563-574.

[69] Sopha, T., Nguyen, T.B.N., Chiew, S.P., Lee, C.K. and Lie, S.T., (2008), "Stress Analysis and Fatigue Test of Partially Overlapped CHS K joints", International Journal of Advanced Steel Construction, Vol. 4, No. 2, pp.134- 146.

[70] ABAQUS (2006), User Manual (Ver. 6.5), Hibbit, Karlsson and Sorensen Inc., USA.

[71] Chiew, S. P., Lie, S.T., Lee, C.K., and Huang, Z.W., (2004), "Fatigue Performance of Cracked Tubular T-Joint under Combined Loads-Part I-Experimental," Journal of Structural Engineering, American Society of Civil Engineers, ASCE, Vol. 130, No. 4, pp. 562-571.

[72] Lee, C.K., Lie, S.T., Chiew, S.P. and Shao, Y.B., (2005), "Numerical models verification of cracked tubular T, Y and K- Joints under combined loads", Engineering Fracture Mechanics, United States, Vol. 72, No. 7, pp. 983 – 1009.

[73] Lie, S.T., Lee, C.K., Chiew, S.P., Shao Yongbo, 2005, "Validation of surface crack stress intensity factors of a tubular K-joint", International Journal of Pressure Vessels and Piping ,(United Kingdom), Vol. 82, No. 8, pp. 610 - 617.

[74] Lie, S.T., Lee, C.K., Chiew, S.P., Shao Yongbo, (2005), "Mesh modelling of cracked uni-planar tubular K-joints", Journal of Constructional Steel Research, United Kingdom, Vol. 61, No. 2, pp. 235 - 264.

[75] Dover, W. D., Dharmavasan, S., Brennan, F. P., and Marsh, K.J., (1995), Fatigue Crack Growth in Offshore Structures, Engineering Materials Advisory Services (EMAS) Ltd., Chameleon Press, London, UK.

[76] Technical Software Consultant Ltd. (TSC), (1991), ACFM Crack Microgauge – Model U10, Milton Keynes, UK.

[77] Technical Software Consultant Ltd. (TSC), (1998), FLAIR User's Manual – Software Version 1.9, Milton Keynes, UK.

[78] Lee, C.K. (1999), "Automatic adaptive mesh generation using metric advancing front approach", Engineering Computations, Vol. 16, No. 2, pp. 230-263.

[79] Xu, Q.X. (2006), "Analysis of thin-walled structural joints using 3D solid

element," PhD Thesis, CEE, NTU, Singapore.

[80] Wardenier, J. (1982), Hollow Sections in Structural Applications, Delft University Press, Delft, The Netherlands.

[81] DataFit (2002), Version 8.0, Oakdale Engineering, USA.

[82] Sabih A. L, (1993), "The Fatigue, Fracture and Ultimate Behaviour of Fillet Welded RHS K-Joints with gap," Ph.D. Thesis, Manchester, UK.

[83] Fatigue Guidance Review Panel, MATSU (1996), Fatigue Background Guidance Document, An Offshore Technology Report. By HSE Books as an Offshore Technology Report.

[84] Zienkiewicz, O. C., Taylor, R. L. and Zhu, J. Z, (2005), "The Finite Element Method: Its Basis and Fundamentals," Sixth Edition, Elsevier Butterworth-Heinemann, UK.

[85] Kuang, J. G., Potvin, A. B., Leick, R. D. and Kahlich, J. L. (1977), "Stress Concentration in Tubular Joints", Society of Petroleum Engineering, USA, August, pp.287-99.

[86] Wordsworth A.C, Smedley G.P. (1978), "Stress concentrations at unstiffened tubular joints," European Offshore Steels Research Seminar, Proceedings, Paper 31, Cambridge, U.K., November, 1978.

[87] Wordsworth A.C. (1981), "Stress concentration factors at K and KT tubular joints", Fatigue of Offshore Structural Steels, Conference Proceedings, February, pp. 59-69.

[88] International Institute of Welding, IIW (1995), Stress Determination for Fatigue Analysis of Welded Components, Edited by Erkki Niemi, Abingtion Publishing.

[89] Liaw C.Y, Litton R.W, Reimer R.B. (1976), "Improved finite element for analysis of welded tubular joints," Offshore Technology Conference, OTC 2642, Houston, Texas, pp. 267–282.

[90] Efthymiou M. (1988), "Development of SCF formulae and generalized functions for use in fatigue analysis," OTJ 88, Surrey, U.K., 1988.

[91] Karamanos S.A, Romeijn A., Wardenier J. (1998), "Stress concentrations in tubular gap K-joints: mechanics and fatigue design," Engineering Structures, Department of Civil Engineering, Delft University of Technology, 1998.

[92] STELCO inc., (1981), "Hollow structural sections design manual for connections", 2nd ed., Hamilton, Canada.

[93] Packer, J. A., Birkemoe, P. C. and Tucker, W. J., (1984), "Canadian implementation of CIDECT Monograph No 6", CIDECT report No 5AJ-84/9-E, IIW Doc. SC-XV-E-84-072.

# *PUBLICATIONS*

JOURNAL PAPERS

1 **Sopha, T**., Nguyen, T.B.N., Chiew, S.P., Lee, C.K. and Lie, S.T., (2008), "Stress Analysis and Fatigue Test of Partially Overlapped CHS K joints", International Journal of Advanced Steel Construction, Vol. 4, No. 2, pp.134-146.

2 Lee, C.K, Chiew, S.P., Lie, S.T., **Sopha, T**. and Nguyen, T.B.N., (2009), "Experimental Studies on Stress Concentration Factors for Partially Overlapped Circular Hollow Section K-Joints", International Journal of Advanced Steel Construction, Vol. 5, No. 4, pp. 481 - 499.

CONFERENCE PAPERS

1 Lee, C.K., Lie, S.T., Chiew, S.P., **Sopha, T**. and Nguyen, T.B.N. (2006), "An experimental study on the fatigue behaviour of partially overlapped CHS K-joints", Proceeding of the 8th International conference on steel space composite structures, Kuala Lumpur, pp. 273-279, Malaysia.

2 Chiew S.P., Lee C.K., Lie, S.T., Nguyen T. B. N. and **Sopha T**. (2007), "Mesh generation for partially overlapped circular hollow section k-joints under fatigue loadings", The 2nd International Maritime-Port Technology and Development Conference (MTEC 2007) ,26-28 September 2007, Singapore

3 Lee, C.K., Lie, S.T., Chiew, S.P., **Sopha, T**. and Nguyen, T.B.N. (2007), "Experimental Studies on Fatigue Behaviour of Partially Overlapped CHS K-joints", International Maritime-Port Technology and Development Conference, Singapore, pp. 280-285.

4 Lee, C.K., Lie, S.T., Chiew, S.P., **Sopha, T**. and Nguyen, T.B.N. (2007), "Experimental Studies on Stress Distributions for Partially Overlapped CHS K-

joints", The 9th International Conference on Steel, Space and Composite Structures, China, pp. 262-272.

5 Lee, C.K., Lie, S.T., Chiew, S.P., **Sopha, T**. and Nguyen, T.B.N., (2007), "On Stress Concentration Factors for Partially Overlapped CHS K-joints by Experimental Studies", The 5th International Conference on Advance in Steel Structures, Singapore, pp. 563-574.

# *APPENDIX A*
# *API (1993) AND AWS (2000) WELDING SPECIFICATIONS*

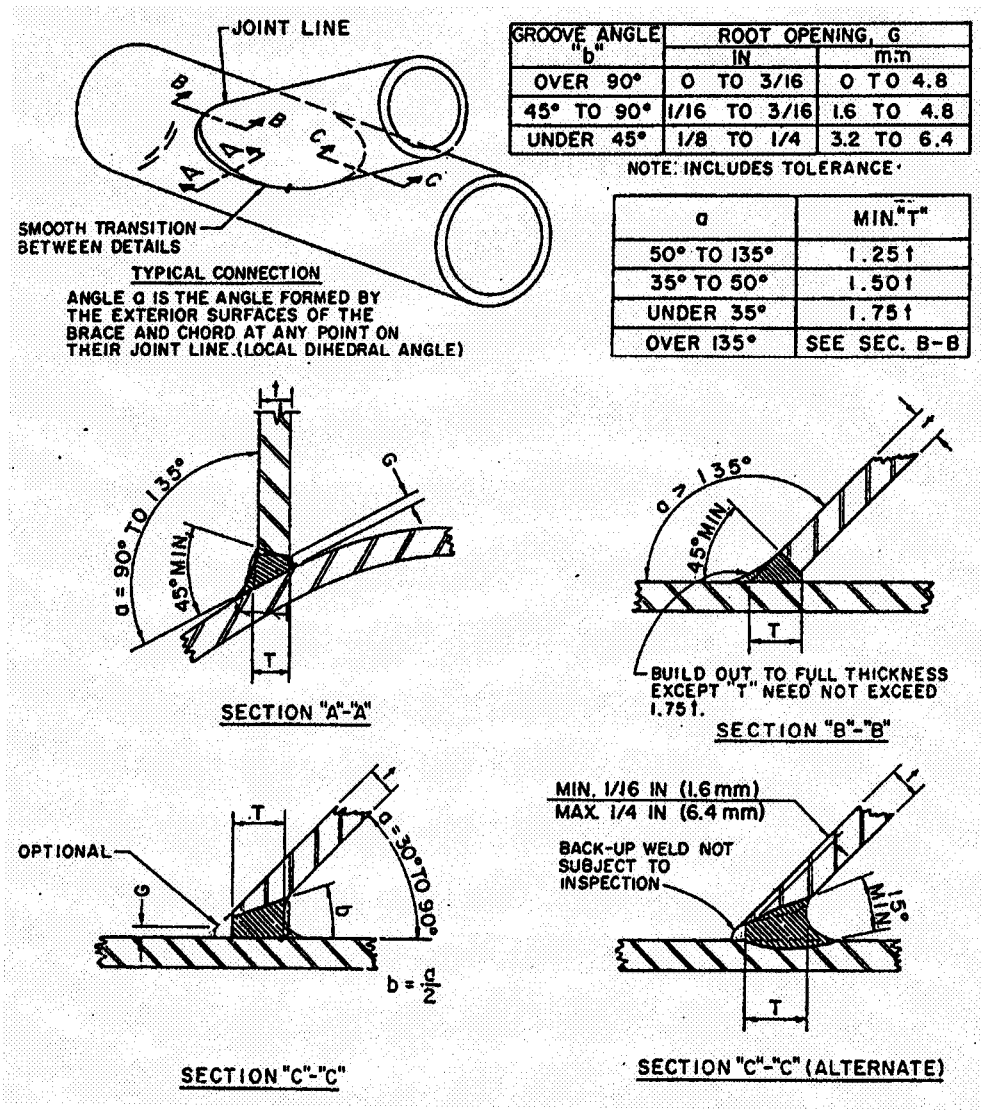


Figure A.1: API welding details for tubular connections [35]

Notes:

1. The dihedral angle is defined as $\alpha$.
2. "T" is the minimum weld thickness.
3. "t" is the thickness of brace.

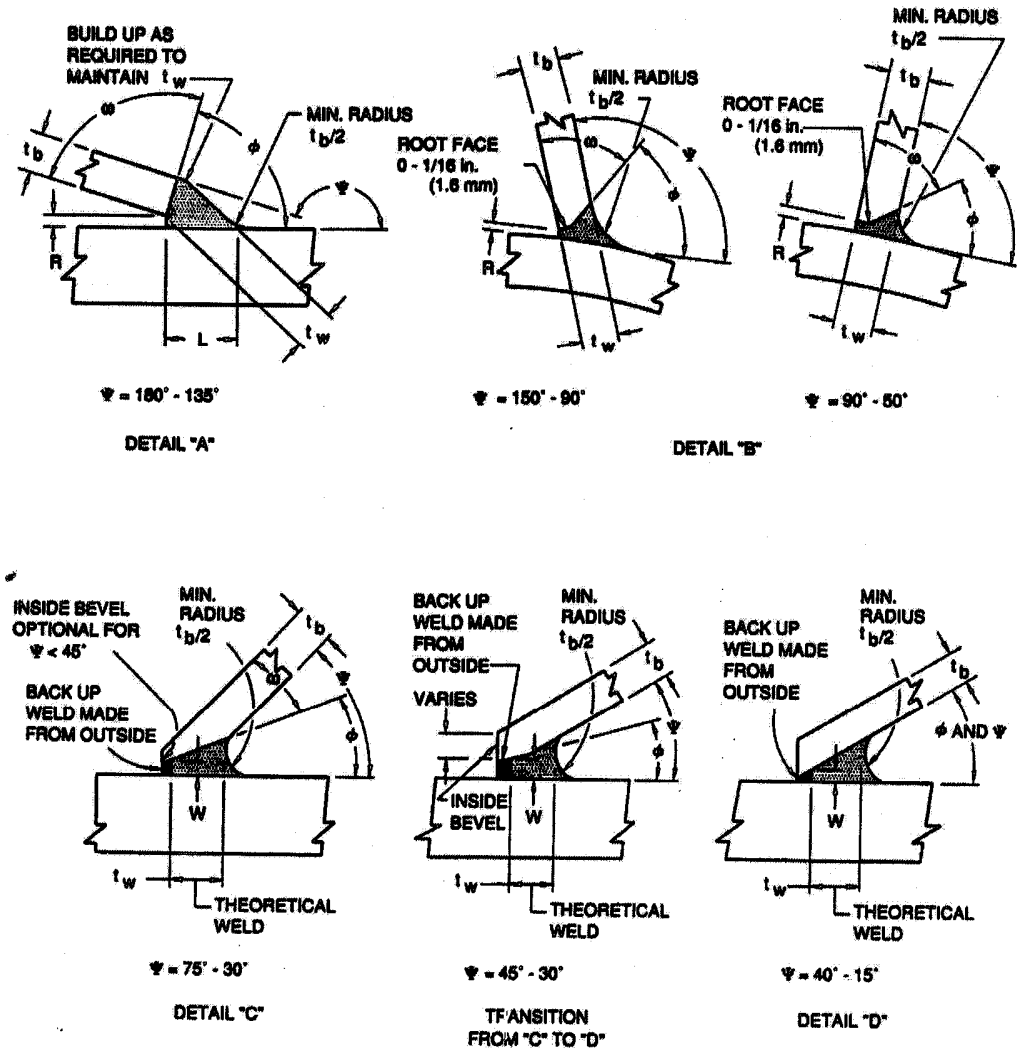


Figure A.2: AWS welding details for complete joint penetration in tubular T-, Y-, K-connections [9]

Notes:

1. The dihedral angle is defined as **Ψ**.
2. "$\mathbf{t}_b$" is the thickness of the brace.
3. ϕ is the joint included angle.
4. ω is end preparation angle.
5. L is the size of fillet.
6. R is the root opening (joint fit-up).
7. W is the backup weld width.

# *APPENDIX B*

## *SHAPE FUNCTIONS OF LAGRANGE LINEAR INTERPOLATION METHOD*

$$N_1 = \frac{\alpha^1 - \alpha_2^1}{\alpha_1^1 - \alpha_2^1} \cdot \frac{\alpha^2 - \alpha_2^2}{\alpha_1^2 - \alpha_2^2} \cdot \frac{\alpha^3 - \alpha_2^3}{\alpha_1^3 - \alpha_2^3} \cdot \frac{\alpha^4 - \alpha_2^4}{\alpha_1^4 - \alpha_2^4} \cdot \frac{\alpha^5 - \alpha_2^5}{\alpha_1^5 - \alpha_2^5}$$

$$N_2 = \frac{\alpha^1 - \alpha_1^1}{\alpha_2^1 - \alpha_1^1} \cdot \frac{\alpha^2 - \alpha_2^2}{\alpha_1^2 - \alpha_2^2} \cdot \frac{\alpha^3 - \alpha_2^3}{\alpha_1^3 - \alpha_2^3} \cdot \frac{\alpha^4 - \alpha_2^4}{\alpha_1^4 - \alpha_2^4} \cdot \frac{\alpha^5 - \alpha_2^5}{\alpha_1^5 - \alpha_2^5}$$

$$N_3 = \frac{\alpha^1 - \alpha_2^1}{\alpha_1^1 - \alpha_2^1} \cdot \frac{\alpha^2 - \alpha_1^2}{\alpha_2^2 - \alpha_1^2} \cdot \frac{\alpha^3 - \alpha_2^3}{\alpha_1^3 - \alpha_2^3} \cdot \frac{\alpha^4 - \alpha_2^4}{\alpha_1^4 - \alpha_2^4} \cdot \frac{\alpha^5 - \alpha_2^5}{\alpha_1^5 - \alpha_2^5}$$

$$N_4 = \frac{\alpha^1 - \alpha_1^1}{\alpha_2^1 - \alpha_1^1} \cdot \frac{\alpha^2 - \alpha_1^2}{\alpha_2^2 - \alpha_1^2} \cdot \frac{\alpha^3 - \alpha_2^3}{\alpha_1^3 - \alpha_2^3} \cdot \frac{\alpha^4 - \alpha_2^4}{\alpha_1^4 - \alpha_2^4} \cdot \frac{\alpha^5 - \alpha_2^5}{\alpha_1^5 - \alpha_2^5}$$

$$N_5 = \frac{\alpha^1 - \alpha_2^1}{\alpha_1^1 - \alpha_2^1} \cdot \frac{\alpha^2 - \alpha_2^2}{\alpha_1^2 - \alpha_2^2} \cdot \frac{\alpha^3 - \alpha_1^3}{\alpha_2^3 - \alpha_1^3} \cdot \frac{\alpha^4 - \alpha_2^4}{\alpha_1^4 - \alpha_2^4} \cdot \frac{\alpha^5 - \alpha_2^5}{\alpha_1^5 - \alpha_2^5}$$

$$N_6 = \frac{\alpha^1 - \alpha_1^1}{\alpha_2^1 - \alpha_1^1} \cdot \frac{\alpha^2 - \alpha_1^2}{\alpha_1^2 - \alpha_2^2} \cdot \frac{\alpha^3 - \alpha_1^3}{\alpha_2^3 - \alpha_1^3} \cdot \frac{\alpha^4 - \alpha_2^4}{\alpha_1^4 - \alpha_2^4} \cdot \frac{\alpha^5 - \alpha_2^5}{\alpha_1^5 - \alpha_2^5}$$

$$N_7 = \frac{\alpha^1 - \alpha_2^1}{\alpha_1^1 - \alpha_2^1} \cdot \frac{\alpha^2 - \alpha_2^2}{\alpha_2^2 - \alpha_1^2} \cdot \frac{\alpha^3 - \alpha_1^3}{\alpha_2^3 - \alpha_1^3} \cdot \frac{\alpha^4 - \alpha_2^4}{\alpha_1^4 - \alpha_2^4} \cdot \frac{\alpha^5 - \alpha_2^5}{\alpha_1^5 - \alpha_2^5}$$

$$N_8 = \frac{\alpha^1 - \alpha_1^1}{\alpha_2^1 - \alpha_1^1} \cdot \frac{\alpha^2 - \alpha_1^2}{\alpha_2^2 - \alpha_1^2} \cdot \frac{\alpha^3 - \alpha_1^3}{\alpha_2^3 - \alpha_1^3} \cdot \frac{\alpha^4 - \alpha_2^4}{\alpha_1^4 - \alpha_2^4} \cdot \frac{\alpha^5 - \alpha_2^5}{\alpha_1^5 - \alpha_2^5}$$

$$N_9 = \frac{\alpha^1 - \alpha_2^1}{\alpha_1^1 - \alpha_2^1} \cdot \frac{\alpha^2 - \alpha_2^2}{\alpha_1^2 - \alpha_2^2} \cdot \frac{\alpha^3 - \alpha_2^3}{\alpha_1^3 - \alpha_2^3} \cdot \frac{\alpha^4 - \alpha_1^4}{\alpha_1^4 - \alpha_1^4} \cdot \frac{\alpha^5 - \alpha_2^5}{\alpha_1^5 - \alpha_2^5}$$

$$N_{10} = \frac{\alpha^1 - \alpha_1^1}{\alpha_2^1 - \alpha_1^1} \cdot \frac{\alpha^2 - \alpha_1^2}{\alpha_1^2 - \alpha_2^2} \cdot \frac{\alpha^3 - \alpha_2^3}{\alpha_1^3 - \alpha_2^3} \cdot \frac{\alpha^4 - \alpha_2^4}{\alpha_2^4 - \alpha_1^4} \cdot \frac{\alpha^5 - \alpha_2^5}{\alpha_1^5 - \alpha_2^5}$$

$$N_{11} = \frac{\alpha^1 - \alpha_2^1}{\alpha_1^1 - \alpha_2^1} \cdot \frac{\alpha^2 - \alpha_1^2}{\alpha_2^2 - \alpha_1^2} \cdot \frac{\alpha^3 - \alpha_2^3}{\alpha_1^3 - \alpha_2^3} \cdot \frac{\alpha^4 - \alpha_1^4}{\alpha_2^4 - \alpha_1^4} \cdot \frac{\alpha^5 - \alpha_2^5}{\alpha_1^5 - \alpha_2^5}$$

$$N_{12} = \frac{\alpha^1 - \alpha_1^1}{\alpha_2^1 - \alpha_1^1} \cdot \frac{\alpha^2 - \alpha_1^2}{\alpha_2^2 - \alpha_1^2} \cdot \frac{\alpha^3 - \alpha_2^3}{\alpha_1^3 - \alpha_2^3} \cdot \frac{\alpha^4 - \alpha_1^4}{\alpha_2^4 - \alpha_1^4} \cdot \frac{\alpha^5 - \alpha_2^5}{\alpha_1^5 - \alpha_2^5}$$

$$N_{13}=\frac{\alpha^1-\alpha_2^1}{\alpha_1^1-\alpha_2^1}\cdot\frac{\alpha^2-\alpha_2^2}{\alpha_1^2-\alpha_2^2}\cdot\frac{\alpha^3-\alpha_1^3}{\alpha_2^3-\alpha_1^3}\cdot\frac{\alpha^4-\alpha_1^4}{\alpha_2^4-\alpha_1^4}\cdot\frac{\alpha^5-\alpha_2^5}{\alpha_1^5-\alpha_2^5}$$

$$N_{14}=\frac{\alpha^1-\alpha_1^1}{\alpha_2^1-\alpha_1^1}\cdot\frac{\alpha^2-\alpha_2^2}{\alpha_1^2-\alpha_2^2}\cdot\frac{\alpha^3-\alpha_1^3}{\alpha_2^3-\alpha_1^3}\cdot\frac{\alpha^4-\alpha_1^4}{\alpha_2^4-\alpha_1^4}\cdot\frac{\alpha^5-\alpha_2^5}{\alpha_1^5-\alpha_2^5}$$

$$N_{15}=\frac{\alpha^1-\alpha_2^1}{\alpha_1^1-\alpha_2^1}\cdot\frac{\alpha^2-\alpha_1^2}{\alpha_2^2-\alpha_1^2}\cdot\frac{\alpha^3-\alpha_1^3}{\alpha_2^3-\alpha_1^3}\cdot\frac{\alpha^4-\alpha_1^4}{\alpha_2^4-\alpha_1^4}\cdot\frac{\alpha^5-\alpha_2^5}{\alpha_1^5-\alpha_2^5}$$

$$N_{16}=\frac{\alpha^1-\alpha_1^1}{\alpha_2^1-\alpha_1^1}\cdot\frac{\alpha^2-\alpha_1^2}{\alpha_2^2-\alpha_1^2}\cdot\frac{\alpha^3-\alpha_1^3}{\alpha_2^3-\alpha_1^3}\cdot\frac{\alpha^4-\alpha_1^4}{\alpha_2^4-\alpha_1^4}\cdot\frac{\alpha^5-\alpha_2^5}{\alpha_1^5-\alpha_2^5}$$

$$N_{17}=\frac{\alpha^1-\alpha_2^1}{\alpha_1^1-\alpha_2^1}\cdot\frac{\alpha^2-\alpha_2^2}{\alpha_1^2-\alpha_2^2}\cdot\frac{\alpha^3-\alpha_1^3}{\alpha_2^3-\alpha_1^3}\cdot\frac{\alpha^4-\alpha_2^4}{\alpha_1^4-\alpha_2^4}\cdot\frac{\alpha^5-\alpha_1^5}{\alpha_2^5-\alpha_1^5}$$

$$N_{18}=\frac{\alpha^1-\alpha_1^1}{\alpha_2^1-\alpha_1^1}\cdot\frac{\alpha^2-\alpha_2^2}{\alpha_1^2-\alpha_2^2}\cdot\frac{\alpha^3-\alpha_2^3}{\alpha_1^3-\alpha_2^3}\cdot\frac{\alpha^4-\alpha_2^4}{\alpha_1^4-\alpha_2^4}\cdot\frac{\alpha^5-\alpha_1^5}{\alpha_2^5-\alpha_1^5}$$

$$N_{19}=\frac{\alpha^1-\alpha_2^1}{\alpha_1^1-\alpha_2^1}\cdot\frac{\alpha^2-\alpha_1^2}{\alpha_2^2-\alpha_1^2}\cdot\frac{\alpha^3-\alpha_2^3}{\alpha_1^3-\alpha_2^3}\cdot\frac{\alpha^4-\alpha_2^4}{\alpha_1^4-\alpha_2^4}\cdot\frac{\alpha^5-\alpha_1^5}{\alpha_2^5-\alpha_1^5}$$

$$N_{20}=\frac{\alpha^1-\alpha_1^1}{\alpha_2^1-\alpha_1^1}\cdot\frac{\alpha^2-\alpha_1^2}{\alpha_2^2-\alpha_1^2}\cdot\frac{\alpha^3-\alpha_2^3}{\alpha_1^3-\alpha_2^3}\cdot\frac{\alpha^4-\alpha_2^4}{\alpha_1^4-\alpha_2^4}\cdot\frac{\alpha^5-\alpha_1^5}{\alpha_2^5-\alpha_1^5}$$

$$N_{21}=\frac{\alpha^1-\alpha_2^1}{\alpha_1^1-\alpha_2^1}\cdot\frac{\alpha^2-\alpha_2^2}{\alpha_1^2-\alpha_2^2}\cdot\frac{\alpha^3-\alpha_1^3}{\alpha_2^3-\alpha_1^3}\cdot\frac{\alpha^4-\alpha_2^4}{\alpha_1^4-\alpha_2^4}\cdot\frac{\alpha^5-\alpha_1^5}{\alpha_2^5-\alpha_1^5}$$

$$N_{22}=\frac{\alpha^1-\alpha_1^1}{\alpha_2^1-\alpha_1^1}\cdot\frac{\alpha^2-\alpha_2^2}{\alpha_1^2-\alpha_2^2}\cdot\frac{\alpha^3-\alpha_1^3}{\alpha_2^3-\alpha_1^3}\cdot\frac{\alpha^4-\alpha_2^4}{\alpha_1^4-\alpha_2^4}\cdot\frac{\alpha^5-\alpha_1^5}{\alpha_2^5-\alpha_1^5}$$

$$N_{23}=\frac{\alpha^1-\alpha_2^1}{\alpha_1^1-\alpha_2^1}\cdot\frac{\alpha^2-\alpha_1^2}{\alpha_2^2-\alpha_1^2}\cdot\frac{\alpha^3-\alpha_1^3}{\alpha_2^3-\alpha_1^3}\cdot\frac{\alpha^4-\alpha_2^4}{\alpha_1^4-\alpha_2^4}\cdot\frac{\alpha^5-\alpha_1^5}{\alpha_2^5-\alpha_1^5}$$

$$N_{24}=\frac{\alpha^1-\alpha_1^1}{\alpha_2^1-\alpha_1^1}\cdot\frac{\alpha^2-\alpha_1^2}{\alpha_2^2-\alpha_1^2}\cdot\frac{\alpha^3-\alpha_1^3}{\alpha_2^3-\alpha_1^3}\cdot\frac{\alpha^4-\alpha_2^4}{\alpha_1^4-\alpha_2^4}\cdot\frac{\alpha^5-\alpha_1^5}{\alpha_2^5-\alpha_1^5}$$

$$N_{25}=\frac{\alpha^1-\alpha_2^1}{\alpha_1^1-\alpha_2^1}\cdot\frac{\alpha^2-\alpha_2^2}{\alpha_1^2-\alpha_2^2}\cdot\frac{\alpha^3-\alpha_2^3}{\alpha_1^3-\alpha_2^3}\cdot\frac{\alpha^4-\alpha_1^4}{\alpha_2^4-\alpha_1^4}\cdot\frac{\alpha^5-\alpha_1^5}{\alpha_2^5-\alpha_1^5}$$

$$N_{26}=\frac{\alpha^1-\alpha_1^1}{\alpha_2^1-\alpha_1^1}\cdot\frac{\alpha^2-\alpha_2^2}{\alpha_1^2-\alpha_2^2}\cdot\frac{\alpha^3-\alpha_2^3}{\alpha_1^3-\alpha_2^3}\cdot\frac{\alpha^4-\alpha_1^4}{\alpha_2^4-\alpha_1^4}\cdot\frac{\alpha^5-\alpha_1^5}{\alpha_2^5-\alpha_1^5}$$

$$N_{27} = \frac{\alpha^1 - \alpha_2^1}{\alpha_1^1 - \alpha_2^1} \cdot \frac{\alpha^2 - \alpha_1^2}{\alpha_2^2 - \alpha_1^2} \cdot \frac{\alpha^3 - \alpha_2^3}{\alpha_1^3 - \alpha_2^3} \cdot \frac{\alpha^4 - \alpha_1^4}{\alpha_2^4 - \alpha_1^4} \cdot \frac{\alpha^5 - \alpha_1^5}{\alpha_2^5 - \alpha_1^5}$$

$$N_{28} = \frac{\alpha^1 - \alpha_1^1}{\alpha_2^1 - \alpha_1^1} \cdot \frac{\alpha^2 - \alpha_1^2}{\alpha_2^2 - \alpha_1^2} \cdot \frac{\alpha^3 - \alpha_2^3}{\alpha_1^3 - \alpha_2^3} \cdot \frac{\alpha^4 - \alpha_1^4}{\alpha_2^4 - \alpha_1^4} \cdot \frac{\alpha^5 - \alpha_1^5}{\alpha_2^5 - \alpha_1^5}$$

$$N_{29} = \frac{\alpha^1 - \alpha_2^1}{\alpha_1^1 - \alpha_2^1} \cdot \frac{\alpha^2 - \alpha_2^2}{\alpha_1^2 - \alpha_2^2} \cdot \frac{\alpha^3 - \alpha_1^3}{\alpha_2^3 - \alpha_1^3} \cdot \frac{\alpha^4 - \alpha_1^4}{\alpha_2^4 - \alpha_1^4} \cdot \frac{\alpha^5 - \alpha_1^5}{\alpha_2^5 - \alpha_1^5}$$

$$N_{30} = \frac{\alpha^1 - \alpha_1^1}{\alpha_2^1 - \alpha_1^1} \cdot \frac{\alpha^2 - \alpha_2^2}{\alpha_1^2 - \alpha_2^2} \cdot \frac{\alpha^3 - \alpha_1^3}{\alpha_2^3 - \alpha_1^3} \cdot \frac{\alpha^4 - \alpha_1^4}{\alpha_2^4 - \alpha_1^4} \cdot \frac{\alpha^5 - \alpha_1^5}{\alpha_2^5 - \alpha_1^5}$$

$$N_{31} = \frac{\alpha^1 - \alpha_2^1}{\alpha_1^1 - \alpha_2^1} \cdot \frac{\alpha^2 - \alpha_1^2}{\alpha_2^2 - \alpha_1^2} \cdot \frac{\alpha^3 - \alpha_1^3}{\alpha_2^3 - \alpha_1^3} \cdot \frac{\alpha^4 - \alpha_1^4}{\alpha_2^4 - \alpha_1^4} \cdot \frac{\alpha^5 - \alpha_1^5}{\alpha_2^5 - \alpha_1^5}$$

$$N_{32} = \frac{\alpha^1 - \alpha_1^1}{\alpha_2^1 - \alpha_1^1} \cdot \frac{\alpha^2 - \alpha_1^2}{\alpha_2^2 - \alpha_1^2} \cdot \frac{\alpha^3 - \alpha_1^3}{\alpha_2^3 - \alpha_1^3} \cdot \frac{\alpha^4 - \alpha_1^4}{\alpha_2^4 - \alpha_1^4} \cdot \frac{\alpha^5 - \alpha_1^5}{\alpha_2^5 - \alpha_1^5}$$